Physico-chimie des atomcules d'hélium antiprotonique : modélisation de processus réactifs en présence d'antimatière

Sebastien Sauge

THÈSE
PRÉSENTÉE PAR

Sébastien Sauge

POUR OBTENIR LE TITRE DE DOCTEUR
DE L'UNIVERSITÉ JOSEPH FOURIER - GRENOBLE 1
(Arrêtés ministériels du 5 juillet 1984 et du 30 mars 1992)

SPÉCIALITÉ PHYSIQUE MOLÉCULAIRE

PHYSICO-CHIMIE DES ATOMCULES D'HELIUM ANTIPROTONIQUE: MODÉLISATION DE PROCESSUS RÉACTIFS EN PRÉSENCE D'ANTIMATIÈRE

DATE DE SOUTENANCE : 06 Juillet 2000

COMPOSITION DU JURY :

M. Jean-Marc RICHARD	Président
M. Philippe MILLIÉ	Rapporteur
M. Till von EGIDY	Rapporteur
M. Jean-Claude RAYEZ	Examinateur
M. Pierre VALIRON	Directeur de thèse

THÈSE PRÉPARÉE AU SEIN DU LABORATOIRE D'ASTROPHYSIQUE,
Observatoire de Grenoble, UJF/CNRS, BP 53, F-38 041 Grenoble CEDEX 9

THÈSE
PRÉSENTÉE PAR

Sébastien Sauge

POUR OBTENIR LE TITRE DE DOCTEUR
DE L'UNIVERSITÉ JOSEPH FOURIER - GRENOBLE 1
(Arrêtés ministériels du 5 juillet 1984 et du 30 mars 1992)

SPÉCIALITÉ PHYSIQUE MOLÉCULAIRE

PHYSICO-CHIMIE DES ATOMCULES D'HELIUM ANTIPROTONIQUE: MODÉLISATION DE PROCESSUS RÉACTIFS EN PRÉSENCE D'ANTIMATIÈRE

DATE DE SOUTENANCE : 06 Juillet 2000

COMPOSITION DU JURY :

M. Jean-Marc RICHARD	Président
M. Philippe MILLIÉ	Rapporteur
M. Till von EGIDY	Rapporteur
M. Jean-Claude RAYEZ	Examinateur
M. Pierre VALIRON	Directeur de thèse

THÈSE PRÉPARÉE AU SEIN DU LABORATOIRE D'ASTROPHYSIQUE,
Observatoire de Grenoble, UJF/CNRS, BP 53, F–38 041 Grenoble CEDEX 9

Je dédie cette thèse à mon frère Nicolas et à mes parents

Remerciements

La rédaction d'un manuscrit de thèse s'apparente assez à l'entrée dans une mer d'eau froide. On commence par y tremper un pied pour l'en retirer aussi sec (si j'ose dire), avec la certitude que "non, non, ça n'est pas pour moi ça". Ce petit manège peut durer plusieurs jours voire plusieurs semaines. Eh puis bon, il faut bien se jeter à l'eau avant qu'invariablement quelqu'un d'autre ne s'en charge, je ne cite personne, encore que si justement mais pour d'autres raisons: cette expérience aura valu principalement par les personnes que j'y ai rencontrées, les amis, les amies, les "amies"... S'il est vrai qu'un manuscrit de thèse est destiné à retourner d'où il vient, autrement dit à prendre la poussière (ou l'eau) ailleurs que sur ce bureau, j'espère que ces amitiés, elles, ne les prendront jamais.

A Pierre Valiron, pour avoir accepté de jouer les "maîtres nageurs", pour ses conseils et encouragements sans lesquels ce travail n'aurait peut être pas abouti.

A István Mayer (le hongrois terrible) et Jaume Carbonell (le catalan volubile) pour leur contribution à ces travaux et leur délicieux sens de l'humour.

A Jean-Marc Richard, Philippe Millié, Till von Egidy et Jean Claude Rayez, pour avoir aimablement accepté de participer au jury de cette thèse, pour l'intérêt qu'ils ont porté à mes travaux et pour leur lecture attentive et critique de ce manuscrit.

A tous les membres du Laboratoire d'Astrophysique pour leur accueil et leur soutien. Aux secrétaires (Fanfan, Cécile, Hélène et Stéphanie) pour leur gentillesse et leur disponibilité. Aux informaticiennes Ginette et Françoise pour leur aide et leur dévouement.

A Alex, l'homme qui marcha sur le web (ou plutôt son top-model directory) quand il ne l'imprimait pas, le physicien ("j= 100 est assez grand pour considérer que c'est l'infini"), le chimiste ("il n'y a pas d'eau dans l'oxygène"), le mathématicien ("mais m..., il me manque un dernier nombre premier, et je les ai déjà tous essayés!"), l'unix best administrator ("j'ai rebooté, y'avait encore des mouches"), mais aussi le père d'un charmant bambin, Paul, qui fera parler de lui. Et à Marie, pour avoir accepté de s'occuper de ces deux lascards. Merci d'avoir fait de ces trois années une franche partie de rigolade.

A Nico dit "chouchou", qui fut mon compagnon de couveuse à la maternité de Besançon. Ça crée des liens, forcément. Vingt huit ans plus tard, Nico vit dans le Gers avec Irène et leur petit Maxime. Il est un spécialiste incontournable des disques de matière dense (gâteau basque) et des fluides parfaits (juransson vendanges tardives). Ils vivent heureux et nous le rendent bien.

A Damien et Erika pour m'avoir initié à l'escalade, au crawl, aux tractions (au secours...); et pour leur précieuse amitié.

A Evy "body" Kersalé et Frédérique pour avoir eu la bonne idée de rédiger en même temps que moi, et pour quelques séances inoubliables de kick-boxing, comics-tracking et autres dérapages peu contrôlés. Frédérique, tu cours toujours pas assez vite pour m'attraper, patate!

A Claudia pour avoir contrasté avec la fiévreuse énergie des énergumènes sus-cités et à Laurent pour m'avoir trouvé un job en planque de l'armée... dans une caserne.

A Jean Charles, pour m'avoir donné l'impression d'être une personne vaguement subtile. Gentle man... et à Nathalie pour cette même gentillesse à la fois discrète et présente.

A Manu, dont le cœur doit être à peu près aussi grand que ce prodigieux estomac. C'est Murielle qui a de la chance (et puis ça fait aussi moins de vaisselle).

A Freddy Plazy, pour m'avoir tiré des griffes de l'ennui qui guettaient dix mois de vie, en caserne aussi.

A Jean Philippe "loutte d'amour" Berger, parce que Jean Philippe Berger sera toujours Jean Philippe Berger.

A Pop, pour des raisons qui m'échappent.

A Gasp pour avoir préféré l'astronomie au football.

A la relève, Pierre, Fabien, Wilfrid, Estelle, Ludo, Gael...

A Bill Evans pour nous avoir maintes fois sauvé la mise des amateurs de Joe Dassin, des frères Jacques ou des Cure.

A quelques potes du côté de la Momie – Marc, Mourad, Cric, Pat et Tal et al. – for invaluable discussions pas piquées des vers.

A tous ceux que j'ai oublié.

A Gilles en souvenir de nos bons et mauvais coups, la différence entre les deux se situant au niveau du délai de prescription. Et à ses drôles de dames...

A Flo pour ce qu'elle sait.

A Corinne, à tort ou à raison.

Et à Becky.

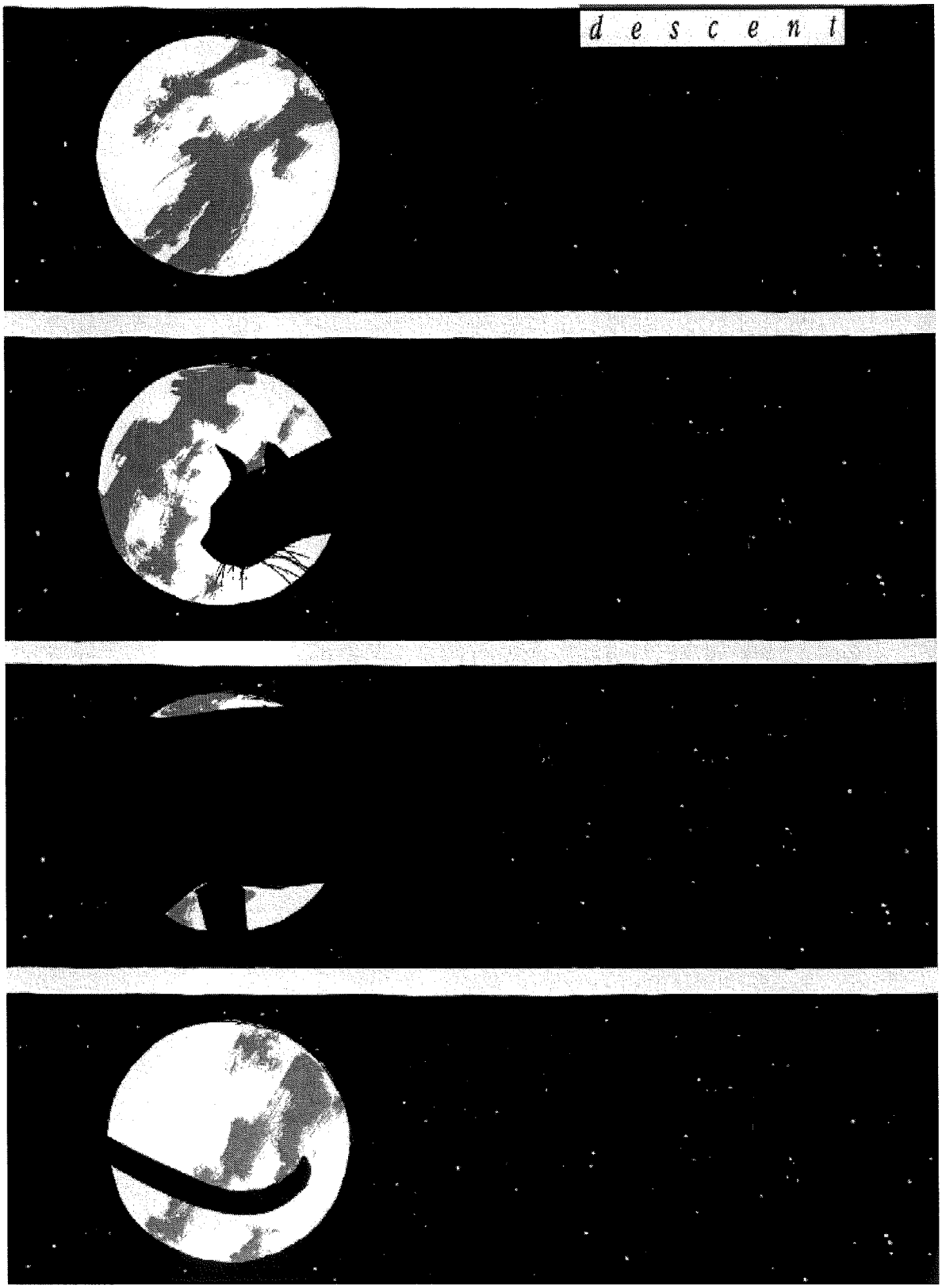
descent

Résumé

Environ 3% des antiprotons ($\bar{p}$) stoppés dans l'helium survivent plusieurs microsecondes, contre quelques picosecondes dans tout autre matériau. Cette métastabilité inhabituelle résulte d'une capture sur des états liés de l'atome exotique $\bar{p}He^+$, dénommé atomcule car il s'apparente à la fois à un atome de Rydberg quasi-circulaire quasi-classique de grand moment angulaire $l \sim n - 1 \sim 37$ et à une molécule diatomique composée d'un noyau chargé négativement et caractérisée par une forte excitation rotationnelle $J = l$. En dehors de cette structure duale originale accessible par spectroscopie laser, la physico-chimie de leur interaction avec d'autres atomes ou molécules a fait l'objet de mesures résolues en état (n, l). Alors que les atomcules résistent à des millions de collisions dans l'helium pur, des contaminants moléculaires comme H_2 les détruisent immédiatement, même à basse température.

Dans le cadre Born-Oppenheimer, nous interprétons l'interaction moléculaire, calculée par des techniques de chimie quantique *ab initio*, en termes de chemins réactifs classiques, qui présentent des barrières d'activation compatibles avec celles mesurées pour He et H_2. Nous montrons par une approche Monte Carlo de trajectoires classiques que la thermalisation détruit fortement les populations initiales, portant la fraction estimée des états de capture à 3 %. Nous étudions aussi la recombinaison dissociative $\bar{p}He^+ + e^+e^-$ dans une approche de trajectoires classiques pour les noyaux: nous prédisons la synthèse d'antihydrogène avec un rapport de branchement de 10 %, ainsi qu'une nouvelle classe d'atomcules métastables (α, $\bar{p}$, e^+, $2e^-$), qui pourrait être confirmée par spectroscopie. Ce travail illustre la transférabilité des concepts de chimie physique à l'étude de processus exotiques en présence d'antimatière, et apporte un éclairage nouveau sur la physico-chimie des radicaux interstellaires froids.

Summary

About 3% of antiprotons ($\bar{p}$) stopped in helium are long-lived with microsecond lifetimes, against picoseconds in all other materials. This unusual longevity has been ascribed to the trapping of $\bar{p}$ on metastable bound states in $\bar{p}He^+$ helium atom-molecules thus named atomcules. Apart from their unique dual structure investigated by laser spectroscopy - a near-circular quasi-classical Rydberg atom with $l \sim n-1 \sim 37$ or a special diatomic molecule with a negatively charged $\bar{p}$ nucleus in high rotational state with $J = l$ - the chemical physics aspects of their interaction with other atoms or molecules constitute an interesting topic for molecular physics. While atomcules may resist to million collisions in helium, molecular contaminants such as H_2 are likely to destroy them in a single one, down to very low temperatures.

In the Born-Oppenheimer framework, we interpret the molecular interaction obtained by *ab initio* quantum chemical calculations in terms of classical reactive channels, with activation barriers accounting for the experiments carried out in He and H_2. From classical trajectory Monte Carlo simulations, we show that the thermalization stage strongly quenches initial populations, thus reduced to a recovered 3 % trapping fraction. Alternatively, we investigate the reactive association of $\bar{p}He^+$ with e^+e^- in a classical trajectory approach for nuclei: we predict antihydrogen synthesis with 10 % branching ratio and a new class of metastable atomcules (α, $\bar{p}$, e^+, $2e^-$), which could be confirmed by spectroscopy. This work illustrates the pertinence of chemical physics concepts to the study of exotic processes involving antimatter. New insights into the physico-chemistry of cold interstellar radicals are anticipated.

Contents

Introduction

Un atome ordinaire se compose d'un noyau chargé positivement, en interaction électromagnétique avec des électrons, ce qui conduit à l'existence d'états liés. On appelle atome exotique un atome pour lequel l'un des électrons a été remplacé par toute autre particule massive chargée négativement, comme un pion (π^-), un kaon (K^-), ou un antiproton ($\bar{p}$). Lorsqu'une telle particule massive pénètre dans la matière, elle est ralentie par collisions inélastiques avec les électrons atomiques. Lorsque son énergie cinétique tombe en dessous du potentiel d'ionisation des atomes environnants, elle est capturée sur des orbites qui présentent le plus fort recouvrement avec la fonction d'onde de l'électron éjecté. Pour l'antiproton, cette condition conduit - compte tenu du rapport M des masses réduites du $\bar{p}$ et de l'électron relativement au noyau d'helium - à une capture sur une orbite de nombre quantique principal $n \sim \sqrt{M} = 38$. Une fois l'antiproton lié, il cascade par une série de transitions radiatives, jusqu'à ce que ces dernières l'amènent à portée de l'interaction forte. La cascade est fortement influencée par les collisions avec les atomes environnants, qui induisent des transitions rapides des états de capture de grand moment angulaire L aux états S ($L = 0$). Ce processus porte le nom d'effet Stark. Dans la mesure où ces états S présentent un fort recouvrement au noyau, les antiprotons vont s'y annihiler rapidement. Dans les atomes exotiques autres que l'atome d'hydrogène où l'effet Stark est dominant, l'émission Auger joue également un rôle important dans la désexcitation des états de capture: si le couplage avec l'un des électrons devient fort, l'antiproton peut communiquer une partie de son énergie à ce dernier qui est alors susceptible d'être éjecté. Une fois ionisé, l'atome exotique polarise l'environnement et se trouve soumis à des champs électriques intenses qui induisent des transitions Stark externes vers les états S. On a longtemps supposé que tout antiproton capturé dans la matière devrait s'annihiler en quelques picosecondes au noyau de l'atome exotique ainsi constitué. Contrairement à cette hypothèse, une faible fraction (3 %) des antiprotons stoppés dans l'helium est capturée sur des états métastables avec une durée de vie moyenne de 3 microsecondes, plus d'un million de fois supérieure aux durées de vie observées dans tous les autres matériaux (Yamazaki *et al.*, 1993).

Des états métastables analogues mais à plus courte durée de vie avaient déjà été observés dans les années soixante avec des pions (π^-) et des kaons (K^-) dans les chambres à bulles d'helium liquide. On doit à Condo (1964) d'avoir suggéré que la métastabilité pourrait être attribuée à la capture de ces particules sur des états de Rydberg, c'est à dire de grand moment

angulaire. Ces états correspondent à des orbites circulaires ($L = n - 1$) ou quasi-circulaires. Dans le cas du système $\bar{p}He^+$, l'écart ΔE_n entre ces niveaux d'énergie est d'environ 2 eV, une valeur bien inférieure à l'énergie d'ionisation, voisine de celle de l'helium (environ 25 eV). En conséquence, un saut ΔL de quatre unité de moment angulaire au moins devient nécessaire pour induire une émission Auger. Des calculs montrent que le taux de transition Auger augmente de trois ordres de grandeur chaque fois que ΔL augmente d'une unité. L'électron $1s$ n'est donc pas éjecté immédiatement. Sa présence assure la neutralité de l'atome, ce qui rend inopérant l'effet Stark externe. Elle lève également la dégénérescence en L des états de capture qui se trouvent décalés de 0.3 eV, ce qui supprime l'effet Stark interne lié au mixing des états de même L. Enfin, la répulsion de Pauli le protège des collisions avec les atomes d'helium environnants, justifiant ainsi la faible sensibilité des spectres d'annihilation à la densité d'helium. La désexcitation de l'atome exotique reste donc dominée par les transitions radiatives, du moins jusqu'à ce que ces dernières l'amènent sur un état instable par effet Auger et annihilation Stark subséquente. Ces transitions sont lentes en raison du faible écart ΔE_n entre les niveaux d'énergie[1]. Les seules transitions permises obéissent à la règle de sélection $\Delta n = \Delta L = 1$ qui conserve le nombre quantique vibrationnel $v = n - L - 1$. Les états métastables se désexcitent ainsi suivant une cascade identifiée par $v = 0, 1, 2 \ldots$ (Yamazaki & Ohtsuki, 1992). Les calculs prédisent ainsi des durées de vie de l'ordre de quelques microsecondes pour les états $n \sim L \sim 38$, en accord avec celles observées. Ici encore, l'électron contribue à prolonger la durée de vie des états métastables. Le terme de répulsion coulombienne e^--$\bar{p}$ polarise l'électron $1s$ à l'opposé du $\bar{p}$, avec pour effet de réduire encore par trois le taux de transition radiatif (Yamazaki & Ohtsuki, 1992). L'antiproton occupe ainsi des états de Rydberg métastables qui correspondent à des orbites quasi-classiques.

L'atome exotique $[\bar{p}He^+]_{nL}$ s'apparente également à une molécule diatomique un peu particulière, puisque l'un de ses noyaux (l'antiproton) porte une charge négative. Cette molécule présente par ailleurs une très forte excitation rotationnelle, avec des nombres quantiques de rotation $J = L$ proches de 40. La force centrifuge issue de ce couplage assure la stabilité de l'"anti-liaison". Malgré sa rotation rapide, l'antiproton demeure encore n fois plus lent que l'électron, dont la distribution s'ajuste ainsi adiabatiquement à la position des noyaux. La séparation Born-Oppenheimer (BO) reste donc un cadre valide d'approximation pour étudier ce système. Pour chaque valeur de $J = L$, le potentiel effectif BO du système ressemble à un potentiel interatomique dans lequel les états métastables se comportent comme des états de vibration faiblement excités ($v = n - L - 1 \sim 0, 1, 2 \ldots$). La dénomination d'"atomcule" a été introduite par Yamazaki *et al.* (1993) pour illustrer cette dualité de description. La figure 1 résume les points développés ci-dessus.

[1] le taux de transition radiatif est proportionnel à $(\Delta E_n)^3$.

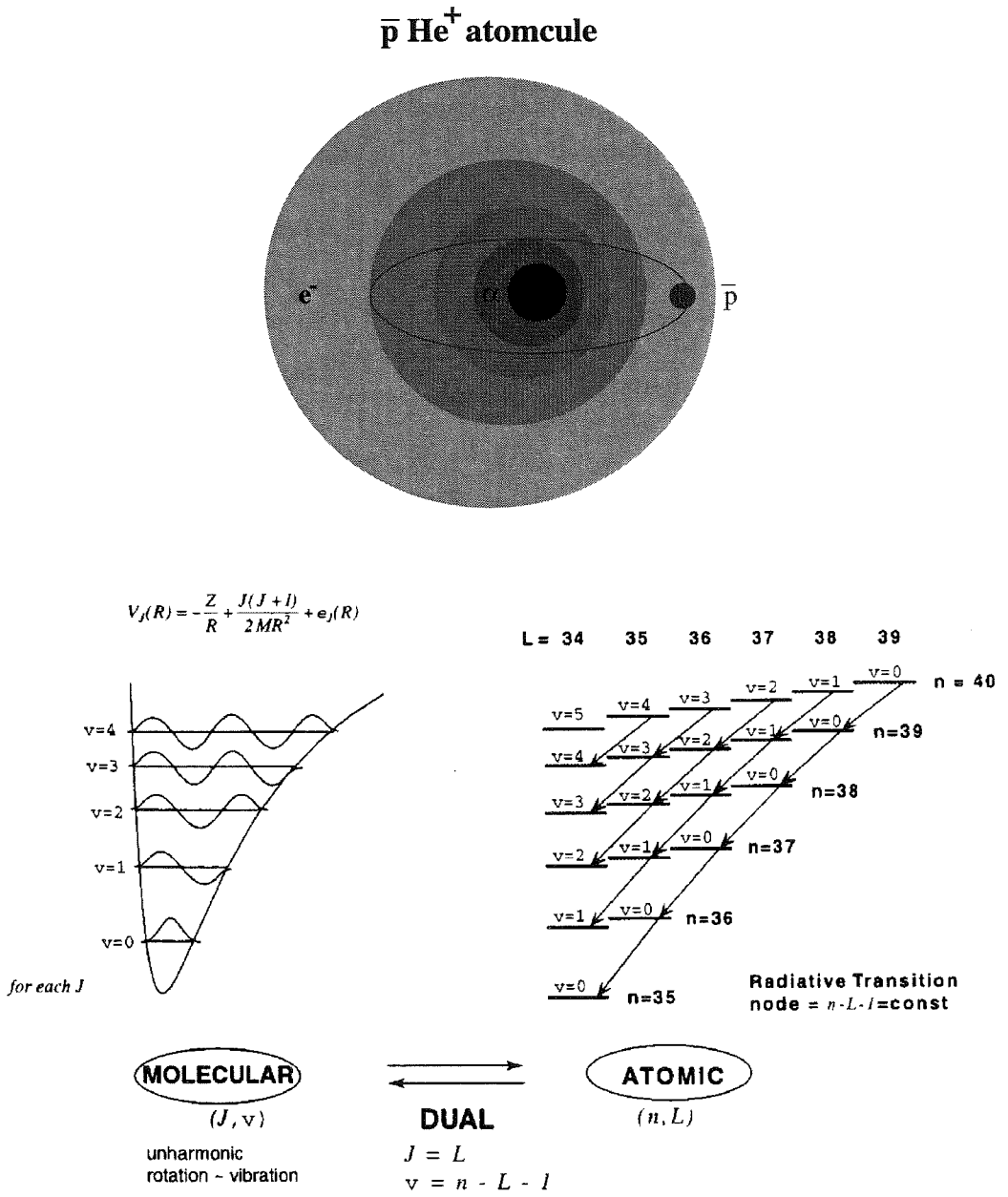

Figure 1: Haut: une représentation de l'atomcule métastable $\bar{p}He^+$, constitué d'un antiproton localisé sur une orbite de Rydberg quasi-circulaire typique $(n, L) = (38, 37)$ (en perspective) autour d'un noyau α (en noir), tandis que le nuage électronique (courbes d'isodensité), est polarisé à l'opposé du $\bar{p}$. L'électron ajuste adiabatiquement sa distribution à la position du $\bar{p}$. Bas: points de vue atomiques et moléculaires illustrant le caractère dual de l'atomcule antiprotonique. Ce dernier peut être d'abord considéré comme un atome de Rydberg $(n, L \sim n - 1)$ qui se désexcite par de lentes transitions radiatives conservant le nombre quantique vibrationnel $v = n - L - 1$. L'atomcule supporte également une description moléculaire. La molécule diatomique caractérisée par les nombres quantiques $(v, J) = (n - L - 1, L)$ a un noyau de charge -1 et une forte excitation rotationnelle $(J = L \sim 40)$. Les niveaux vibrationnels $v = 0, 1, 2 \ldots$ sont quantifiés dans le potentiel effectif $V_J(R)$. Figure du bas tirée de Yamazaki (1998).

L'hypothèse de Condo fut pour la première fois étudiée théoriquement par Russell (1969). Ce dernier suggéra de reconduire les expériences avec des antiprotons qui sont stables intrinsèquement, à l'inverse des pions et kaons qui se désintègrent en quelques dizaines de nanosecondes. Il fallut attendre presque trente ans avant que les faisceaux d'antiprotons mono-énergétiques délivrés par l'anneau de stockage LEAR du CERN ne permettent l'étude détaillée et systématique du phénomène, après que le laboratoire national de physique des hautes énergies du Japon (le KEK) l'ait "redécouvert". Un spectre typique d'annihilation est présenté à la figure 2. Les spectres confirment qu'environ 3 % des antiprotons ont une durée de vie moyenne de 3 microsecondes. Aucun état métastable n'a été observé dans le lithium ou dans un gaz rare autre que l'helium.

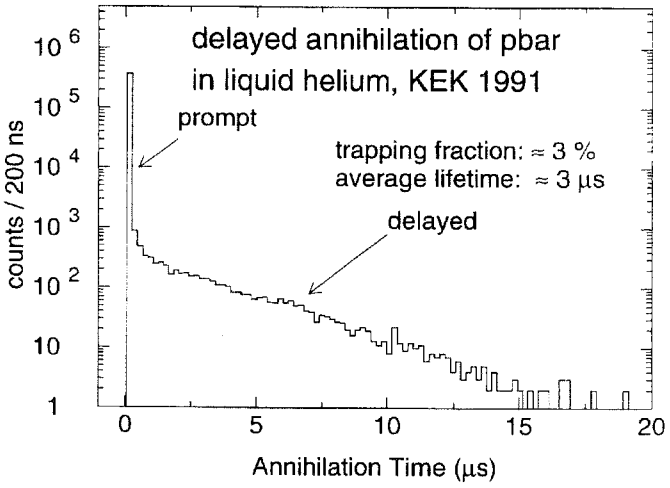

Figure 2: Spectre typique d'annihilation d'antiprotons dans l'helium pur. Près de 3 % des $\bar{p}$ capturés survivent avec une durée de vie moyenne de 3 microsecondes, alors que 97 % s'annihilent normalement au noyau en quelques picosecondes (Iwasaki *et al.*, 1991).

L'existence d'atomcules reçut une première confirmation lorsque les spectres d'annihilation mirent en évidence un effet isotopique prédit théoriquement par Yamazaki & Ohtsuki (1992) dans le cadre du modèle atomique de Condo: la durée de vie des antiprotons dans ^{3}He est inférieure de 15 % à celle mesurée dans ^{4}He. Toutefois, cet effet isotopique seul ne constituait pas une signature non-équivoque de la formation de ces états atomiques particuliers. Il était clair qu'une expérience conclusive consisterait à induire des transitions laser résonnantes entre les niveaux d'énergie de l'atome exotique. Avec la détermination toujours plus précise de ces derniers (Yamazaki & Ohtsuki, 1992; Shimamura, 1992; Korobov, 1996), un test portant sur la structure du système $\bar{p}He^+$ put être envisagé. La nouvelle méthode de spectroscopie développée par le LEAR a permis dans un premier temps d'accéder aux transitions entre états métastables et états adjacents instables par effet Auger. L'irradiation laser à la longueur d'onde de la transition provoque une désexcitation résonnante des premiers vers les seconds détruits par annihilation Stark, ce qui se traduit par l'apparition d'un pic

résonnant sur les spectres (Morita *et al.*, 1994). La découverte de deux premières transitions en 1993 et 1994 avec une incertitude relative de 5 ppm seulement (liée à la faible largeur de bande des lasers) motiva d'autres avancées théoriques, dans la mesure où les prédictions des approches atomiques d'interaction de configuration et moléculaires dans le cadre Born-Oppenheimer présentaient encore un écart relatif de 200-2000 ppm. Après les calculs de Korobov incluant les corrections non Born Oppenheimer, l'écart entre les longueurs d'onde de transition théoriques et expérimentales tomba à 50 ppm (et la recherche des transitions passa de 5 jours à quelques heures de balayage de faisceau dans la bande de longueurs d'onde considérée). Treize transitions ont ainsi été identifiées à ce jour (dix dans ^{4}He, trois dans ^{3}He), validant sans aucun doute possible le modèle de Condo et l'existence des atomcules.

La spectroscopie laser des atomcules antiprotonique a aujourd'hui deux objets, qui sont développés dans la première partie de ce manuscrit: le premier concerne la poursuite de l'étude structurale détaillée de ce système à trois corps; le second étudie les aspects de leur formation et de leur destruction, c'est à dire de leur interaction avec d'autres atomes ou molécules. Ce dernier point intéresse tout particulièrment la physique des collisions atomiques et la physico-chimie moléculaire. La survie collisionnelle des atomcules d'helium antiprotonique révèle en effet une grande variété de comportements. La figure 3 présente différents spectres d'annihilation mesurés dans l'helium pur sous différents états (gaz, liquide, solide) et en présence de gaz rares (Ne, Ar, Kr, Xe) ou d'impuretés moléculaires (H_2, N_2, O_2). Dans l'helium pur, les atomcules survivent plusieurs microsecondes dans des conditions variées de pression et d'état. La faible dépendance des spectres à la densité suggère que les états métastables sont pratiquement insensibles aux collisions avec He. Avec des fréquences de collision typiques de 10^{13} Hz, ces durées de vie de l'ordre de la microseconde impliquent que l'atomcule survit à plusieurs millions de collisions dans l'helium pur. L'addition de gaz rares (Ne, Ar, Kr) jusqu'à des concentrations de 20% préserve la métastabilité, à l'exception du Xenon qui affecte plus sensiblement les spectres, même à l'état de traces (quelques centaines de ppm). En revanche, la stabilité collisionnelle des atomcules est très sensible à la présence d'impuretés moléculaires dans le réservoir d'helium où ils sont formés. L'effet le plus spectaculaire est observé avec O_2 et H_2 qui détruisent la métastabilité presque complètement à des concentrations de quelques centaines de ppm, tandis que N_2 à des concentrations d'environ 1% n'a pas autant d'effet. La spectroscopie permet aujourd'hui l'étude des propriétés individuelles des états métastables (durée de vie, sections efficaces de collision), obtenues en induisant des transitions laser vers des états rendus sélectivement instables par leur interaction avec des contaminants moléculaires. Pour H_2, des sections efficaces géométriques ont ainsi été mesurées à très basse température ($\sim$ 30 K) pour les états normalement métastables $n = 38$ et $n = 39$ (Ketzer *et al.*, 1998). Ceci signifie qu'H_2 a une probabilité significative de détruire ces derniers dès la première collision. Si la stabilité collisionnelle des atomcules dans l'helium pur a déjà été étudiée théoriquement (Korenman, 1996; Voronin & Dalkarov, 1998), aucun mécanisme n'a encore été proposé pour interpréter le fort "quenching" collisionnel par H_2 ou O_2.

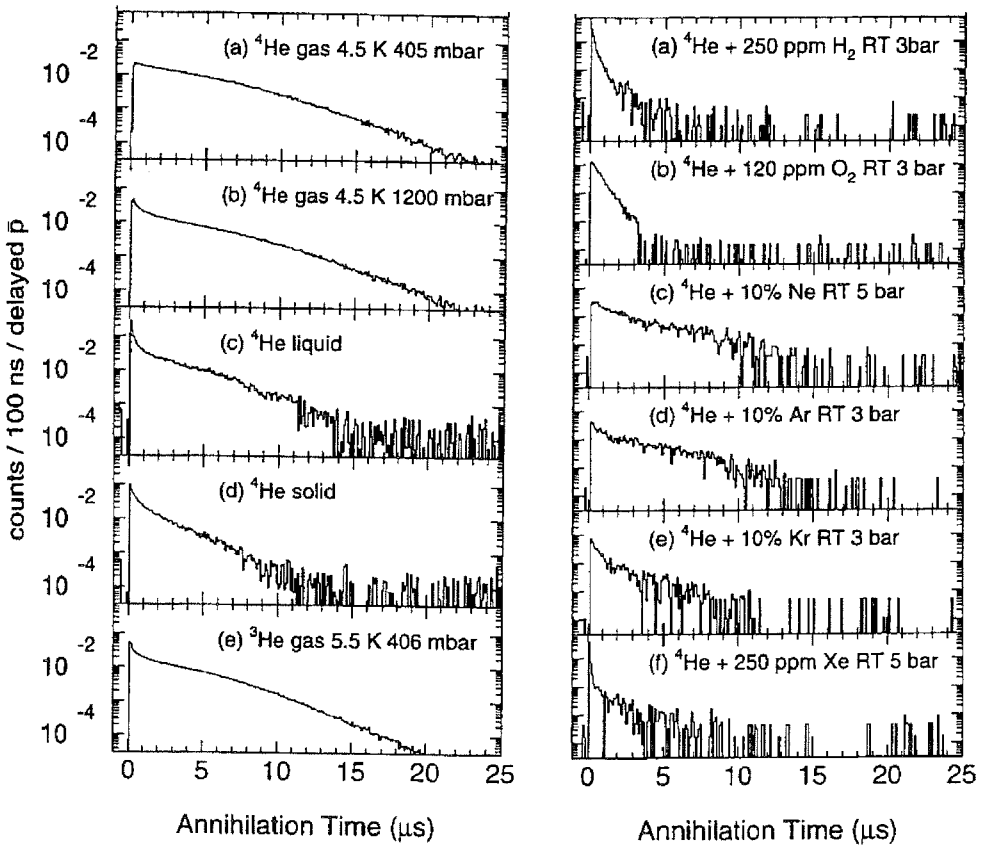

Figure 3: Comparaison des spectres d'annihilation des antiprotons dans l'helium pur sous différents états (gaz, liquide, solide, isotopique) et en présence de gaz rares (Ne, Ar, Kr, Xe) ou d'impuretés moléculaires (H_2, O_2, N_2). Tiré de (Yamazaki *et al.*, 1993; Widmann *et al.*, 1996).

L'objectif premier de cette thèse a été d'interpréter ces différences de comportement collisionnel à partir de concepts simples de physique moléculaire. Nous avons étudié plus particulièrement la survie collisionnelle des atomcules dans l'helium et l'hydrogène moléculaire qui constituent les deux cas limites représentatifs. Il serait intéressant de comprendre notamment pourquoi l'interaction d'échange responsable de la répulsion de Pauli semble protéger les états métastables de collisions avec He mais pas H_2, alors que ces deux systèmes ont le même nombre d'électrons. L'autre intérêt à étudier ces systèmes tient au fait qu'ils sont constitués d'un petit nombre de particules dont l'interaction peut être calculée précisément en utilisant des techniques standards de chimie quantique *ab initio*. D'autres aspects physico-chimiques ont également été abordés, parmi lesquels: la synthèse possible d'antihydrogène ($\bar{H}$=$\bar{p}e^+$) par recombinaison dissociative d'atomcules $\bar{p}He^+$ avec du positronium (Ps=e^+e^-), l'existence d'autres familles d'atomcules métastables, et le confinement d'antiprotons au sein de cages nanométriques. L'ensemble de ces résultats fait l'objet de la seconde partie de ce manuscrit.

Part I

Antiprotonic helium atomcules: a bibliographic review

Chapter 1

Theoretical studies of antiprotonic helium atomcules

Contents

1.1 Introduction

This chapter studies the structure of the metastable antiprotonic atomcule. Most of its general features can be infered by modeling the $\bar{p}e^{-}He^{2+}$ system as a simple Bohr atom, as illustrated in Section 1.2. Beyond this description, a wide range of techniques has been used in order to reckon the energy levels of this unusual three-body system with an accuracy hardly ever achieved, as we reviewed in Section 1.3.

1.2 General features of antiprotonic helium atomcules

Antiprotonic atoms are formed when $\bar{p}$ are slowed down in helium, where they excite and ionize atoms. Atomic capture takes place when the $\bar{p}$ energy falls below the ionization potential of the surrounding atoms. When the exotic atoms are formed, the populated atomic states are those for which the $\bar{p}$ orbit most strongly overlaps the wave function of the displaced electron. This condition can be investigated in the framework of the Bohr model, providing one neglects the interaction with the remaining electron. The Bohr radius of the $\bar{p}$ captured

on a state with principal quantum number n is [1]

$$r_n^{\bar{p}} = \frac{n^2}{MZ}, \tag{1.1}$$

where M is the reduced mass of the $\bar{p}$-He^+ system and Z the screened charge of the α nucleus felt by the $\bar{p}$ ($Z < Z_0 = 2$). Assuming the electron occupies the $1s$ orbital (with principal quantum number $n_e = 1$), its Bohr radius is given by

$$r_{1s}^{e} = \frac{1}{z}, \tag{1.2}$$

where z denotes the effective nuclear charge felt by the electron. Since both $\bar{p}$ and e^- occupy orbits of same spatial extension, it is straightforward to assume that $z \sim Z$. Accordingly, the most probable $\bar{p}$ orbit under the condition $r_n^{\bar{p}} = r_{1s}^{e}$ has a principal quantum number close to

$$n_0 = \sqrt{M} = 38, \tag{1.3}$$

and the Bohr energies of the $\bar{p}He^+$ atom are given by

$$E_n^{\bar{p}} = -\frac{M}{2}\left(\frac{Z}{n}\right)^2. \tag{1.4}$$

In the vinicinity of n_0, $E_n^{\bar{p}}$ matches the orbital energy of the electron, so that the total energy of the atomcule in this state is close to the energy of the He atom

$$E_{1s,n}^{\bar{p}He^+} \sim E_{n_0}^{\bar{p}} + E_{1s}^{e^-} = -\frac{M}{2}\left(\frac{Z}{n_0}\right)^2 - \frac{Z}{2} = -Z^2 \sim E_{1s^2}^{He} = -2.9\ au. \tag{1.5}$$

This approximation leads to an effective nuclear charge

$$Z \sim 1.7\,. \tag{1.6}$$

The maximum $\bar{p}$ available kinetic energy can be taken as roughly equal to the ionization potential I_0 (0.90 au for helium), since above this value, ionization still competes strongly with capture. The maximum angular momentum brought in by the $\bar{p}$ is then

$$l_{max} = r_n^{\bar{p}}\sqrt{2\,m_{\bar{p}}\,I_0}\,. \tag{1.7}$$

For helium, l_{max} is about 50, a value which allows all possible angular momentum (up to $l = n - 1$) to be populated [2]. The $\bar{p}$ wavelength at these energies,

$$\lambda_{\bar{p}} = \frac{h}{p_{\bar{p}}} = \frac{h}{\sqrt{2ME_n^{\bar{p}}}} \propto \frac{1}{n}, \tag{1.8}$$

[1] Throughout the rest of this manuscript, we assume atomic units, wherein $\hbar$, the electron mass and charge are all equal to unity. Conversions from atomic units are given in Appendix 7.4.

[2] For a given principal quantum number n, the orbital angular momentum l takes values of 0, 1, 2 ... $n-1$. The last one ($l = n - 1$) is a circular state and is characterized by a nodeless wave function.

is about n times smaller than the mean radius of the electron cloud, which implies that the $\bar{p}$ orbit is quasi-classical. In the case of helium, the $\bar{p}$ orbital velocity is smaller than that of the remaining electron by the same factor n

$$\sqrt{\langle v_{\bar{p}}^2 \rangle_n} \sim \frac{2|E_n^{\bar{p}}|}{M} \sim \frac{1}{n}. \tag{1.9}$$

Therefore, the rotation frequency of both particles vary in the same ratio. Accordingly, the Born-Oppenheimer separation of electronic and nuclear motions is a valid approximation.

Once the antiproton is bound, it cascades to the nucleus through a serie of radiative transitions, until it comes within range of strong interaction and annihilates. The cascade is strongly influenced by collisions with neighbouring atoms, which induce fast Stark transitions from high-n, high-l states to high-n s states, which have a strong overlap to the nucleus. In exotic atoms other than those formed in hydrogen, Auger emission of the remaining 1s electron is also expected to strongly compete with the radiative decay. This process occurs when the correlation between the antiproton and the remaining electron becomes strong, so that the $\bar{p}$ imparts some of its energy to the e^- which is then emitted in a time of about 10^{-15} s. Annihilation should then occur within picoseconds, since the charged $\bar{p}He^{2+}$ ion is subject to strong electric fields via polarizing the environment, thus inducing fast external Stark transitions to n s states. Contrary to this common belief, about 3% of the $\bar{p}$ stopped in helium survive several microseconds, that is one million times longer thain in any other materials, thus arising the question of this unusual metastability.

Condo (1964) had suggested that in some of the high-l, high-n atomic states formed by pions and kaons in helium, fast Auger transitions could be strongly supressed, essentially because the energy spacing between these states is small compared to the ionization energy. In the case of antiprotons, the energy spacing in the vincinity of n_0 is roughly obtained from (1.4) by considering that both $\bar{p}$ and electron nearly equally share the total binding energy

$$\triangle E_n = E_n^{\bar{p}} - E_{n-1}^{\bar{p}} \sim -\frac{2n-1}{(n-1)^2} E_n^{\bar{p}} \sim \frac{2}{n} \left| \frac{E_{1s^2}^{He}}{2} \right| = \frac{2.9}{n}. \tag{1.10}$$

In the case of antiprotonic helium, $\triangle E_n$ is only 0.08 au, much smaller than the ionization energy of the helium atom (0.9 au). As a result, Auger transitions to lower-lying $\bar{p}He^{2+}$ states require a large jump in both n and l values, namely $|\triangle n| \sim 6$, $|\triangle l| > 3$. The $|\triangle n| \sim 6$ criterium can be found qualitatively by considering that in the vincinity of n_0, a transition to an Auger-dominated level with quantum number n_A occur when

$$E_{n_0}^{\bar{p}} > E_{n_A}^{\bar{p}He^{2+}} = -\frac{MZ_0^2}{2n_A^2}, \tag{1.11}$$

thus leading to

$$n_A < n_0 \frac{Z_0}{Z}. \tag{1.12}$$

With $n_0 = 38$, one gets $n_A < 32$, so that $|\Delta n| \sim 6$. Calculations show that the Auger transition rate increases by three orders of magnitude as $|\Delta l|$ increases by one unit (Morita *et al.*, 1993). Therefore, fast Auger transitions are energetically impossible. Protected during collisions by the charge cloud of the remaining electron, the exotic atom will not be able to reach ns states quickly by collision-induced Stark transitions. The Stark mixing of high-l with low-l levels is suppressed because the electron removes the degeneracy of l-states with the same n from about 0.1 au. Besides, the neutrality prevents the atomcule to be destroyed by external Stark effect, and for close encounters with He atoms, the $\bar{p}$ should be shielded by the Pauli repulsion. As a result, the deexcitation of the $\bar{p}He^+$ atom is mainly dominated by radiative transitions, until they are brought on a state from which a fast $\Delta l \leq 3$ Auger decay becomes energetically possible. These transitions are slow because of the small energy levels spacing[3] and obey the selection rule $\Delta n = \Delta l = 1$ Yamazaki & Ohtsuki (1992), which conserves the vibrational quantum number $v = n - l - 1$, so that metastable states can be grouped into cascade chains $v = 0, 1, 2, \ldots$, as illustrated in Fig. 1.1.

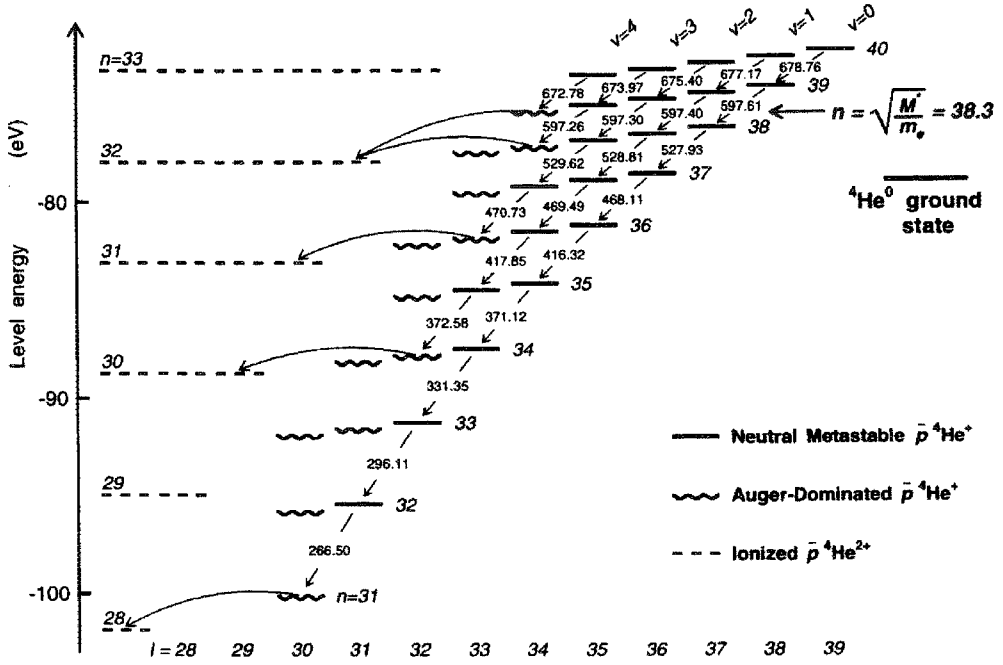

Figure 1.1: Level structure of the $\bar{p}^4He^+$ atom. The solid lines indicate the radiation-dominated metastable states with lifetimes of $1 - 2$ μs, the wavy lines Auger-dominated short-lived levels. The broken lines show the final $\bar{p}He^{2+}$ ionic states formed after Auger emission of the remaining electron. The curved arrows indicate Auger transitions with minimum $|\Delta l|$. The theoretical absolute energy of each state (n, l) is relative to the three-body-breakup threshold. The calculated resonance wavelengths of radiative transitions following the constant-v propensity rule are given in nanometers (Hori *et al.*, 1998).

[3]The transition rate λ is proportional to $(\Delta E_n)^3$. Considering (1.10), λ depends upon n^{-3}. Accordingly, radiative lifetimes are about 1-2 μs.

1.3 Energy levels of antiprotonic helium atomcules

The two main theoretical descriptions of the $[\bar{p}e^{-}\alpha]$ three-body system are the atomic approach (section 1.3.2) and the molecular approach (section 1.3.3). Recently they have been supplemented by large configuration-space variational methods, including relativistic and higher-order QED corrections (section 1.3.4). The present calculations agree with experimental transition wavelengths to a relative accuracy of a few 10^{-6}.

1.3.1 Hamiltonian

The nonrelativistic spinless Hamiltonian for the three-body system ($\bar{p}$, e^{-}, He^{2+}) $\equiv$ $\bar{p}He^{+}$, after separating the center of mass motion, can be written in Jacobian coordinates as

$$H = -\frac{1}{2M}\triangle_{\mathbf{R}} - \frac{1}{2m}\triangle_{\mathbf{r_I}} - \frac{2}{R} - \frac{2}{r} + \frac{1}{|\mathbf{r}-\mathbf{R}|}, \tag{1.13}$$

where $\mathbf{R}$ is the position vector of the $\bar{p}$ nucleus relative to the α particle; $\mathbf{r}$ and $\mathbf{r_I}$ denote the position vectors of the electron relative to the α particle and the center of mass of the two nuclei, respectively (see Fig. 1.2). M and m are the reduced masses

$$\frac{1}{M} = \frac{1}{m_\alpha} + \frac{1}{m_{\bar{p}}}, \tag{1.14}$$

$$\frac{1}{m} = \frac{1}{m_e} + \frac{1}{m_\alpha + m_{\bar{p}}}. \tag{1.15}$$

In this formulation of the Hamiltonian, the separation of both electronic and nuclear motions appears through the position vector $\mathbf{r_I}$ and the reduced mass m.

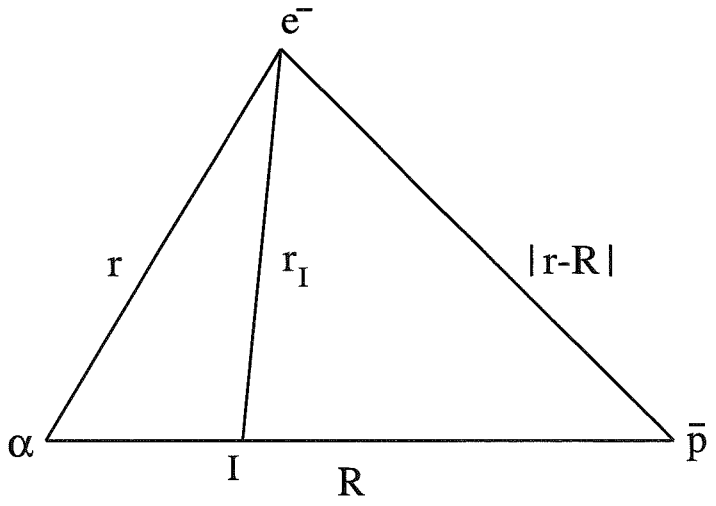

Figure 1.2: Set of jacobian coordinates for the description of the ($\bar{p}$,$e^{-}He^{2+}$) exotic atomcule.

1.3.2 Energy levels in the atomic picture

As previously mentioned, the antiproton within the $\bar{p}He^+$ system can be viewed as a heavy electron bound to the α nucleus in a near-circular quasi-classical Rydberg state with $l \simeq 40$.

The independent-particles approximation

Because of the $\bar{p}$–e^- interaction, the Schrödinger equation for the $\bar{p}He^+$ system cannot be solved exactly. One first approximation consists in neglecting the interaction term $\frac{1}{|\mathbf{r}-\mathbf{R}|}$, thus reducing the Hamiltonian H to the sum of two non-interacting hydrogenlike Hamiltonians. The total wave function comes down to the simple product of the two one-particle eigenfunctions relative to the e^- and $\bar{p}$ particles

$$\Psi(\mathbf{r},\mathbf{R}) = \psi^{e}_{100}(\mathbf{r})\,\psi^{\bar{p}}_{nlm}(\mathbf{R}). \tag{1.16}$$

For hydrogenic Hamiltonians, we can write the wave function in spherical polar coordinates (r,θ,ϕ) as the product of a radial function, $\mathcal{R}_{nl}(R)$ by an angular function, $\Omega_{lm}(\theta,\phi)$, which is constructed from the one-particle angular momentum eigenfunctions, namely the spherical harmonics. The radial function is the solution of the radial Schrödinger equation

$$\left[-\frac{1}{2M}\left(\frac{\partial^2}{\partial R^2}+\frac{2}{R}\frac{\partial}{\partial R}\right)+U(R)\right]\mathcal{R}_{nl}(R) = E_n\mathcal{R}_{nl}(R), \tag{1.17}$$

where

$$U(R) = -\frac{Z_0}{R}+\frac{l(l+1)}{2MR^2}\,. \tag{1.18}$$

$U(R)$ consists in an attractive long-range Coulomb potential and a repulsive short-range centrifugal potential. The solution of this equation gives the well-known Bohr energies. Eventually, the eigenenergies of the Hamiltonian operator are the sum of the hydrogenlike energies of both $\bar{p}$ and e^- particles moving in their effective potential, namely

$$E_{n,1s} = -\frac{M}{2}\left(\frac{Z_0}{n}\right)^2-\frac{mZ_0^2}{2}\,. \tag{1.19}$$

For each value of n, the multiplet $(l = 0, 1...n-1)$ is degenerate in energy.

The variational approach

The repulsive Coulomb interaction between the electron and the antiproton leads each particle to screen the other from the α nucleus. As a result, both $\bar{p}$ and e^- are subject to an effective nuclear charge less than the full nuclear one. Moreover, the $\bar{p}$–e^- interaction perturbs the central symmetry of the potential in a dynamic way, thus removing the degeneracy of states with different l but the same n. As a consequence, the electron is polarized away from the $\bar{p}$. The screening of the α can be accounted for in the framework of the variational principle.

Considering the weak mass ratio between the electron and the α nucleus, we can safely assume the α particle as fixed, so that the Hamiltonian can be rewritten as

$$H = -\frac{1}{2M}\,\triangle_{\mathbf{R}} - \frac{1}{2}\,\triangle_{\mathbf{r}} - \frac{2}{R} - \frac{2}{r} + \frac{1}{|\mathbf{r}-\mathbf{R}|}\,. \tag{1.20}$$

The variational theorem states that the expectation value of the energy operator $E_{\Psi_T} = \langle\Psi_T|H|\Psi_T\rangle$ over a trial normalized wave function $\Psi_T(\zeta)$ depending on variational parameters ζ's provides an upper bound to the exact ground state energy, which can be assessed asymptotically by minimizing E_{Ψ_T} with respect to the ζ's. For excited states, the variational method requires the trial wave function be orthogonal to all energetically lower-lying state eigenfunctions, since the eigenfunctions of an hermitian operator are orthogonal. For circular states, i.e. for the energetically lower-lying states of given angular momentum l, this condition is automatically fullfilled if the total wave function of the $\bar{\text{p}}$-He^+ system is expressed as a product of normalized hydrogenlike wave functions (centered on the helium nucleus), owing to the othogonality of the spherical harmonics. The trial wave function can be expressed as

$$\Psi_T(z,Z) = \psi^e_{100}(\mathbf{r},z)\,\psi^{\bar{p}}_{nlm}(\mathbf{R},Z), \tag{1.21}$$

where

$$\psi^e_{100}(\mathbf{r},z) = \mathcal{R}^e_{10}(r,z)\,Y_{00}(\theta,\phi), \tag{1.22}$$

and

$$\psi^{\bar{p}}_{nlm}(\mathbf{R},Z) = \mathcal{R}^{\bar{p}}_{nl}(R,Z)\,Y_{lm}(\Theta,\Phi)\,. \tag{1.23}$$

$\mathcal{R}^e_{10}(r,z)$ and $\mathcal{R}^{\bar{p}}_{nl}(R,Z)$ represent the radial Coulomb wave functions of the $1s$-electron and of the antiproton lying in a state with quantum numbers n,l,m, whereas Y_{lm} designates the spherical harmonics (eigenfunctions of both L^2 and L_z operators). The effective nuclear charges z and Z are variational parameters, which account for the screening of the α particle. They are determined by minimizing the variational integral

$$\begin{aligned} E_{\Psi_T}(z,Z) &= \langle\Psi_T(z,Z)|H|\Psi_T(z,Z)\rangle & (1.24)\\ &= \left\langle\Psi_T\left|-\frac{1}{2M}\,\triangle_{\mathbf{R}} - \frac{Z}{R}\right|\Psi_T\right\rangle + \left\langle\Psi_T\left|\frac{Z-2}{R}\right|\Psi_T\right\rangle \\ &\quad + \left\langle\Psi_T\left|-\frac{1}{2}\,\triangle_{\mathbf{r}} - \frac{z}{r}\right|\Psi_T\right\rangle + \left\langle\Psi_T\left|\frac{z-2}{r}\right|\Psi_T\right\rangle \\ &\quad + \left\langle\Psi_T\left|\frac{1}{|\mathbf{r}-\mathbf{R}|}\right|\Psi_T\right\rangle\,. & (1.25)\end{aligned}$$

As previously recalled, hydrogenlike wave functions ψ^H_{nlm} are solutions of the eigenvalue equation

$$\left(-\frac{1}{2M}\,\triangle_{\mathbf{R}} - \frac{Z}{R}\right)\psi^H_{nlm} = E_n\,\psi^H_{nlm}, \text{with} En = -\frac{MZ^2}{2n^2}\,. \tag{1.26}$$

Moreover, the Virial theorem states that for any hydrogenlike atom stationary state, the expectation value of the kinetic– and potential–energy operators vary as

$$\langle T \rangle = -E_n, \qquad \langle V \rangle = 2E_n \,. \tag{1.27}$$

As a result,

$$\left\langle \Psi_T \left| \frac{Z}{R} \right| \Psi_T \right\rangle = 2E_n = -\frac{MZ^2}{n^2} \,. \tag{1.28}$$

Therefore, the expectation value of the hamiltonian operator is

$$E_{\Psi_T}(z,Z) = \left(-\frac{MZ^2}{2n^2} + \frac{Z-2}{Z}\frac{MZ^2}{n^2} \right) + \left(-\frac{z^2}{2} + \frac{z-2}{z} z^2 \right) + J_{nlm}, \tag{1.29}$$

where J_{nlm} denotes the Coulomb-integral

$$J_{nlm} = \int d^3R\, d^3r\, \frac{|\psi^e_{100}(\mathbf{r})|^2\, |\psi^{\bar{p}}_{nlm}(\mathbf{R},Z)|^2}{|\mathbf{r}-\mathbf{R}|} \,. \tag{1.30}$$

To evaluate J_{nlm}, we can expand $\frac{1}{|\mathbf{r}-\mathbf{R}|}$ in terms of spherical harmonics:

$$\frac{1}{|\mathbf{r}-\mathbf{R}|} = \sum_{l'=0}^{\infty} \sum_{m'=-l'}^{l'} \frac{4\pi}{2l'+1} \frac{\min(r,R)^{l'}}{\max(r,R)^{l'+1}} Y^{\star}_{l'm'}(\theta_r,\phi_r)\, Y_{l'm'}(\theta_R,\phi_R) \,. \tag{1.31}$$

As previously recalled, the Y_{lm} functions are orthogonal and can be normalized. Thus, they obey the orthonormality condition:

$$\int sin\theta\, d\theta\, d\phi\, Y^{*}_{l'm'}(\theta,\phi)\,.\,Y_{lm}(\theta,\phi) = \delta_{ll'}\,\delta_{mm'} \,. \tag{1.32}$$

Let us denote by $\mathbf{L}$ the total angular momentum $\mathbf{L} = \mathbf{L_e} + \mathbf{L_{\bar{p}}}$. The Kronecker deltas make all terms vanish except the single term with $m = 0$, since the vanishing commutator $[\mathbf{L}, \frac{1}{|\mathbf{r}-\mathbf{R}|}]$ does not depend of m. After integration over angular variables, we obtain

$$J_{nl0} = \int dR\, R^2 \int dr\, r^2\, |\mathcal{R}^e_{10}(r)|^2\, |\mathcal{R}^{\bar{p}}_{nl}(R)|^2\, \frac{1}{\max(r,R)} \,. \tag{1.33}$$

The radial one-particle wave functions for the $1s$-electron and for the antiproton lying in the $(n, l = n-1)$ circular state are given by

$$\mathcal{R}^e_{10}(r,z) = 2\, z^{3/2}\, e^{-zr}, \tag{1.34}$$

and

$$\mathcal{R}^{\bar{p}}_{n,n-1}(R,Z) = \frac{1}{\sqrt{(2\,n)!}} \left(\frac{2\,Z\,M}{n} \right)^{n+1/2} R^{n-1}\, e^{-ZMR/n} \,. \tag{1.35}$$

After integration over radial coordinates, we get

$$J_{nl0} = -\frac{1}{n^2} \left[Z^{2n+1} M^{2n+1} z \frac{n^2}{(MZ+nz)^{2n+1}} + Z^{2n+1} M^{2n+1} \frac{1}{(MZ+nz)^{2n}} - ZM \right] . \tag{1.36}$$

Eventually, the variational integral comes down to

$$\langle \Psi_T | H | \Psi_T \rangle = E_T(z, Z) = -\frac{MZ}{2n^2}(2 - Z) - \frac{1}{2}z(4 - z) - MzZ\left(\frac{MZ}{MZ + nz}\right)^{2n}\left(\frac{1}{MZ + nz} + \frac{1}{n^2 z}\right). \quad (1.37)$$

The results of the numerical minimization of (1.37) are presented in Fig. 1.3. The screening of the nuclear charge is illustrated in Fig. 1.3a, where z and Z are drawn as a function of principal quantum number n. For high n values, the $\bar{p}$ moves outside of the electronic cloud, thus seeing an effective nuclear charge, which tends asymptotically to $Z_0 - 1 = 1$. Alternatively, for inner states, the screening of the α particle is weaker and the $\bar{p}$ sees a nuclear charge close to $Z_0 = 2$. For the binding of the electron, the results are reversed. Fig. 1.3b presents the energy levels E_T^{min} of the atomcule circular states.

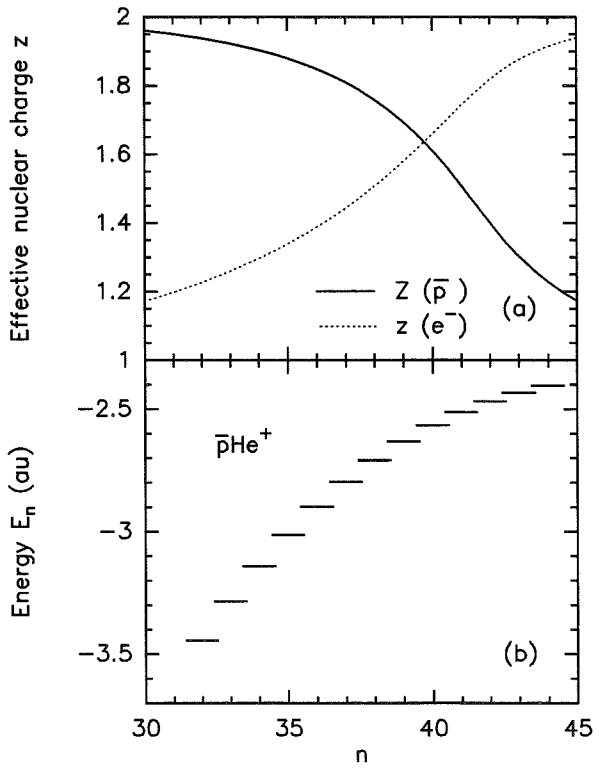

Figure 1.3: (a) Effective nuclear charge z and Z as a function of principal quantum number n. (b) Variational energies E_T^{min} for circular states of the $\bar{p}He^+$ system. After Ketzer (1999).

The configuration interaction method

The independent-particle wave function $\Psi_T = \Psi_T^{(0)}$ corresponds to a zeroth-order wave function, whereas the expectation value $E_{\Psi_T}(z, Z)$ of the Hamiltonian over Ψ_T (1.37) provides a first-order contribution to the exact energy in a perturbative approach, assuming the e^-–$\bar{p}$ interaction, which renders this three-body problem non-separable, is treated as a perturbation. However, we expect this term to be of the same order of magnitude than the α–e^- and α–$\bar{p}$ interaction energies. The ratio between these terms,

$$\rho = \frac{1/|\mathbf{r}-\mathbf{R}|}{2/R+2/r} \sim \frac{1/R}{4/R} = \frac{1}{4}, \tag{1.38}$$

is rather high for a perturbative treatment, since the interaction between the electron and the $\bar{p}$ is dealt with in an average way, both particles being thus placed in spherical symmetry around the α nucleus. Actually, this comes down to neglect the polarization of the e^- away from the $\bar{p}$. The first way to consider the dynamical instantaneous e^-–$\bar{p}$ correlation is to introduce explicitly the interleptonic distance $\frac{1}{|\mathbf{r}-\mathbf{R}|}$ into the wave function. This method, which is only praticable for systems with a few leptons, will not be discussed here. The second method is configuration interaction (CI), which will be presented in further details in Appendix 7.8.1. The main idea behind CI is that first- and higher-order corrections to the wave functions will mix in contributions from excited configurations, giving rise to configuration mixing. In the case of the $\bar{p}He^+$ system, this comes down to mix into the wave function $\Psi_{nlm}(\mathbf{r}, \mathbf{R})$ contributions from other configurations besides $1s$ or $(n, l = n-1)$

$$\Psi_{nlm}(\mathbf{r}, \mathbf{R}) = \sum_{k_e, k_{\bar{p}}} C_{k_e}^{k_{\bar{p}}} \psi_{k_e}(\mathbf{r}), \psi_{k_{\bar{p}}}(\mathbf{R}), \tag{1.39}$$

where $k_{e,\bar{p}}$ denote a state of quantum numbers (n_e, l_e, m_e) and $(n_{\bar{p}}, l_{\bar{p}}, m_{\bar{p}})$ with respect to the electron and the antiproton, respectively. The rules governing the composition of angular momentum demand that the magnitude l of the total angular momentum $\mathbf{L} = \mathbf{L_e} + \mathbf{L_{\bar{p}}}$ only takes the values

$$|l_{\bar{p}} - l_e| \leq l \leq |l_{\bar{p}} + l_e| \,. \tag{1.40}$$

Moreover, the product of one-particle wave functions relative to both e^- and $\bar{p}$ has to conserve the total parity $(-1)^l$ of the atomcule, meaning that only the terms with $(l_e, l_{\bar{p}}) = (s, l)$, $(p, l \pm 1)$, $(d, l \pm 2)$... appear in the expansion. The most common way to do a configuration-interaction calculation on an atom or molecule uses the variational method. One starts by choosing a basis set of one-particle functions ϕ_i. In principle, this basis set should be complete, but in practice, one is limited to a basis set of finite size. One hopes that a good choice of basis functions will give a good approximation to a complete set. For atomic calculations, Slater type orbitals (STOs) are often used

$$\phi_i = N\, r^{n-1}\, e^{-zr}\, Y_{lm}(\theta, \phi), \tag{1.41}$$

where (n, l, m) is a set of quantum numbers describing an hydrogenic state, N a normalization factor, and z a variational parameter accounting for the nuclear screening. The atomic orbitals ψ_{k_e} or $\psi_{k_{\bar{p}}}$ are then written as linear combinations of the basis-set functions ϕ_i. For his calculations, Ohtsuki used a primitive Slater-type function (STF) for each ψ_{k_e}, whereas he expressed each $\psi_{k_{\bar{p}}}$ as a linear combination of 18 STO functions, whose expansion coefficients as well as the screening factor z were obtained by solving the Schrödinger equation

$$\left[-\frac{1}{2M}\,\triangle_{\mathbf{R}} + \epsilon_\sigma^e(R)\right]\psi_{k_{\bar{p}}}(\mathbf{R}) = E_{k_{\bar{p}}}\psi_{k_{\bar{p}}}\,. \tag{1.42}$$

In (1.42), $\epsilon_\sigma^e(R)$ is an adiabatic potential of the $1s_\sigma$ electronic state for a fixed R internuclear α-$\bar{\text{p}}$ separation. $E_{k_{\bar{p}}}$ corresponds to the energy level E_{vJ} of the state $|1s_\sigma, vJ\rangle$ in the dual molecular picture, where $v = n_{\bar{p}} - l_{\bar{p}} - 1$ and $J = l_{\bar{p}}$ denote vibrational and rotational quantum numbers respectively, as will be detailed in next Section. In the calculations made by Ohtsuki, $\Psi_{nlm}(\mathbf{r}, \mathbf{R})$ consisted of 10 $s-$, 9 $p-$ and 8 $d-$STOs for the electron (thus including all contributions up to $n_e = 10$) and the first 15 $\bar{\text{p}}$ orbitals for each $l_{\bar{p}}$ ($n_{\bar{p}} = l_{\bar{p}} + 1,\ l_{\bar{p}} + 2,\ \ldots,$ $l_{\bar{p}} + 15$). All possible angular momenta $(l_e, l_{\bar{p}}) = (0, l),\ (1, l \pm 1),\ (2, l \pm 2)$ were used. The $C_{k_e}^{k_{\bar{p}}}$ coefficients were eventually derived by applying the variational method. Fig. 1.4 shows the CI $\bar{\text{p}}$ and e^- wave function for the circular state $(n, l) = (38, 37)$. As can be seen in Fig. 1.4c, the $\bar{\text{p}}$ is localized at an average distance $\langle R \rangle \sim 0.57$ au from the α nucleus. The electron cloud adjusts itself to the $\bar{\text{p}}$ location, since it moves about n times faster. Because of the repulsive interaction, the 1 s electron is polarized away from the $\bar{\text{p}}$ (Fig. 1.4b). Comparing the CI and $1s$ electronic wave functions in Fig. 1.4a points out that the polarization is substantial. Yamazaki & Ohtsuki (1992) have shown that this slows down the radiative process by a factor of about 3.

1.3.3 Energy levels of $\bar{\text{p}}\text{He}^+$ in the molecular picture

Correspondence between the atomic and molecular pictures

Although the effective potential of the $\bar{\text{p}}\text{He}^{2+}$ ion, $U_{eff}(R) = -\frac{Z_0}{R} + \frac{l(l+1)}{2MR^2}$, has an atomic origin – an attractive long-range Coulomb potential and a repulsive short-range centrifugal potential –, it also resembles an interatomic potential, when the $\bar{\text{p}}$ has a large angular momentum. This picture remains valid when an electron is coupled to large-l circular or quasi-circular orbitals: the electronic energy $\epsilon_\sigma^e(\mathbf{R})$, which can be computed in the adiabatic approximation as a function of the α-$\bar{\text{p}}$ internuclear distance, is slowly varying and thus plays no essential role in the stability of the anti-binding, which is ensured by the centrifugal force from the high rotational coupling. The electron only modifies the binding energies so as to remove the degeneracy of different l-states with the same n. Thus, the $\bar{\text{p}}$-He^+ system can be also considered as a diatomic molecule, presenting low vibrational $v = n - l - 1 \sim 0..3$ and high rotational $J = l \sim 38$ quantum numbers, where large-l orbitals behave like bound states in a ro-vibrational potential. However, although the potential $V_{eff}(R) = U_{eff}(R) + \epsilon_\sigma^e(\mathbf{R})$ looks like an interatomic potential in shape, it is very different from those of normal molecules, for

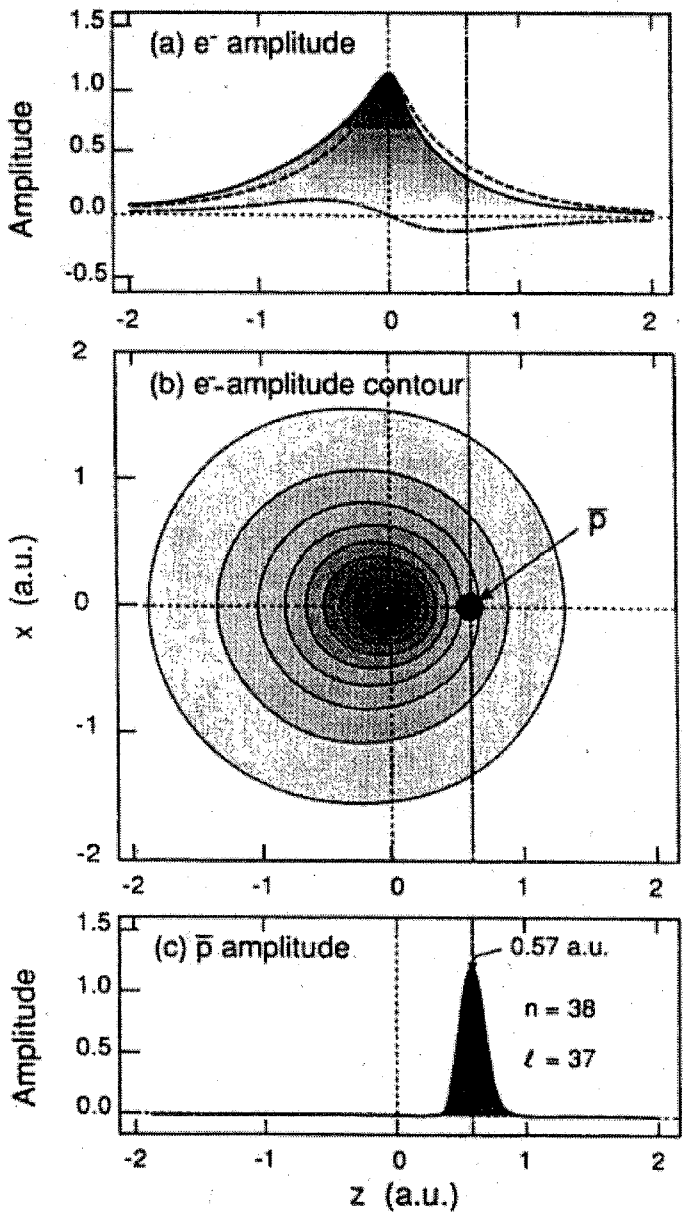

Figure 1.4: Spatial distributions of e^- and $\bar{p}$ for the $(n, l) = (38, 37)$ circular capture state of the $e^-\bar{p}He^{2+}$ atom, as calculated by solving Eq. (1.42). The $\bar{p}$ is well localized, as shown in (*c*), moves slowly compared with the electron motion, and polarizes the latter in the opposite direction, as shown in contour mapping of the electronic wave function in (*b*) and its projection (*a*), where the dashed curve shows the non-polarized wave function (Yamazaki & Ohtsuki, 1992).

which the long-range part comes from the molecular binding force mediated by the electrons and the short-range one arises from the internuclear repulsion. As a result, the structure of the energy levels remains essentially of atomic type. Anyway, treating the $\bar{p}He^+$ system in an atomic approach requires to take into account a large number of configurations in the CI ex-

pansion and affords no simple independent-particle picture, because the antiproton captured in a quasi-Rydberg state (with large l values) correlates strongly with the electron. In the molecular approach however, the vibrational motion is separable from the electronic motion in a good approximation.

Energy levels in the Born-Oppenheimer approximation

The validity of the Born-Oppenheimer approximation can be infered in the framework of a simple atomic independent-particle model, as a consequence of the Virial theorem, which provides the averaged squared velocities of the $\bar{\mathrm{p}}$ and $1s_\sigma$ electron:

$$\langle v_{\bar{p}}^2 \rangle = \frac{Z^2}{n_{\bar{p}}^2}, \tag{1.43}$$

and

$$\langle v_e^2 \rangle = Z^2 \,. \tag{1.44}$$

As a result, the σ electron of the (n,l) atomcule moves about n times faster than the antiproton (Shimamura, 1992). Since the electron in the molecule quickly adjust its distribution to changing nuclear positions, one can reasonably assume that the electron distribution depends only on the instantaneous positions of the nuclei and not on their velocities. In other words, the quantum-mechanical problem of electron motion in the field of fixed nuclei may first be solved, leading to an effective electronic energy $E_\sigma^e(\mathbf{R}) = -\frac{2}{R} + \epsilon_\sigma^e(\mathbf{R})$ which depends on the relative nuclear coordinate $\mathbf{R}$, namely,

$$H_e \, \psi_\sigma^e(\mathbf{r}|\mathbf{R}) = \epsilon_\sigma^e(\mathbf{R}) \, \psi_\sigma^e(\mathbf{r}|\mathbf{R}), \tag{1.45}$$

where H_e denotes the electronic Hamiltonian

$$H_e = -\frac{1}{2} \triangle_{\mathbf{r}} - \frac{2}{r} + \frac{1}{|\mathbf{r} - \mathbf{R}|}, \tag{1.46}$$

and $\psi_\sigma^e(\mathbf{r}|\mathbf{R})$, the electronic wave function depending on the electronic coordinate $\mathbf{r}$ at fixed internuclear separation $\mathbf{R}$. As a consequence of the Born-Oppenheimer separation, the total wave function takes the separable form

$$\Psi_{\sigma v J M}(\mathbf{r}, \mathbf{R}) = \psi_\sigma^e(\mathbf{r}|\mathbf{R}) \, \psi_{vJM}(\mathbf{R}), \tag{1.47}$$

where $\psi_{vJM}(\mathbf{R})$ is the nuclear wave function for the $\bar{\mathrm{p}}$ lying in the (v, J, M) state. The fixed-nuclei energy $E_\sigma^e(\mathbf{R}) = -\frac{2}{R} + \epsilon_\sigma^e(\mathbf{R})$ is then used as a potential energy for a subsequent study of the nuclear motion, which obeys the equation

$$\left[-\frac{1}{2M} \triangle_{\mathbf{R}} + E_\sigma^e(\mathbf{R}) \right] \psi_{vJM}(\mathbf{R}) = E_{vJM} \, \psi_{vJM}(\mathbf{R}) \,. \tag{1.48}$$

Since $E^e_\sigma(\mathbf{R}) = E^e_\sigma(R)$ is rotation invariant, the wave function ψ_{vJM} can be separated into radial and angular parts:

$$\psi_{vJM}(\mathbf{R}) = \frac{1}{R}\chi_{vJ}(R)\, Y_{JM}(\theta,\phi)\,. \tag{1.49}$$

The vibrational wave function $\chi_{vJ}(R)$ satisfies the one-dimensional Schrödinger equation

$$\left[-\frac{1}{2M}\frac{d^2}{dR^2} + V_{eff}(R)\right]\chi_{vJ}(R) = E_{vJ}\,\psi_{vJ}(R), \tag{1.50}$$

where the effective potential

$$V_{eff}(R) = -\frac{2}{R} + \epsilon^e_\sigma(R) + \frac{J(J+1)}{2MR^2} \tag{1.51}$$

is the sum of the attractive long-range Coulomb potential, the BO electronic potential, and the repulsive short-range centrifugal potential. Next paragraphs are devoted to the resolution of both electronic and nuclear Schrödinger equations.

Resolution of the electronic Schrödinger equation

We present here two schemes for computing the Born-Oppenheimer electronic energy $\epsilon^e_\sigma(R)$ as a function of internuclear separation R. The first method is only approximate but provides a quasi-analytical variational solution, which accounts for the asymptotic features of the electronic potential. The second method presents the accurate numerical procedure in use for treating one-electron diatomic molecules.

Behavior of the electronic potential The asymptotic features of the electronic potential can be sketched from a variational treatment describing the variation of the effective nuclear charge with internuclear separation. Let us express the electronic wave function as an hydrogenlike $1s$ normalized atomic orbital centered on the α particle

$$\psi^e_\sigma(\mathbf{r}|\mathbf{R}) = \frac{1}{\sqrt{\pi}}\, z^{3/2}\, e^{-zr}\,. \tag{1.52}$$

Here z denotes the effective nuclear charge, which is considered as a variational parameter. This wave function accounts for the correct asymptotic behavior: for $R \to 0$, the electron sees a central potential with an effective nuclear charge $z \to Z_0 - 1 = 1$, whereas for $R \to \infty$, the atomcule dissociates into an antiproton and an helium atom, so that $z \to Z_0 = 2$. According to the variational principle, an upper bound to the electronic energy $\epsilon^e_\sigma(R)$ is obtained by minimizing the variational integral

$$\epsilon^e_\sigma(R,z) = \langle\psi^e_\sigma|H_e|\psi^e_\sigma\rangle = \left\langle\psi^e_\sigma\left|-\frac{1}{2}\,\triangle_{\mathbf{r}} - \frac{2}{r}\right|\psi^e_\sigma\right\rangle + \left\langle\psi^e_\sigma\left|\frac{1}{|\mathbf{r}-\mathbf{R}|}\right|\psi^e_\sigma\right\rangle\,. \tag{1.53}$$

The first integral in the summation is derived from the Virial theorem applied to a Coulomb potential

$$\left\langle\psi^e_\sigma\left|-\frac{1}{2}\,\triangle_{\mathbf{r}} - \frac{2}{r}\right|\psi^e_\sigma\right\rangle = -\frac{1}{2}z^2 - \frac{2-z}{z}z^2 = \frac{1}{2}z^2 - 2z\,. \tag{1.54}$$

The potential energy term in the second bracket is easily integrated in elliptical coordinates, leading to

$$\left\langle \psi_\sigma^e \left| \frac{1}{|\mathbf{r}-\mathbf{R}|} \right| \psi_\sigma^e \right\rangle = \frac{1}{R}\left\{1-[Rz+1]e^{-2zR}\right\} . \tag{1.55}$$

Eventually, the variational energy comes down to

$$\epsilon_\sigma^e(R,z) = \frac{1}{2}z^2 - 2z + \frac{1}{R}\left\{1-[Rz+1]e^{-2zR}\right\} . \tag{1.56}$$

Numerical minimization of (1.56) with respect to z provides an estimation of the effective nuclear charge and the adiabatic electronic potential as a function of internuclear separation R, as presented in Fig. 1.5. The electronic energy behaves as expected: for $R = 0$, the α and $\bar{\text{p}}$ have come together to form a ground-state hydrogen atom; hence $\epsilon_\sigma^e(0) = -0.5$ au. For $R = \infty$, the atomcule is dissociated into a $\bar{\text{p}}$ and an He^+ ion with a binding energy $\epsilon_\sigma^e(\infty) = -2$ au.

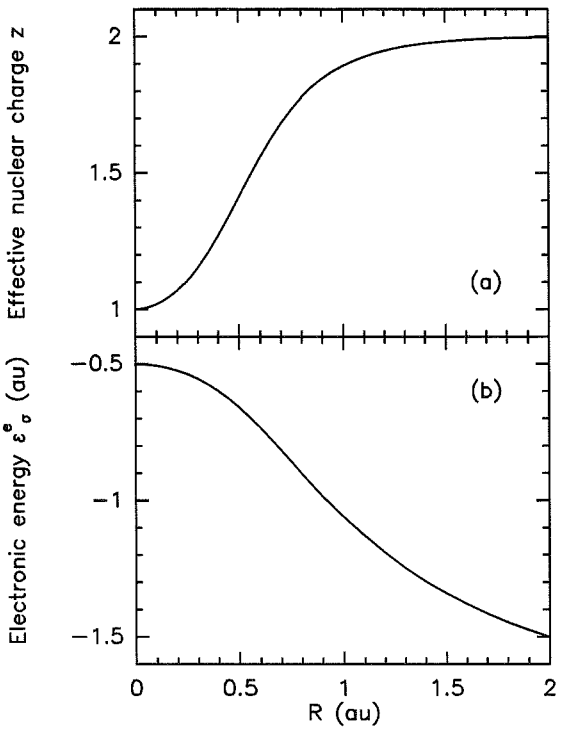

Figure 1.5: Results of the variational procedure achieved to calculate the Born-Oppenheimer electronic potential of the $\bar{\text{p}}$-He^+ system. (a) Effective nuclear charge for the electron and (b) electronic energy $\epsilon_\sigma^e(R,z)$ of the $1s\sigma$ state as a function of $\bar{\text{p}}$-He^+ internuclear distance R. After Ketzer (1999).

Numerical procedure In the framework of the Born-Oppenheimer approximation, the binding energies of a one-electron diatomic molecule can be obtained accurately, the same way as for the simple H_2^+ molecule. The electronic Schrödinger equation is separable using cofocal elliptic coordinates $\mathbf{r} = (\xi, \eta, \phi)$. The coordinate ϕ is the angle of rotation of the electron about the internuclear (z) axis, the same as in spherical polar coordinates. The coordinates ξ and η are defined by

$$\xi = (r_\alpha + r_{\bar{p}})/R, \qquad \eta = (r_\alpha - r_{\bar{p}})/R, \tag{1.57}$$

where r_α and $r_{\bar{p}}$ denote the electron distance to the respective nuclei. The range of these coordinates are

$$0 \le \phi \le 2\pi, \qquad 0 \le \xi \le \infty, \qquad -1 \le \eta \le 1\,. \tag{1.58}$$

The volume element is

$$d\tau = \frac{R^3}{8}\,(\xi^2 - \eta^2)\,d\xi\,d\eta\,d\phi\,. \tag{1.59}$$

In this coordinate system, we have

$$r_\alpha = \frac{1}{2}R(\xi + \eta), \qquad r_{\bar{p}} = \frac{1}{2}R(\xi - \eta)\,. \tag{1.60}$$

In this coordinate system, the electronic Hamiltonian from (1.45) is

$$\begin{aligned} H_e \;=\; & \frac{4}{R^2(\xi^2 - \eta^2)}\left\{\frac{\partial}{\partial\xi}\left[(\xi^2-1)\frac{\partial}{\partial\xi}\right] + \frac{\partial}{\partial\eta}\left[(1-\eta^2)\frac{\partial}{\partial\eta}\right] + \right. \\ & \left. + \left(\frac{1}{\xi^2-1} + \frac{1}{1-\eta^2}\right)\frac{\partial^2}{\partial\phi^2}\right\} - \frac{4}{R(\xi+\eta)} + \frac{2}{R(\xi-\eta)}\,. \end{aligned} \tag{1.61}$$

Since the $\bar{p}$-He^+ system has axial symmetry, H_e commutes with the z component L_z of the angular momentum operator ($[L_z, H_e] = 0$). Therefore, the electronic wave functions can be chosen to be eigenfunctions of $L_z = -i\hbar(\frac{\partial}{\partial\phi})$. The eigenfunctions of L_z are

$$\lambda(2\pi)^{-1/2}\,e^{im\phi}, \quad m = 0, \pm1, \pm2, \pm3, \ldots\,, \tag{1.62}$$

m denoting the z angular component of the electronic angular momentum in $\bar{p}He^+$. As a result, the atomcule electronic wave function has the form

$$\psi^e_\sigma(\mathbf{r}, R) = L_\sigma(\xi)\,M_\sigma(\eta)\,(2\pi)^{-1/2}e^{im\phi}\,. \tag{1.63}$$

Substitution of (1.63) into $H_e\psi^e_\sigma = \epsilon^e_\sigma\psi^e_\sigma$ gives an equation in which the variables are separable. The functions $L_\sigma(\xi)$ and $M_\sigma(\eta)$ satisfy the equations

$$\frac{d}{d\xi}\left((\xi^2-1)\frac{dL_\sigma}{d\xi}\right) + \left(A_\sigma + R\xi + \frac{1}{2}R^2\xi^2\epsilon^e_\sigma - \frac{m^2}{\xi^2-1}\right)L_\sigma(\xi) = 0, \tag{1.64}$$

and

$$\frac{d}{d\eta}\left((1-\eta^2)\frac{dM_\sigma}{d\eta}\right)+\left(-A_\sigma-3R\eta-\frac{1}{2}R^2\eta^2\epsilon_\sigma^e-\frac{m^2}{1-\eta^2}\right)M_\sigma(\eta)=0\,. \tag{1.65}$$

These ordinary differential equations are solvable in terms of series expansion. The process of solving for $L_\sigma(\xi)$ and $M_\sigma(\eta)$ is very complicated and will be omitted here (Wind, 1965). The condition that ψ_σ^e be well behaved requires that, for each value of R, only certain values of ϵ_σ^e are allowed: this gives a set of different electronic states. Fig. 1.6 illustrates an electronic charge distribution $|\psi_{1\sigma}(r|R)|^2$ at $R = 0.505$ au calculated from (1.63). The 1σ electron is polarized opposite to the $\bar{\mathrm{p}}$, as expected.

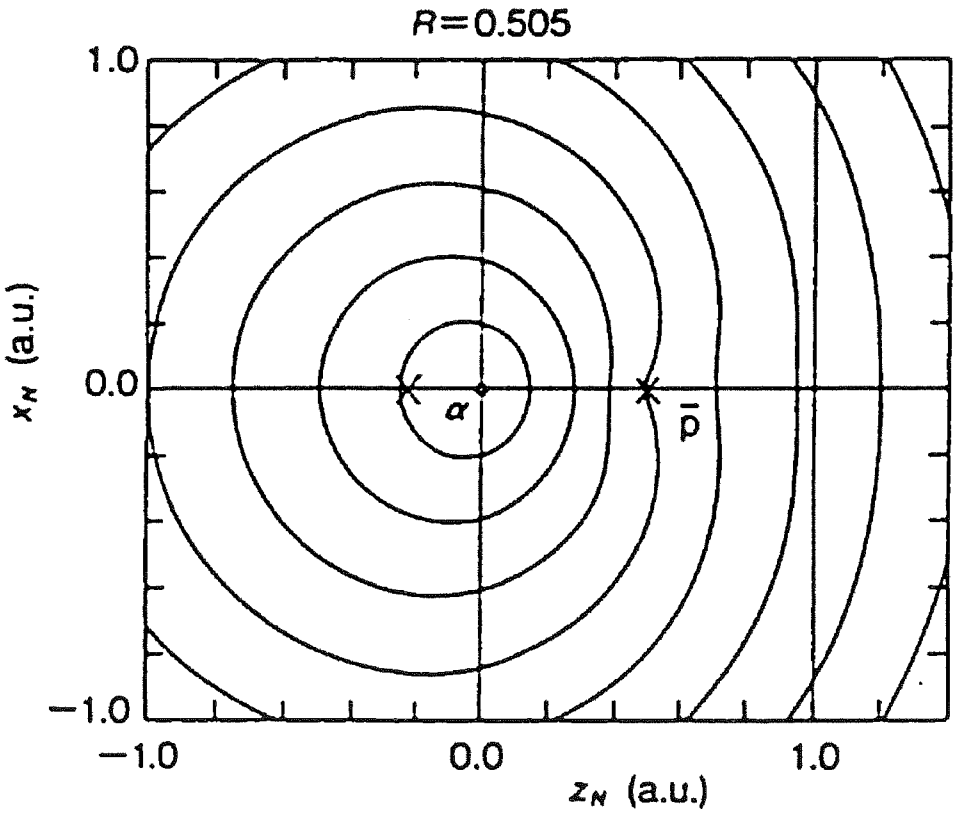

Figure 1.6: Isodensity curves of the electronic charge distribution $|\psi_{1\sigma}(r|R)|^2$ for an internuclear separation R of 0.505 au, which is the equilibrium α-$\bar{\mathrm{p}}$ distance R_e for the circular state $(n,l) = (37,36)$ or $(v,J) = (0,36)$. The contours are drawn at intervals of a factor $\frac{1}{2}$. The coordinate center is the position of the α particle, and the right cross is the position of the $\bar{\mathrm{p}}$. An elementary negatively charged particle located at the left cross would contribute the same dipole moment as the electron cloud does (Shimamura, 1992).

Resolution of the nuclear Schrödinger equation

The vibrational potential $E^e_\sigma = -\frac{2}{R} + \epsilon^e_\sigma(R)$, which looks like a screened Coulomb potential, is strongly attractive for small R and looks quite different from the usual molecular potentials. If the centrifugal potential is added to the electronic one however, the effective potential $V_{eff}(R) = E^e_\sigma(R) + \frac{J(J+1)}{2MR^2}$ for high J resembles an interatomic potential, as shown in Fig. 1.7.

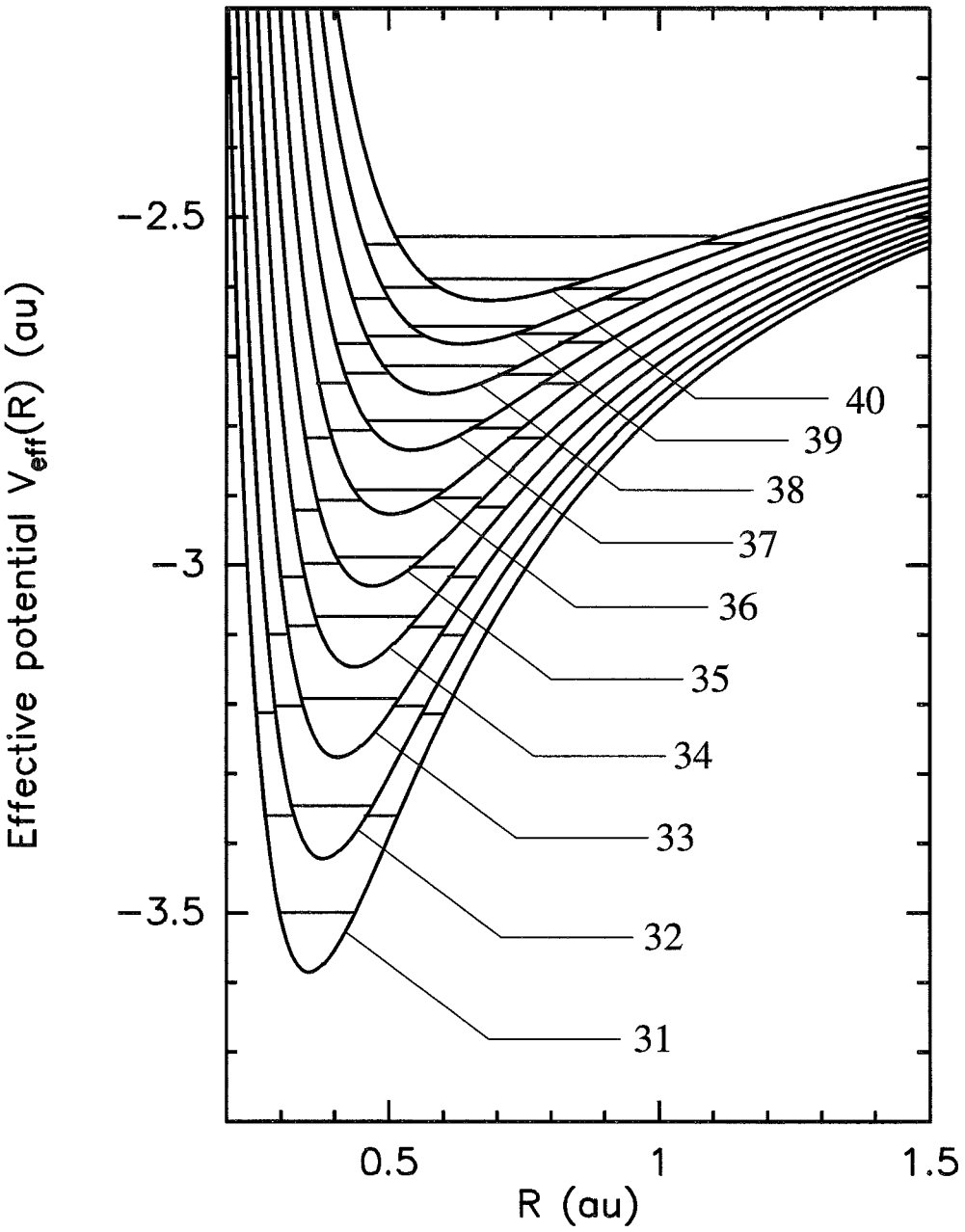

Figure 1.7: The effective potentials $V_{eff}(R)$ obtained in the adiabatic approximation for $J = 31-40$. Some rovibrational E_{vJ} levels are indicated by horizontal lines. The figure gives also an idea of the $\bar{p}$-He^+ equilibrium distance R_e and its dependence on J. After Shimamura (1992).

As previously recalled, the vibrational wave function $\chi_{vJ}(R)$ satisfies the one-dimensional Schrödinger equation

$$\left[-\frac{1}{2M}\frac{d^2}{dR^2} + V_{eff}(R)\right] \chi_{vJ}(R) = E_{vJ}\,\psi_{vJ}(R)\,. \tag{1.66}$$

The eigenvalue E_{vJ}, which is the total energy of an eigenstate of the exotic helium molecule, is independent of the quantum number M. The one-dimensional eigenvalue equation (1.66) can be easily solved numerically with a high accuracy by standard methods. We present here an analytical treatment, which provides a semi-quantitative description of the rovibronic levels structure. An analytical function which fits both repulsive short-range and attractive long-range parts of V_{eff} is the Morse potential

$$U(r) = E_e + D(1 - e^{-a(R-R_e)})^2, \tag{1.67}$$

where E_e denotes the minimum potential energy corresponding to the α-$\bar{\text{p}}$ equilibrium distance R_e; D is the dissociation energy of the molecule and a is a constant accounting for the anharmonicity of the potential. Using this fitting formula, the internal energy of the diatomic molecule becomes

$$E_{vJ} = E_e + \nu_e(v+\frac{1}{2}) - \nu_e x_e(v+\frac{1}{2})^2 + B_e J(J+1) - D_e J^2(J+1)^2 - \alpha_e(v+\frac{1}{2})J(J+1), \tag{1.68}$$

where

$$\nu_e = a\sqrt{\frac{2D}{M}}, \qquad x_e = \frac{\nu_e}{4D}, \tag{1.69}$$

$$B_e = \frac{1}{8\pi^2 I_e}, \qquad D_e = \frac{4B_e^3}{\nu_e^2}, \qquad I_e = MR_e^2, \tag{1.70}$$

$$\alpha_e = 6\sqrt{\frac{x_e B e^3}{\nu_e}} - \frac{6B_e^2}{\nu_e}. \tag{1.71}$$

In (1.68), the second term is the energy of a pure vibrator in the harmonic approximation. The third term is obtained because of the vibrational potential is anharmonic. The term of the form $B_e J(J+1)$ is the solution of a rigid rotor problem, while the next to last term comes from centrifugal stretching of the rotating molecule. The last term arises from vibration-rotation interaction, thus allowing for the change in average moment of inertia I_e due to vibration and the consequent change in rotational energy. In ordinary molecules, vibrational energy differences are much greater than rotational energy differences. Due to the high rotational excitation of the atomcule, the former is about a little smaller than the latter. For example, the $(v, J) = (1, 38) \rightarrow (0, 38)$ transition energy is about 0.06 eV, whereas the $(v, J) = (0, 38) \rightarrow (0, 37)$ transition energy is about 0.08 eV. Once again, although V_{eff} looks like an interatomic potential in shape, it is essentially different from the case of normal molecules.

Beyond this semi-qualitative treatment, it is possible to obtain the exact analytical solution for a Morse potential. Using this fitting function, the energy of the v^{th} vibrational level is

$$E_{vJ} = E_e + D - D\left[1 - \frac{a\hbar}{\sqrt{2MD(J)}}(v+\frac{1}{2})\right]^2 . \tag{1.72}$$

It should be noted that the J dependence of E_{vJ} comes from the fitting coefficients D and E_e. Fig. 1.7 includes some of the ro-vibrational levels, as calculated from (1.72). The vibrational eigenfunction is given by

$$\chi_{vJ} = \frac{1}{r} e^{-\xi/2}\, \xi^s\, \omega(\xi), \tag{1.73}$$

where

$$s = \frac{\sqrt{-2ME_v}}{a\hbar}, \xi = \frac{2\sqrt{2MD}}{a\hbar} e^{-a(r-r_e)}, \tag{1.74}$$

$$\omega = 1 + \frac{-v}{2s+1}\frac{\xi}{1!} + \frac{-v(-v+1)}{(2s+1)(2s+2)}\frac{\xi^2}{2!} + ... \tag{1.75}$$

until the term $-v(-v+1)...$ becomes zero (for circular states, $\omega = 1$). Fig. 1.8 illustrates the radial probability densities of the $\bar{p}$ for the states with $n = 39$ and $v = n - l - 1 = 0, 1, 2, 3$.

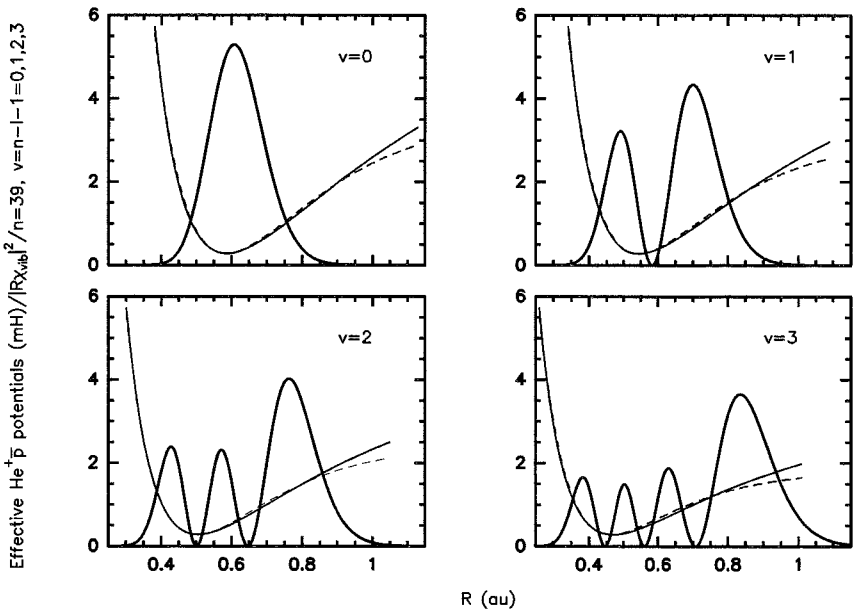

Figure 1.8: Radial probability densities of the $\bar{p}$ (bold curves) for the states with $n = 39$, $v = n - l - 1 = 0, 1, 2, 3$. They were obtained by fitting a Morse potential (dashed curves) to the effective $[\bar{p}He^+]_{n,l}$ potential (solid curves).

1.3.4 High-precision calculations

Large configuration-space variational methods

Direct evidence for the existence of antiprotonic atomcules was established with the advent of a new laser spectroscopy technique, which used theoretical predictions as a guide in searching for the expected transitions (Shimamura, 1992; Yamazaki & Ohtsuki, 1992). The experimental technique involves laser-induced transitions between metastable states (n, l) and adjacent Auger-dominated short-lived levels $(n-1, l-1)$ at the end of each cascade with vibrational quantum number $v = n - l - 1 = const.$ Such transitions are almost immediately followed by $\bar{\mathrm{p}}$ annihilation and are thus detectable as a spike in the delayed annihilation time spectra[4]. In the first phase of experiments, transition energies of the states in the $v = 2$ and $v = 3$ bands were determined, with an uncertainty lower that 5 ppm. Previous theoretical predictions however, based either on atomic configuration interaction (Yamazaki & Ohtsuki, 1992) or molecular Born-Oppenheimer (BO) approach (Shimamura, 1992), provided energy transitions with a relative precision of $200 - 2000$ ppm only. The breakthrough was made by Korobov, which treated the non adiabatic couplings of excited electronic states to the BO ground state. His work is reviewed here briefly.

Since the Hamiltonian operator (1.13) is rotation invariant, it commutes with each component of the angular momentum operator $\mathbf{L}$ ($[H, L_i] = 0, i = x, y, z$). Therefore, H, $\mathbf{L}^2$ and L_z are compatible observables, which admit a common set of eigenfunctions, on which they are simultaneously diagonalizable. Let us denote by $\Psi_{LM}(\mathbf{R}, \mathbf{r})$ one such eigenstate in a space-fixed coordinate system, L and M being the eigenvalues of the $\mathbf{L}$ and L_z operators, respectively. The same state will be represented by $\Psi_{Lm}(\mathbf{R}', \mathbf{r}')$ in a body-fixed coordinate system, where m is the projection of the $L_{z'}$ operator over the z' internuclear axis. $\Psi_{LM}(\mathbf{R}, \mathbf{r})$ and $\Psi_{Lm}(\mathbf{R}', \mathbf{r}')$ are related by the Wigner– or $\mathcal{D}^L_{Mm}$–functions, which are eigenfunctions of the $\mathbf{L}^2$, L_z and L'_z operators[5]

$$\Psi_{LM}(\mathbf{R}, \mathbf{r}) = \sum_{m=-L}^{L} \mathcal{D}^L_{Mm}(\epsilon, \zeta, \varsigma)\, \Psi_{Lm}(\mathbf{R}', \mathbf{r}')\,. \tag{1.76}$$

(ϵ, ζ, ς) is the set of Euler angles, which defines the rotation from the space-fixed to the body-fixed frame in the unitary transformation $\mathcal{D}^{\mathcal{L}}(\epsilon, \zeta, \varsigma)\Psi_{LM}(\mathbf{R}, \mathbf{r}) = \Psi_{Lm}(\mathbf{R}', \mathbf{r}')$ ($\mathcal{D}^L_{Mm} = \langle \Psi_{LM} | \mathcal{D}^{\mathcal{L}} | \Psi_{Lm} \rangle$). It is also possible to express (1.76) by using the symmetrized Wigner $\mathcal{D}$ functions

$$\mathcal{D}^{L\lambda}_{Mm}(\epsilon, \zeta, \varsigma) = \left[\frac{2L+1}{16\pi^2(1+\delta_{m0})}\right]^2 [\mathcal{D}^L_{Mm}(\epsilon, \zeta, \varsigma) + \delta(-1)^{L-m}\mathcal{D}^L_{M,-m}(\epsilon, \zeta, \varsigma)], \tag{1.77}$$

where $\lambda = (-1)^L$ is the parity[6] of the metastable atomcule with remaining electron lying in the ground state. Since H is rotation invariant, $\Psi_{Lm}(\mathbf{R}', \mathbf{r}')$ only depends on the three

[4] The principles of this new spectroscopy are reviewed in further details in Section. 2.4.

[5] $\mathbf{L}^2\mathcal{D}^L_{Mm} = \hbar^2 L(L+1)\mathcal{D}^L_{Mm}$, $L_z\mathcal{D}^L_{Mm} = \hbar M \mathcal{D}^L_{Mm}$ and $L'_z\mathcal{D}^L_{Mm} = \hbar m \mathcal{D}^L_{Mm}$, where L, M and m are constants of motion.

[6] λ is the eigenvalue of the parity operator, which replaces each cartesian coordinate with its negative.

coordinates R', r' and θ, which describe the respective positions of the three particles in the body-fixed frame: in jacobian coordinates, $\mathbf{R}'$ is the position vector of the $\bar{\mathrm{p}}$ nucleus relative to the α particle, $\mathbf{r}'$ denotes the position vector of the electron relative to the center of mass of the two nuclei, and θ is the angle between $\mathbf{R}'$ and $\mathbf{r}'$. $\Psi_{Lm}(\mathbf{R}', \mathbf{r}')$ can be written

$$\Psi_{Lm}(\mathbf{R}', \mathbf{r}') = F_m^L(R', r', \theta)\,. \tag{1.78}$$

Accordingly, Korobov used for his calculations the large-configuration molecular-expansion trial function

$$\Psi_{LM}(\mathbf{R}, \mathbf{r}) = \sum_{m=0}^{L} \mathcal{D}_{Mm}^{L\lambda}(\epsilon, \zeta, \varsigma) F_m^{L\lambda}(R, r, \theta)\,. \tag{1.79}$$

After separating the centre of mass motion, the six-dimensional Schrödinger equation comes down, to the determination of the three dimensional functions $F_m^{L\lambda}(R, r, \theta)$. If one retains only the term with azimuthal quantum number $m = 0$ in the variational expansion (1.79), one recovers the adiabatic approximation, since $\mathcal{D}_{M0}^{L\lambda}(\epsilon, \zeta, \varsigma) = \text{const.} \times Y_{LM}(\epsilon, \zeta)$. The non adiabatic couplings arise from contributions with $m > 0$, which are mixed to the σ ($m = 0$) ground state wave function. In his calculations, Korobov included all contributions from the π ($m = 1$) and δ ($m = 2$) components. The components $F_m^{L\lambda}$ were expanded as a power serie of R

$$F_m^{L\lambda}(R, \xi, \eta) = R^m \left[(\xi^2 - 1)(1 - \eta^2)\right]^{m/2} R^N \sum_n c_n R^{i_n} \xi^{j_n} \eta^{k_n} e^{-(\alpha + \beta\xi)R}, \tag{1.80}$$

where ξ and η are the spheroidal coordinates of the electron, as defined in (1.57), and $i_n \geq j_n$. The factor R^N was introduced to meet the requirement that the antiproton occupies mainly the rotational state with high angular momentum L and $\Psi(R) \sim R^L$ for $R \to 0$. The coefficients c_n in (1.80) were obtained by solving the generalized eigenvalue problem

$$\mathbf{A}\,\mathbf{v_k} = E_k\,\mathbf{B}\,\mathbf{v_k}, \tag{1.81}$$

where

$$\mathbf{A} = \langle\Psi|H|\Psi\rangle, \text{ and } \mathbf{B} = \langle\Psi|\Psi\rangle. \tag{1.82}$$

The nonlinear parameters α, β and N were optimized using a set of 528 basis functions and were then set fixed. The final results were obtained with a trial function containing 1728 terms. Maximum powers of $(i^{max} \times j^{max} \times k^{max}) = (12 \times 10 \times 5)$ were used for the σ component, $(8 \times 6 \times 4)$ for the π component and $(6 \times 4 \times 3)$ for the δ component. The contribution of the π component to the energy levels of the metastable atom is about $5\,10^{-4}$ au while that of the δ component is about 10^{-7} au. With this method, the theoretical transition wavelengths showed an agreement with experimental ones at the level of 50 ppm. Table 1.1 compares the accuracy level of all methods stated above to Korobov's high-precision calculations.

Method	Energy shift	
	(au)	relative
Bohr model	1	$3\ 10^{-1}$
Effective nuclear charge (ENC)	10^{-1}	$3\ 10^{-2}$
Configuration interaction (CI)	10^{-4}	$3\ 10^{-5}$
Born-Oppenheimer (BO)	10^{-4}	$3\ 10^{-5}$

Table 1.1: Accuracy level of various atomic or molecular calculations for the $\bar{p}He^+$ energy levels relative to Korobov's large-configuration space calculations.

Relativistic corrections

Korobov's calculations helped observing new resonance transitions. Thus, not only favoured $\Delta v = 0$ but also unfavoured $\Delta v = 2$ transitions were found (Yamazaki *et al.*, 1997b). However, a systematic deviation as much as 50 ppm for the $\Delta v = 0$ and 100 ppm for the $\Delta v = 2$ transition remained. When his calculations were augmented by relativistic corrections (Korobov & Bakalov, 1997), the agreement became as good as a few ppm, as shown in Fig. 1.9.

The main corrective term, which results from the relativistic effects of the electron motion, leads to a shift in the energy levels $\frac{\delta_e(E)}{E} \propto \alpha^2$, relative to Korobov's non relativistic calculations[7]. Recently, Elander & Yarevsky (1997), Kino *et al.* (1998) and Korobov (1998) came up with calculations including the Lamb shift, another effect of vacuum fluctuations, which confer to the electron an erratic motion, leading to a slight shift in the energy levels. With both relativistic corrections and the Lamb shift taken into account, the discrepancies between theoretical and experimental values came down to a few ppm. Also, his estimations shows that the contributions of higher-order relativistic and QED corrections to the energies are at least one order of magnitude smaller than the Lamb shift, as shown in Table 1.2. According to Korobov, these values should be precise within a computational accuracy of 0.5 ppm. Theoreticians are currently working for even more accurate values and further results are anticipated.

[7]The fine structure Hamiltonian can be expressed as powers of $\frac{v_e}{c}$, where v_e is the electron velocity. The relativistic energy of a classical particle with mass at rest m_e and impulse $\mathbf{p_e}$ is given by $E = \sqrt{\mathbf{p_e^2} + m_e^2 c^2}$. A Taylor expansion of E as powers of $\mathbf{p_e}/m_e c$ leads to

$$E = m_e c^2 + \frac{\mathbf{p_e^2}}{2m_e} - \frac{\mathbf{p_e^4}}{8m_e^3 c^2} + \ldots \tag{1.83}$$

In addition to the energy at rest ($m_e c^2$) and to the non relativistic energy ($\frac{\mathbf{p_e^2}}{2m_e}$), one gets the first corrective term to the energy, due to the relativistic variation of the electon mass with velocity. The magnitude of this correction is given by

$$\frac{\frac{\mathbf{p_e^4}}{8m_e^3 c^2}}{\frac{\mathbf{p_e^2}}{2m_e}} = \frac{\mathbf{p_e^2}}{4m_e^2 c^2} = \frac{1}{4}\left(\frac{v_e}{c}\right)^2 \sim \alpha^2 \sim \left(\frac{1}{137}\right)^2, \tag{1.84}$$

where α is the fine structure constant.

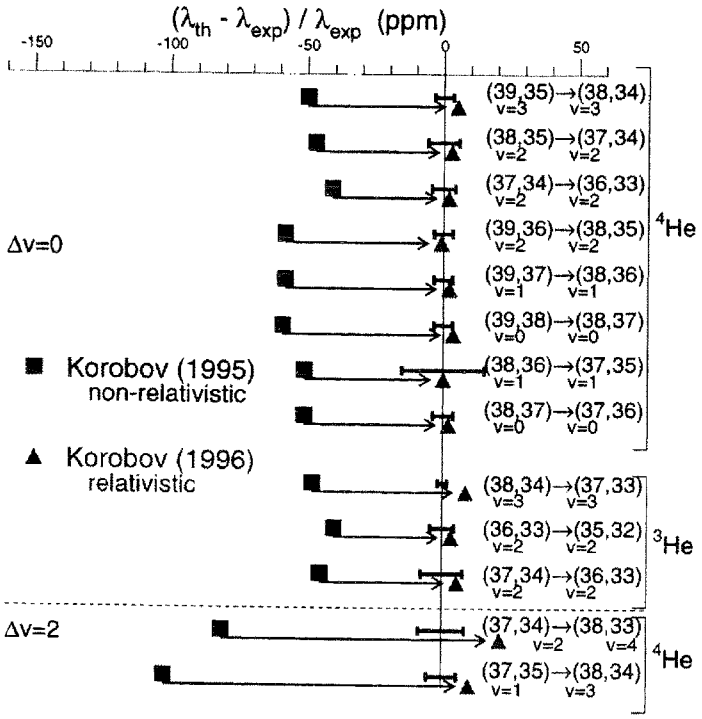

Figure 1.9: Comparison of the experimental transition wavelengths observed in ^{4}He or ^{3}He with Korobov's theoretical predictions. The deviation between experiments and Korobov's nonrelativistic calculations (filled squares) (Korobov, 1996) turns out to be about $\sim$ 50 ppm and always positive. With relativistic corrections (filled triangles) (Korobov & Bakalov, 1997), the discrepancies with experimental values become only a few ppm or less. The error bars are the experimental ones (Yamazaki *et al.*, 1997b).

1.3.5 Hyperfine structure

At the ppm level, fine and hyperfine structure start to appear as in other atoms. The energy levels of the $\bar{p}He^+$ atomcule are split, owing to the coupling of the $\bar{p}$ angular momentum ($\mathbf{L}$) with the magnetic momenta associated with the spins of the $\bar{p}$ ($\mathbf{S_{\bar{p}}}$) and the electron ($\mathbf{S_e}$). The largest effect arises from the interaction of $\mathbf{L}$ with $S_e = \frac{1}{2}$, which is responsible for the hyperfine structure. This splits each level into a doublet with quantum numbers $F^{\pm} = L \pm S_e$. This dominant hyperfine doublet is further split into superhyperfine doublets with quantum numbers $J^{\pm} = F^{\pm} \pm S_{\bar{p}}$. Fig. 1.10 shows the quadruplet structure, as predicted by Bakalov & Korobov (1998). Recently, a precise scan of the previously discovered laser-induced transition $(n, l) = (37, 35) \rightarrow (38, 34)$ in $\bar{p}He^+$ revealed the dominant doublet structure (Widmann *et al.*, 1997). Further prospects for direct measurements of level splittings are being planned with the use of a micro-wave technique, which may ultimately lead to a precise determination of the antiproton magnetic moment.

Correction	Energy shift	
	(au)	relative
Relativistic motion of the electron	$0.5\,10^{-4}$	20 ppm
Lamb shift	$0.6\,10^{-5}$	2 ppm
Vacuum polarization	$0.4\,10^{-6}$	150 ppb
Relative mass of $\bar{p}$ and α in the kinetic energy	$0.3\,10^{-7}$	10 ppb
Retardation effects of the particles electromagnetic field	$0.3\,10^{-7}$	10 ppb
Electromagnetic structure of $\bar{p}$ and α	$1.5\,10^{-9}$	0.5 ppb

Table 1.2: Relativistic and higher-order QED energy shifts to the energy levels of antiprotonic helium atomcules (Korobov & Bakalov, 1997).

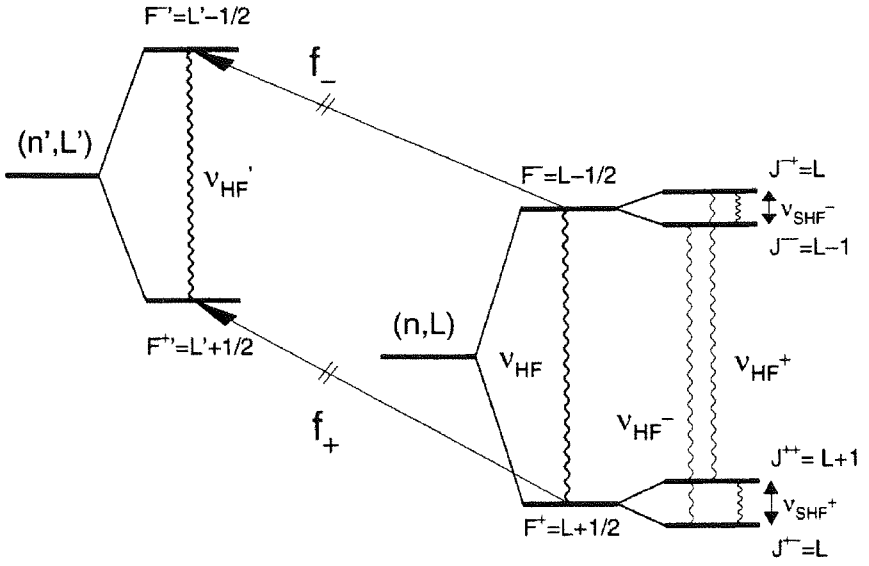

Figure 1.10: Hyperfine quadruplet structure of the $\bar{p}He^+$ atomcule predicted by Bakalov and Korobov (Bakalov & Korobov, 1998). The dominant doublet structure was recently revealed as a doublet in the $(37, 35) \rightarrow (38, 34)$ unfavoured resonance transition by Widmann et al. (Widmann *et al.*, 1997).

1.3.6 Towards a determination of the $\bar{p}$ fundamental constants

The excellent agreement between theory and experiment is now able to impose stringent constraints on the $\bar{p}$ fundamental constants (mass $M_{\bar{p}}$ and charge $-Q_{\bar{p}}$), which are equal to those of the proton if one assumes the CPT invariance. Alternatively, if we allow $\Delta M_{\bar{p}}/M_{\bar{p}} = \frac{M_{\bar{p}}-M_p}{M_{\bar{p}}}$ and $\Delta Q_{\bar{p}}/Q_{\bar{p}} = \frac{Q_{\bar{p}}-Q_p}{Q_{\bar{p}}}$ to be free, the present agreement between theory and experiments yields a constraint on these two values, since the transition wavelengths depend upon the $\bar{p}$ Rydberg constant, according to

$$R_\infty(\bar{p}) \propto M_{\bar{p}} \times Q_{\bar{p}}^2 . \tag{1.85}$$

This imposes a linear relation between $\Delta M_{\bar{p}}/M_{\bar{p}}$ and $\Delta Q_{\bar{p}}/Q_{\bar{p}}$. On the other hand, the charge-to-mass ratio $Q_{\bar{p}}/M_{\bar{p}}$ of the antiproton is known with a high-precision of 10^{-9} to be the same as that of the proton (Gabrielse *et al.*, 1990), thus setting also another severe constraint,

$$\left| \frac{\delta Q_{\bar{p}}}{e} - \frac{\delta M_{\bar{p}}}{M_{\bar{p}}} \right| < 1 \times 10^{-9}, \tag{1.86}$$

which does not mean however that the charge and the mass are determined with that high precision. This constraint crosses the line set by the high-resolution spectroscopy of the $\bar{p}He^+$ atomcule, as shown in Fig. 1.11. Thus, it was found that

$$\Delta M_{\bar{p}}/M_{\bar{p}} < 5 \times 10^{-7}, \text{ and } \Delta Q_{\bar{p}}/Q_{\bar{p}} < 5 \times 10^{-7} \tag{1.87}$$

In the past, only a poor constraint ($\sim 5\,10^{-5}$) was known by using antiprotonic x-ray data (Hugues & Deutch, 1992).

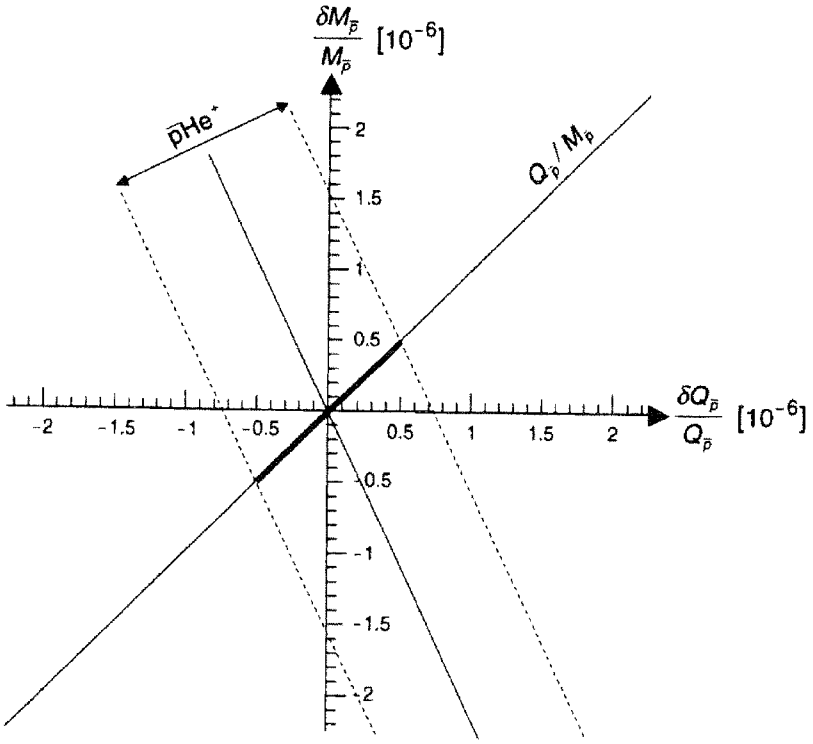

Figure 1.11: Two-dimensional constraint on $\Delta M_{\bar{p}}/M_{\bar{p}} = \frac{M_{\bar{p}}-M_p}{M_{\bar{p}}}$ and $\Delta Q_{\bar{p}}/Q_{\bar{p}} = \frac{Q_{\bar{p}}-Q_p}{Q_{\bar{p}}}$ obtained from the $\bar{p}$ cyclotron frequency (Gabrielse *et al.*, 1990) and from the present spectroscopic studies of $\bar{p}He^+$ (Torii *et al.*, 1999).

1.4 Conclusions

In this chapter, we showed that the highly unusual three-body system consisting of an helium nucleus, an electron and an antiproton has now reached a level where QED corrections like the Lamb shift have to be calculated to explain the measured transition energies. If both theoretical and experimental accuracy can be improved in the future, the atomcule may surpass the ordinary helium atom as the best calculated and experimentally verified three-body system, allowing for stringent tests on the accuracy of three-body calculations. Experimental studies of antiprotonic atomcules are presented hereafter.

Chapter 2

Experimental studies of antiprotonic helium atomcules

Contents

2.1 Introduction

This chapter is devoted to experimental studies of metastable antiprotonic helium atomcules $\bar{p}He^+$. Experiments can be divided into two subjects, one dealing with the structure of the atomcule and another one with its formation and decay, i.e. its interaction with other atoms (helium and other noble gases), molecules (H_2, O_2, N_2), as well as exotic systems (Ps). This latter aspect is reviewed here. Integral informations about the properties of atomcules are presented in a first part, from the analysis of delayed annihilation time spectra as a function of helium density or impurity level. Microscopic (state-dependent) studies from laser spectroscopic measurements are reviewed in a second part. The last section is devoted to the possible formation of anti-hydrogen from $\bar{p}He^+$ atomcules.

2.2 Delayed annihilation of antiprotons in pure helium

2.2.1 The experimental setup

The PS205 experiment was performed at the low energy antiproton ring (LEAR) of CERN, which provides a high-intensity, mono-energetic and low-energy beam. Fig. 2.1 shows a plan view of the setup used in the experiments for measuring the delayed annihilation lifetimes of antiprotons in helium, from the detection of the annihilation products (charged pions $\pi^{\pm}$ as well as γ's from π^0 decay).

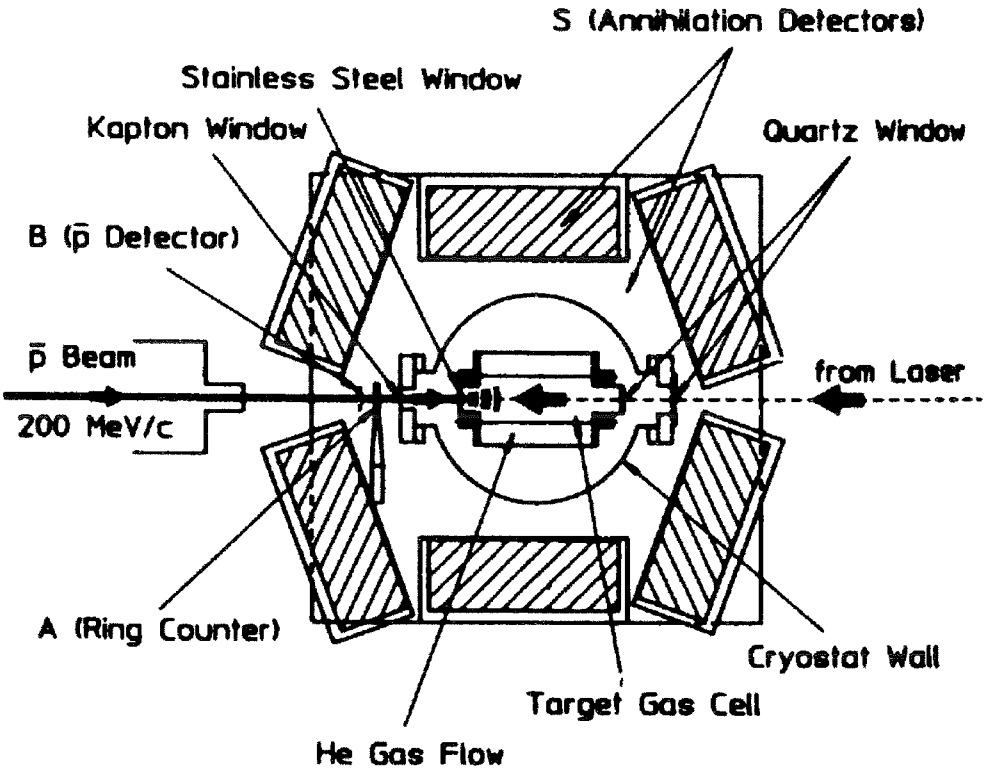

Figure 2.1: Experimental setup. The antiprotons, extracted with a momentum of 200 Mev/c, traverse two beam counters (B and A) and are stopped in a target chamber containing helium, which is cooled to $5 - 10$ K at $0.7 - 1$ bar. Both charged and neutral $\bar{p}$ annihilation products are detected by seven scintillation counter arrays (S, 6 sides and 1 bottom). Two laser beams enter the target chamber through quartz windows from the direction opposite to the $\bar{p}$ beam (Morita *et al.*, 1994).

A 200 Mev/c $\bar{p}$ beam with an intensity of about 10^4 $\bar{p}$ s^{-1} is delivered from LEAR. At the end of the beam line, the antiprotons pass through a plastic scintillator (B), which serves as a beam counter to provide the start signal for the annihilation time measurements. The time delay between each antiproton's arrival in the gas and its annihilation is digitized. It is important to minimize the detection inefficiency of the beam scintillator, as undetected antiprotons may follow a given antiproton within the time range of interest, and produce fake

delayed events. The average multiplicity of $\pi^{\pm}$ for $p\bar{p}$ annihilation is approximately three. As a result, only annihilations in which three simultaneous charged particles are recorded in the scintillation counters are accepted. This requirement eliminates events of 2.2 μs mean lifetime caused by the $\pi^+ \rightarrow \mu^+ \rightarrow e^+$ decay chain of prompt annihilation pions stopped in material surrounding the target chamber.

2.2.2 Delayed annihilation time spectra

Since the discovery of long-lived antiprotons in liquid helium in 1991 at KEK, which showed anomalous longevity some million times longer than the usual belief, delayed annihilation time spectra of antiprotons (DATS) in helium were measured at the LEAR in CERN. Typical DATS are presented on Fig. 2.2. As previously reported, a small fraction of the $\bar{p}$ stopped in various helium materials are effectively found to live up to 25 μs.

To represent the time spectra $n(t)$ by a single value, the delayed average lifetime T_{av} can be introduced as

$$T_{av}(> t_0) = \frac{\int_{t_0}^{t_{max}} t\, n(t) dt}{\int_{t_0}^{t_{max}} n(t) dt} - t_0, \tag{2.1}$$

where events occuring at $t > t_0$ are considered as delayed. t_{max} defines the observation time. t_0 and t_{max} were fixed at 20 nsec and 50 μs, respectively. The trapping fraction f is defined by

$$f = \frac{n(t_0 < t < t_{max})}{n_{total}}. \tag{2.2}$$

The DATS show that about 3 % of antiprotons undergo delayed annihilation with an average lifetime of 3 μs. The average lifetime in DATS decreases slowly from 4 to 3 μs as the density increases from a gas phase to solid phase. The weak dependence of the $\bar{p}$ average lifetime on the helium density implies that the metastable atoms are essentially insensitive to collisions with He atoms. Besides, all spectra present a downward bending in $\ln n(t)$ vs t at $t > 15 \mu s$, suggesting the presence of metastable states in the decay chain, as asserted by the Condo model. Eventually, the average lifetime in ^{3}He is found to be 15 % shorter than in ^{4}He gas.

2.2.3 Trapping fraction

In this section, we try to account for the 3% fraction of $\bar{p}$ captured on metastable states. Let us denote by $l_0 \sim 35$ the angular momentum which divides the metastable and the prompt zone. The trapping fraction is then given by the fraction of populated levels with angular momentum $l \geq l_0$. One may expect the initial population $P(l)$ of metastable states to follow a statistical distribution corresponding to the degenerescence order of the levels considered,

$$P(l) = 2l + 1, \qquad l < l_{max}, \tag{2.3}$$

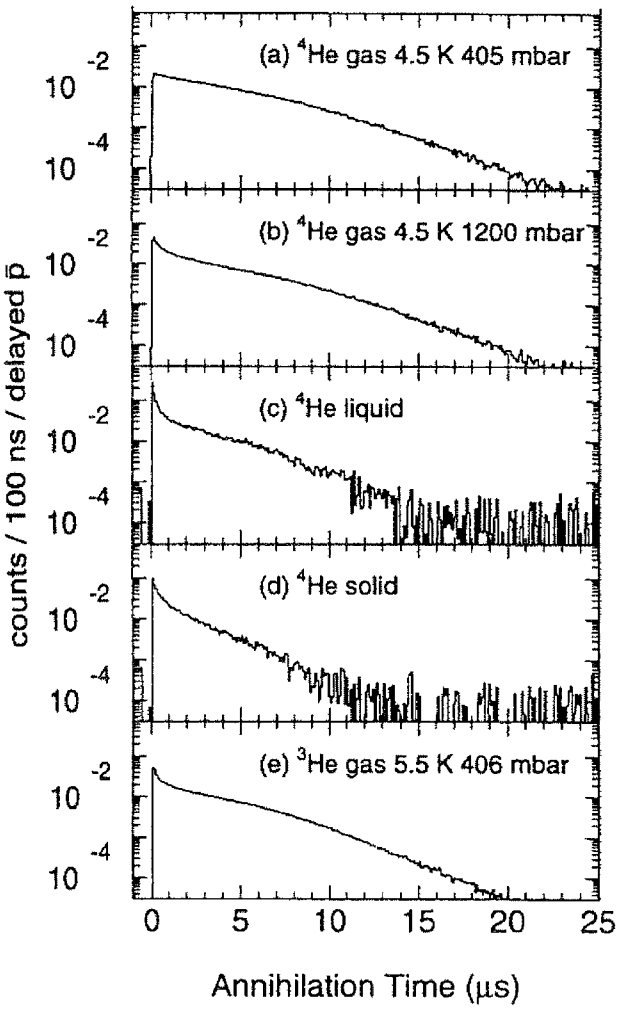

Figure 2.2: Comparison of the time spectra of $\bar{p}$ annihilation in various helium media. Besides, no evidence for a delayed annihilation of antiprotons in pure Li, Ne, Kr or Xe was observed (Widmann *et al.*, 1993).

at least up to a certain limit value of l_{max} close to the maximum angular momentum brought in by the $\bar{p}$ before capture. According to initial population estimates (Beck *et al.*, 1993), l_{max} might be about 42. Under this assumption, the trapping fraction would be

$$f = \frac{\sum_{l=l_0+1}^{l_{max}} P(l)}{\sum_{l=0}^{l_{max}} P(l)} = 1 - \frac{\sum_{l=0}^{l_0} P(l)}{\sum_{l=0}^{l_{max}} P(l)} = 1 - (\frac{l_0+1}{l_{max}+1})^2 \simeq 0.3, \tag{2.4}$$

which is too large when compared with the observed trapping fraction. In Section 3, we will try to account for the 3 % value, by estimating the populations of individual states after the thermalization stage, which is expected to strongly quench the latter, since the atomcule at birth is formed with a large recoil energy of about 4-5 eV ($\equiv 3\,10^4$ kT).

2.2.4 Isotopic effect

The delayed annihilation of antiprotonic helium atoms has been studied in isotopically pure low-temperature ^{3}He and ^{4}He gas at various densities. Fig. 2.3 shows two typical DATS from ^{4}He and ^{3}He. The DATS are very similar in shape except for a small difference in the time scale and the presence of a distinct fast decay component in the case of ^{3}He.

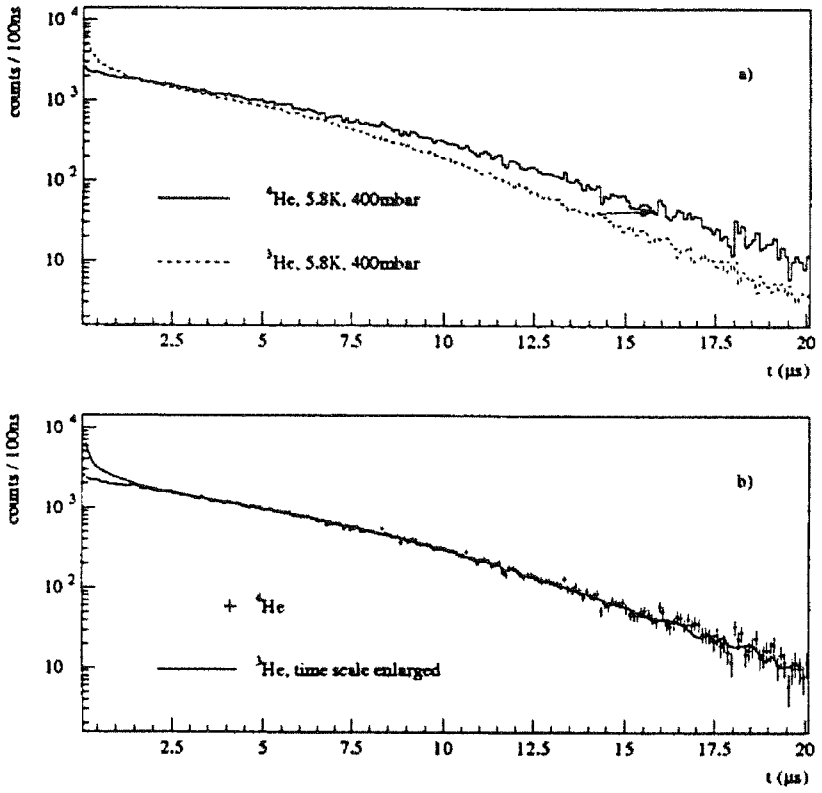

Figure 2.3: Time spectra of the delayed $\bar{p}$ annihilation in ^{3}He (solid line) and ^{4}He (dashed line). (a) reveals the small difference in the time scale between ^{3}He and ^{4}He DATS for $t > 2\mu s$. (b) shows the same spectrum as in (a), with the time scale of the ^{3}He spectrum enlarged by 14.6 % (Ketzer *et al.*, 1996).

As shown in Fig. 2.3.b, the long-lived component of both spectra match, if one enlarge the time scale of the ^{3}He spectrum by a factor of 1.144. This scaling factor can be readily interpreted as the ratio of overall trapping times

$$\tau = \frac{T_{trap}(^4He)}{T_{trap}(^3He)} = 1.144\,. \tag{2.5}$$

Moreover, the ratio of average lifetimes in ^{3}He and ^{4}He as defined in (2.1) is

$$\frac{T_{av}(^4He)}{T_{av}(^3He)} = 1.153, \tag{2.6}$$

showing that T_{av} indeed reflects the overall trapping time of antiprotons, providing that the different time scales in ^{3}He and ^{4}He are taken into consideration [1]. Anyway, the experimental results for this ratio, as given by (2.5) or (2.6) are in excellent agreement with the simple theoretical estimation based on the atomic model and presented hereafter (Yamazaki & Ohtsuki, 1992). In the atomic model, the only difference between both isotopic species arises from the ratio of their reduced masses

$$R = \frac{M(^4He)}{M(^3He)} \sim 1.14\,. \tag{2.7}$$

This ratio causes sizable difference in the transition energies and lifetimes. If one assumes that the formation mechanism and the subsequent collisional processes are exactly the same for ^{3}He and ^{4}He, the difference in the overall lifetime τ comes only from:

- the lifetime of the representative (n, l) level, which is inversely proportional to the transition rate λ, which is proportional to $(\Delta E_n)^3$. For $l \sim n-1$, $\Delta E_n \propto n^{-3}$.
- the average number of metastable states constituting the $v = n - l - 1$ cascade. Since the metastable states are quite uniformly distributed over a given energy interval, the number of metastable cascades is expected to be proportional to the density of energy levels, namely to $(\triangle E_n)^{-1}$.

Accordingly, the overall lifetime

$$\tau \propto \frac{1}{\lambda}\frac{1}{\triangle E_n} \propto \frac{1}{\triangle E_n^4} \sim n^4 \sim M^2\,. \tag{2.8}$$

Thus,

$$\frac{\tau(^4He)}{\tau(^3He)} \propto \frac{M(^4He)}{M(^3He)} = R\,. \tag{2.9}$$

This procedure implicitly assumes that the number of the contributing metastable cascades is rather small. This view is consistent with the experimental fact that the overall trapping time is about 3 microseconds. Anyway, this estimation agrees very well with the observed isoptopic effect.

Both DATS differ also by the presence of a distinct fast decay component in ^{3}He. By fitting a simple sum of two exponential functions to the ^{3}He spectrum, the lifetime of the fast component was determined to be 0.154 μs. The fraction of all trapped antiprotons annihilating with this relatively short lifetime (compared to radiative transitions) was found to be around 13 %. This suggests that the $\bar{p}^3He^+$ atom has some states of intermediate lifetime on the border between a metastable zone and an Auger-dominated short-lived zone. Auger transition rates were computed by Fedotov *et al.* (1996) and appear to be larger in ^{3}He, thus accounting for the presence of the fast component. Alternatively, we investigated the possible influence of collisional effects to the isotopic effect. Results are presented in Section 3.

[1] In Eq. (2.1), T_{av} is defined for an initial time t_0. if a value of t_0 is set for ^{3}He, a value of $t_0\tau$ should be used for ^{4}He.

2.2.5 Descriptive models of the DATS in pure He

A close look at the DATS suggests that T_{av} is not the best parameter to describe their shape in detail since they are not single exponentials. All DATS deviate from a single exponential slope, exhibiting a downward bent structure for long decay times. This shape indicates that the $\bar{p}$ cascades down a ladder of successive metastable levels, before coming to a state from which a fast Auger transition is possible. The simplest model which is able to reproduce the characteristic downward bending of the annihilation spectra is a $\bar{p}$ cascade over three metastable levels followed by an Auger-dominated short-lived state, as shown in Fig. 2.4.

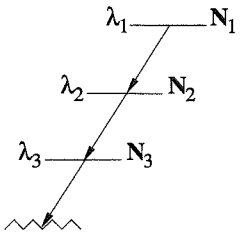

Figure 2.4: Three-level cascade model. λ_1, λ_2, and λ_3 are the radiative decay rates of the metastable states. N_1, N_2 and N_3 represent the population of the respective levels (Ketzer *et al.*, 1996).

The rate equations for the populations of the different levels are then

$$\frac{dN_1}{dt} = -\lambda_1 N_1, \tag{2.10}$$

$$\frac{dN_2}{dt} = -\lambda_2 N_2 + \lambda_1 N_1, \tag{2.11}$$

$$\frac{dN_3}{dt} = -\lambda_3 N_3 + \lambda_2 N_2, \tag{2.12}$$

with λ_i being the radiative decay rates of the metastable states. The large number of free parameters can be reduced to three by setting $\lambda_1 = \lambda_2$ and by assuming the initial populations of all three levels to be equal ($= N_0$). In view of the high level density and the small level spacing around $n = n_0$, this is probably justified. The annihilation rate $\lambda_3 N_3(t)$ is then given by

$$\lambda_3 N_3(t) = N_0 \left\{ \frac{\lambda_1^2 t}{\lambda_3 - \lambda_1} - \frac{\lambda_1^2}{(\lambda_3 - \lambda_1)^2} + \frac{\lambda_1}{\lambda_3 - \lambda_1} \right\} e^{-\lambda_1 t} + N_0 \left\{ 1 - \frac{\lambda_1}{\lambda_3 - \lambda_1} + \frac{\lambda_1^2}{(\lambda_3 - \lambda_1)^2} \right\} e^{-\lambda_3 t}. \tag{2.13}$$

Fig. 2.5 (left) shows the results of a fit of the annihilaton rate to typical spectra recorded in ^{3}He and ^{4}He. The shape of DATS from ^{4}He is described satisfactorily, while the simplified three-level fitting function cannot reproduce the short-lived component and the downward bent structure of DATS for longer decay times in ^{3}He. A $\bar{p}$ cascade over four metastable

states instead of three reproduces the behavior of DATS both for short and long decay times, as shown in Fig. 2.5 (right) and detailed herafter.

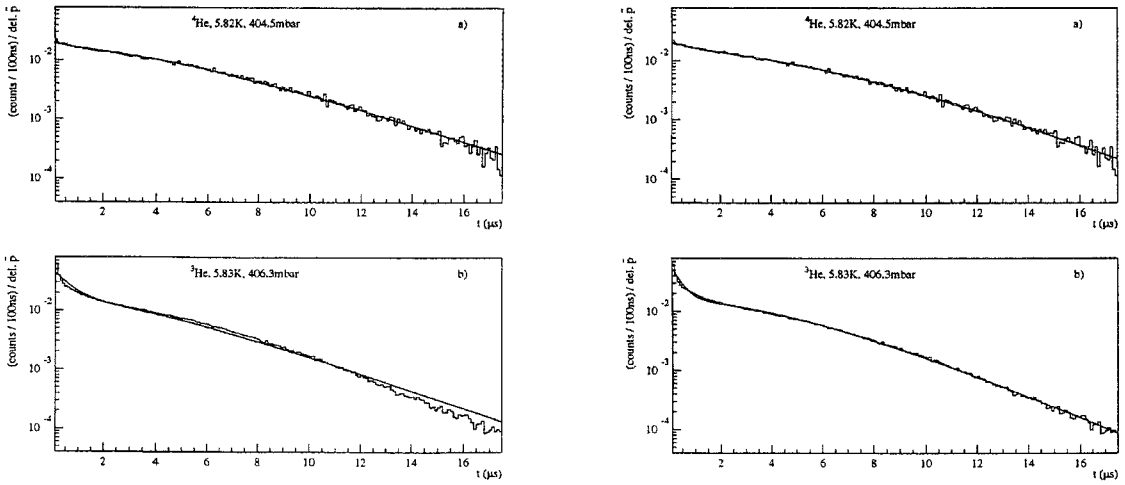

Figure 2.5: Left: fits of a three-level model with three free parameters (λ_1, λ_3 and N_0) to typical spectra. Right: fits of a four-level model with four free parameters to typical spectra (Ketzer *et al.*, 1996).

Since the downward bent shape of the DATS indicates a reduced feeding from higher levels at longer decay times, the initial population of the highest state was introduced as an additional free parameter (N_0^1). The initial populations of the lower levels were assumed to be equal (N_0). To ensure stable fit results, the decay rates were set to be equal for the three upper levels ($\lambda_1 = \lambda_2 = \lambda_3$), as in the three-level model. Comparing values of λ_1 for ^{3}He and ^{4}He at "standard" conditions, we find an average ratio

$$\frac{\lambda_1(^3He)}{\lambda_1(^4He)} = 1.14, \tag{2.14}$$

which is in good agreement with the ratio obtained from the direct comparison of DATS in (2.5). Thus λ_1 determines the overall trapping time in the model. The decay rate of the last metastable level, λ_4, represents the fast decaying component of DATS: it is roughly a factor of 3 higher in ^{3}He than in ^{4}He, again suggesting the existence of at least one border state with an intermediate lifetime between metastability and Auger dominance.

The ratio of initial populations N_0/N_1 is in all cases smaller than unity, indicating that the initial population of metastable states decreases with increasing principal quantum number n. Alternatively, Ohtsuki (Yamazaki, 1994) made calculations of the level populations, level lifetimes and Auger rates and found that the experimental DATS in pure He can be accounted for only when an external constraint such as $n_{max} = 40$ (namely $l_{max} = 39$) is imposed on the initial distribution, as shown on Fig. 2.6. In Section 3, we will investigate the thermalization stage of individual states and provide collisional branching ratios for estimating the thermalized populations.

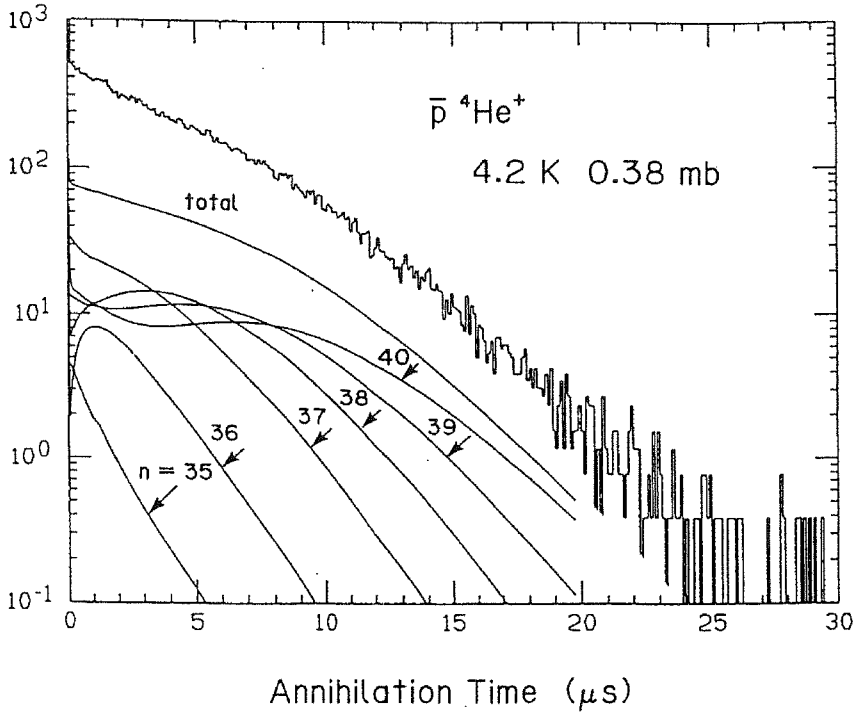

Figure 2.6: Calculated delayed annihilation time spectra with a cut-off at $n = 40$ in comparison with the observed spectral shape (Yamazaki, 1994).

2.3 Quenching by impurity atoms and molecules

2.3.1 Introduction

The metastability of the isolated $\bar{p}$-He^+ atomcule is well understood in the framework of the Condo-Russell model (Condo, 1964; Russell, 1970); however the collisional stability of atomcules remains mysterious: while metastable in pure helium for densities varying over several orders of magnitude, atomcules are extremely sensitive to molecular contaminants such as H_2 (Ketzer *et al.*, 1998) and O_2 (Pohl *et al.*, 1998): geometrical "quenching" cross sections were deduced from DATS, meaning that a single collision with H_2 or O_2 is able to destroy the metastability[2]. Besides, the admixture of light noble gases (Ne, Ar, Kr) up to 20 % reduces the observed lifetimes only slightly, whereas already 200 ppm of Xe shows a much stronger influence. Fig. 2.7 presents typical DATS, which illustrate the collisional quenching of atomcules by noble gases, H_2 and O_2. No mecanism has been provided thus far for interpreting such huge variations in their collisional (meta)stability.

[2] An atom has a typical size of 1 Å , ie a geometrical cross-section of 1 $Å^2 \equiv 10^{-16}$ cm^2.

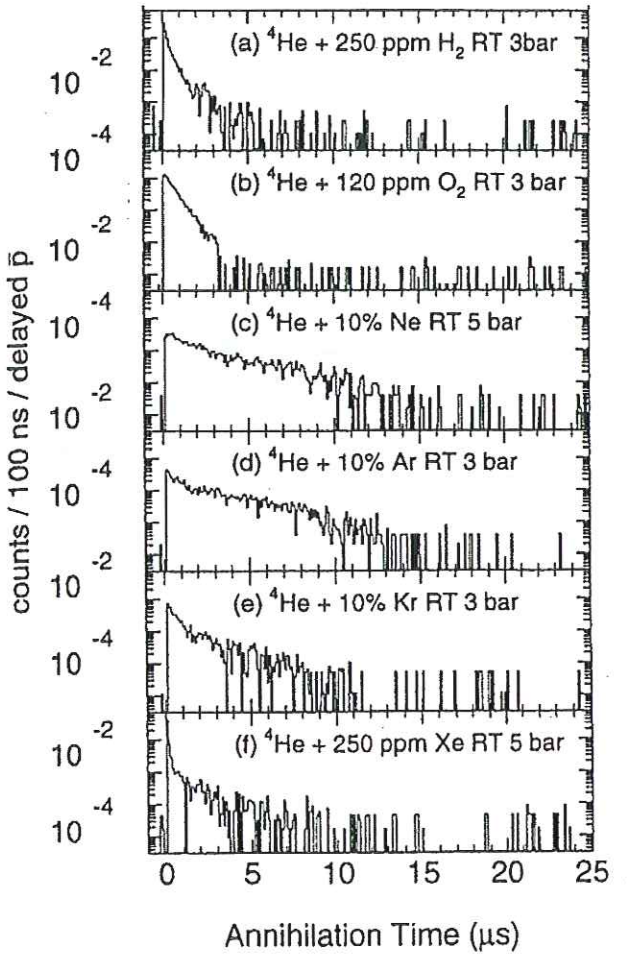

Figure 2.7: Quenching of the $\bar{p}He^+$ metastability in gaseous helium induced by molecular (H_2, O_2) or noble gas (Ne, Ar, Kr, Xe) impurities (Widmann *et al.*, 1993).

2.3.2 Descriptive models of the DATS

A two exponential model provides a better description of the delayed annihilation time spectra than the three or four-level cascade model, which is unable to reproduce the steep fast component. The annihilation rate was then fitted by

$$n(t) = A\left[\lambda_f\, f\, e^{-\lambda_f t} + \lambda_s\,(1-f)\, e^{-\lambda_s t}\right]. \tag{2.15}$$

The model is based on the assumption that the capture states are distributed on two reservoirs of particles, which are in weak interaction: the one containing the fraction f of high l states is quenched by collisions (mostly during the thermalization stage) with a decay rate λ_f, the particles of the second essentially follow a radiative decay. Fig. 2.8 shows the density dependence of the fitted decay rates λ_s for admixtures of either noble gases (Ne, Ar, Kr, Xe) or molecular contaminants (O_2, H_2, N_2).

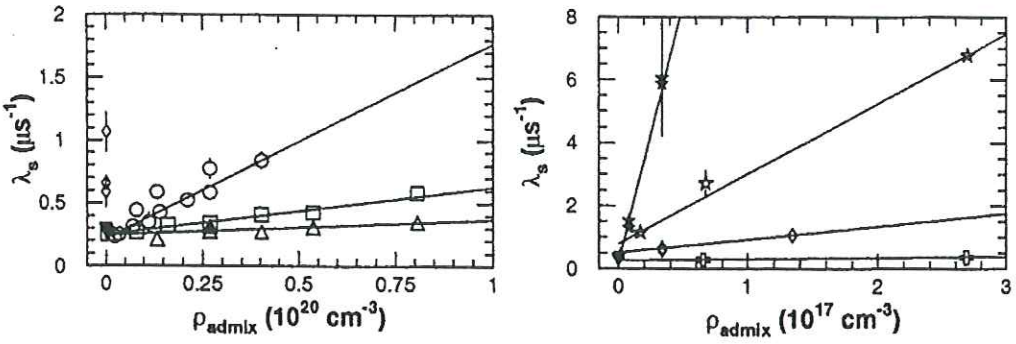

Figure 2.8: Density dependence of λ_s for noble gas admixtures (left column) and molecular admixtures (right column) (Widmann *et al.*, 1995). The relation is linear with density, increasing from Ne to Xe, whose behavior is similar to the one of N_2.

Since the fitted decay rates exhibit a fairly linear relation with the admixture density, it is justified to apply a simple quenching model of metastable states by binary collisions with the admixture atoms or molecules. The decay rate dependence of λ upon the admixture density n can then be expressed as

$$\lambda = \lambda_0 + n\, v_{th}\, \sigma_q, \tag{2.16}$$

where λ_0 is the intrinsic decay rate of the metastable state, σ_q the quenching cross section, and $v_{th} = \sqrt{8k_BT/\pi\mu}$ is the relative thermal velocity of the collision partners. Here, k_B denotes the Boltzmann constant, T the target gas temperature and μ the reduced mass of the admixture atom or molecule relative to the $\bar{p}He^+$ atomcule. Table 2.1 gives the quenching cross sections deduced from this fit.

type	Ne	Ar	Kr	Xe	N_2	H_2	O_2
σ_q (cm^2)	$9\ 10^{-21}$	$2.9\ 10^{-20}$	$1.2\ 10^{-19}$	$3\ 10^{-18}$	$3\ 10^{-18}$	$9.7\ 10^{-17}$	$1.2\ 10^{-15}$

Table 2.1: Quenching cross sections σ_q in cm^2 obtained from a fit of (2.16) to the experimental values for the decay rates (Widmann *et al.*, 1996).

As a result, light noble gases (Ne, Ar, Kr) in concentrations of 10 % change the DATS only slightly, with quenching cross sections of 10^{-19} cm^2. Both Xe and N_2 quench the metastable states much more strongly, with cross sections of about 10^{-18} cm^2. The most striking effect is observed with O_2 and H_2, for which geometrical quenching cross-sections are measured, meaning that a single collision with H_2 or O_2 is able to destroy the metastability, whereas the atomcule may resist to millions of collisions in pure helium.

2.3.3 Discussion

It should be noted that the aforementioned model of destruction by binary collisions with contaminants assumes that the quenching takes place after formation (and thermalization) of the metastable states. This assumption is certainly valid when dealing with impurities: since the newly formed $\bar{p}He^+$ system is slowed down from a few eV kinetic energy to thermal velocity in about ten elastic collisions with He atoms (Hartmann *et al.*, 1998), it is therefore thermalized before it encounters any impurity atom. As a proof, the total delayed fraction remains nearly constant no matter how short the lifetime becomes. However, large noble gas admixtures up to 20 % concentrations may influence the formation stage itself: due to their electronic cloud, noble gases would act as moderators, thus reducing the angular momentum brought in by the $\bar{p}$ before capture. Accordingly, the quenching induced by true mixtures of noble gases would have no collisional origin (Yamazaki *et al.*, 1993). This assumption is supported by our calculations, as will be detailed in Section 3.

On the other hand, the strong collisional quenching by molecular gases remains mysterious. It was suggested that molecular gases, with their many internal "ro-vibronic" degrees of freedom, may absorb the exact amount of energy and angular momentum required to move the $\bar{p}$ from a metastable to a short-lived state. The resonance conditions for H_2 were investigated (Yamazaki *et al.*, 1997a) by comparing the energies released from the de-excitation of the atomcule with the excitation energies of H_2 for various vibrational (v) and rotational (J) modes. Only the energy releases for $(n,l) \rightarrow (n-1,l-1)$ transitions were considered, since the ones for $(n,l) \rightarrow (n,l-1)$ transitions are around 0.30 eV, smaller than the H_2 excitation energy to the $v=1$ band ($\hbar\omega = 0.516$ eV) and much larger than the rotation energies (the smallest $J = 0 \rightarrow 1$ energy is 0.03 eV). The results for H_2 are presented in Fig. 2.9, which provides no clear resonance condition.

For larger de-excitation energies of the atomcule, dissociation or ionization of molecular gases may occur, thus moving the $\bar{p}$ from a metastable to a short-lived state (the dissociation and ionization energies for H_2 are 4.48 eV and 15.44 eV, respectively). Alternatively, if the binding energy between $\bar{p}He^+$ and H is stronger than the H-H one (due to the larger effective charge of $\bar{p}He^+$), the [($\bar{p}He^+$)-H] exotic molecule may be formed and the metastability may disappear. Eventually, one may invoke some possible chemical reaction, thus explaining why the chemically less active N_2 has a weaker effect on the atomcule.

Recently, state to state quenching cross-sections were deduced at 30 K for the atomcule-H_2 interaction (Ketzer *et al.*, 1998), owing to the laser resonance transitions induced by making use of the selective quenching of high-n states by appropriate H_2 admixtures. These low temperature experiments, which are presented in Section 2.5.

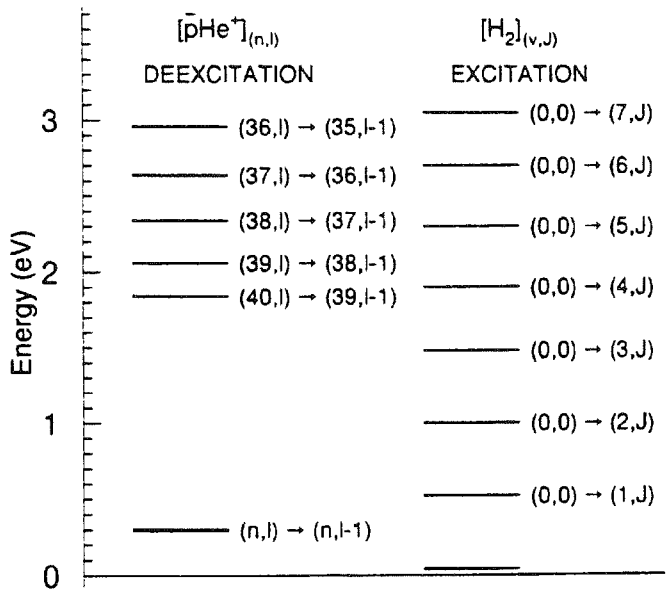

Figure 2.9: Comparison between the released energies of the $\bar{p}He^+$ atomcules and the excitation energies of H_2 (Yamazaki *et al.*, 1997a).

2.4 Laser spectroscopic studies of metastable states

2.4.1 Principle

As previously mentioned, the high-(n, l) antiprotonic metastable states predominantly decay via a cascade of slow radiative transitions with constant vibrational quantum number $v = n - l - 1$, each state having a lifetime of about 1 microsecond. These microsecond lifetimes are long enough to carry laser spectroscopy measurements of these transition wavelengths, which fall in the visible light range. Inasmuch as the de-excitation photon during such a transition is emitted with arbitrary orientation, it proves rather difficult to detect it in a spectrometer. Looking for some measurement technique which would instead rely on the possible detection of annihilation products, Morita *et al.* (1993) proposed a new spectroscopic method for investigating the structure of atomcules. The principles of this method are presented hereafter.

Any change in the level population of metastable states should reveal itself in the observed annihilation spectrum. By irradiating the metastable states with a laser, their populations will be equalized. However, since many metastable states around $n = 38$ are populated and the difference of level population of adjacent levels may not be large enough, only a slight change in a time spectrum would be expected. Fortunately, certain metastable states have adjacent Auger-dominated short-lived levels. Accordingly, these metastable states can be resonantly de-excited to short-lived ones by irradiation with laser light, resulting in immediate annihilation of the antiproton with the helium nucleus. Besides, the population of metastable

states adjacent to Auger-dominated short-lived levels are expected to have a sufficient population. This laser-induced transition from a "parent" to a "daughter" state, which prompts the annihilation, will cause a spike in the $\bar{p}$ annihilation time spectrum. This method presents therefore the net advantage that the detection of the de-excitation photon is now replaced by the detection of the annihilation products, which is easily done by surrounding the target with Cerenkov counters.

2.4.2 Evidence for the existence of $\bar{p}He^+$ atomcules

Following this proposal, the experimental setup was completed. Recent theoretical calculations by Ohtsuki (Yamazaki, 1994) of $\bar{p}He^+$ energy levels, populations, Auger and radiative rates were used as a guide in searching for suitable transitions. One resonance detected at 597.26 nm (see Fig. 2.10) was ascribed to the transition $(n, l) = (39, 35) \rightarrow (38, 34)$ located at the end of the metastable cascade chain $v = 3$ (Morita *et al.*, 1994). Another transition detected at 470.72 nm was ascribed to $(37, 34) \rightarrow (36, 33)$, where the $v = 2$ cascade terminates (Maas *et al.*, 1995).

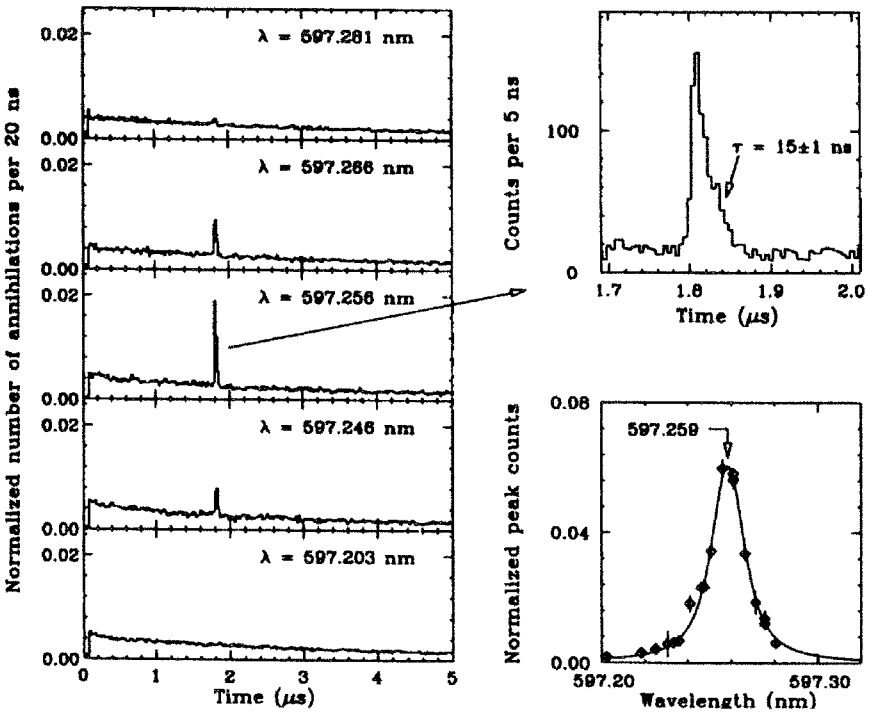

Figure 2.10: left: Time spectra of delayed annihilation obtained with laser irradiation at wavelengths near 597.2 nm. Spikes due to forced annihilation through the resonance transitions are seen at 1.8 μs. Upper right: enlarged time profile of the resonance spike. The peak profile shows an exponential decay with a time constant of 15 ± 1 ns, which reflects the lifetime of the Auger-dominated short lived state. Lower right: normalized peak count versus vacuum wavelength in the resonance region, showing a central wavelength 597.259 ± 0.002 and width of 0.018 nm (Morita *et al.*, 1994).

The whole picture was later completed by Korobov (1996) high-precision calculations of the relevant transitions, including the electron relativistic correction. The difference between the relativistic theory and experiment for all the wavelengths so far observed is only several ppm. Thus, these laser-spectroscopy experiments confirmed both the existence of the metastable $\bar{p}He^+$ atom and the description of its life history, as recalled in section 1.2.

2.4.3 Density-dependent lifetime shortening of metastable states

The laser-spectroscopic method offered a way to map the lifetimes of individual states, when supplemented by a simplified model of the cascade. The lifetimes of the metastable states in the $v = 3$ cascade appeared to be in good agreement with theoretical estimations. Thus, the metastable state $(n, l) = (39, 35)$ showed a lifetime of 1.5 μs, regardless of density. However, measurements of the $v = 2$ cascade indicated that the lifetime of the energetically lower-lying state $(37, 34)$ was found to shorten from 1.3 to 0.1 μs with increasing density. As can be seen on Fig. 2.11, the decay rate of the state $(37, 34)$ increases nonlinearly with target density, from the purely radiative value $\lambda = 1.2\ \mu s^{-1}$ at $\rho = 10^{21} cm^{-3}$ to $\lambda = 8\ \mu s^{-1}$ at $\rho = 3\,10^{21} cm^{-3}$, then levels off at higher densities. It was speculated that the shorter lifetime might be due either to contributions from an internal Auger process or from collisions with ordinary helium atoms. We investigated the latter assumption, which is discussed in Section 3.

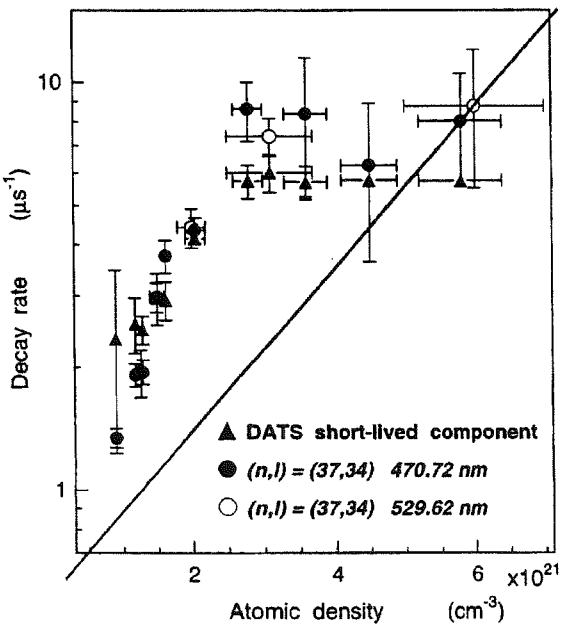

Figure 2.11: Decay rate of the state $(n, l) = (37, 34)$ measured at various densities using the 470.72 nm and 529.62 nm resonances (Hori *et al.*, 1998).

2.4.4 The hydrogen-assisted inverse resonances (HAIR) method

The experimental technique used until now, however, was restricted to laser-stimulated transitions between metastable states (n, l) and adjacent non metastable ones $(n-1, l-1)$ at the end of each cascade with vibrational quantum number $v = n - l - 1 = const.$ Experimentalists have now overcome this restriction by taking advantage of state-dependent quenching effects observed when H_2 is added to helium at ppm levels. It has been shown earlier that outer states are much more strongly quenched by H_2 than inner ones. This can be partially attributed to a reduction of Pauli shielding, as the $\bar{p}$ moves outside the electronic cloud for high n states. This selective quenching of high-n states by appropriate H_2 admixtures opens the possibility to study transitions between two normally metastable states by converting the upper state into a short-lived one while keeping the lower state still long-lived. This transition can be then unambigously identified by applying a laser pulse of the corresponding wavelength to induce the "inverse" transition $(n, l) \rightarrow (n+1, l+1)$ between the long-lived lower level and the now-short lived upper one. The 'H_2 assisted inverse resonance method' (HAIR) was carried out and led to the first observation of five new laser induced transitions, namely $(n, l) = (38, l) \rightarrow (39, l+1), l = 35, 36, 37$ and $(n, l) = (37, l) \rightarrow (38, l+1), l = 35, 36$. Thus, not only all the dipole transitions from metastable states between $n = 39$ and 37 have been identified as laser resonances, but also the first two transitions in the $v = n - l - 1 = 0$ cascade have been found. The experiment and derivation of the decay rates are described in Section 2.5.

2.5 Collisional quenching of $\bar{p}He^+$ atoms by H_2 molecules

The HAIR method requires that the laser pulse be applied early enough after the antiproton arrival to ensure that there is still a sufficiently large population in the lower level, which to some extent is affected as well by the presence of H_2. This is hardly effective in the technique used until now, since the laser, which is triggered by a randomly arriving antiproton, can be fired only after an intrinsic ignition time of about 1 μs. On the other hand, using long antiproton bunches instead meets this requirement, in so far as the laser can be ignited prior to the bunch arrival in the He buffer. In the experiment, each bunch contained some 10^8 particles, producing about $3\,10^6$ metastable atomcules, the Cerenkov light released by the charged annihilation products being detected by a fast photomultiplier tube. As a result however, this pulsed extraction mode did not allow to distinguish delayed annihilation pions from the $\pi^+ \rightarrow \mu^+ \rightarrow e^+$ decay chain of prompt annihilation pions stopped in the vincinity of the target chamber. Figure 2.12 shows a typical DATS with the laser wavelength tuned to the transition $(n, l) = (38, 35) \rightarrow (39, 36)$. The target gas was maintained at low temperature, around 30 K, to avoid H_2 condensation and contamination by other molecular impurities such as O_2 and N_2.

The DATS observed without laser irradiation reflects the many decay channels of antiprotons, surimposed on the exponential component with a 2.2 μs lifetime, arising from the

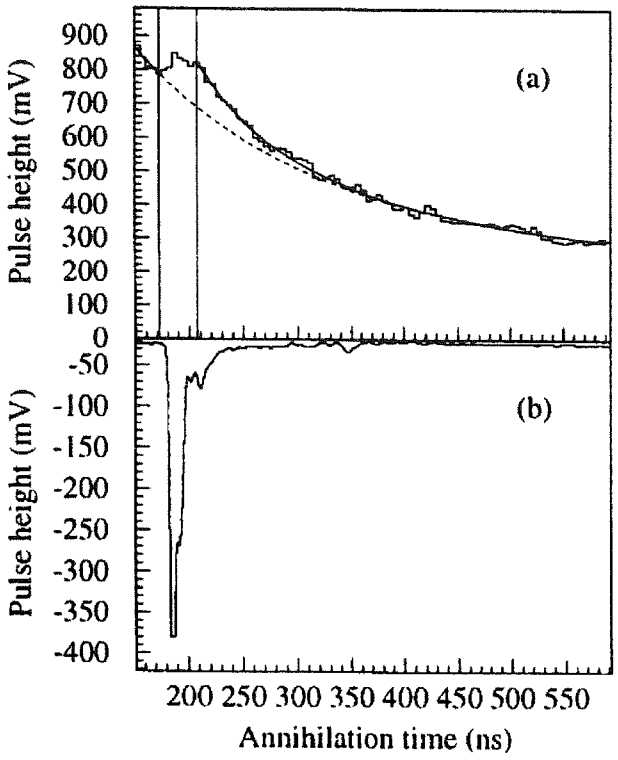

Figure 2.12: (a) DATS of the transition $(n, l) = (38, 35) \rightarrow (39, 36)$ obtained at 30.2 K, 4.8 bar, and an H_2 concentration of 98.6 ppm. The solid line is the result of simultaneously fitting Eq. (2.18) to a set of 27 analog DATS (including the one displayed), the dashed line represents the "background" function (2.17), ie DATS without the laser-induced peak. The vertical lines indicate the duration of the laser pulse. (b) Time structure of the corresponding laser pulse (Ketzer *et al.*, 1998).

$\pi^+ \rightarrow \mu^+ \rightarrow e^+$ decay mentioned above. The shape of this background is easily reproduced by a sum of two exponential functions

$$B(t) = N\left[\lambda_1 f e^{-\lambda_1 t} + \lambda_2 (1-f) e^{-\lambda_2 t}\right], \tag{2.17}$$

where λ_1 denotes the decay rate of stopped π^+ ($\lambda_1 \sim 2.2\ \mu s^{-1}$), while λ_2 is treated as a free parameter; f weights the contribution of prompt pions decay to the total spectrum and N is an overall normalization parameter. The exponentially decaying laser-induced peak was then described by adding to the background a single exponential with an amplitude A_p and a decay rate λ_p:

$$A(t) = \begin{cases} N\left[\lambda_1 f e^{-\lambda_1 t} + \lambda_2 (1-f) e^{-\lambda_2 t}\right] & t < t_L^{on} \\ N\left[\lambda_1 f e^{-\lambda_1 t} + \lambda_2 (1-f) e^{-\lambda_2 t} + A_p \lambda_p e^{-\lambda_p t}\right] & t > t_L^{off} \end{cases}, \tag{2.18}$$

where t_L^{on} and t_L^{off} denote the beginning and the end of the laser pulse, respectively.

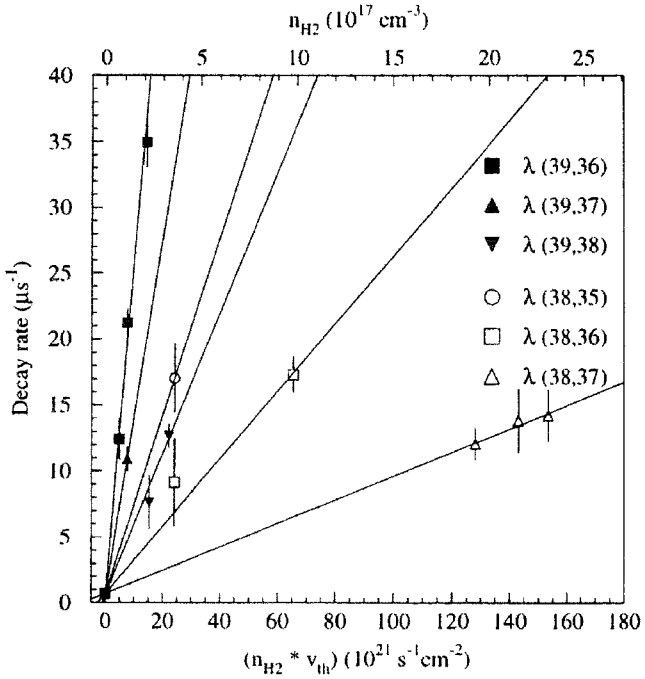

Figure 2.13: Decay rates of the six HAIR transitions for different H_2 number densities (Ketzer *et al.*, 1998).

Figure 2.13 presents the measured decay rates as a function of the number density of H_2 molecules. Since the fitted decay rates exhibit a fairly linear relation with the admixture density, it is justified to apply the same quenching model as described in Section 2.3.2. The decay rate dependence of a given state (n, l) on the admixture density n_{H_2} can then be expressed as

$$\lambda(n,l) = \lambda_0(n,l) + n_{H_2}\, v_{th}\, \sigma_q(n,l), \tag{2.19}$$

where $\lambda_0(n,l)$ is the theoretical decay rate for an isolated $\bar{p}He^+$ system, $\sigma_q(n,l)$ the state-dependent quenching cross section, and $v_{th} = \sqrt{8k_BT/\pi\mu}$ is the relative thermal velocity of the collision partners. Here, k_B denotes the Boltzmann constant, T the target gas temperature and μ the reduced mass of the H_2 molecule relative to the $\bar{p}He^+$ atomcule. The value used for $\lambda_0(n,l)$ includes both radiative and Auger contributions. Radiative transition rates between states (n,l) and $(n+\Delta n, l\pm 1)$ were obtained in a Born-Oppenheimer calculation (Shimamura, 1992), whereas Auger transition rates were calculated with a variational method based on a molecular expansion of the wave function (Korobov & Shimamura, 1997). All calculations however do not take into account the $\bar{p}He^+$-He interaction at finite target densities, which is known experimentally to shorten the lifetime of the state $(37,34)$ considerably, as discussed in Section 2.4. Besides, the lifetime of the state $(38,35)$ is expected to be ≤ 15 % with respect to the theoretical result, while the state $(39,35)$ has been

observed to remain nearly unaffected. Hence, a 15 % error was ascribed to the theoretical decay rates ($n = 38, 39, l \geq 35$) as an upper limit for this quenching process. Table 2.2 gives the quenching cross sections deduced from this fit.

l	34	35	36	37	38
n					
39		28	25.8	13.6	5.4
38		6.8	2.57	0.89	
37	1.1				

Table 2.2: Quenching cross sections $\sigma_q(n,l)$ in units of 10^{-16} cm^2, obtained from a fit of Eq. (2.19) to the experimental values for the decay rates.

The geometrical cross section for a $\bar{p}He^+$-H_2 collision is expected to be 21 10^{-16} cm^2, as deduced from the van der Waals radii of a He atom, ($r_{He} = 1.2$ Å) and an H_2 molecule ($r_{H_2} = 1.38$ Å) (Ketzer *et al.*, 1998). The fact that the quenching cross sections deduced for states with $n = 39$ are of the same order of magnitude as the geometrical cross sections means that they are quenched to almost 100 % in a single collision with an H_2 molecule, while the probability to quench the energetically lower lying states with $n = 38$ is much smaller. Fig. (2.14) summarizes the observed (n,l) dependence of the H_2 quenching cross section σ_q.

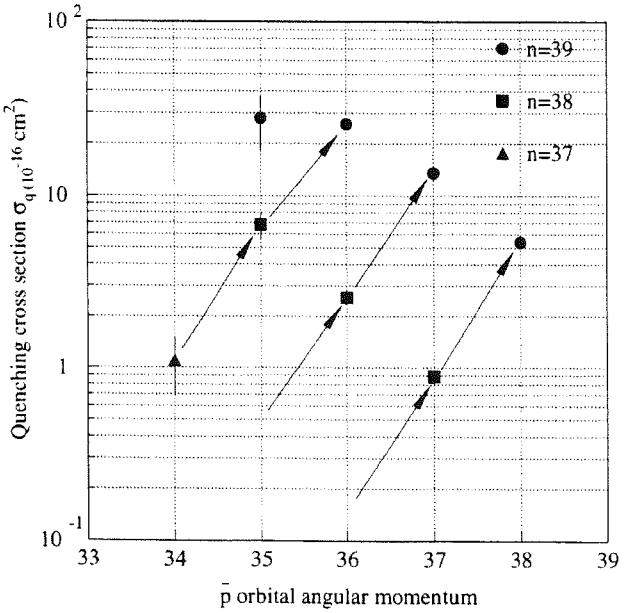

Figure 2.14: The (n,l) dependence of the H_2 quenching cross section σ_q. The arrows indicate HAIR transitions between a long-lived lower state and an H_2-induced short-lived upper state (Ketzer *et al.*, 1998).

The results give a quantitative confirmation of the strong n-dependence of the quenching by H_2 molecules: within a given cascade, the lifetime of the upper state is more sensitive to H_2 by a factor of $4-6$ than that of the lower state. It was this fact that facilitated the HAIR method. In addition, the quenching cross sections depend on the angular momentum number l: for constant principal quantum number n, states with higher l are less affected by H_2 admixtures than those with lower l, by a factor $2-3$.

A qualitative interpretation of this selective quenching was proposed from the charge distributions of both antiproton and electron in the isolated atomcule, as calculated by Korobov & Bakalov (1997) and displayed in Fig. 2.15 for different (n,l) capture states.

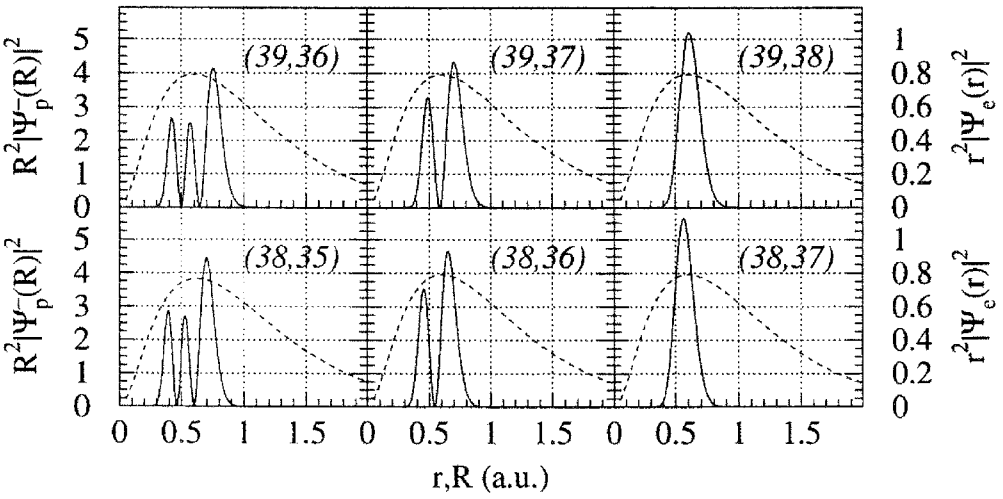

Figure 2.15: Radial probability densities of the antiproton $R^2|\Psi_{\bar{p}}(R)|^2$ (solid curve) and the electron $r^2|\Psi_e(r)|^2$ (dashed curve) for each of the six HAIR daughter states, calculated by Korobov (Korobov, 1996; Korobov & Bakalov, 1997), as a function of the $\bar{p}$-He^+ distance R and the e^-–He^{2+} distance r. All angular variables have been integrated over, thus neglecting the polarization of the electron cloud due to the repulsive interaction between the antiproton and the electron (Ketzer *et al.*, 1998).

As can be seen, the mean radius of the antiproton increases with increasing n or v values, which corresponds to excited or elliptic states, respectively. The reduction of Pauli shielding for these outer states may be invoked, the same way it accounts for the quenching of high n states in pure helium. This discussion however is based on the sole determination of the charge distributions in the *isolated* atomcule and allows no definite conclusion for interpreting at the same time the collisional stability in pure helium and the strong selective quenching by H_2 molecules. In Section 4, we will present a molecular physico-chemistry approach to account for collisional effects arising with from the detailed features of the intermolecular interaction $\bar{p}He^+$–H_2.

2.6 A route to synthetize antihydrogen from $\bar{p}He^+$?

Antihydrogen, the bound state of antiproton and positron, $\bar{H}$=$\bar{p}e^+$, is the most basic building block of antimatter. Recently, antihydrogen ($\bar{H}$= $e^+\bar{p}$) synthesis was proposed (Yamazaki, 1992) from metastable antiprotonic helium via the collision with positronium (Ps= e^+e^-)[3]

$$[\bar{p}He^+]_{nl} + Ps \rightarrow \bar{H} + He + 6.8\ eV\,. \tag{2.20}$$

This process seems likely since the reaction is exothermic, and the positroniums in helium tend to be isolated from neighbouring atoms, due to "Ps bubbles" formation, which are relatively long-lived. Energetic positrons traversing He media are slowed down due to ionization and excitation losses. When their kinetic energy falls below He ionization potential $I_0 \sim 24.6$ eV, they can form positronium by electron abstraction reaction

$$e^+ + He \rightarrow Ps^\star + He^+\,. \tag{2.21}$$

The reaction occurs with 23 % branching ratio. Since the threshold energy of this endothermic process, E_{th}, is about 18.8 eV, Ps emerge with kinetic energies up to $I_0 - E_{th} \sim 6.8$ eV. This energy is smaller than the first electronic excitation energy (= 19.8 eV for He), therefore inelastic collisions do not take place any longer and the slowing-down of positroniums is governed by elastic collisions which are slow, owing to Ps small mass. The slowing-down process before annihilation is characterized by a time constant $\tau_{Ps}^{s.d.}$

$$\tau_{Ps}^{s.d.} \times n_{He} = \text{constant}, \tag{2.22}$$

where n_{He} denotes the He gas density. In 37 atm He gas, n_{He} is about 10^{21} cm^{-3} and $\tau_{Ps}^{s.d.}$ is about 50 ns. The number $\nu_{Ps}^{s.d.}$ of elastic collisions required to slow down Ps from $E_i = I_0 - E_{th}$ to E_f can be estimated, according to the procedure of neutron thermalization theory, as

$$\nu_{Ps}^{s.d.} = \frac{\ln E_i/E_f}{1 + \alpha/(1-\alpha)\ln\alpha}, \text{ where } \alpha = \left(\frac{m_{He}/m_{Ps} - 1}{m_{He}/m_{Ps} + 1}\right)^2 . \tag{2.23}$$

For Ps, $m_{Ps} = 2m_e$ and $\nu_{Ps}^{s.d.} \sim 10^4$ either in liquid helium or room temperature gas. In this thermalization stage, the probability for any Ps to encounter one of the metastable antiprotonic helium atoms is

$$P_{Ps}^{s.d.} = \nu_{Ps}\frac{n(\bar{p}He^+)}{n_{He}}, \tag{2.24}$$

where $n(\bar{p}He^+)$ is the density of atomcules per burst per cm^3. Thus, the formation rate of antihydrogen atoms per burst in the slowing-down process is given by

$$R_{\bar{H}}^{s.d.} = N_{Ps}\, P_{Ps}^{s.d.}, \tag{2.25}$$

[3] The positronium (Ps) atom consists of an electron (e^-) and a positron (e^+) orbiting their mutual center of mass. It is similar to an hydrogen atom with the positron replacing the proton. The binding energy of Ps is 6.80285 eV, i.e. half the binding energy of the hydrogen ground state. The spatial extent of the Ps ground state is twice as large as hydrogen ground state. The average electron-positron distance is 3.0 a_0.

where N_{Ps} is the total number of Ps, which stop in the same spatial region as the antiprotons. The above formula assumes that an antihydrogen atom is formed at every encounter of Ps with $\bar{p}He^+$. However, only a few $\bar{H}$ atoms are expected to be produced from one bunch of 10^9 $\bar{p}$ and 10^8 e^+ during the thermalization stage.

The thermalization stage is followed by an equilibrium stage, which shows an exponential lifetime component. Ground state positronium comes in two different spin states with almost the same energy: $S = 0$ (para-Ps) and $S = 1$ (ortho-Ps). Only ortho-Ps ($S = 1$) with a 150 ns lifetime may contribute to $\bar{H}$ formation. Besides, ortho-Ps, as a triplet spin state, is three times more abundant than the para component. The mobility of ortho-Ps in the equilibrium state is dominated by a diffusion process. The encounter probability P_{Ps}^{eq} for one Ps with the $\bar{p}He^+$ atoms can then be estimated by

$$P_{Ps}^{eq} = 4\pi\, D\, r\, n(\bar{p}He^+)\tau_{Ps}, \tag{2.26}$$

where D denotes the diffusion constant of Ps (cm^2/s), r the reaction radius ($r \sim 0.2\ nm$), $n(\bar{p}He^+)$ the density of $\bar{p}He^+$ per cm^3, and τ_{Ps} the mean lifetime of Ps. The Ps diffusion constant in He is not known but can be estimated from the known mobility of electrons. To obtain the antihydrogen yield per bunch, P_{Ps}^{eq} has to be multiplied by the total number N_{Ps} of Ps

$$R_{\bar{H}}^{eq} = N_{Ps} P_{Ps}^{eq}. \tag{2.27}$$

Since the stopping distribution of positrons which form Ps is narrower than that of antiprotons, this gives the total antihydrogen yield per bunch. In a typical experimental situation, a bunch of 10^9 $\bar{p}$ and 10^8 e^+ can be produced, leading to the formation of $3\,10^7$ metastable $\bar{p}He^+$ and $23\,10^6$ Ps in helium. According to Ito's estimations (Ito & Yamazaki, 1993), 10^3-10^4 thermalized Ps might subsequently encounter $\bar{p}He^+$ atomcules, using a high pressure He buffer. Reaction (2.20) could thus synthetize about 10^3-10^4 antihydrogen atoms per bunch, assuming $\bar{H}$ formation is the dominant output channel. We investigated these other channels and corresponding branching ratios, in order to better estimate the effective $\bar{H}$ formation cross-sections. Our results are presented in Section 5.

Besides, the question arises, how to detect the formation of $\bar{H}$ in this experimental situation. Most probably, $\bar{H}$ atoms will be destroyed in atomic collisions with other He atoms. In this case, the $\bar{p}$ annihilation time spectrum will show a spike from increased $\bar{p}$ annihilation. Such a spike however only indicates that the $\bar{p}He^+$ atoms have reacted with Ps. The only unique way to identify $\bar{H}$ is to ionize it by laser excitation and to observe the associated $\bar{p}$ annihilation. For this purpose the produced antihydrogen atoms are required to survive for some time around 10 ns. Such a long survival can be realized in 1 atm medium. Thus, more sophisticated experimental techniques need to be developped to stop and confine antiprotons and positrons at high densitites in a dilute gas medium.

2.7 Conclusions

Laser spectroscopy measurements provided direct evidence for the existence of metastable antiprotonic atomcules, as 13 resonant transitions of the antiproton in both $\bar{p}^4He^+$ and $\bar{p}^3He^+$ were observed, in remarkable agreement with the theoretical predictions. Besides, the structure of the atomcule was completed by the observation of a hyperfine splitting in one transition. Apart from the high-precision structural study of atomcules, the aspects of their interaction with other atoms, molecules or exotic systems constitute a very interesting subject for atomic collision and chemical physics research, since laser-tagging of individual levels provides state-dependent information on the change of level lifetimes. Next chapters are devoted to the study of these chemical physics aspects.

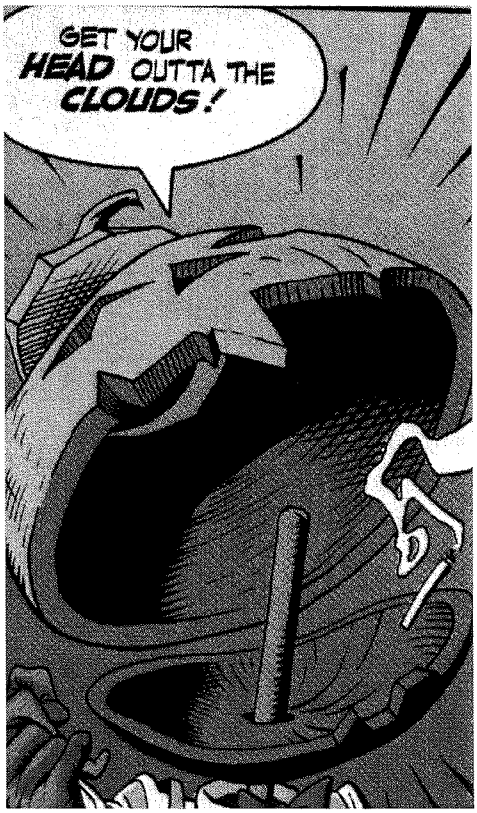

Part II

Chemical physics aspects

Chapter 3

Collisional survival of antiprotonic helium atomcules

Contents

3.1 Présentation générale de l'étude

Introduction

Si la métastabilité des atomcules $\bar{p}He^+$ isolés est bien comprise dans le cadre du modèle de Condo, leur stabilité collisionnelle demeure mystérieuse: bien que résistant à des millions de collisions dans l'helium pur (presque indépendamment de sa densité) ou d'autres gaz rares (jusqu'à des concentrations pouvant atteindre 20 % en nombre de moles), quelques collisions avec H_2 ou O_2 (à des concentrations de 100 ppm ou moins) suffisent à détruire la métastabilité. Afin d'interpréter ces différences, nous avons développé une approche physico-chimique, basée sur une détermination précise du potentiel intermoléculaire. Des premiers résultats sont présentés ici pour l'interaction d'atomcules avec l'helium ou d'autres gaz rares.

Démarche et résultats

Dans la mesure où les états métastables sont des états de Rydberg, un traitement classique des trois noyaux lents ($\alpha\bar{p}$-α) dans le potentiel d'interaction Born-Oppenheimer (BO) constitue une première étape satisfaisante vers un traitement quantique complet de la dynamique collisionelle. Dans notre approche moléculaire, nous décrivons les orbites de Rydberg du sous système $\bar{p}He^+$ par une quantification semi-classique du potentiel effectif ro-vibronique. Le potentiel d'interaction BO est calculé par des techniques standards de chimie quantique *ab initio* qui sont détaillées dans l'annexe 7.

Dans un premier temps, nous simplifions la dynamique de la collision en moyennant classiquement le potentiel d'interaction sur l'orbite quasi-classique rapide de l'antiproton, dont la fréquence de rotation est environ 100 fois plus grande que la fréquence de collision. Ceci permet une interprétation préliminaire du potentiel moyen en termes de chemins réactifs classiques. Nous attribuons la stabilité collisionnelle des atomcules thermalisés dans l'helium pur à l'existence d'une barrière d'activation élevée due à la répulsion de Pauli. Notre modèle prédit la réduction des barrières pour les orbites externes et rend ainsi compte de la destruction des états de grand n par les atomes d'helium.

Dans un deuxième temps, nous étudions la phase de thermalisation des atomcules, formés avec une énergie de recul suffisante pour franchir les barrières d'activation. L'évolution d'un atomcule créé dans un état (n, l) est simulée par un chainage Monte Carlo de collisions jusqu'à thermalisation à 1000 K, en intégrant classiquement le mouvement des noyaux ($\alpha\bar{\text{p}}$–α) dans le potentiel d'interaction Born-Oppenheimer. Nous estimons des rapports de branchement pour tous les états métastables et nous montrons que la voie principale de désexcitation collisionelle correspond à des transferts élastique de moment angulaire, c'est à dire sans changement de n. Nos résultats rendent compte de la destruction des états de $n > 40$ durant la phase de thermalisation et prédisent la dépopulation significative de toutes les couches $n \leq 40$ à des taux supérieurs à 50 %. En faisant l'hypothèse que la population initiale des atomcules se distribue statistiquement sur les niveaux de moment angulaire, nous reproduisons la fraction observée de 3 % des états métastables.

Conclusions

Cette étude illustre la transférabilité des concepts simples de physique moléculaire à la physico-chimie de systèmes exotiques. Toutefois, des approches quantiques seront nécessaires pour interpréter les expériences menées à basse température dans le cadre des projets LEAR et AD. Au chapitre suivant, nous présentons une première analyse de la destruction des atomcules par H_2 à 30 K, basée sur une moyenne quantique de l'état de transition.

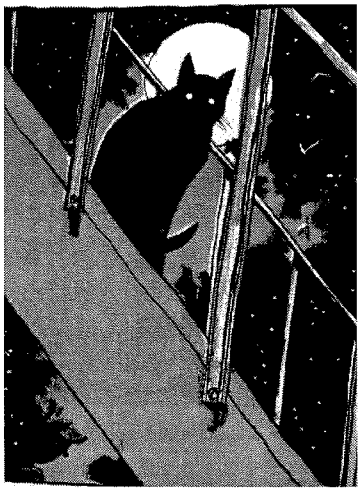

Publication

Accepted in *Chemical Physics* (2000)

Collisional survival of antiprotonic atomcules

Sébastien Sauge and Pierre Valiron

Collisional survival of antiprotonic helium atoms

Sébastien Sauge, Pierre Valiron

Laboratoire d'Astrophysique de l'Observatoire de Grenoble, UMR 5571 CNRS - Université Joseph Fourier, B.P. 53, 38041 Grenoble Cedex 09, France

Abstract

We investigate the collisional survival of antiprotonic $\bar{p}He^+$ atomcules in pure helium from a detailed *ab initio* analysis of their intermolecular interaction. After averaging over classical $\bar{p}$ orbits, we attribute the collisional stability of thermalized atomcules to the existence of a high activation barrier due to Pauli repulsion. Our model predicts the reduction of the barrier for outer $\bar{p}$ orbits, thus accounting for the quenching of high n states by He atoms. We also investigate the thermalization stage of newly formed atomcules from a classical trajectory Monte Carlo approach. Our results support the destruction of the states with $n \geq 41$, as well as the strong depopulation of all $n < 41$ layers, with a quenching rate of 50 % at least. Assuming a statistical distribution of newly formed atomcules with respect to their initial angular momentum, we account for the 3 % observed trapping fraction of metastable states.

1 Introduction

About 3% of antiprotons ($\bar{p}$) stopped in helium are long-lived with microsecond lifetimes, against picoseconds in all other materials [1]. This unusual longevity has been ascribed to the trapping of $\bar{p}$ on metastable bound states in exotic helium atoms $\bar{p}e^-He^{2+} \equiv \bar{p}He^+$. The atomic model of Condo [2] identifies the longer-lived $\bar{p}$ states to near-circular quasi-classical Rydberg orbits with large angular momentum $l \sim n - 1 \sim 37$. For these states, the Auger emission of the remaining electron and the subsequent Stark annihilation of the $\bar{p}$ to the nucleus are strongly suppressed, because of the small energy level spacing compared to the ionization energy of the exotic atom, which therefore predominantly decay via slow radiative transitions [1]. The existence of atomcules was unambigously established by the spectroscopic measurement of their transition wavelengths [3], which were theoretically confirmed with a few ppm accuracy [4].

Beside the atomic description, the $\bar{p}He^+$ system can be also considered as a special diatomic molecule with a negatively charged $\bar{p}$ nucleus in low vibrational $v = 0, 1, 2 \ldots$, high rotational $J = l \sim 37$ state. Due to its high J, the $\bar{p}$ remains n times slower than the electron [5]. Therefore, the Born-Oppenheimer (BO) approximation is expected to be usable for studying this system. The denomination of atomcule was introduced to account for this duality of description [1].

While the metastability of isolated atomcules is well understood, their collisional quenching remains puzzling. On one hand, with typical collision frequencies of about 10^{13} Hz in dense helium, microseconds lifetimes imply that atomcules undergo several millions encounters before annihilating. On the other hand, an analysis of the shape of delayed annihilation time spectra (hereafter referred as to DATS) implies that the states with $n > 40$ are not populated [6], whereas initial population estimates predict that the $\bar{p}He^+$ at birth should exist in many higher states [7,8]. Eventually, a strong density-dependent lifetime shortening was found for the lower-lying $(37, 34)$ state, whereas the lifetime of the higher-lying $(39, 35)$ state remains unaffected [9]. Besides, the admixture of noble gases (Ne, Ar, Kr) up to 20% affects the metastability only slightly [10], except for Xe which reduces the $\bar{p}$ lifetime much more strongly in concentrations of a few hundred ppm only. In addition, the collisional stability of atomcules is very sensitive to the presence of molecular contaminants [10]. The most spectacular effect is observed with O_2 and H_2, which destroy the metastability almost completely in concentrations of a few hundred ppm only, while the presence of about 1% of N_2 has a weaker effect.

We present here a molecular *physico-chemistry* approach to account for collisional effects arising from the detailed features of the intermolecular interaction. The present study is devoted to the collisional survival of $\bar{p}He^+$ atomcules interacting with helium or other noble gases (the quenching of atomcules by molecular contaminants will be presented elsewhere). Since metastable states are Rydberg ones, a classical treatment of the three slow nuclei ($\alpha\bar{p}$-α) in the BO interaction potential provides a first step towards a full quantum mechanical study, at least as far as finer quantum effects such as tunneling or electronic nonadiabaticity are not considered. In this molecular picture, we described Rydberg metastable states of the $\bar{p}He^+$ subsystem by enforcing a semi-classical quantization, which is considered in Section 2. *Ab initio* calculations of the $\bar{p}He^+$-He BO potential energy surface (PES) are presented in Section 3. In Section 4, we provide a first interpretation of the interaction in terms of classical reactive channels with high activation barriers. In Section 5, we simulate the thermalization stage of individual states by classical trajectory Monte-Carlo calculations. State-dependent destruction probabilities as well as collisional branching ratios are presented in Section 6, thus providing an estimate for the total trapping fraction of metastable states. Last section is devoted to stress some limitations and perspectives of our work.

2 Classical BO description of the $[\bar{p}He^+]_{nl}$ atomcule

The classical analog of a Rydberg (n, l) state is a circular or elliptical orbit of angular momentum $l + 1$ and radius or semi-major axis r_{nl}, which we determined by a semi-classical quantization of the effective ro-vibronic potential of the fast rotating atomcule,

$$V_J(r) = \epsilon(r) + \frac{J(J+1)}{2Mr^2}, \tag{1}$$

which is the sum of the ground state BO electronic potential $\epsilon(r)$ and of the repulsive short-range centrifugal potential. M is the reduced mass of the diatomic ($\bar{p}$, He^+) system.

We computed $\epsilon(r)$ by using standard *ab initio* techniques [11,12]. In the BO framework, the Hartree-Fock limit is exact, since this system involves no electronic correlation. For the atomcule, specific polarization orbitals are required, in order to describe the anti-bounding and the strong polarization of the electronic cloud. Exponents ξ for such polarization orbitals were experimented in order to approach the SCF limit for representative α–$\bar{p}$ separations. For the $\bar{p}$, we used a set of 4 shared exponents sp orbitals (ξ= 1, 3, 10, 30) and 1 pure d function (ξ= 0.6). For the α, we expanded the helium's 311++G basis set [13] into an uncontracted set of 3 s (ξ= 98.1243, 14.7689, 0.086), 3 sp (ξ= 3.31883, 0.874047, 0.244564) and 1 pure d (ξ= 1) functions. This resulted in a total of 41 basis functions.

For high $J = l$ values, $V_J(r)$ resembles an interatomic potential, in which large-l states for a given principal quantum number n behave like bound vibrational states with $v = n - l - 1 \sim 0, 1, 2 \ldots$ Reproducing theoretical energies [4] of given n states constrains the classical orbit of the circular state and semi-major axis of the elliptic ones, as illustrated in Fig. 1.

Alternatively, we can predict the actual energies of the circular states by using a Bohr quantization of the classical angular momentum $L(r) = \sqrt{Mr^3 \frac{d\epsilon(r)}{dr}}$, according to $L(r) = (l + 1) = n$. This quantization constrains the radii r_n of the circular orbits and the bound states energies $E_n = \epsilon(r_n) + \frac{n^2}{2Mr_n^2}$. Our values achieve a relative accuracy of a few 10^{-3} with respect to high-precision quantum calculations [4], thus validating our simple quasi-classical approach. Corresponding energy levels for the circular states are presented in Table 1.

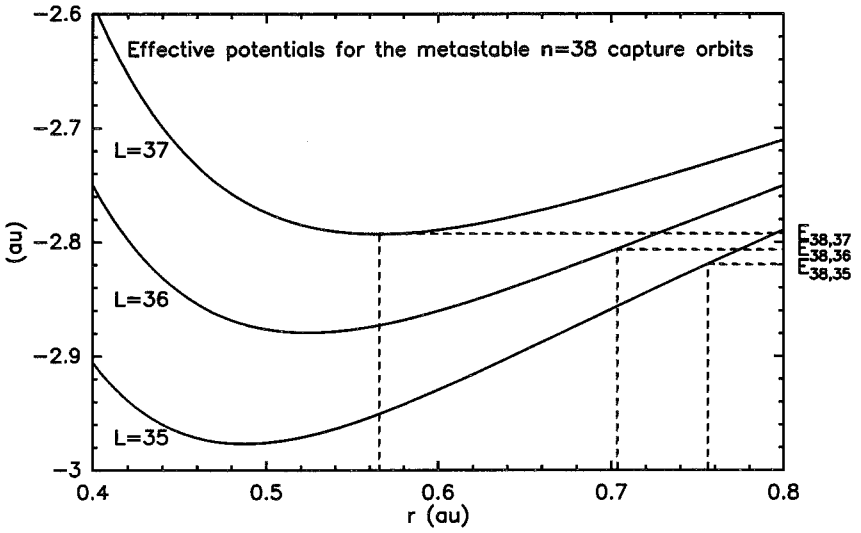

Fig. 1. Semi-classical quantization of the effective $[\bar{p}He^+]_{n,l=J}$ potential (solid lines). Reproducing theoretical energies [4] of given (n,l) states constrains the classical orbit of the circular state $(n, n-1)$ and semi-major axis of the elliptic ones (dashed lines). The semi-minor axis is constrained analogously.

	classical			quantum	
n	R_n (au)	E_n (au)	$\Delta\lambda^n_{n-1}$ (nm)	E_n (au)	$\Delta\lambda^n_{n-1}$ (nm)
42	0.778	-2.541	896.8		
41	0.716	-2.591	779.2		
40	0.660	-2.650	680.7		
39	0.610	-2.717	597.8	-2.724	597.6
38	0.565	-2.793	527.6	-2.800	527.9
37	0.524	-2.879	467.6	-2.887	468.1
36	0.487	-2.977	415.7	-2.984	416.3
35	0.453	-3.086	370.6	-3.093	371.1
34	0.422	-3.209	330.9	-3.212	331.3
33	0.393	-3.347	295.8	-3.353	296.1

Table 1
Classical radius, energy levels and transition wavelengths for the $[\bar{p}He^+]_{n,l=n-1}$ circular states. Transition wavelengths between circular states are consistent with Korobov's non relativistic values [4] within a few Å.

3 The Born-Oppenheimer $\bar{p}He^+$-He interaction potential

The 3-D interaction potential $\bar{p}He^+$-He was parametrized by using the usual Jacobi coordinates (r, $\cos\theta$, R), as shown in Fig. 2. The choice of the cosinus is imposed by the invariance of the potential in the transformation $\theta \rightarrow -\theta$.

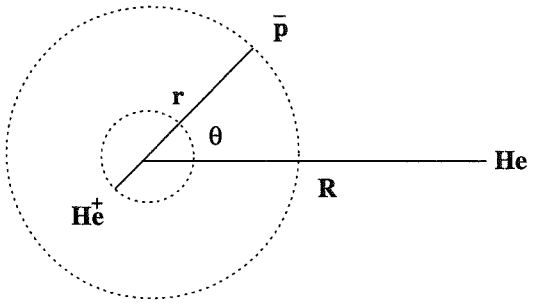

Fig. 2. Jacobi coordinate system used to describe the $\bar{p}He^+$-He interaction. R is the intermolecular separation between both molecules centers of mass.

For an accurate treatment of electronic correlation, we used Unrestricted Møller-Plesset fourth order perturbation theory, including contributions from Single, Double, Triple and Quadruple excitations (UMP4-SDTQ) [11]. In addition to the basis mentioned for the description of the $\bar{p}He^+$ subsystem, we used the helium's 311++G basis set [13] for the description of the interacting He atom, thus resulting in a total of 59 basis functions.

An inevitable difficulty arising from the use of finite basis sets in *ab initio* calculations is the appearance of the basis set superposition error (BSSE). The interaction energy was computed by using the usual counterpoise (CP) scheme [14] in the supermolecular basis (SM):

$$\Delta E = E_{\bar{p}He^+-He}(SM) - E_{\bar{p}He^+}(SM) - E_{He}(SM)\,. \qquad (2)$$

The total potential energy was then obtained by adding to the interaction energy the internal energy $\epsilon(r)$ of the isolated atomcule, *calculated in its own basis set* (see Section 2). This procedure fulfills a generalized hierarchical counterpoise scheme for N-body clusters [15].

All calculations used the *Gaussian94* package [12]. The CPU time for a single UMP4-SDTQ/CP-corrected calculation was about 90 seconds on a RS/6000 Model 590 IBM workstation. The 3-D PES was computed over a fine 3-D mesh in order to permit a spline interpolation of the hypersurface. The mesh sampled from 0.1 au to 1.5 au by step of 0.025 au in r and from 0^o to 180^o by step of 20^o in θ. Intermolecular separation R was sampled from 1.25 to 8 au by step of 0.25 au until $R = 4$ au and by step of 0.5 au beyond. The calculation of the whole PES on this 11400 points grid required about 300 CPU hours.

4 Classical PES averaging

4.1 Collisional stability and quenching of $\bar{p}He^+$ states

The $\bar{p}He^+$-He PES for α-$\bar{p}$ separation $r = 0.565$ au corresponding to the radius of the $(n, l) = (38, 37)$ circular capture orbit is shown in Fig. 3. The instantaneous potential is modulated along the $\bar{p}$ trajectory (i.e. along θ) when He is approached. The magnitude of the modulation is given by the energy difference between the most attractive (α-$\bar{p}$-He, $\theta = 180^o$) and repulsive ($\bar{p}$-α-He, $\theta = 0$) conformations. For a collision energy of 300 kT, the modulation of the PES has a value of 0.1 eV at the classical turning point, whereas typical transition energies between adjacent states with the same n are about 0.3 eV. This modulation might induce weak l-changing transitions in a quantal description of thermal collisions.

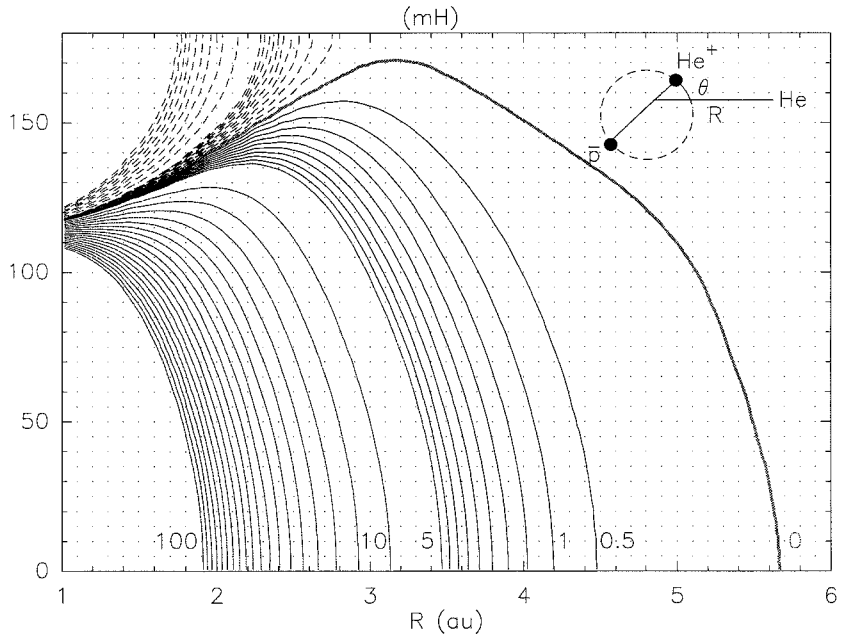

Fig. 3. $\bar{p}He^+$-He interaction potential for α-$\bar{p}$ separation $r = 0.565$ au corresponding to the radius of the $(n, l) = (38, 37)$ circular capture orbit (UMP4-SDTQ-CP level of theory).

Assuming an interaction length of few au, the typical duration of a thermal collision is about 40 times longer than a $\bar{p}$ revolution. Averaging accordingly the PES over the $\bar{p}$ fast rotating orbit allows a preliminary interpretation in terms of classical reactive channels for frozen geometries, the metastability depending upon the existence and magnitude of an activation barrier. For the sake of simplicity, the averaging was made over circular Bohr capture orbits only. Obviously, $\bar{p}$ are also captured on slightly elliptic states, but considering the magnitude of the activation barrier for He, the qualitative conclusions of our model should also apply. The PES was averaged for the coplanar approach (i.e. He lying in the $\bar{p}$ orbital plane), as this approach was found to minimize the barrier. The PES averaged over different circular states is presented in Fig. 4, as a function of intermolecular separation. It presents a high activation barrier with a height corresponding to an energy of 2.5 10^4 kT, which explains the collisional stability of atomcules in the He buffer. Besides, the averaged PES presents a net reduction of its activation barrier for orbits with $n > 42$, thus suggesting that collisional quenching might be favoured for high n states. This effect can be attributed to a reduction of Pauli shielding of the $\bar{p}$, which moves towards the tail of the electronic cloud for higher n states. Thus, collisional quenching could provide a depopulation mechanism of states with $n > 42$, accounting for the spectroscopic observation that these states are not populated [6]. This point will be studied in sections 5 and 6.

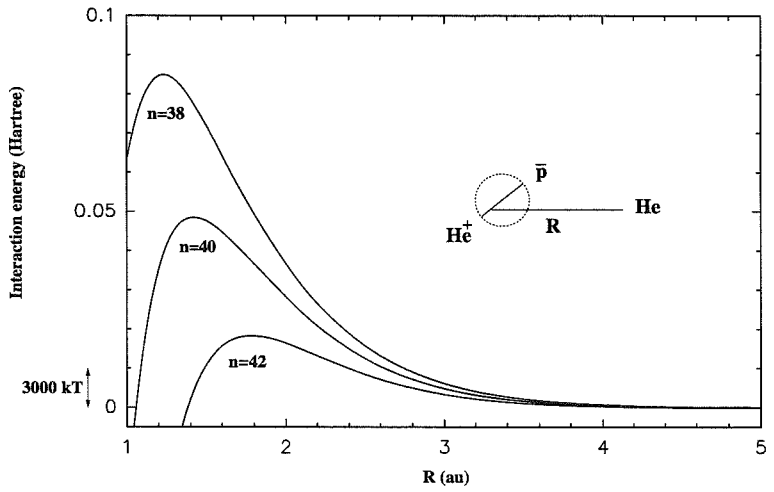

Fig. 4. $[\bar{p}He^+]_{nl}$-He interaction potential for different circular capture orbits. Activation barriers present a net reduction for orbits with $n > 42$, accounting for the spectroscopic observation that these states are not populated [6]. This can be attributed to a reduction of Pauli shielding for high n states.

4.2 Comparison with the He-He interaction potential

We also compared the $\bar{p}He^+$-He interaction with the He-He potential computed by Aziz [16]. Both potentials are presented in Fig. 5. The $\bar{p}He^+$-He barrier appears to be less repulsive than the He-He one. We attribute this lower repulsion to the reduction of the Pauli exchange term, since only one electron remains in the atomcule versus two electrons in normal He.

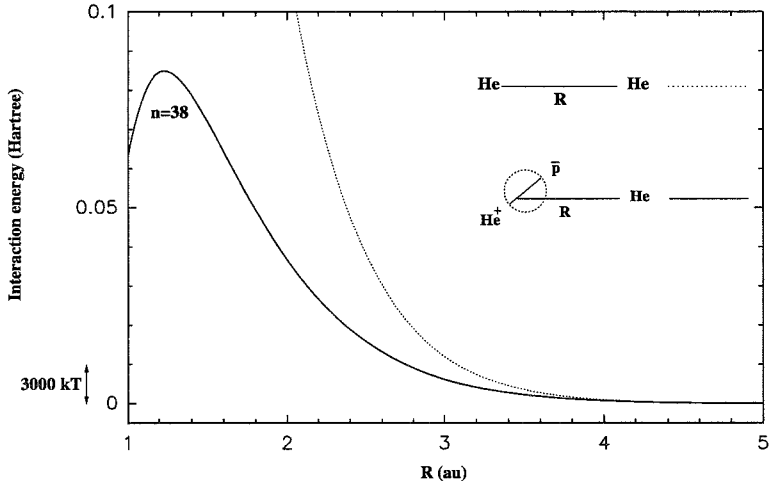

Fig. 5. Comparison of the $[\bar{p}He^+]_{n=38,l=37}$-He averaged PES to the He-He repulsion [16].

4.3 Isotopic effect

We considered also isotopic effects, by comparing interaction potentials for both ^{3}He and ^{4}He. The respective PES are presented in Fig. 6 for the $n = 38$ circular state. On one hand, the activation barrier appears to be lower in ^{3}He than in ^{4}He. This might account for an overall collisional lifetime lower in ^{3}He. On the other hand, the most probable capture orbit is $n_0 = 37$ in ^{3}He instead of 38 in ^{4}He, as for a Bohr-like orbit $n_0 \propto \sqrt{M}$, where M denotes the ratio between the $\bar{p}He^+$ and e^-He^+ reduced mass. The metastability would thus be increased in ^{3}He, due to a larger Pauli shielding of the $\bar{p}$. Auger transition rates, which are larger in ^{3}He [18], most probably explains the shorter lifetimes observed in ^{3}He.

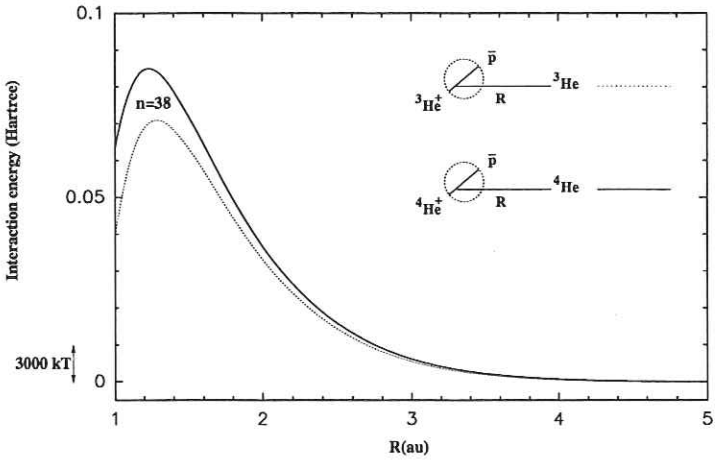

Fig. 6. Comparison of the $[\bar{p}He^+]_{nl}$-He interaction potentials in ^{3}He and ^{4}He for the $(n,l) = (38,37)$ circular state.

4.4 Quenching by noble gases

We also investigated the moderate quenching of atomcules by noble gases, by computing the interaction with neon. The PES averaged over the $n = 38$ circular orbit is presented in Fig. 7 and compared to the $\bar{p}He^+$-He interaction for the same state. The PES for Ne exhibits a slightly higher activation barrier than in He, with a value of about 0.1 au (corresponding to an energy of 3.10^4 kT). Therefore, our computations with Ne weaken the possibility of collisional de-excitation processes and supports the assumption that large noble gas concentrations would influence the formation stage itself: due to their large electronic cloud, noble gases would act as moderators, thus reducing the angular momentum brought in by the $\bar{p}$ before capture. The antiprotons would be then captured preferentially on weakly shielded elliptic states, and the quenching induced by true mixtures of noble gases would have no collisional origin, as previously suggested [1].

4.5 Lifetime shortening of the $(37,34)$ *state with increasing density*

The reduction of Pauli shielding was invoked in section 4.1 to account for the quenching of high n states by He atoms. Nethertheless, this argument fails to explain the intriguing density-dependent lifetime of certain inner orbits, which was observed through laser spectroscopic measurements performed at temperatures between 5 and 7 K [9]. While the metastable state $(n,l) = (39,35)$ shows a lifetime of 1.5 μs, regardless of density, the lifetime of the energetically lower-lying state $(37,34)$ was found to shorten from 1.3 to 0.1 μs with increasing density.

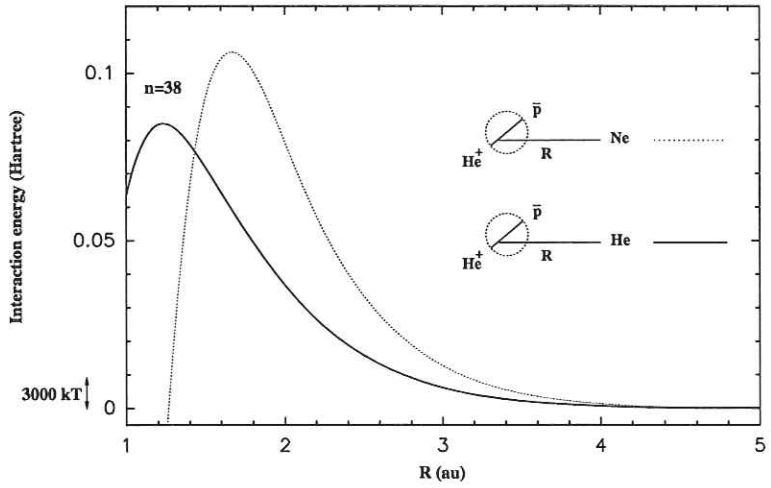

Fig. 7. Comparison of the $[\bar{p}He^+]_{nl}$ interaction with He and Ne, for the $(n,l) = (38,37)$ circular state.

We considered a ternary process, which could account for the experimentally observed quadratic dependence of the decay rate with density, namely

$$He + \bar{p}He^+ + He \rightarrow (He, \bar{p}He^+) + He\,. \tag{3}$$

The cluster ($He^+\bar{p}$ + He) might be bound by the dipole-induced dipole interaction arising from the delocalisation of the $\bar{p}He^+$ electronic cloud, which is larger for inner orbits. Assuming such clusters are only bound for inner orbits, the quenching may be explained by the collisions the $\bar{p}$ now encounters at each revolution with the helium companion. Accordingly, we performed an estimation of cluster binding energies.

We computed interaction energies by averaging the PES over $\bar{p}$ elliptic trajectories corresponding to the states with $(n,l) = (39,35)$ and $(37,34)$. In addition, the atomcule was allowed to relax its geometry while interacting with the He atom. The classical trajectories of the α and $\bar{p}$ nuclei were predicted by integrating the classical equations of motion from the initial conditions determined in Section 2. For the calculation of the interaction energy at a given intermolecular separation, the interaction potential was branched *adiabatically* from zero, i.e. with a time constant τ much greater than the typical $\bar{p}$ revolution period. Fig. 8 shows the $[\bar{p}He^+]_{nl}$-He interaction potentials for the states $(37,34)$ and $(39,35)$. Binding energies for such clusters are no greater than a few kT units, implying that clustering is rather unlikely at very low temperatures. Besides, binding energies are predicted to be greater for outer orbits than for inner ones, implying that the destructive clustering would be more efficient for the $(39,35)$ state than for the shorter-lived $(37,34)$ level. Another possible quenching mechanism might involve an internal Auger process [19].

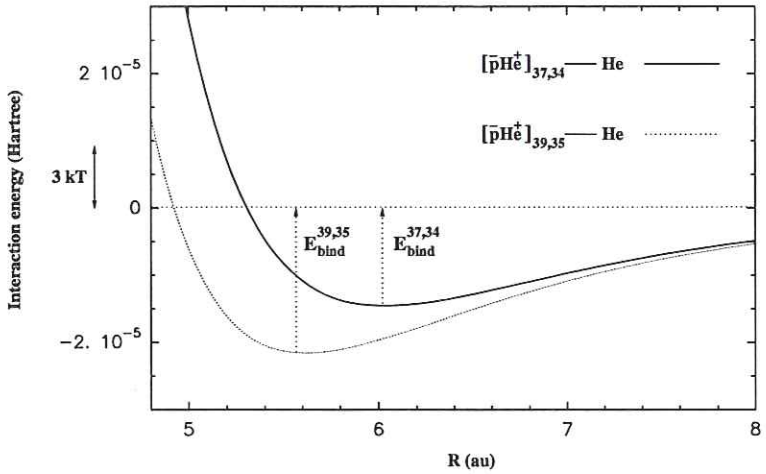

Fig. 8. Estimation of $[\bar{p}He^+]_{nl}$-He cluster binding energies for the states $(37, 34)$ and $(39, 35)$.

5 Simulation of the thermalization stage

The evolution of an atomcule formed in the state (n, l) with a recoil energy of $4 - 5$ eV was simulated by multiple collisions until thermalization at 1000 K. Each collision was treated by integrating the classical equations of motion for the nuclei $\alpha\bar{p}$-α (see section 5.1), providing a careful Monte Carlo selection of initial conditions (see section 5.2). After thermalization, the classical state $(n, l - \Delta L)$ was reprojected on the most probable quantum state, according to a procedure described in section 5.3.

5.1 Hamiltonian

The thermalization stage was studied in the laboratory frame, where the helium bath is thermalized. In this frame, the total Hamiltonian can be written

$$H = T + \epsilon(r) + \Delta E, \tag{4}$$

where $\epsilon(r)$ is the BO electronic potential of the $\bar{p}He^+$ system, ΔE is the interaction energy and

$$T = \frac{\mathbf{p_G}^2}{2M_t} + \frac{\mathbf{p_r}^2}{2M} + \frac{\mathbf{p_R}^2}{2\mu} \tag{5}$$

is the total nuclear kinetic energy. The $\mathbf{p_i}$ are the conjugated momenta, G the center of mass of the $\bar{p}He^+$-He system with total mass M_t and reduced mass μ. The equations of motion for the $\alpha\bar{p}$-α nuclei were derived from Hamilton's

equations:

$$\frac{\partial H}{\partial p_i} = \dot{q}_i \text{ and } \frac{\partial H}{\partial \dot{q}_i} = -\dot{p}_i, \tag{6}$$

which were numerically integrated in cartesian coordinates by using a fourth-order Runge-Kutta algorithm [20]. The conservation of energy and angular momentum provided a numerical consistency check for the whole procedure. We achieved an accuracy of 10^{-10} over all trajectories.

5.2 Initial and final conditions

Fig. 9 summarizes the initial conditions specified for simulating the thermalization stage in the laboratory frame.

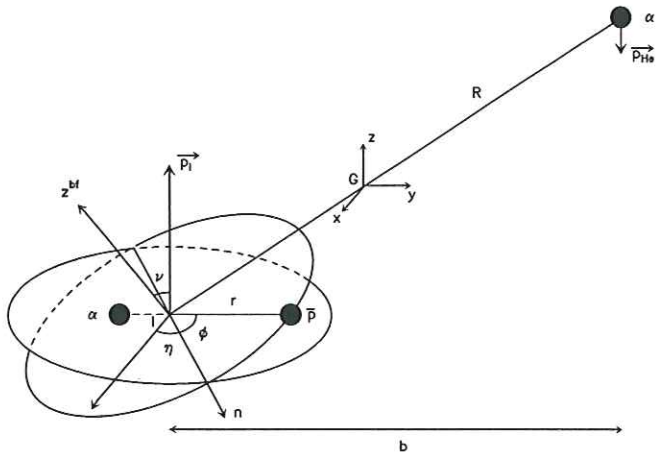

Fig. 9. Initial conditions for simulating the thermalization of a newly formed atomcule.

The recoil energy $E^r_{\bar{p}He^+}$ of the newly formed atomcule is estimated from the conservation of the total impulse during the capture process $\bar{p}$+He $\rightarrow$ $\bar{p}He^+ + e^-$. One can safely neglect the impulse of both thermalized helium atom and light ejected electron with respect to the $\bar{p}$ one, since the capture is expected to favor nearly resonant conditions where the $\bar{p}$ kinetic energy $E_{\bar{p}}$ matches the ionization potential $I_0 = 24.6$ eV of the helium atom. Thus, the recoil energy

$$E^r_{\bar{p}He^+} \sim \frac{m_{\bar{p}}}{(m_{\bar{p}} + m_{He^+})} E_{\bar{p}}, \tag{7}$$

is about 5 eV for $E_{\bar{p}} = I_0$.

In our simulations, the newly-formed atomcule was created with recoil energies of 4 and 5 eV. The kinetic energy of thermalized helium atoms was sampled from a Maxwell Boltzmann distribution at 1000 K. The approach distance $R(t = 0)$ prior to each new collision corresponded to the range of the interaction potential ΔE, namely 6 au (the mean distance between particles for typical helium densities $\rho = 10^{-3}$ mol/cm^3 is about 20 au). The sample of impact parameter b was constructed from a uniform distribution in b^2, in the range $[0, b_{max}]$, where b_{max} is the upper limit beyond which no significant angular momentum transfer for the atomcule is observed. b_{max} was set to 3.5 au, a value corrresponding to the classical turning point at 1000 K, as determined from Fig. 4.

The orientation of the atomcule orbital plane with respect to its center of mass frame was described by a set (η, ϕ, ν) of Eulerian angles, which were selected uniformly in the 4π steradians, leading to a flat sampling of η, ϕ in [0,2π] and of $\cos\nu$ in [-1,1]. In the body-fixed frame referential, the quantization condition for the $\bar{p}He^+$ angular momentum is $Mr^2\dot{\phi} = l + 1$.

The collisions were chained until each newly-formed atomcule was (a) thermalized at 1000 K ($E_I(t) < 1.5\ kT$) or (b) destroyed either by overcome of the activation barrier or by collision-induced transitions on Auger-dominated short-lived levels. Batches of 1000 trajectories were run for each (n, l) metastable capture state. A typical simulation is shown in Fig. 10. By adjusting the collision energy, we were able to produce integer ΔL transfers from an initial (n, l) state. The internal energy of atomcules after such collisions matches the quantum energy of the $(n, l-\Delta L)$ level with a relative accuracy of 10^{-2}. Therefore, collisions produce an *elastic* angular momentum transfer, i.e. without n changing. This feature is illustrated in Fig. 10B and 10C.

Reducing the buffer temperature below 1000 K produced no noticeable change in the results at the expense of a large increase in computation time.

5.3 Reprojection of classical states after thermalization

In our model, the $\bar{p}He^+$ atomcule undergoes classical ΔL angular momentum transfers by collisions with surrounding helium atoms. In the simple case where ΔL is an integer, the quantum probability $P_{\Delta l=\Delta L}$ of a classical integer ΔL transition is unambigously equal to unity. What is the correspondence rule when ΔL is not an integer?

Let us first address the case $\Delta L < 1$. As an approximation, we can consider that each elastic collision leads to a mixing of the states (n, l) and $(n, l-1)$

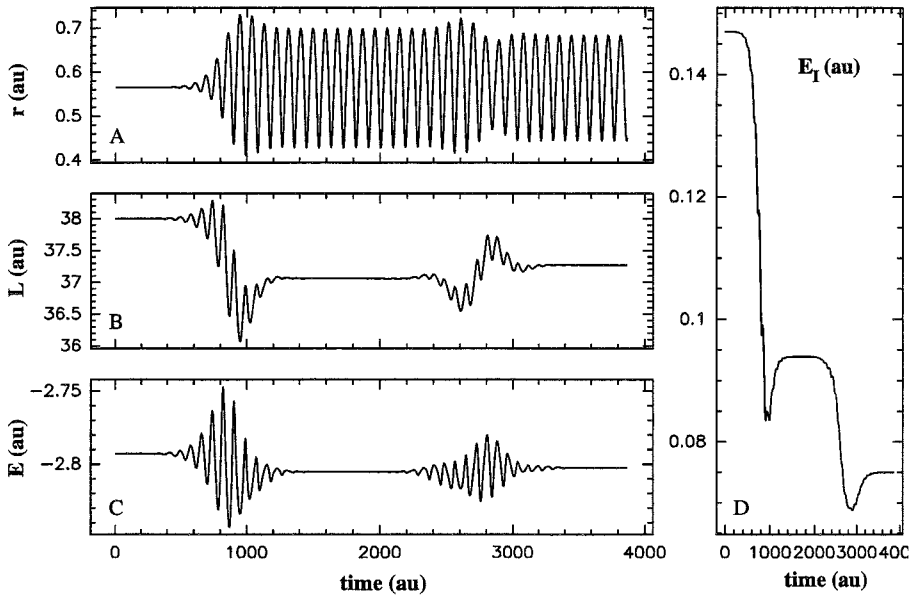

Fig. 10. Thermalization of a newly formed 4 eV atomcule in the $(n, l) = (38, 37)$ circular state. Figure displays time evolution of radius (A), angular momentum (B) and energy (C) of atomcule, which thermalizes its kinetic energy E_I in a T=1000 K helium bath (D). The initial angular momentum obeys the classical limit $L = l + 1$. The first collision produces an angular momentum transfer $\Delta L \sim 1$. ΔE corresponds to the $(38, 37) \rightarrow (38, 36)$ transition energy. Therefore, collisions produce an elastic ΔL transfer (n does not change).

bracketing $l - \Delta L$. The final state Ψ can be then written:

$$\Psi = a\,\Phi(n, l) + b\,\Phi(n, l-1) \;\text{ with }\; |a|^2 + |b|^2 = 1\,. \tag{8}$$

The determination of $P_{\Delta l=1} = |b|^2$ can be achieved by equaling the expectation value of the L^2 operator with its classical homolog $(l - \Delta L)\,(l - \Delta L + 1)$:

$$\langle \Psi \mid L^2 \mid \Psi \rangle = (l - \Delta L)\,(l - \Delta L + 1)\,. \tag{9}$$

The left-hand side of Eq. (9) can be expanded as

$$\langle \Psi \mid L^2 \mid \Psi \rangle = |a|^2 \langle \Phi(l) \mid L^2 \mid \Phi(l) \rangle + |b|^2 \langle \Phi(l-1) \mid L^2 \mid \Phi(l-1) \rangle \tag{10}$$

$$+ \text{ interference term.}$$

The interference term is zero since the Φ functions are eigenfunctions of the L^2 operator and orthogonal in this respect. By identifying the right-hand sides of Eq. (9) and (10), one gets

$$(1 - |b|^2)\,l(l+1) + |b|^2\,(l-1)l = (l - \Delta L)\,(l - \Delta L + 1)\,. \tag{11}$$

Thus, the quantum probability of a $\Delta l = 1$ angular momentum transfer is

$$P_{\Delta l=1} = |b|^2 = \Delta L - \frac{\Delta L(\Delta L - 1)}{2l} \sim \Delta L\,. \tag{12}$$

For any ΔL value, we can still consider that the classical state after collision corresponds to a mixing of the states $(n, l - E(\Delta L))$ and $(n, l - E(\Delta L) - 1)$ bracketing $l - \Delta L$, $E(\Delta L)$ denoting the integer part of ΔL. The probability densities for a transition on each of these two states are then:

$$P_{\Delta l=E(\Delta L)+1} = \Delta L - E(\Delta L) \text{ and } P_{\Delta l=E(\Delta L)} = 1 - (\Delta L - E(\Delta L))\,. \tag{13}$$

Fig. 11 presents the quantum probability $P_{\Delta l=0,1,2}$ as a function of classical angular momentum transfer ΔL. After the last thermalizing collision, a random number (ξ) with flat distribution on the interval [0, 1] was selected and the classical state was reprojected on the state $(n, l - E(\Delta L) - 1)$ if $\xi > \Delta L - E(\Delta L)$ and on the state $(n, l - E(\Delta L))$ otherwise.

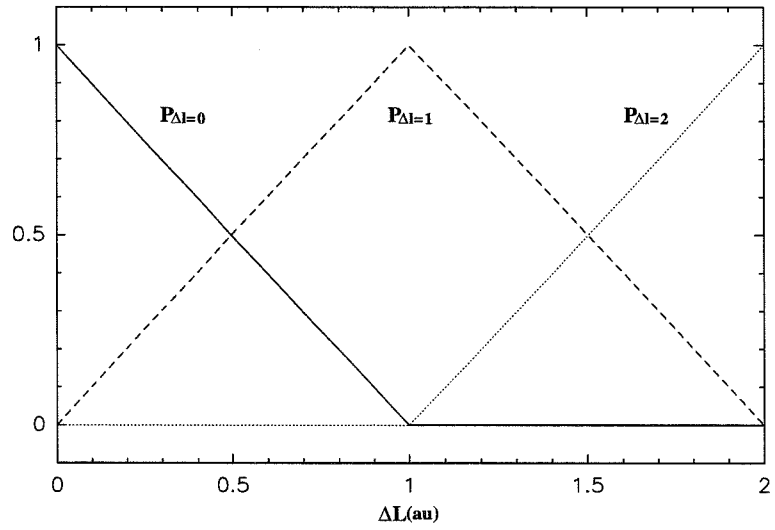

Fig. 11. Reprojection of classical states after collision. As an approximation, a classical $(n, l - \Delta L)$ state was assumed to be a mixing of the 2 quantum states bracketing $l - \Delta L$ (with same n since collisions are elastic ones). The correspondence between $P_{\Delta l=0,1,2...}$ and classical ΔL was then obtained by identification of $< \Psi|L^2|\Psi >$ with its classical homolog $(l - \Delta L)\,(l - \Delta L + 1)$.

6 Results

6.1 Destruction probabilities

Table 2 presents the destruction probabilities $P_d(n,l)$ for each of the metastable states from $n = 33$ to $n = 42$, resulting from the thermalization stage with a recoil energy of 5 eV. Our results support the destruction of the states with $n > 40$, consistent with the spectroscopic observation that such states seem not populated. Nevertheless, the quenching by helium atoms is not complete for these states, which might correspond to the few longer-lived atomcules observed with lifetimes up to 25 μs. Besides, the frontier between metastability and collisional quenching is not clean, e.g. 30 to 90% of the initial population of each state with $n \leq 40$ is destroyed during the first few collisions. Eventually, we observe the strong depopulation of the elliptic states adjacent to Auger-dominated short-lived levels, thus confirming the weaker collisional stability of such states, which are less shielded than the circular one with same n.

n \ l	41	40	39	38	37	36	35	34	33	32
42	0.98	0.98	0.98	0.98	0.98	0.98				
41		0.90	0.92	0.93	0.94	0.96				
40			0.72	0.80	0.85	0.90	0.94			
39				0.53	0.69	0.83	0.92			
38					0.42	0.70	0.87			
37						0.27	0.60	0.86		
36							0.36	0.82		
35								0.36	0.76	
34									0.35	0.77
33										0.93

Table 2
State dependent destruction probabilities of the metastable states after thermalization from a recoil energy of 5 eV.

6.2 Trapping fraction

Assuming the atomcule at birth is formed with a principal quantum number n ranging from n_m to n_M and a statistical distribution $P(n,l) \propto 2l+1$ with respect to angular momentum l, the initial trapping fraction is

$$f_i = \frac{\sum_{n=n_m}^{n_M} \sum_{l=l_A+1}^{n-1} (2l+1)}{\sum_{n=n_m}^{n_M} \sum_{l=0}^{n-1} (2l+1)}, \tag{14}$$

where $l_A = l_A(n)$ is the angular momentum dividing the metastable and the prompt zone, from which fast Auger transitions occur. Of course a statistical distribution is not conceivable for unlimited l- and therefore n-values, but we should not be concerned with the expected cutoff in the initial populations if we assume that the collisional quenching occurs prior to the cutoff. According to classical trajectory Monte Carlo calculations [21], the initial population would extend from $n_m = l_m + 1 = 34$ to $n_M = l_M + 1 = 44$. Thus, the total fraction of newly-formed metastable states would amount up to about 20 % prior to any quenching mechanism. We estimated an effective trapping fraction by convoluting the initial distribution of metastable states by the state-dependent survival probabilities:

$$f = (1 - P_d(n,l)) \otimes f_i = \frac{\sum_{n=34}^{44} \sum_{l=l_A+1}^{n-1} (1 - P_d(n,l)) \times (2l+1)}{\sum_{n=34}^{44} \sum_{l=l_A+1}^{n-1} (2l+1)} \times 20\ \% \sim 3\ \%. \tag{15}$$

This estimation agrees surprisingly well with the experimental value. The fraction would be close to 9%, assuming that only the states with $n > 40$ (the observed limit) are affected by the thermalization stage. Therefore, the quenching of normally metastable states with $n \leq 40$ contributes also to the lowering of the effective trapping fraction.

6.3 Redistribution of the states after thermalization

Atomcules can be grouped into cascade chains with $n = \textit{constant}$ with respect to collisions (whereas radiative transitions obey the selection rule $\Delta v = \Delta(n - l - 1) = 0$). We investigated the redistribution of individual states on adjacent levels with same n. Results are illustrated in Table 3 for the states with $n = 39$. For each batch of $N = 1000$ atomcules formed in the state $(n,l) = (39,l)$, the redistribution on each adjacent levels $(39, 38-\Delta l)$, $\Delta l = 0,1,2,3$ is presented. Although the vast majority of states undergo transitions to lower l-states, we note that a small fraction is promoted on higher-l levels. Each state (n,l) has a statistical weight $W_n(l) = (2l+1)/(2(n-1)+1)$ with respect to the circular state $(n, n-1)$. By averaging the redistribution of a given (n,l) state over all

possible Δl values, we get back the survival probability $P_s(n,l) = 1 - P_d(n,l)$ of this state. By averaging the redistribution of all (n,l) levels on a given state $(n, l - \Delta l)$, we obtain the total population of this state after thermalization.

$l/l - \Delta l$	38	37	36	35	$W_n(l) \times N$	$P_s(n,l)$
38	150	194	83	44	1000	0.47
37	0	209	64	26	974	0.31
36	0	82	61	14	948	0.17
35	0	28	29	18	922	0.08
$\langle l \rangle$	150	513	237	102	3844	0.26

Table 3
Redistribution of each metastable state $(39, l)$ on adjacent states $(39, l - \Delta l)$ after thermalization from a 5 eV recoil energy.

Fig. 12 shows that within a cascade of given n, the first elliptic state (with $v = n - l - 1 = 1$) benefits from the strongest repopulation during the thermalization.

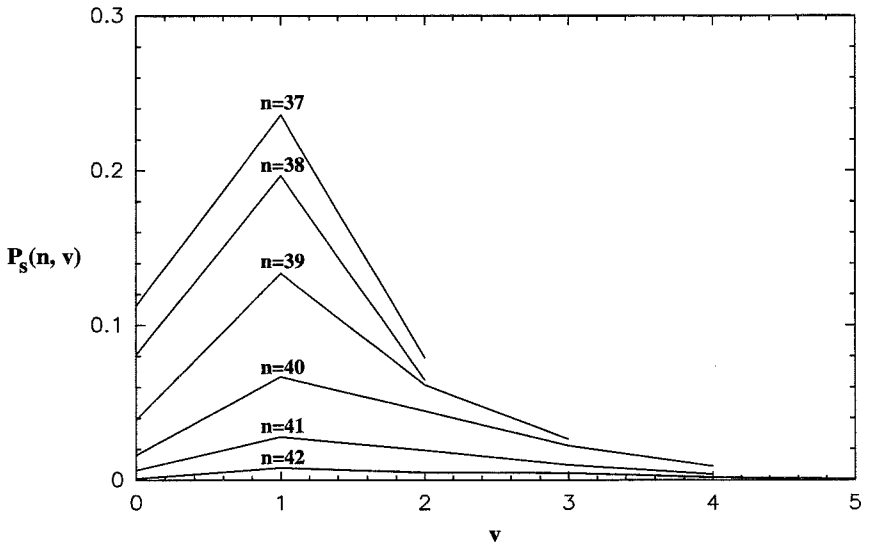

Fig. 12. Collisional branching ratios within each n layer, as a function of vibrational quantum number $v = n - l - 1$. Each curve is normalized with respect to the initial (statistical) population of the n layer. After thermalization, the first elliptic state $l = n - 2$ $(v = 1)$ is the most populated level.

Eventually, averaging the redistribution over all l and Δl values provides the survival probability of the n layer through thermalization:

$$P_s(n, \langle l \rangle) = \sum_l W_n(l) \times P_s(n,l)\,. \tag{16}$$

n-dependent survival probabilities are presented in Fig. 13 for a recoil energy of atomcules between 4 and 5 eV. As can be seen, the thermalization stage from a 5 eV recoil energy (grey filled rectangles) quenches all n layers significantly, with a destruction rate of 50 % at least. High-n layers are strongly quenched because of a weaker Pauli shielding of the $\bar{p}$, whereas lower-n states are destroyed because a smaller Δl transfer is required for reaching an Auger-dominated level. The quenching from a 4 eV recoil energy (unfilled rectangles) remains efficient with a destruction rate of 40 % at least.

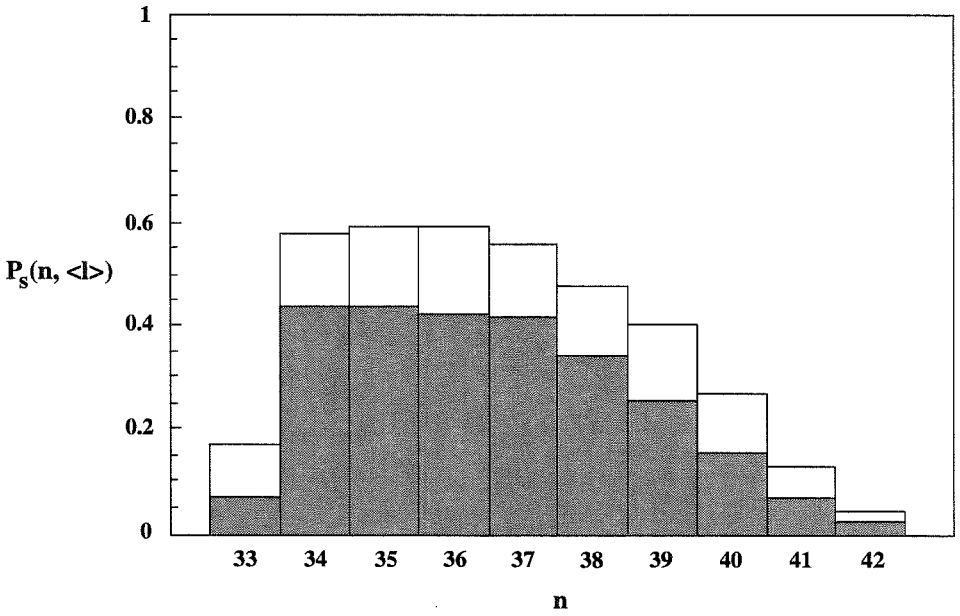

Fig. 13. Survival probability of each layer with principal quantum number n from a recoil energy of newly-formed atomcules between 4 and 5 eV (grey filled rectangles).

Trapping fractions f_n within each n layer are obtained by multiplying the normalized statistical population of the layer by its survival probability:

$$f_n(n_m \leq n \leq n_M) = \frac{\sum_{l=l_A+1}^{n-1} W_{n_M}(l)\, N}{\sum_{n=n_m}^{n_M} \sum_{l=l_A+1}^{n-1} W_{n_M}(l)\, N} \times P_s(n, \langle l \rangle)\,. \qquad (17)$$

The diagram shows that the thermalized populations are almost uniformly distributed around the observed 3 % trapping fraction (about 2.5 % for the states with $n = 34 - 36$, about 3.5 % for the states with $n = 37 - 39$). In view of the high level density and the small level spacing around $n = 38$, a uniform distribution is a consistent prediction.

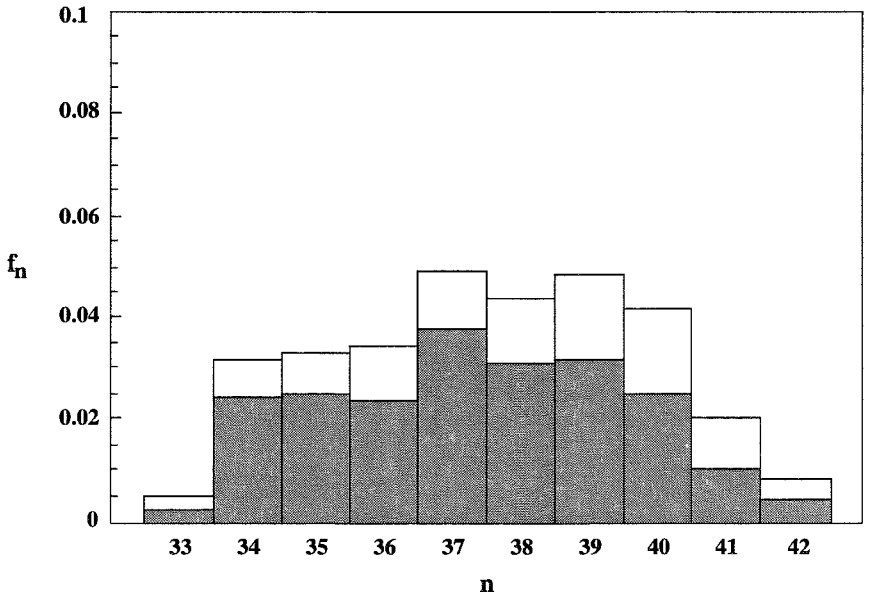

Fig. 11. Trapping fraction within each layer of principal quantum number n, from a recoil energy between 4 and 5 eV (grey filled rectangles).

7 Conclusions

This study illustrates the transferability of simple molecular physics concepts to the physico-chemistry of exotic processes involving antiprotonic atomcules.

The remarkable collisional stability of atomcules in pure helium results from the existence of a high activation barrier in the classically-averaged potential energy surface. This barrier can only be crossed during the initial thermalization stage of the newly-formed atomcules with typical recoil energies of several eV. Monte Carlo classical trajectory simulations demonstrate that this thermalization stage strongly quenches initial populations, especially for $n > 40$. Assuming a statistical distribution of newly-formed atomcules, we retrieve the 3 % observed trapping fraction.

The sole molecular picture cannot account for finer details such as isotopic effects, quenching by heavier noble gases or lifetime shortening of the (37,34) state with increasing density.

However the present approach provides a first step towards a global quantum treatment integrating all aspects of the collisional processes involved. Such developments will be especially required for interpreting the low temperature experiments from the LEAR and AD projects [22]. As a first attempt, we will present in a forthcoming paper a preliminary analysis of the strong quenching by H_2 at 30 K, based upon a quantum averaging of the reactive state.

Acknowledgements

Calculations have been carried out on the workstations of the "Service Commun de Calcul Intensif de l'Observatoire de Grenoble". One of us (S.S.) was supported by a fellowship of the Ministère de l'Enseignement Supérieur et de la Recherche. We warmly acknowledge Dr. J. Carbonell and his colleagues from the few-body community for numerous informal discussions.

References

[1] T. Yamazaki, E. Widmann, R.S. Hayano, M. Iwasaki, S.N. Nakamura, K. Shigaki, F.J. Hartmann, H. Daniel, T.v. Egidy, P. Hofmann, Y.-S. Kim, J. Eades, Nature 361 (1993) 238.

[2] G.T. Condo, Phys. Lett. 9 (1964) 65.

[3] N. Morita, T. Yamazaki, F.J. Hartmann, D. Horváth J. Eades et al., Phys. Rev. Lett. 72 (1994) 1180.

[4] V.I. Korobov, Hyp. Int. 101/102 (1996), 479.

[5] I. Shimamura, Phys. Rev. A46 (1992) 3776.

[6] T. Yamazaki, Prospects of spectroscopy with antiprotonic exotic atoms, International Conference on Low-Energy Antiprotons Physics, 1994.

[7] W.A. Beck, L. Wilets, M.A. Alberg, Phys. Rev. A 48 (1993), 2779.

[8] G. Ya. Korenman, Hyp. Int. 103 (1996) 341.

[9] M. Hori, H.A. Torii, R.S. Hayano, T. Ishikawa, F.E. Maas, H. Tamura, B. Ketzer, F.J. Hartmann, R. Pohl, C. Maierl, M. Hasinoff, T.v. Egidy, M. Kumakura, N. Morita, I. Sugai, D. Horváth, E. Widmann, J. Eades, T. Yamazaki, Phys. Rev. A 57 (1998) 1698.

[10] E. Widmann, I. Sugai, T. Yamazaki, R.S. Hayano, T. Ishikawa, S.N. Nakamura, H. Tamura, T.M. Ito, A. Kawachi, N. Nishida, W. Higemoto, Y. Ito, N. Morita, F.J. Hartmann, H. Daniel, T.v. Egidy, W. Schmid, F.J. Hofmann, J. Eades, Phys. Rev. A 53 (1996) 3129

[11] W.J. Hehre, L. Radom, P.v.R. Schleyer, J.A. Pople, Ab Initio Molecular Orbital Theory, Ed. Wiley & Sons, United States, 1986.

[12] Gaussian 94, Revision D.3, M.J. Frisch, G.W. Trucks, H.B. Schlegel, P.M.W. Gill, B.G. Johnson, M.A. Robb, J.R. Cheeseman, T. Keith, G.A. Petersson, J.A. Montgomery, K. Raghavachari, M.A. Al-Laham, V.G. Zakrzewski, J.V. Ortiz, J.B. Foresman, J. Cioslowski, B.B. Stefanov, A. Nanayakkara, M. Challacombe, C.Y. Peng, P.Y. Ayala, W. Chen, M.W. Wong, J.L. Andres, E.S. Replogle,

R. Gomperts, R.L. Martin, D.J. Fox, J.S. Binkley, D.J. Defrees, J. Baker, J.P. Stewart, M. Head-Gordon, C. Gonzalez, and J.A. Pople, Gaussian, Inc., Pittsburgh PA, 1995; J.B. Foresman and A. Frish, Exploring Chemistry with Electronic Structure Methods (Gaussian Inc., 1996).

[13] R. Krishnan, J.S. Binkley, R. Seeger, J.A. Pople, J. Chem. Phys. 72 (1980) 650.

[14] S.B. Boys, F. Bernardi, Mol. Phys. 19 (1970) 553.

[15] P. Valiron, I. Mayer, Chem. Phys. Lett., 275 (1997) 46.

[16] R.A. Aziz, M.J. Slaman, J. Chem. Phys. 94 (1991) 8047.

[17] E. Widmann, I. Sugai, T. Yamazaki, R.S. Hayano, T. Ishikawa, S.N. Nakamura, H. Tamura, T.M. Ito, A. Kawachi, N. Nishida, Y. Ito, N. Morita, F.J. Hartmann, H. Daniel, T.v. Egidy, W. Schmid, F.J. Hofmann, J. Eades, Phys. Rev. A 51 (1995) 2870.

[18] S.I. Fedotov, O.I. Kartavtsev, D.E. Monakhov, Phys. of Atoms and Nucl. 59 (1996) 1717.

[19] G. Ya. Korenman, Hyp. Int. 119 (1999) 227.

[20] W.H. Press, B.P. Flannery, S.A. Teukolsky, W.T. Vetterling, Numerical Recipes, Ed. Cambridge University Press, 1986.

[21] W.A. Beck, private communication.

[22] B. Ketzer, F.J. Hartmann, T.v. Egidy, C. Maierl, R. Pohl, J. Eades, E. Widmann, T. Yamazaki, M. Kumakura, N. Morita, R.S. Hayano, M. Hori, T. Ishikawa, H.A. Torii, I. Sugai, D. Horváth, J. Chem. Phys., 109 (1998) 424.

Chapter 4

Collisional quenching of cold antiprotonic atomcules by H_2 molecules

Contents

4.1 Présentation générale de l'étude

Introduction

Nous étudions la destruction collisionnelle sélective des atomcules par l'hydrogène moléculaire afin d'interpréter les mesures résolues en état obtenues à basse température. Ces mesures mettent en évidence la persistence d'une destruction collisionnelle à 30 K avec des sections efficaces quasi-géométriques pour les états $n = 38$ et 39.

Démarche et résultats

Nous analysons la surface d'énergie potentielle complète (6-D) calculée en *ab initio*, à partir des concepts simples de physique moléculaire issus du cadre Born-Oppenheimer. Notre stratégie consiste à moyenner la surface d'énergie potentielle sur les mouvements rapides des noyaux afin de réduire la dimensionalité du problème. Après une moyenne sur les orbites rapides de l'antiproton et plus généralement sur les états ro-vibroniques quantiques de l'atomcule et de H_2, nous identifions des chemins réactifs avec des barrières d'activation de quelques 100 μH. Ainsi, nous rendons compte qualitativement de l'ordre de grandeur des sections efficaces géometriques mesurées à 30 K pour les états $n = 38$ et 39 avec leur dépendance en l. Cependant, l'écart entre les barrières demeure surestimé d'un facteur 2.

Le résultat le plus inattendu est l'effet de délocalisation quantique ro-vibronique des noyaux légers (p,$\bar{p}$): les corrections vibrationnelles abaissent les barrières d'environ 0.2 mH, alors que la moyenne sur l'état de rotation de H_2 est fortement répulsive: la moyenne est défavorable à l'état $J = 0$ (para-H_2) et nous attribuons la destruction collisionnelle à 30 K à l'espèce orientée $J = 1$ (ortho-H_2). A des températures plus élevées, les espèces ortho et para contribueraient efficacement à la destruction collisionnelle via des états de J plus élevé.

Nous discutons l'importance relative d'autres effets à prendre en compte pour faire des prédictions quantitatives. Une surface d'énergie convergée à quelques 10 μH – au niveau de théorie coupled-cluster CCSD(T) ou CCSD(T)-R12 – est à portée des calculateurs actuels. Une réduction du coût numérique nécessitera le développement de bases d'orbitales moléculaires spécifiques pour d'écrire l'anti-liaison et la polarisation du nuage électronique autour de la particule α. Sauf pour de très grandes bases, les corrections d'erreur de superposition de base sont nécessaires. Les effets de relaxation de géométrie des monomères et de relaxation dynamique sont plus faibles que les corrections ro-vibroniques mais restent significatifs par rapport à 30 kT. En plus de ces effets, les modèles devront également tenir compte de la relaxation correspondante des énergies vibrationnelles de point zéro pour les deux monomères. Enfin, traiter la dynamique collisionnelle sera inévitable pour prédire des sections efficaces absolues et pour la prise en compte d'autres effets (couplages non Born-Oppenheimer, effet tunnel, résonances et transitions Auger induites par collision).

Conclusions

Ces mesures basse température résolues en état imposent des contraintes très stimulantes sur les modèles théoriques et devraient fournir des résultats de référence pour des études physico-chimiques détaillées à quatre corps. Ces mesures pourraient par ailleurs éclairer la physico-chimie des molécules ou radicaux terrestres et interstellaires froids. En particulier, les corrections ro-vibroniques et les effets de relaxation dynamique pourraient se révéler significatifs dans les processus d'excitation faisant intervenir des liaisons légères.

Publication

Submitted to *Chemical Physics* (2001)

Quenching of cold antiprotonic helium atoms by collisions with H_2 molecules

Sébastien Sauge and Pierre Valiron

Quenching of cold antiprotonic helium atoms by collisions with H_2 molecules

Sébastien Sauge and Pierre Valiron

Laboratoire d'Astrophysique de l'Observatoire de Grenoble, UMR 5571 CNRS — Université Joseph Fourier, B.P. 53, 38041 Grenoble Cedex 09, France

Abstract

We investigate the collisional quenching of cold metastable antiprotonic atomcules $[\bar{p}He^+]_{n,l}$ by H_2 molecules in view of the recent state-resolved measurements at CERN. Firstly, we determine *ab initio* the 6-D intermolecular interaction between the four (anti)nuclei at the CCSD(T)/CP level. After averaging the interaction over the fast $\bar{p}$ orbits, we exhibit reactive channels and activation barriers below few 100 μH. Hence, we account qualitatively for the order of magnitude and (n, l) dependence of the quenching cross sections measured at 30 K. However improving this overall agreement requires the determination of numerous finer contributions. We monitor the saturation of electronic correlation with larger basis sets; we estimate the importance of dynamical relaxation effects; and we stress the role of quantum vibrational and rotational delocalization for the light (p, $\bar{p}$) nuclei. The latter vibrational corrections lower the barriers, while the rotational H_2 averaging defavours isotropic para-H_2 ($J = 0$). As a result, we attribute the quenching at 30 K to ortho-H_2 ($J = 1$). Additional experiments at several temperatures and with para-H_2 would better constrain this ortho-para quenching selectivity, and would provide an ideal four-body benchmark for further chemical physics investigations (including tunneling, collision-induced Auger decay, etc).

1 Introduction

About 3% of antiprotons ($\bar{p}$) stopped in helium are trapped on $\bar{p}He^+$ metastable bound states named atomcules, which survive several microseconds, for helium densities varying over several orders of magnitude [1]. Apart from their unique dual structure investigated by spectroscopy [2] — a near-circular quasi-classical Rydberg atom with $l \sim n - 1 \sim 37$ or alternatively, a special diatomic molecule with a negatively charged $\bar{p}$ nucleus in high rotational $J = l$ state — the chemical physics aspects of their interaction with other atoms or molecules constitute also a challenging topic for molecular physics. While the

exotic atoms may resist to millions of collisions in pure helium, molecular contaminants are likely to destroy them effectively in one or few collisions [3]. The most spectacular effect is observed with H_2 [4] and O_2 [5], which destroy the metastability almost completely in concentrations of a few hundred ppm only. State-resolved decay rates could be measured at 30 K for various H_2 admixtures, using laser-induced lifetime shortening of high n-states [6]. Geometrical quenching cross sections of $10^{-15} - 10^{-16}$ cm^2 were then derived for the normally metastable states with $n=38$ and 39. In particular, the quenching cross sections increase by a factor of 2 with decreasing l values, which correspond to ascending elliptic states. Within a cascade of constant $v = n - l - 1$, inner states with $n = 38$ are found to be less quenched by a factor of 4 than those with $n = 39$. These data are likely to put severe constraints upon quenching models.

From the theoretical side, the case of pure helium has been already investigated in detail [7–9]: all models support the collisional stability of thermalized states with $n \leq 40$, which can be further attributed to the existence of a high activation barrier due to Pauli repulsion [7]. In addition, all models account for the destruction of the states with $n \geq 41$ during the thermalization stage, either by crossing of the activation barriers [7], Auger decay enhancement due to collisions [7,9], Stark mixing with Auger nonstable states [8,9], or via the formation of an He^+-$\bar{p}$-He^+ molecular ion [9]. Eventually, the molecular model complemented by Monte Carlo simulations of the thermalization stage [7] roughly accounts for the 3% observed trapping fraction of metastable states. To our present knowledge however, no mechanism has been provided so far for interpreting the strong collisional quenching by H_2 and O_2 molecules and its state-selectivity.

Pursuing earlier investigations relating the strong quenching by H_2 to the existence of reactive channels with low activation barriers [10], we present a *molecular physico-chemistry* approach to account for collisional effects arising from the detailed features of the potential energy surface (PES) to a few kT accuracy, while preserving a good description of the exotic system, which lies many atomic units above its ground state. Since both $\bar{p}He^+$ and H_2 molecules are constituted by a small number of particles, an accurate determination of their interaction by using elaborate *ab initio* quantum chemistry techniques is attainable, in spite of the high dimensionality of the PES.

Ab initio calculations of the $\bar{p}He^+$-H_2 Born-Oppenheimer 6-D PES are presented in Section 2. In Section 3, we identify the main reactive channel from a mere *classical* averaging over the fast rotating $\bar{p}$ Rydberg orbit [1] and we intro-

[1] Averaging the PES over $\bar{p}$ orbits is justified, in as much as the typical duration of a collision at 30 K is about 100 times longer than a $\bar{p}$ revolution, assuming an interaction length of few au.

duce state-dependent $[\bar{p}He^+]_{n,l}$-H_2 classical activation barriers for the reactive complex. The simplicity of the classical approach permits an estimation of geometry relaxation effects for both $\bar{p}He^+$ and H_2 molecules. In Section 4, we introduce step by step the *quantum* averaging over nuclear ro-vibronic states, thus allowing to sketch the interplay of finer "nuclear averaging" effects. In last Section, we discuss the convergence of the PES with respect to the largest standard basis sets available and we present estimated activation barriers for ortho- and para-H_2. Finally we stress the limitations and perspectives of our work in view of the remaining discrepancies with experimental data.

2 The Born-Oppenheimer $\bar{p}He^+$-H_2 interaction potential

Experiments establish the persistence of a strong state-selective collisional quenching down to 30 K. Accordingly, a reliable calculation should provide effective interaction potentials and — presumably — activation barriers converged to better than 0.1 mH. The Born Oppenheimer (BO) separation allows a very accurate determination of electronic energies for any internuclear configuration by using standard *ab initio* quantum chemistry techniques. This approximation is applicable since the $1s$ electron of a $[\bar{p}He^+]_{nl}$ atomcule moves about $n \sim 40$ times faster than the antiproton [11]. However, non adiabatic corrections might be larger than for normal molecules due to the fast $\bar{p}$ motion and would deserve subsequent studies.

The potential energy surface (PES) is 6-D, as illustrated in Fig. 1 using Jacobi coordinates. With respect to a spherical space-fixed reference frame with z intermolecular axis, each molecule is oriented by a set of spherical angles (θ_i, ϕ_i), $i = 1, 2$. Since the system is rotation invariant onto the intermolecular axis, the interaction potential solely depends upon the relative dihedral angle $\phi = \phi_r - \phi_\rho$, instead of ϕ_r *and* ϕ_ρ.

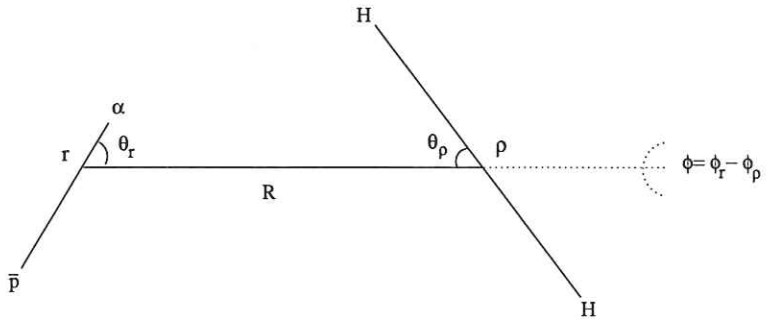

Fig. 1. Jacobi coordinate system used to describe the $\bar{p}He^+$-H_2 interaction. R is the intermolecular separation between both molecules centers of mass. ϕ is the out-of-plane dihedral angle.

State of art calculations may prove very time consuming to achieve MP2 saturation. We present here a compromise between accuracy and computational efficiency for sampling the *whole* PES. Convergence studies will be presented in Section 5 and Tables 3, 4.

The accuracy of individual points crucially depends upon (a) the method used for the treatment of electronic correlation and (b) the saturation of the basis set used. Both aspects are discussed hereafter.

(a) For an accurate treatment of correlation, we used the Coupled Cluster CCSD(T) method [13], which should approach the full CI energy for the present system involving *3* electrons, as it treats exactly all Single and Double excitations and provides a good approximation of Triples ones. One would anticipate the remaining contribution of triple excitations to be very small, since only one electron — the polarized e^- of the atomcule — is expected to play a specific role in the state-dependent quenching. This assumption has been confirmed a posteriori by the rapid convergence of the post-MP2 correlation energy and by the small contribution of Triples (see Section 5.1 and Table 4).

(b) Actually, no optimized basis set has been designed yet for investigating the physico-chemistry of exotic processes involving such $\bar{p}$ atomic bound states. For the atomcule, we included specific polarization orbitals, in order to describe the "anti-bounding" around the $\bar{p}$, and the strong polarization of the electronic cloud around the α by the closely orbiting $\bar{p}$. In addition, we uncontracted the He basis set to better model the hydrogenic 1s orbital. Exponents ξ of the α and $\bar{p}$ polarization orbitals were experimented in order to approach the SCF limit for representative α–$\bar{p}$ separations. For the α, we expanded the helium's 311++G basis set [14] into an uncontracted set of 3 s (ξ= 98.1243, 14.7689, 0.086), 3 sp (ξ= 3.31883, 0.874047, 0.244564) and 1 pure d (ξ= 1) functions. For the $\bar{p}$, we used a set of 3 shared exponents sp orbitals (ξ= 3, 10, 30) and 1 pure d function (ξ= 0.6). For the description of the H_2 molecule, we used the standard *triple zeta* 6-311++G(3pd) basis set [14] which contains an *s*-shell of 6 primitives, and multiple polarization functions (3 p and 1 d functions). This resulted in a total of 73 basis functions.

An inevitable difficulty arising from the use of finite basis sets in *ab initio* calculations is the appearance of the basis set superposition error (BSSE). The interaction energy was computed by using the usual counterpoise (CP) scheme [15] in the supermolecular basis (SM):

$$\Delta E_{int} = E_{\bar{p}He+-H_2}(SM) - E_{\bar{p}He+}(SM) - E_{H_2}(SM). \qquad (1)$$

The CP scheme can be generalized to cope with the geometry relaxation of monomers. The *total* potential energy is then obtained by adding to the *interaction* energy the *internal* energies of the (possibly relaxed) monomers,

calculated in their respective basis set [16]:

$$E_T = \Delta E_{int} + [E_{\bar{p}He^+} - E^0_{\bar{p}He^+}](\bar{p}He^+) + [E_{H_2} - E^0_{H_2}](H_2), \qquad (2)$$

where superscript "0" refers to the equilibrium geometry of the free monomers. For the isolated atomcule, $E_{\bar{p}He^+}$ was computed at the Hartree-Fock limit, which is exact for this one electron system. See [7] for further details.

All calculations used the *Gaussian94* package [17]. The CPU time for a single CCSD(T)/CP-corrected calculation at an intermolecular separation of 3.5 au is about 7 minutes on a RS6000/590 IBM workstation. Calculations at shorter distances are more expensive, mainly due to slower Hartree-Fock convergence. The resulting 6-D PES was computed over a mesh of 14400 points and required about 2400 CPU hours. With respect to the atomcule internal coordinates (r, θ_r), the mesh extends from 0.3 au to 1 au in r (0.3, 0.5, 0.7, 0.85, 1 au) and from 0 to 360° in θ_r, by step of 30° in the range $[-120, 120]$ and 20° outside. The more detailed sampling corresponds to the highest attractive regions of the PES. With respect to the H_2 molecule, ρ was sampled from 1 to 2 au by step of 0.25 au, and θ_ρ from 0 to 90° (0, 30, 45, 60, 90), making use of the PES invariance in the transformation $(\theta_r, \theta_\rho) \rightarrow (-\theta_r, \theta_\rho + \pi/2)$. In addition, the potential was assumed to be weakly dependent upon dihedral angle $\phi = \phi_r - \phi_\rho$. This statement is exact for $\theta_\rho = 0$ and will be validated a posteriori in Section 4.4, after averaging the PES over H_2 rotation states (see Fig. 11 and 12). Accordingly, the ϕ dependence was sampled for $\phi = 0$ and $\pi/2$ only. Intermolecular separation R was sampled regularly from 3.2 to 4.4 au by step of 0.4 au for $\phi = \pi/2$, complemented by 5 and 6 au for $\phi = 0$. For each value of ϕ and intermolecular distance R, a spline interpolation of the 4-D stripes of the PES was performed. *Ab initio* PES and interpolation routines are available in electronic form in demand [18]. Classical and quantum averaging of the PES over ro-vibronic nuclear states are presented in the next two sections, respectively.

3 Classical PES averaging

3.1 Introduction

Since metastable Rydberg states bear large (n, l) quantum numbers, a classical treatment of the slow (α, $\bar{p}$) nuclei in the BO interaction potential provides a first step towards a full quantum mechanical study, at least as far as finer quantum effects are not considered. From a classical description of both $\bar{p}He^+$ and H_2 molecules, which is discussed in Section 3.2, we identify the main reactive channel in Section 3.3 and we estimate activation barriers

in Section 3.4. We investigate dynamical and geometrical relaxation of both interacting monomers in Section 3.5. Resulting cross sections are presented in Section 3.6.

3.2 Classical BO description of the $[\bar{p}He^+]_{nl}$ and H_2 molecules

In our classical picture, the antiprotonic Rydberg states are described by enforcing a semi-classical quantization of the orbits in the effective $[\bar{p}He^+]_{n,l=J}$ potential, which is the sum of the corresponding ground state BO electronic potential and of the centrifugal potential. Reproducing theoretical energies [19] of given n states constrains the classical orbit of the circular state and semi-major axis of the elliptic ones, as illustrated in Fig. 2. Alternatively, Bohr quantization of the circular states is sufficient to provide a few 10^{-3} relative accuracy on the energies [7].

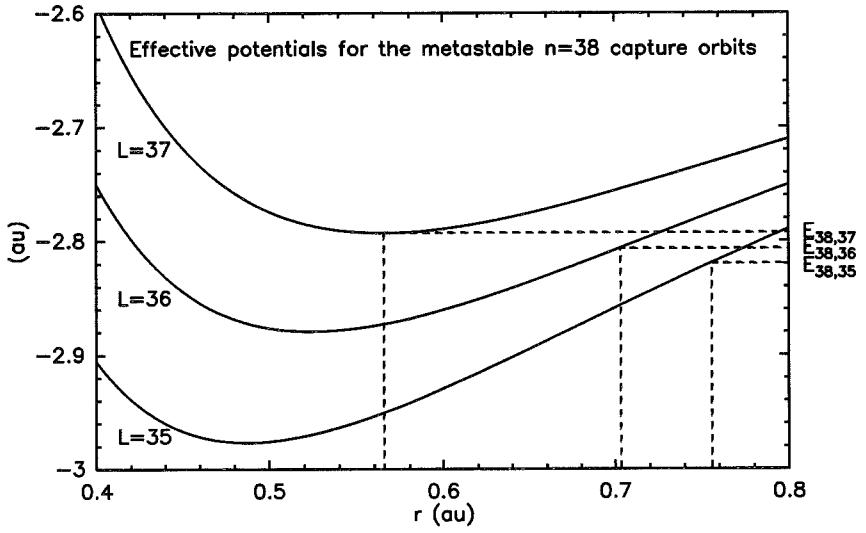

Fig. 2. Semi-classical quantization of the effective $[\bar{p}He^+]_{n,l=J}$ potential (solid lines). Reproducing theoretical energies [19] of given (n,l) states constrains the classical orbit of the circular state $(n, n-1)$ and semi-major axis of the elliptic ones (dashed lines). The semi-minor axis is constrained analogously.

The H_2 molecule is described as a rigid rotor, with an equilibrium bond length of 1.4 au. Below 100 K, only $J = 0, 1$ rotation states of H_2 are significantly populated. Para-H_2 ($J = 0$) is isotropic and can be modeled in our classical picture by averaging the potential over three orthogonal orientations. Ortho-H_2 ($J = 1$) is orientable and matches very roughly the rigid body picture for $m_J = 0$, while it corresponds to a rotating disk for $m_J = \pm 1$.

3.3 Classical reactive channels: illustration for the $n = 38$ circular orbit

Looking for classical reactive channels, we considered limiting conformations of both atomcule and H_2. As a first step, we neglected the geometry relaxation of the atomcule and we averaged the PES over a typical unperturbed circular $\bar{p}$ orbit, namely the $n = 38$ one with classical radius $r_n = 0.565$ au. As can be seen in Fig. 3, the height of the activation barriers is of the order of a few mH, to be compared with the much higher ones obtained in He, which are about 100 mH [7]. The classical molecular picture therefore provides a first qualitative explanation of the quenching of atomcules by H_2, while already accounting for their collisional survival in pure He. The most reactive channel presents a barrier below 1 mH and corresponds to the coplanar and colinear approach for H_2 (see Fig. 3 d). Considering this approach, the quenching by colinear ortho-H_2 ($J = 1, m_J = 0$) would be efficient down to room temperature at least (1 mH $\equiv$ 300 kT). Alternatively, quenching by isotropic para-H_2 ($J = 0$) would be described by averaging the barriers over the three orthogonal orientations in Fig. 3 a, b, d. The resulting averaged barrier is obviously higher by several mH. Quenching by para-H_2 ($J = 0$) is thus expected to be negligible at lower temperatures and defavoured at room temperature. Quenching by ortho-H_2 ($J = 1, m_J = \pm 1$) would be similarly defavoured for all atomcule orientations[2]. All other metastable (n, l) orbits present a similar behaviour. Better estimates of activation barriers will be presented in Section 4 based upon a proper quantum averaging.

3.4 Classical activation barriers

Due to the screening by the remaining electron, the (α, $\bar{p}$) interaction is not coulombian, and the antiprotonic system follows unclosed precessing orbits for all elliptical states. In consequence there is no closed circuit available for averaging the intermolecular interaction, with depends over both phase and precession angles. We present here an alternate treatment in order to estimate activation barriers for both circular and elliptic states without any explicit averaging. As in the previous section, we keep fixed the center of mass of both monomers.

The interaction energy $E_a^{nl}(R)$ corresponds to the energy required to bring H_2 from infinity to R. Equivalently, it can be determined while keeping H_2 at fixed intermolecular separation R, and branching the interaction *adiabatically*, i.e. with a time constant τ much greater than the typical $\bar{p}$ revolution and

[2] For the atomcule orientation depicted in Fig. 3, the interaction was estimated by averaging over panels a and b; similar results were obtained in the parallel-parallel configuration (not depicted in the Figure).

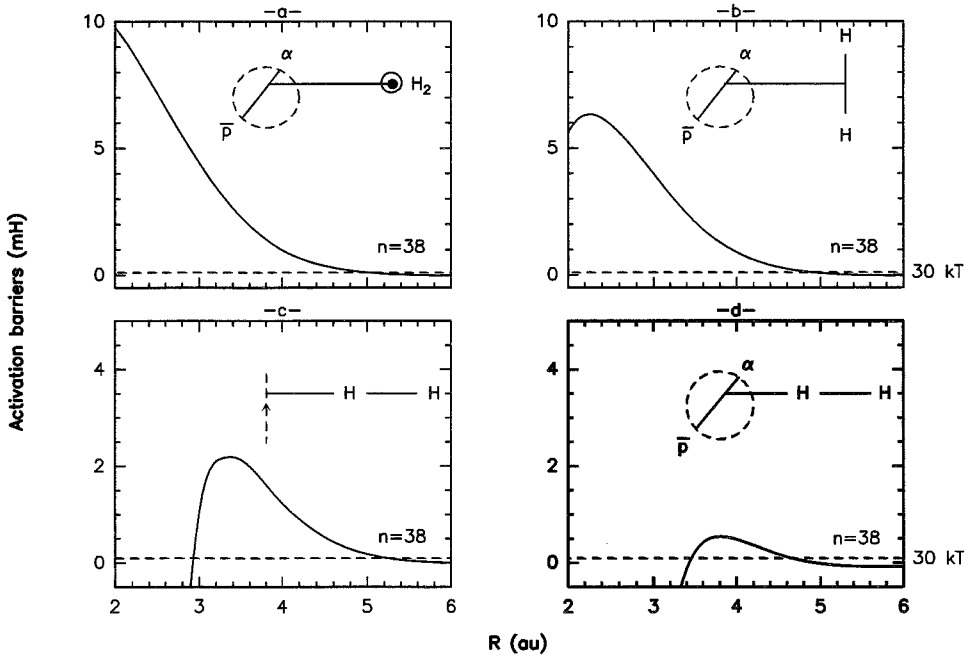

Fig. 3. $[\bar{p}He^+]_{n=38,l=37}$-$H_2$ interaction potential (in mH units) for several mutual orientations of atomcule and H_2. The most reactive orientation is depicted in panel d (in bold).

precession periods. Thus, $E_a^{nl}(R)$ is given by the total energy difference with respect to the time τ during which the interaction is branched between both monomers kept at fixed intermolecular separation R:

$$E_a^{nl}(R) \equiv E_T(R, t = \tau) - E_T(R, t = 0)\,. \tag{3}$$

For the atomcule, the trajectories of the α and $\bar{p}$ nuclei in the slowly rising PES were predicted by integrating the classical equations of motion. The initial $\bar{p}$ Rydberg orbits were those determined from the semi-classical quantization of the effective $[\bar{p}He^+]_{n,l=J}$ potential (see Section 3.2, Fig. 2). The initial angular momentum $L(t = 0)$ obeys the classical limit $L(t = 0) = l + 1$. Technically, the center of mass of the atomcule was kept fixed by zeroing the PES gradient with respect to the R intermolecular coordinate. This condition is equivalent to solving the dynamical equations for the (α, $\bar{p}$) reduced particule. Analogously to the previous section, H_2 was kept rigid. Fig. 4 illustrates the time evolution of the atomcule classical radius and angular momentum, as well as the rise of the interaction energy, until the branching is complete. When increasing the branching duration, the convergence of the interaction energy is faster than the disappearance of the residual tiny oscillations visible in panel C.

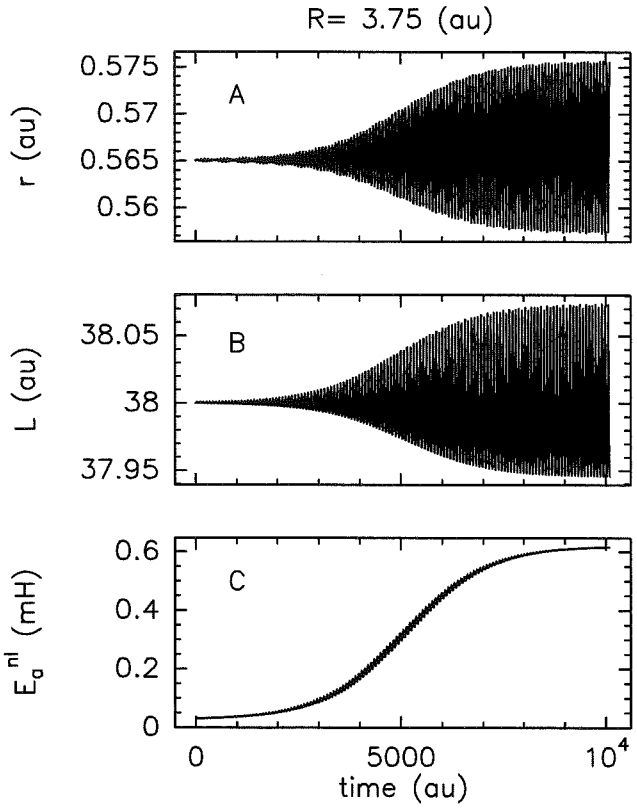

Fig. 4. Classical observables of an atomcule lying in the circular state $(n, l) = (38, 37)$ and interacting adiabatically with H_2 distant from R= 3.75 au. The figure displays time evolution of the classical radius (A) and angular momentum (B) of the atomcule. The initial angular momentum obeys the classical limit $L(t = 0) = l + 1$. The activation barrier (C) rises as the interaction is branched.

State dependent $[\bar{p}He^+]_{n,l}$-H_2 interaction potentials $E_a^{nl}(R)$ were subsequently derived as a function of intermolecular distance R. They are presented in Fig. 5 for the circular state and first two elliptic ones, for principal quantum numbers n ranging from 37 to 40. As can be seen, interaction potentials present a net reduction of their activation barrier with increasing n values. The activation barriers even vanish for the states with $n \geq 39$, accounting for the geometrical quenching cross sections measured for these states. A moderate decrease is also observed for the adjacent elliptic states. This can be attributed to a reduction of Pauli shielding, as the $\bar{p}$ moves outside the electronic cloud for high n states or more extended elliptic levels[3]. Therefore our model accounts — at least very qualitatively — for the (n, l) dependence of the experimental quenching cross sections.

[3] This effect already accounted for the quenching of high n states by He [7].

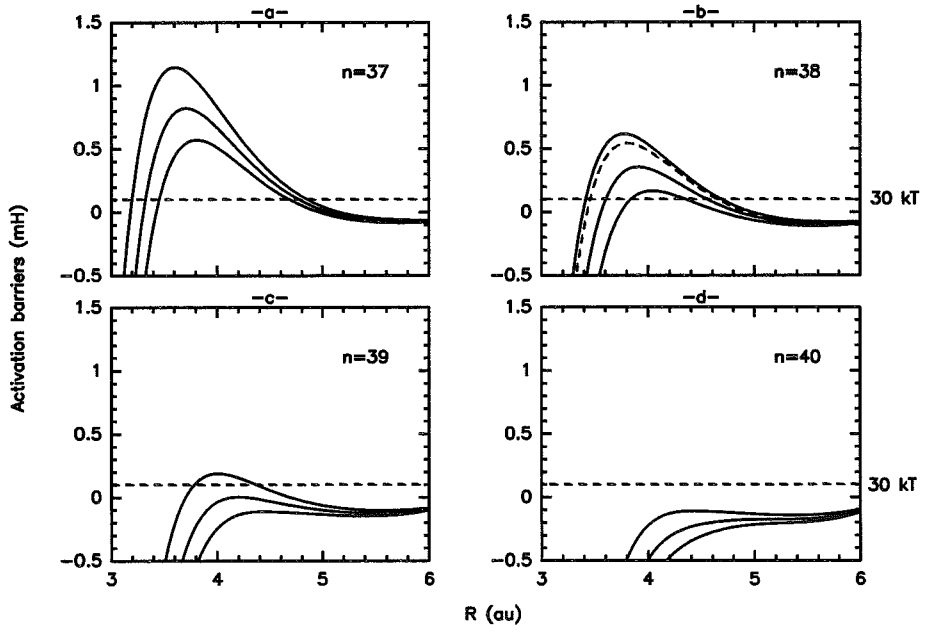

Fig. 5. State dependent $[\bar{p}He^+]_{n,l}$-H_2 interaction potentials derived by a classical averaging over nuclear motions in the adiabatic approximation and for the most reactive approach (see Fig. 3 d). Within each box, the three curves correspond to the states with vibrational quantum number $v = n-l-1 = 0, 1, 2$ (circular state and first two elliptic ones). The dashed curve in panel b corresponds to the averaging over the rigid $n = 38$ circular orbit displayed in Fig. 3 d.

3.5 Dynamical and geometry relaxation effects

Neglecting internal vibration modes, usual molecules can be approximated as rigid bodies. Geometry relaxation effects describe the subsequent adjustment of bond lengths and angles in response to the intermolecular interactions. The rigid-body picture itself needs to be generalized for dynamical systems such as atomcules, which must be averaged over their internal degree of freedom. In Section 3.3 we averaged the potential over a fixed orbit. In Section 3.4 we still fixed the atomcule's center of mass but we let the orbit relax under the influence of the intermolecular interactions. We shall discuss here independently (a) the validity of this "restricted" dynamical relaxation of the atomcule and (b) the geometry relaxation of H_2. The more general dynamical relaxation problem — where the intermolecular separation is only enforced *in average* — would deserve further study.

The dynamical relaxation effects are related to the angular anisotropy of the PES along both p and $\bar{p}$ trajectories. If for instance we only consider the most

reactive approach (see Fig. 3 d), the magnitude of this modulation for the atomcule is given by the energy difference between the most attractive (α-$\bar{p}$-H_2) and repulsive ($\bar{p}$-α-H_2) conformations. For a collision energy of 30 kT, the modulation of the PES for the α-$\bar{p}$ separation corresponding to the circular state $n = 38$ has a value of 0.1 eV at the classical turning point, whereas typical transition energies between adjacent states with same n are about 0.3 eV. In addition to orbit relaxation effects, this modulation might also induce non-diagonal effects in a quantum framework, such as l-changing transitions, which could in turn affect the state-resolved quenching cross-sections.

(a) The effect of the "restricted" dynamical relaxation of the atomcule is apparent in Fig. 5, panel b for the circular state $n = 38$ (where the dashed curve refers to the unrelaxed interaction). The contribution of this "restricted" relaxation is *repulsive* by about 0.1 mH. As relaxation effects are always attractive, this result manifests the need for an unrestricted model where the atomcule center of mass is only fixed in average. In order to fulfill invariance properties of the global center of mass, the center of mass of H_2 should also be allowed to wiggle around its average position. Thus this fully "unrestricted" treatment of dynamical relaxation implies to consider the correlation of the dynamical fluctuations of the centers of mass of both monomers under the field of the interacting potential. This more difficult problem will be postponed to a later study. We assumed that the "unrestricted" dynamical relaxation presents a comparable magnitude to the spurious repulsion above, about 0.1 mH, but in the *attractive* direction.

(b) H_2 also undergoes some relaxation, which is weaker since the H-H potential is very steep. We estimated the relaxed H-H bond length by adding the relaxation energy of the H_2 molecule to the interaction energy, following Eq. (2). For each intermolecular separation, the PES was calculated for three H_2 bond lengths (ρ = 1.4, 1.45, 1.5 au) and interpolated by a quadratic polynomial. Eventually, the minimum energy was estimated, thus constituting the relaxed PES [4], which is shown in Fig. 6. Taking into account H_2 relaxation lowers the barrier of the circular state $n = 38$ by few 0.01 mH in the vicinity of the activation barrier.

Therefore, the distorsion of both monomers is weak but not negligible at 30 K. By properly taking into account above relaxation effects, activation barriers should be shifted *down* by about -0.10 mH ($\equiv$ 30 kT) or more. In addition to these effects of classical origin, one should also take into account the relaxation of zero-point vibrational energies of both monomers.

[4] The calculations were carried out at the UMP4-SDTQ level of theory, for reasons of computational efficiency (thus the barrier is higher and slightly shifted left).

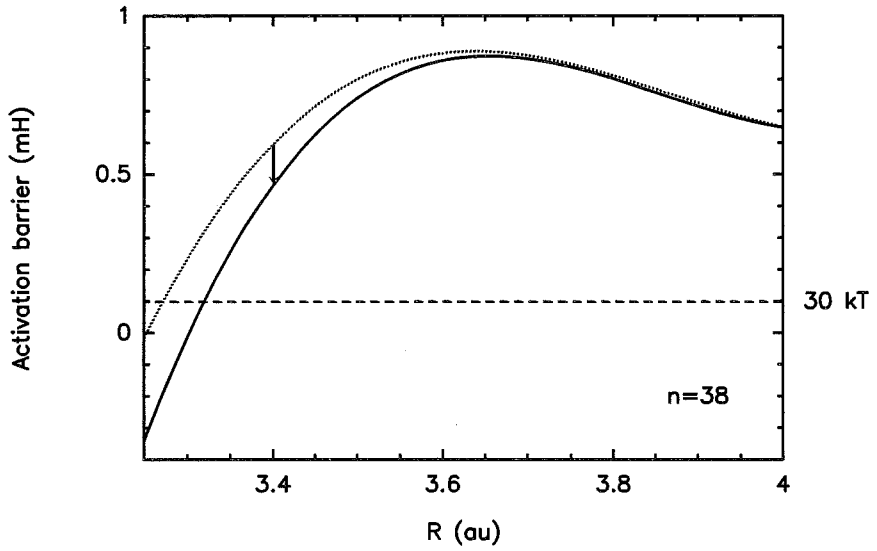

Fig. 6. Influence of geometry relaxation of the H_2 equilibrium bond length for the atomcule lying in the $n=38$ circular state. The relaxed PES (solid line) is compared with the unrelaxed one (dotted line).

3.6 Quenching cross sections estimates

In order to compare to experimental data, we tried to relate activation barriers E_a^{nl} to quenching cross sections, by considering a simple hard sphere reaction model. This results in an Arrhenius law for the quenching cross sections, which are given by

$$\sigma_q^{Arr} = \sigma_0 \exp\left(-\frac{E_a^{nl}}{kT}\right), \tag{4}$$

where σ_0 is the geometrical cross section for the $[\bar{p}He^+]_{nl}$-H_2 collision. σ_0 can be estimated from the van der Waals radii of the He atom ($r_{He} = 1.2$ Å) and H_2 molecule ($r_{H_2} = 1.38$ Å), which leads to a value of 21 10^{-16} cm^2 [4]. The results are compared to experimental quenching cross sections in Table 1. Of course, this very crude model is only applicable for the states which present a positive activation barrier, and the comparison of cross-section ratios is expected to be more instructive than the direct comparison of absolute cross-section values. In short, the interpretation of activation barriers in term of Arrhenius laws leads to cross sections ratios of 70 between the circular states $n = 39$ and $n = 38$, in disagreement with experiments by a factor of 10.

Accordingly, the spacing between these activation barriers should be reduced to 0.2 mH instead of 0.4 mH. Besides, predicted cross sections ratios between adjacent l states are about 3 times too large. Thus the spacing between the corresponding activation barriers should also be reduced to about 0.1 mH instead of 0.2 mH. As a preliminary conclusion, the predicted activation barrier spacings are overestimated by a factor of two.

Despite these discrepancies, there is a promising agreement with experimental data. The largest experimental cross sections match the channels predicted with no activation barriers, and the Arrhenius cross sections are consistent with geometrical estimates as expected in this case. In addition, the ordered sequence of experimental cross sections is nicely consistent with the theoretical activation barriers.

n	l	E_a^{nl}	σ_q^{Arr}	σ_q^{Exp}
38	37	0.618	0.043	0.89
37	34	0.573	0.068	1.1
38	36	0.356	0.60	2.6
39	38	0.189	3.1	5.4
38	35	0.168	3.9	6.8
39	37	0.004	20	13
39	36	-0.110	(63)	26
39	35	-0.183	(130)	28

Table 1
State-dependent activation barriers E_a^{nl} (mH), predicted quenching cross sections σ_q^{Arr} (see text) and experimental quenching cross sections σ_q^{Exp} (in units of 10^{-16} cm^2) at 30 K ($\equiv$ 0.1 mH).

4 Quantum PES averaging

4.1 Introduction

A proper determination of state-dependent interaction potentials requires a quantum averaging of the PES over the nuclear ro-vibronic states. In the Born-Oppenheimer (BO) framework, the total nuclear wave function is expressed as a tensorial product of the monomers ro-vibrational wave functions. Since geometry relaxation processes are weak, we can safely assume that the relevant vibrational eigenstates are very close to those of the unperturbed monomers. In addition H_2 lies in its zero point vibrational eigenstate at sub-thermal con-

ditions. However, we emphasize that the determination of interactions energies should take into account the spatial extension of vibrational wave functions for such "light" molecules, contrarily to the common "lazy" practice of substituting vibrational delta functions located over the equilibrium geometries of each monomer. Quantum ro-vibronic wave functions are determined in Section 4.2, whereas the PES averaging is explicited in further details in Section 4.3. State dependent interaction potentials are presented in Section 4.4 via a step by step averaging, which allows to estimate the respective influence of ro-vibronic nuclear effects on the height of the activation barriers. The proper quantum description of relaxation effects depicted classically in Section 3.5 will be investigated elsewhere.

4.2 Quantum ro-vibronic states

In the standard BO framework, the total nuclear wave function ψ_N is expressed as the product of the respective ro-vibronic wave functions, which can be separated into radial and angular parts, if we assume a weak coupling between vibration and rotation:

$$\psi_N = \phi_{v_1 J_1 m_1} \cdot \phi_{v_2 J_2 m_2} = \chi_{v_1}(r) Y_{J_1}^{m_1}(\Omega_r) \cdot \chi_{v_2}(\rho) Y_{J_2}^{m_2}(\Omega_\rho) \,. \qquad (5)$$

Hereafter, subscripts "1" and "2" refer to the atomcule and H_2 molecule, respectively. χ_{v_i} and $Y_{J_i}^{m_i}$ $(i = 1, 2)$ denote the vibrational wave function and the usual spherical harmonic for the state (v_i, J_i, m_i) with vibrational (v_i) and rotational (J_i, m_i) quantum numbers, respectively. $\Omega_r = (\theta_r, \phi_r)$ and $\Omega_\rho = (\theta_\rho, \phi_\rho)$ describe the orientation of the atomcule $(\mathbf{r})$ and H_2 molecule (ρ) with respect to the intermolecular vector $(\mathbf{R})$, as illustrated in Fig. 1.

One should expect the vibrational wave functions to relax adiabatically, as the interacting monomers undergo some weak distorsion. In order to model relaxation effects, the ground state vibrational wave function should either depend explicitely upon the intermolecular separation or alternatively, be coupled to higher excited states corresponding to closed vibrational channels. However the distorsion of monomers is weak, as shown in Section 3.4. As a consequence, we assume here that both atomcule and H_2 will remain unrelaxed in their original vibrational state, down to intermolecular separations corresponding to the crossing of the activation barriers. Subsequent corrections for relaxation effects should also take into account the corresponding zero-point energy shifts for the atomcule and for H_2, as noted previously.

Vibrational wave functions were estimated analytically by fitting a Morse function to the interaction potentials [20]. The complete derivation is recalled in Appendix. Radial probability densities for both atomcule and H_2 are displayed in Fig. 7 and 8. Considering the spatial extension of vibrational wave functions

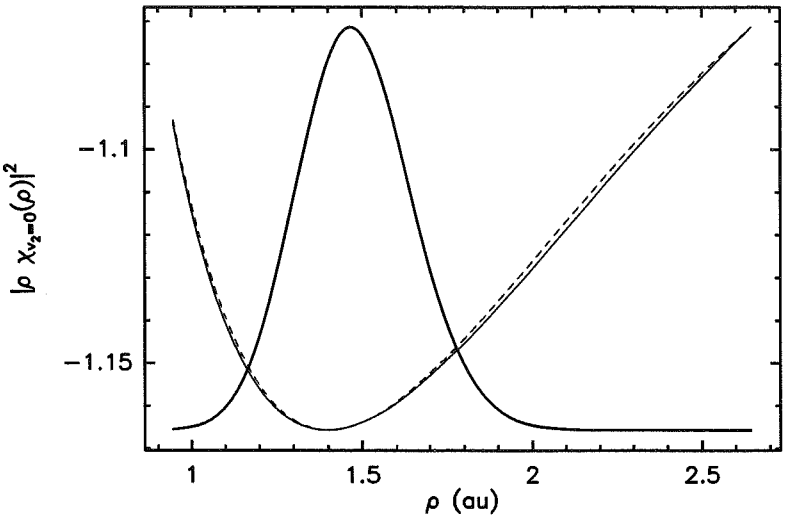

Fig. 8. Zero point vibrational eigenfunction (bold curve) in the H_2 well (solid curve). The parameters of the Morse potential (dashed curve) for H_2 are derived from spectroscopic measurements [21].

coordinates, and express the equation for ψ_N as

$$H_N\,\psi_N = e\,\psi_N, \tag{8}$$

with $H_N = T_N + E_T$. E_T depends upon intramolecular (internal) coordinates (r and ρ) and intermolecular ones (R), as shown in Fig. 1. Likewise, the nuclear kinetic operator can be written

$$T_N = T_{\bar{p}He^+} + T_{H_2} + T_{\bar{p}He^+-H_2}, \tag{9}$$

where the first two terms denote the internal kinetic operators of the respective monomers and the last term is the intermolecular kinetic operator. The Hamiltonian H_N can thus be rewritten as

$$H_N = [T_{\bar{p}He^+} + E_{\bar{p}He^+}] + [T_{H_2} + E_{H_2}] + T_{\bar{p}He^+-H_2} + \Delta E_{int}\,. \tag{10}$$

The averaged PES is recovered from the expectation value of H_N over the nuclear ro-vibronic wave function ψ_N from Eq. (5)

$$\langle H_N\rangle = E_{v_1J_1} + E_{v_2J_2} + \langle T_{\bar{p}He^+-H_2}\rangle + \langle \Delta E_{int}\rangle, \tag{11}$$

where $E_{v_1J_1}$ and $E_{v_2J_2}$ are the energies of the isolated molecules, which are constant within our model as we do not consider monomer relaxation effects

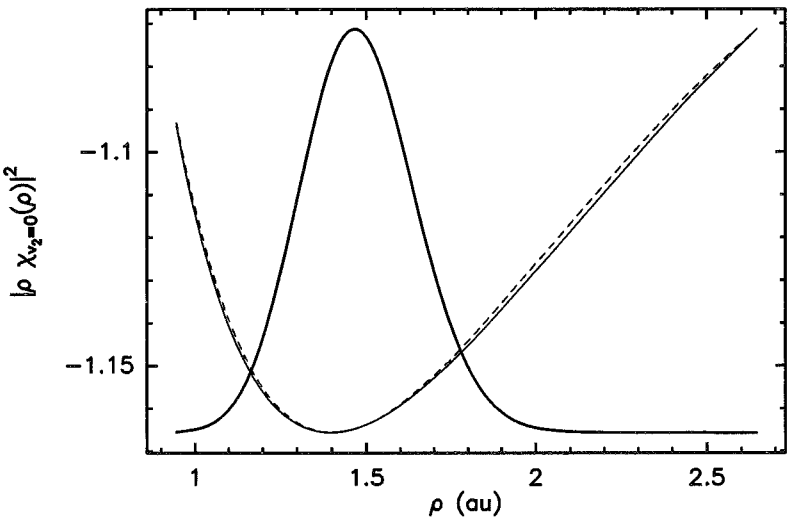

Fig. 8. Zero point vibrational eigenfunction (bold curve) in the H_2 well (solid curve). The parameters of the Morse potential (dashed curve) for H_2 are derived from spectroscopic measurements [21].

coordinates, and express the equation for ψ_N as

$$H_N \psi_N = e \psi_N, \tag{8}$$

with $H_N = T_N + E_T$. E_T depends upon intramolecular (internal) coordinates (r and ρ) and intermolecular ones (R), as shown in Fig. 1. Likewise, the nuclear kinetic operator can be written

$$T_N = T_{\bar{p}He^+} + T_{H_2} + T_{\bar{p}He^+-H_2}, \tag{9}$$

where the first two terms denote the internal kinetic operators of the respective monomers and the last term is the intermolecular kinetic operator. The Hamiltonian H_N can thus be rewritten as

$$H_N = [T_{\bar{p}He^+} + E_{\bar{p}He^+}] + [T_{H_2} + E_{H_2}] + T_{\bar{p}He^+-H_2} + \Delta E_{int}\,. \tag{10}$$

The averaged PES is recovered from the expectation value of H_N over the nuclear ro-vibronic wave function ψ_N from Eq. (5)

$$\langle H_N \rangle = E_{v_1 J_1} + E_{v_2 J_2} + \langle T_{\bar{p}He^+-H_2} \rangle + \langle \Delta E_{int} \rangle, \tag{11}$$

where $E_{v_1 J_1}$ and $E_{v_2 J_2}$ are the energies of the isolated molecules, which are constant within our model as we do not consider monomer relaxation effects

and subsequent zero-point energy shifts. $T_{\bar{p}He^+-H_2}$ corresponds to the scattering kinetic operator. The remaining term is a convolution of the interaction potential over the nuclear ro-vibronic eigenfunctions: it is readily interpreted as the state dependent $[\bar{p}He^+]_{v_1 J_1 m_1}$-$[H_2]_{v_2 J_2 m_2}$ interaction potential:

$$E_a^{nl}(R) = \langle \psi_{v_1 J_1 m_1} \psi_{v_2 J_2 m_2} | \Delta E_{int} | \psi_{v_1 J_1 m_1} \psi_{v_2 J_2 m_2} \rangle \,. \tag{12}$$

The vibrational PES averaging generalizes the usual rigid body approximation, which is recovered by replacing the trial wave functions by dirac functions located over the equilibrium geometries of each monomer. This effect is generally omitted in any practical calculations, except for very accurate few-body systems, such as H_2+H_2 or H_2+HD.

Prior to any approximation, state dependent interaction potentials are given by the following 5-D integral

$$E_a^{nl}(R) = \int_{(5)} r^2 dr\, \rho^2 d\rho\, d\Omega\, |\chi_{v_1}(r)\, Y_{J_1}^{m_1}(\Omega_r)|^2\, \Delta E_{int}\, |\chi_{v_2}(\rho)\, Y_{J_2}^{m_2}(\Omega_\rho)|^2, \tag{13}$$

where the solid angle element $d\Omega = \sin\theta_r\, d\theta_r\, \sin\theta_\rho\, d\theta_\rho\, d\phi$. In so far as we only consider the reactive colinear approach, the projection of the angular momentum of both atomcule and H_2 along the intermolecular axis chosen as quantization axis is zero. Accordingly, $m_1 = m_2 = 0$. In addition, the integral over $\phi = \phi_r - \phi_\rho$ was replaced by a discrete summation, since the activation barriers are weakly dependent upon ϕ (see Fig. 11 and 12):

$$\int d\phi = (2\pi)^2 \times \frac{1}{2} \sum_{\phi=0,\frac{\pi}{2}}, \tag{14}$$

where the $(2\pi)^2$ factor arises from the normalization of the 2 spherical harmonic functions with respect to ϕ_r and ϕ_ρ. The subsequent 4-D integral was then estimated by performing a cubic spline interpolation of the PES in each dimension. This interpolation scheme proved to be adequate since the integrand in the last dimension appeared to be very smooth (see confirmation below). The state-dependent interaction potentials obtained from the evaluation of the PES integral in Eq. (13) are presented in next sub-section.

4.4 Resulting quantum PES

In order to sketch a hierarchy of the different nuclear averaging effects, we estimated the PES integral in Eq. (13) by a step by step averaging over the ro-vibronic nuclear states. The PES was first averaged over the ro-vibronic

states ($v_1 = n-l-1, J_1 = l$) of the atomcule [5], while keeping H_2 as a classical rigid-body with a fixed bond length ($\rho = 1.4$ au) in the most reactive colinear approach ($\theta_\rho = 0$, $\phi = 0$), resulting in a 2-D PES integral in Eq. (13). In a second step, H_2 was considered as a non rotating colinear molecule lying in the $v_2 = 0$ vibrational ground state ($\phi = 0$) and the subsequent 3-D PES integral was computed. Eventually, we investigated in a third step the ortho-para selectivity effects by averaging the PES over H_2 rotation states, either $J_2 = 0$ (isotropic para-H_2) or $J_2 = 1$ (ortho-H_2 in the colinear orientation $m_2 = 0$), leading to the complete 4-D PES integral.

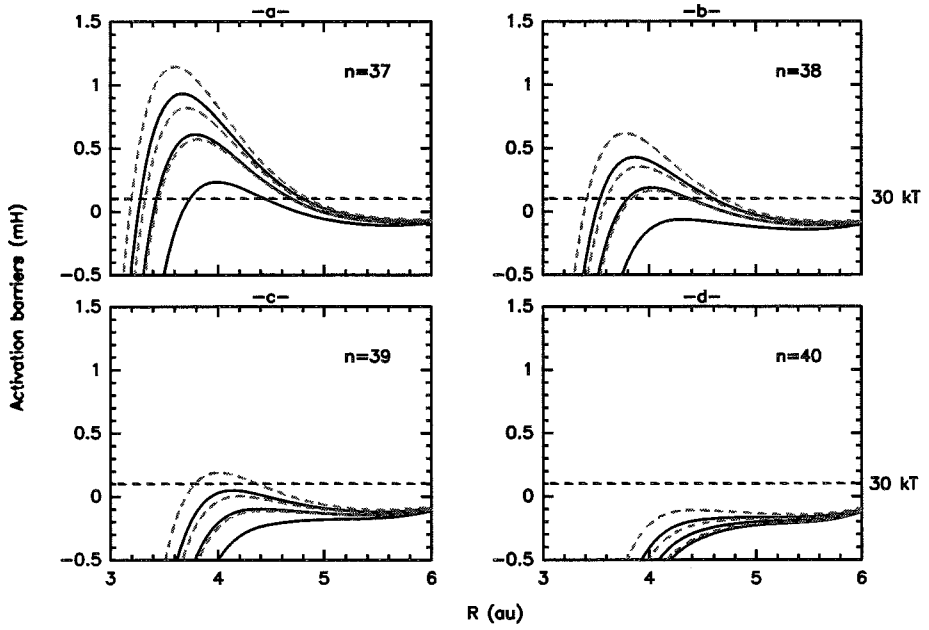

Fig. 9. State-dependent $[\bar{p}He^+]_{n,l}$-H_2 first-step quantum PES (solid lines, see text). The classical activation barriers from Fig. 5 are reproduced in grey dotted lines. For each value of n, the circular state and the first two elliptic ones are represented.

The first-step PES (quantum-averaged over the atomcule ro-vibronic states only) are presented in Fig. 9 and compared to the classically-averaged PES taken from Fig. 5. All activation barriers appear to be shifted down by about 0.2 mH, namely $(n,l) = (37, 34..36)$, $(38, 35..37)$ and $(39, 38)$. The latter tiny barrier is pushed below 30 kT. The other states — which present no positive activation barrier — are also shifted down by comparable shifts in the same intermolecular range. However this comparison exaggerates the importance of the first step shift as the classically averaged PES includes a spurious positive shift of about 0.1 mH (see discussion in Section 3.5).

[5] Since the atomcule is a molecule in dynamical equilibrium, it was not wise to average the PES over the sole vibrational v_1 or rotational J_1 state.

For the second-step PES, we also averaged the PES over colinear H_2 zero-point vibrational eigenfunction ($\theta_\rho = 0$, $\phi = 0$), resulting in a 3-D PES integral in Eq. (13). The corresponding activation barriers are presented in Fig. 10.

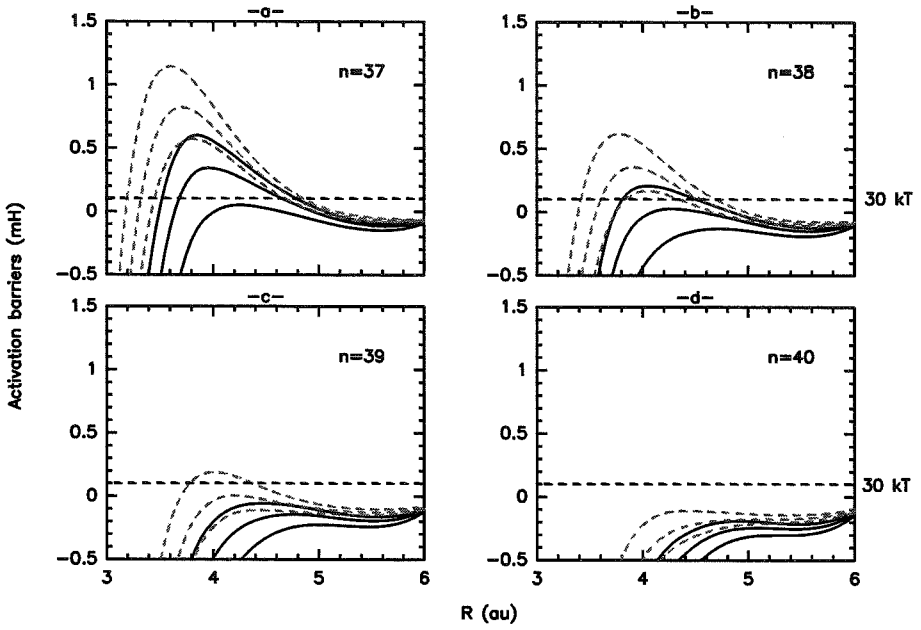

Fig. 10. State-dependent $[\bar{p}He^+]_{n,l}$-$[H\text{-}H]_{v=0}$ second-step quantum PES (solid lines, see text). The classical activation barriers from Fig. 5 are reproduced in grey dotted lines. For each value of n, the circular state and the first two elliptic ones are represented.

Taking into account the spatial extension of H_2 vibrational wave function thus lowers the remaining activation barriers by about 0.1 mH more. After correcting for the spurious classical positive shift, the cumulated effect of vibrational PES delocalizations is about 0.2 mH ($\equiv$ 60 kT). This shift can be crucial for slow collisions, and should also affect excitation or reactive processes involving similar "light" bonds in cold (astrophysical) media. As could be anticipated from the rapid cutoff in the tails of the vibrational eigenfunctions, these (first and second step) vibrational shifts are strongly R-dependent. This feature in turn affect the anisotropy of rotational interactions involving non spherical molecules.

Eventually, the averaging over H_2 rotation states was completed in the third step and the selective quenching by colinear ortho- and by isotropic para-H_2 was investigated, resulting in the interaction potentials presented in Fig. 11 and 12, respectively. For each state, the PES was averaged independently for $\phi = 0, \pi/2$ and $\phi = 0$ only. The differences between these two limiting approximations is about 0.05 mH and 0.1 mH for the ortho- and para-H_2 case,

respectively. Therefore, our ϕ sampling is sufficient for the present study, but should be improved for more quantitative predictions.

As can be seen, the shape of the activation barriers is significantly modified, under the steep repulsive contributions of non-colinear H_2 orientations in the averaging process (see Fig. 3). In addition, the quantum averaged PES for these orthogonal ortho-H_2 ($J_2 = 1$, $m_2 = \pm 1$) states are more repulsive than the para-H_2 ones, and are similar to the analogous classical PES depicted in Fig. 3 (panels a and b).

The collisional quenching by H_2 at 30 K is thus mainly governed by the ortho-species in the colinear orientation which presents the lowest reactive barriers, excepting all the higher barrierless states. Obviously the latter are not defavoured by ortho-para selectivity, and thus present large cross sections close to geometrical ones. The statistical ortho-para distribution is dominated by the room temperature one in usual experimental conditions, due to the very long intermixing timescale between the two species [which differ only by nuclear spins]. In this higher temperature limit, the ortho species is favoured in a three to one ratio with respect to the para species, and the colinear ortho- and para-H_2 are equally populated.

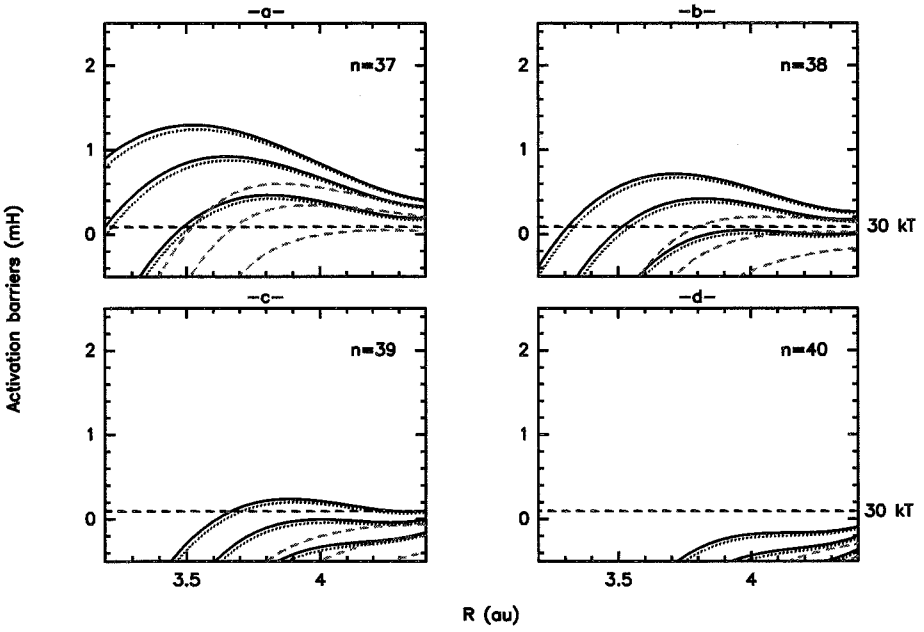

Fig. 11. State-dependent $[\bar{p}He^+]_{n,l}$-[colinear ortho-$H_2]^{m=0}_{v=0,J=1}$ interaction potentials (third quantum step, see text). Solid lines: PES averaged over $\phi = 0, \pi/2$; dotted lines: averaged using $\phi = 0$ hypersurface only). Grey dashed lines: activation barriers resulting from the second quantum step averaging (see previous Fig. 10).

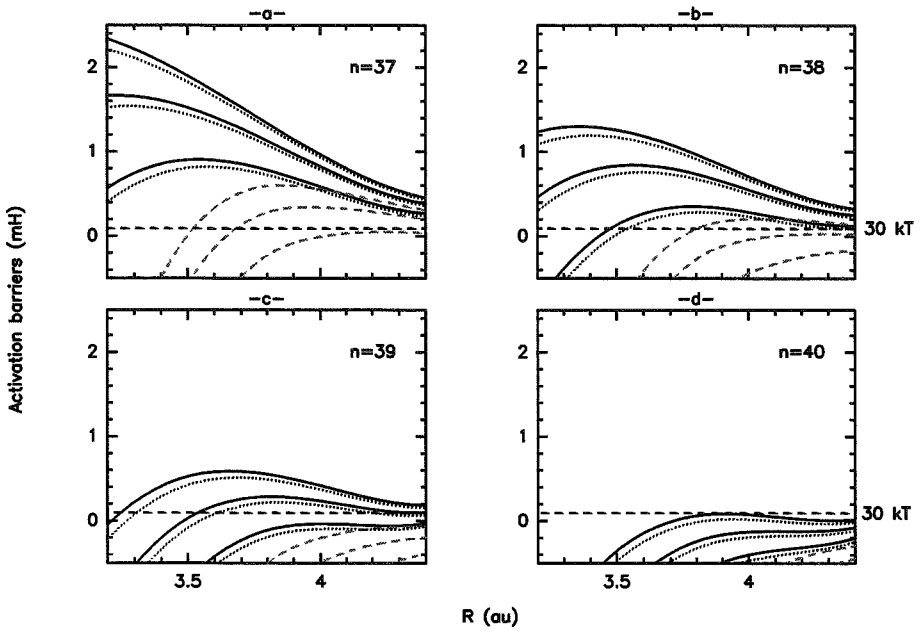

Fig. 12. Same as Fig. 11 for [para-H_2]$_{v=0,J=0}$.

Table 2 displays the activation barriers obtained at each step of the PES averaging. While the barriers remain too high, their respective order however accounts qualitatively well for the (n, l) dependence of the experimental quenching cross sections at 30 K. However most barriers remain too high. For instance, after averaging over ortho-H_2 rotation states, the activation barrier of the circular state $(39, 38)$ raises to 0.24 mH, a value which cannot account for the large cross section measured for this state (see qualitative discussion in Section 3.4).

We recall that the latter barriers have been quantum-averaged over *unrelaxed* ro-vibronic eigenfunctions. In the next section we discuss the *ab initio* PES accuracy and the consequences of relaxation effects. In conclusion we sketch several additional corrections that might be crucial on the harsh road towards quantitative agreement with experimental data.

n	l	E_1	E_2	E_3	E_4	E_5	σ_q^{Exp}
38	37	0.618	0.430	0.208	0.716	1.301	0.89
37	34	0.573	0.234	0.051	0.465	0.907	1.1
38	36	0.356	0.189	0.029	0.422	0.844	2.6
39	38	0.189	0.050	-0.058	0.239	0.589	5.4
38	35	0.168	-0.062	-0.129	0.048	0.355	6.8
39	37	0.004	-0.098	-0.144	-0.004	0.287	13
39	36	-0.110	-0.175	-0.225	-0.263	-0.036	26

Table 2
State-dependent activation barriers (in mH units) obtained after averaging the PES over (1) the classical $\alpha\bar{p}$ trajectories; (2) the atomcule ro-vibronic quantum state [first quantum step]; (3) same plus H_2 zero point vibrational wave function [second step]; (4) and (5), same as (3) plus colinear ortho-H_2 ($J = 1$, $m = 0$) or para-H_2 ($J = 0$) rotational states, respectively [third step]. Experimental quenching cross sections are expressed in 10^{-16} cm^2 units. See text for details.

5 Discussion and conclusions

5.1 Ab initio PES convergence study

By enlarging the size of the basis-set, one would expect to lower the activation barriers. We monitored the convergence of the basis set used so far for the PES (referred to hereafter as "basis set 1") upon the height of the activation barrier for the $n = 38$ circular state. We used the high-precision aug-cc-pV*Z series of correlation-consistent basis sets [22–24] which provide generous polarization and diffuse orbitals on all nuclei. We used the H basis set for both protons and for the $\bar{p}$, and the He basis set for the α. The aug-cc-pVTZ, aug-cc-pVQZ and aug-cc-pV5Z basis sets are of (4s,3p,2d), (5s,4p,3d,2f) and (6s,5p,4d,3f,2g) quality, respectively. All calculations were carried out at the CCSD(T)/CP level of theory.

In view of the dramatically increasing computational cost of such calculations, we did not attempted to evaluate the whole PES. We fixed the intermolecular separation to $R = 3.75$ au, corresponding to the location of the activation barrier for the $n = 38$ circular state. We considered the most reactive colinear approach (see Fig. 3 d). The height of the barrier was obtained by a crude averaging over the classical $\bar{p}$ orbit with the corresponding radius 0.565 au [7], based upon the three $\bar{p}$ orientations $\theta_r = (0, 90, 180)$. Orientations $\theta_r = (\pm 90)$ are degenerate by symmetry. The corresponding weights are (1/4,1/2,1/4), respectively.

Table 3 shows that the convergence of the basis set is seemingly but slowly achieved. Actually, the convergence is slower for MP2 calculations, whereas post-MP2 corrections are already accurate with the aug-cc-pVTZ basis set, as illustrated in Table 4. The contribution of triple excitations to the PES — as approximated by the CCSD(T) scheme — is small, slightly below 0.1 mH. Hence the present limit is expected to be very close to the full-CI one, as no higher diagrams are present in this three-electron system.

In order to accelerate the computation of converged PES data, one should (a) develop specific basis-sets for an efficient modeling of the polarization in the $\bar{p}He^{2+}e^-$ atomcule, and (b) improve the convergence at MP2 and further levels by an appropriate treatment of the correlation cusps (see for instance [25,26] and references therein).

As can be seen by comparing the interaction energies ΔE_{int} with and without CP corrections (values in parenthesis), the BSSE is quite significant (amounting up to 0.1 mH) and should therefore not be ignored, except for the largest basis sets. In view of the monotonous convergence of ΔE_{int} from top with CP corrections and from bottom without CP, we expect that the true interaction energy is bracketed by these two values.

basis set on $\bar{p}$ and H atoms		ΔE_{int}	CPU time
basis set 1	(3s,3p,1d)	0.493 (0.431)	7
aug-cc-pVTZ	(4s,3p,2d)	0.380 (0.285)	22
aug-cc-pVQZ	(5s,4p,3d,2f)	0.322 (0.298)	119
aug-cc-pV5Z	(6s,5p,4d,3f,2g)	0.308 (0.299)	1602

Table 3
Effects of polarization and diffuse orbitals added on $\bar{p}$ and H atoms on the height ΔE_{int} of the activation barrier for the circular state $n=38$ and for the most reactive approach (see text). CCSD(T)/CP interaction energies ΔE_{int} are expressed in millihartree units. Values in parenthesis correspond to the non-CP corrected interaction energies. The CPU time for a single geometry is expressed in minutes (referring to a RS6000/590 IBM workstation for the first basis set and to a faster O2K mainframe for the augmented ones).

	aug-cc-pVTZ	aug-cc-pVQZ	aug-cc-pV5Z
MP2	1.170	1.126	1.082
CCSD(T) - MP2	-0.79	-0.78	-0.77

Table 4
MP2 interaction energies (in mH units) and CCSD(T) values (with respect to the MP2 reference) for size-increasing basis sets. MP2 calculations are slowly converged contrary to post-MP2 energies, as attested by the almost constant CCSD(T) - MP2 energy differences for each basis set.

The energy shift corresponding to the saturation of the electronic correlation — as depicted above — is close to -0.2 mH. This shift obviously depends upon the intermolecular distance, but this dependence should not be too serious, as all activations barriers lie in a very close R range. However it may also depend upon the monomers ro-vibronic states. For the $n = 38$ circular state, we completed our previous colinear estimation by considering the orthogonal coplanar H_2 orientation. The corresponding shift, as computed using the aug-cc-vQZ basis set, is unchanged. Thus the dependence of the energy shift with respect to the H2 orientation is expected to be very weak, and the same negative 0.2 mH shift is also applicable for the rotationally-averaged PES. For the discussion, we will subsequently apply this same shift to all (n, l) states. However the possible dependence of this energy correction to other atomcule orbits (and to different H_2 separations intervening in vibrational corrections) should be investigated in more details.

5.2 Additional relaxation effects

Considering geometry relaxation effects already discussed in Section 3.5, the barriers from Table 2 should be also shifted by a value of about -0.10 mH. Inasmuch as relaxation processes cannot be neglected at 30 K, zero-point corrections should be also investigated. At that level of accuracy, the analytic estimates of the vibrational eigenfunctions should also be revisited.

In the present analysis, we shall only consider the two negative energy shifts corresponding to basis set and relaxation effects, amounting to -0.3 mH. Estimated activation barriers are given in Table 5 and 6 for ortho- and para-H_2, respectively.

For properly oriented ortho-H_2, the barriers vanish for all states which present large (quasi-geometric) quenching cross sections, except for the $n = 38$ circular state. As the corresponding Arrhenius factor $\exp -(E_a^{nl}/kT)$ is close to 0.016, the resulting quenching cross section should be 64 times smaller than the geometrical one. Therefore, we conclude that the present shifted quantum activation barriers remain too high.

For para-H_2, most states keep significant activation barriers with respect to 30 kT ($\equiv$ 0.1 mH). In view of the present values, we anticipate that their quenching by para-H_2 is strongly defavoured at sub-thermal temperatures. On the contrary, para-H_2 ($J = 2$) becomes populated at room temperatures and is favoured by statistical weight. Its rotational eigenfunction is more peaked than for ortho-H_2 ($J = 1$) and will result in lower barriers in the colinear orientation. Thus para-H_2 ($J = 2$) should become the dominant quenching species at higher temperatures.

n \ l	38	37	36	35	34
37			0.996	0.623	0.165
38		0.416	0.122	-0.252	
39	-0.061	-0.304	-0.563		

Table 5
Estimated state-dependent activation barriers E_a^{nl} (mH) for colinear ortho-H_2 ($J = 1$) including the -0.3 mH shift (see text).

n \ l	38	37	36	35	34
37			>1.917	>1.357	0.607
38		1.001	0.544	0.055	
39	0.289	-0.013	-0.336		

Table 6
Same as Table 5 for para-H_2 ($J = 0$).

Experiments using an helium buffer enriched with para-H_2 contaminants are therefore eagerly awaited.

5.3 Conclusions

In this paper, we studied the collisional quenching of $\bar{p}He^+$ atomcule metastable states by H_2 molecules, in a pioneering attempt to interpret the state-resolved data recently obtained at CERN. We focused upon the exploration of the whole *ab initio* potential energy surface (6-D PES), using standard molecular physics concepts at the Born-Oppenheimer (BO) level. Our strategy was to average the PES over the fast nuclear motions — especially the rotation of the $\bar{p}$, and more generally the ro-vibronic nuclear states of the atomcule and H_2 — in order to reduce the dimensionality of the problem and to facilitate its analysis. This simple approach permitted the identification of classical reactive channels with low activation barriers. These results account qualitatively for the large quasi-geometrical quenching cross sections measured for the states $n = 38$ and $n = 39$ at 30 K, and for their l-dependence. However the spacing of (n, l) activation barriers is apparently overestimated by a factor of two by both classical and quantum averaging models. Our quantum averaging model also predicts that quenching by para-H_2 ($J = 0$) is strongly defavoured at 30 K while both ortho- and para-H_2 species would contribute very efficiently to quenching at higher temperatures via higher J H_2 states.

We further attempted to discuss the relative importance of the various processes that should be taken into account to pave the way towards a *quantitative* prediction of the experimental data.

The present PES was helpful to identify the convergence issues in terms of basis set, method and mesh. A fully converged PES is attainable with present computers and large basis sets at the CCSD(T) or CCSD(T)-R12 level, and the effort would be alleviated if specific basis sets were developed for the atomcule. Excepted for very large basis sets, counterpoise corrections will remain necessary. Our preliminary mesh proved also nearly sufficient, it should be doubled over ϕ and slightly extended over r and ρ for computing more accurate ro-vibrational corrections and relaxation effects.

The most unexpected result was the importance of ro-vibrational averaging effects including the influence of the $v = 0$ delocalization of H_2. In this respect, our simple corrections based upon approximate Morse-like eigenfunctions may prove unsufficient. Geometry and dynamical relaxation effects are smaller, but remain significant in view of a detailed interpretation of l-dependent quenching cross-sections. In particular, a throrough investigation of dynamical relaxation effects seems unavoidable. Due to possible zero-point vibrational shifts, it should be carried on at the quantum level. It is not excluded that couplings between geometry and dynamical relaxation effects may prove important at the 30 kT accuracy level.

We did not attempted a quantum treatment of the collision dynamics over the averaged PES. Such an effort would be unavoidable to predict *absolute* quenching cross-sections, and would permit to take into account additional effects such as non-BO couplings, resonances, tunneling effects, and collision-induced Auger decay. In particular, non-BO effects could prove more important than for ordinary systems due to the special dynamical nature of the atomcule, for which the orbital $\bar{p}$ time is only 40 times smaller than the collision time, and due to the longer timescale of precession effects for elliptical orbits. Dynamical relaxation effects could also induce additional nondiagonal couplings.

Undoubtly, such state-resolved low temperature quenching experiments impose very challenging constraints on theoretical models and should provide ideal four-body benchmarks for further detailed chemical physics studies. In this respect, additional measurements of the temperature dependence of the quenching cross-sections and corresponding investigations of the ortho-para quenching selectivity would be welcomed in order to check the predictions of our preliminary study and to stimulate more detailed theoretical investigations.

Alternatively, these low temperature studies might provide new insights into the physico-chemistry of cold terrestrial and interstellar molecules and rad-

icals. In particular, the ro-vibrational averaging corrections and the corresponding dynamical relaxation effects might prove significant for reactive or excitation processes involving light bonds. They might also contribute to a better understanding of the various isotopic H/D fractionation processes which are incredibly effective in cold interstellar or early protostellar clouds.

Appendix. Zero-point eigenfunction of a diatomic molecule vibrating in a Morse potential

Let us recall that the Morse function has the following form

$$U(r) = -D + D(1 - e^{-\alpha(r-r_e)})^2, \tag{15}$$

where D is the dissociation energy of the molecule, r_e denotes the equilibrium distance between nuclei and α is a constant. Using this fitting formula, the energy and eigenfunction of the v^{th} vibrational level are

$$E_v = -D\left[1 - \frac{\alpha\hbar}{\sqrt{2\mu D}}(v + \frac{1}{2})\right]^2 \tag{16}$$

$$\psi_v = \frac{1}{r}\, e^{-\xi/2}\, \xi^s\, \omega(\xi), \tag{17}$$

where μ is the reduced mass of the diatomic molecule and

$$s = \frac{\sqrt{-2\mu E_v}}{\alpha\hbar}, \tag{18}$$

$$\xi = \frac{2\sqrt{2\mu D}}{\alpha\hbar} e^{-\alpha(r-r_e)}, \tag{19}$$

$$\omega = 1 + \frac{-v}{2s+1}\frac{\xi}{1!} + \frac{-v(-v+1)}{(2s+1)(2s+2)}\frac{\xi^2}{2!} + ..., \tag{20}$$

until the term $-v(-v+1)...$ becomes zero.

Acknowledgement

Calculations have been carried out on the workstations of the "Service Commun de Calcul Intensif de l'Observatoire de Grenoble" and on the "Centre Informatique National de l'Enseignement Supérieur" (projects c990820 and x2000-04-20820). One of us (S.S.) was supported by a fellowship of the Ministère de l'Enseignement Supérieur et de la Recherche. We warmly acknowledge Dr. J. Carbonell, Pr. J.M. Richard and various colleagues from the few-body community for their encouragements and for numerous informal discussions.

References

[1] T. Yamazaki, E. Widmann, R.S. Hayano, M. Iwasaki, S.N. Nakamura, K. Shigaki, F.J. Hartmann, H. Daniel, T.v. Egidy, P. Hofmann, Y.-S. Kim, J. Eades, Nature 361 (1993) 238.

[2] N. Morita, T. Yamazaki, F.J. Hartmann, D. Horváth J. Eades et al., Phys. Rev. Lett. 72 (1994) 1180.

[3] E. Widmann, I. Sugai, T. Yamazaki, R.S. Hayano, T. Ishikawa, S.N. Nakamura, H. Tamura, T.M. Ito, A. Kawachi, N. Nishida, W. Higemoto, Y. Ito, N. Morita, F.J. Hartmann, H. Daniel, T.v. Egidy, W. Schmid, F.J. Hofmann, J. Eades, Phys. Rev. A 53 (1996) 3129.

[4] B. Ketzer, F.J. Hartmann, T.v. Egidy, C. Maierl, R. Pohl, J. Eades, E. Widmann, T. Yamazaki, M. Kumakura, N. Morita, R.S. Hayano, M. Hori, T. Ishikawa, H.A. Torii, I. Sugai, D. Horváth, J. Chem. Phys., 109 (1998) 424.

[5] R. Pohl, M. Hori, H.A. Torii, R.S. Hayano, T. Ishikawa, F.J. Hartmann, B. Ketzer, C. Maierl, T.v. Egidy, J. Eades, E. Widmann, T. Yamazaki, M. Kumakura, N. Morita, I. Sugai, D. Horváth, Phys. Rev. A 58 (1998) 4406.

[6] T. Yamazaki, B. Ketzer, E. Widmann, J. Eades, H. Daniel, F.J. Hartmann, M. Hasinoff, R. Pohl, R. Schmidt, T.v. Egidy, D. Horváth, M. Kumakura, N. Morita, I. Sugai, Y. Fujita, H.A. Torii, M. Hori, T. Ishikawa, F.E. Maas, H. Tamura, R.S. Hayano, Chem. Phys. Lett. 265 (1997) 137.

[7] S. Sauge, P. Valiron, "Collisional survival of antiprotonic helium atomcules", Chem. Phys., accepted.

[8] G. Ya. Korenman, Hyp. Int. 103 (1996) 341.

[9] A. Voronin, O. Dalkarov: Private Communication.

[10] S. Sauge, P. Valiron, J. Carbonell, Few-Body Syst. Suppl. 10 (1998) 211.

[11] I. Shimamura, Phys. Rev. A46 (1992) 3776.

[12] W.J. Hehre, L. Radom, P.v.R. Schleyer, J.A. Pople, Ab Initio Molecular Orbital Theory, Ed. Wiley & Sons, United States, 1986.

[13] R. J. Bartlett, Ann. Rev. Phys. Chem. 32 (1981) 359.

[14] R. Krishnan, J.S. Binkley, R. Seeger, J.A. Pople, J. Chem. Phys. 72 (1980) 650.

[15] S.B. Boys, F. Bernardi, Mol. Phys. 19 (1970) 553.

[16] P. Valiron, I. Mayer, Chem. Phys. Lett., 275 (1997) 46.

[17] Gaussian 94, Revision D.3, M.J. Frisch, G.W. Trucks, H.B. Schlegel, P.M.W. Gill, B.G. Johnson, M.A. Robb, J.R. Cheeseman, T. Keith, G.A. Petersson, J.A. Montgomery, K. Raghavachari, M.A. Al-Laham, V.G. Zakrzewski, J.V. Ortiz, J.B. Foresman, J. Cioslowski, B.B. Stefanov, A. Nanayakkara, M. Challacombe,

C.Y. Peng, P.Y. Ayala, W. Chen, M.W. Wong, J.L. Andres, E.S. Replogle, R. Gomperts, R.L. Martin, D.J. Fox, J.S. Binkley, D.J. Defrees, J. Baker, J.P. Stewart, M. Head-Gordon, C. Gonzalez, and J.A. Pople, Gaussian, Inc., Pittsburgh PA, 1995; J.B. Foresman and A. Frish, Exploring Chemistry with Electronic Structure Methods (Gaussian Inc., 1996).

[18] mailto: Pierre.Valiron@obs.ujf-grenoble.fr

[19] V.I. Korobov, Hyp. Int. 101/102 (1996) 479.

[20] L. Landau, E. Lifchitz, Quantum Mechanics, Mir Pub., Moscow, 1980.

[21] K.P. Huber, G. Herzberg, Constants of Diatomic Molecules, Ed. VNR (1979)

[22] R. A. Kendall, T. H. Dunning, Jr. and R. J. Harrison, J. Chem. Phys. 96 (1992) 6796.

[23] T. H. Dunning, Jr., J. Chem. Phys. 90 (1989) 1007.

[24] K. A. Peterson, D. E. Woon and T. H. Dunning Jr., J. Chem. Phys. 100 (1994) 7410.

[25] J. Noga, W. Klopper and W. Kutzelnigg, Rec. Adv. in Comput. Chem., Vol. 3, Ed. R.J. Bartlett, World Scientific, 1997, p 48.

[26] J. Noga and P. Valiron, Chem. Phys. Lett. 324 (2000) 166

Chapter 5

Towards antihydrogen synthesis?

Contents

5.1 Présentation générale de l'étude

Introduction

Nous avons étudié une voie de synthèse de l'antihydrogène ($\bar{H} = e^+\bar{p}$) par réaction d'helium antiprotonique ($[\bar{p}He^+]_{nl}$) avec du positronium (Ps= e^+e^-) (Ito & Yamazaki, 1993):

$$[\bar{p}He^+]_{nl} + Ps \rightarrow \bar{H} + He + 6.8\ eV. \tag{5.1}$$

Dans des conditions expérimentales typiques, cette réaction pourrait produire environ 10^3-10^4 atomes d'antihydrogène par paquets de 10^9 $\bar{p}$ et 10^8 e^+, si on suppose que cette synthèse constitue la voie de sortie prépondérante. Une étude des autres voies de sortie et des rapports de branchement correspondants est donc souhaitable, afin d'estimer des sections efficaces effectives de formation.

Démarche et résultats

Dans le cadre de l'approximation de Born-Oppenheimer (BO), nous discutons l'évolution et la stabilité du complexe intermédiaire (α, $\bar{p}$, e^+, $2e^-$) en utilisant une approche de trajectoires classiques pour le mouvement des noyaux (α, $\bar{p}$) dans le potentiel BO crée par les trois leptons (e^+, $2e^-$). Ce dernier a été calculé au niveau Hartree-Fock, ce qui constitue une bonne approximation dans la mesure où les effets de corrélation représentent quelques pourcents seulement de l'énergie totale[1].

[1] Un calcul plus précis utilisant des méthodes Monte Carlo variationnelles est en cours de réalisation et est présenté à l'annexe 8.

Nous prédisons deux voies de sortie possibles pour la réaction atomcule-Ps, qui dépendent du nombre quantique principal n de l'atomcule: les états de $n \geq 38$ dissocient pour former de l'antihydrogène, tandis que ceux de $n < 38$ forment une nouvelle classe d'atomcules métastables(α, $\bar{p}$, e^+, $2e^-$), dont l'existence pourrait être confirmée par spectroscopie.

Conclusions

Ce travail illustre la transférabilité des concepts de physique moléculaire à la physico-chimie d'atomes-molécules exotiques. Par ailleurs, la nouvelle classe d'atomcules (α, $\bar{p}$, e^+, $2e^-$) pourrait constituer un système de référence pour le traitement de la corrélation dans des molécules composées de leptons et d'antileptons. Le chapitre suivant essaie d'ouvrir des perspectives tournées vers la recherche d'autres clusters antiprotoniques (méta)stables.

Publication

Accepted in *Chemical Physics Letters*. In press.

Dissociative recombination of antiprotonic atomcules $\bar{p}He^+$ with positronium: towards antihydrogen synthesis?

Sébastien Sauge, Pierre Valiron and István Mayer

Dissociative recombination of antiprotonic atomcules $\bar{p}He^+$ with positronium: towards antihydrogen synthesis?

Sébastien Sauge [a], Pierre Valiron [a], István Mayer [b]

[a] *Observatoire de Grenoble, Laboratoire d'Astrophysique (UMR 5571 du CNRS), Université Joseph Fourier, 414 rue de la Piscine, BP53X, 38041 Grenoble Cedex, France*

[b] *Institute of Chemistry, Chemical Research Center, Hungarian Academy of Sciences, P.O. Box 17, H-1525 Budapest, Hungary*

Abstract

We investigate the reactive association of metastable antiprotonic helium "atomcules" ($[\bar{p}He^+]_{nl}$) with positronium (Ps). In the framework of the Born-Oppenheimer approximation, we further discuss the evolution and stability of the intermediate complex (α, $\bar{p}$, e^+, $2e^-$) using a classical trajectory approach for treating the nuclei (α, $\bar{p}$). We predict two possible channels for the atomcule–Ps reaction depending upon the atomcule principal quantum number n: $n \geq 38$ states dissociate to $\bar{H}$, whereas $n < 38$ states form a new class of metastable atomcules, which could be confirmed by laser spectroscopy. The present work illustrates the pertinence of simple chemical physics concepts to the study of exotic processes involving antimatter.

1 Introduction

As widely reported [1], about 3% of antiprotons ($\bar{p}$) stopped in helium are long-lived with an average lifetime of a few microseconds (against a few picoseconds in all other materials). This unusual metastability was attributed to the formation of the so-called antiprotonic helium "atomcule" ($[\bar{p}He^+]_{nl}$), which can be regarded either as a near-circular quasi-classical Rydberg atom with $l \sim 40$ or, alternatively, as a special diatomic molecule with a negatively charged $\bar{p}$ nucleus in a low vibrational, high rotational $J \sim 40$ state. Direct evidence for the existence of such atomcules has been established by their laser detection performed at the LEAR in CERN [2], in remarkable agreement with the theoretical predictions of transition wavelengths [3]. Atomcules are easy to produce by stopping a beam of low energy $\bar{p}$ in a buffer of pure helium

and they survive through millions of collisions with the buffer atoms [4]. In addition, atomcules are quenched by various molecular contaminants [5] and thus constitute an original probe for exploring the stability and reactivity of antiprotonated species. In this respect, many concepts of molecular physics are transferable to the physico-chemistry of exotic atom-molecules, as we shall illustrate in this Letter.

Recently, Ito *et al.* proposed a route to synthetize antihydrogen ($\bar{H} = e^+\bar{p}$) by reaction of antiprotonic helium with positronium ($Ps = e^+e^-$) [6]

$$[\bar{p}He^+]_{nl} + Ps \rightarrow He + \bar{H} + 6.8\ eV\ . \qquad (1)$$

According to Ito's estimations, reaction (1) could synthetize about 10^3-10^4 antihydrogen atoms per bunch of 10^9 $\bar{p}$ and 10^8 e^+, assuming $\bar{H}$ formation is the dominant output channel. An investigation of other channels and corresponding branching ratios is thus desirable, in order to better estimate the effective $\bar{H}$ formation cross-sections.

We suggest to decompose the atomcule-Ps reaction into a two-step process.

In the first step, the approach of the Ps leads to the formation of a molecular complex involving two leptons and one antilepton. Due to the light mass of the colliding Ps, this process cannot be described within the Born-Oppenheimer (BO) framework and is beyond the scope of the present study.

In the second step, the dynamical evolution of the molecular complex $[\alpha, \bar{p}, e^+, 2e^-]_{n'l'}$ may lead to $\bar{H}$ synthesis. In a pioneering work, the BO framework was used by Ahlrichs [7] and then by Shimamura [8] to determine the energies of the atomcule metastable states. In the molecular picture, the BO separation is usable since the $1s$ electron of a $[\bar{p}He^+]_{nl}$ atomcule moves about $n \sim 40$ times faster than the antiproton [8]. The BO framework is expected to remain valid once the complex has been formed, since the velocity of leptons and baryons is not expected to change significantly. The nuclei will then be affected by the *new* BO potential produced by the three leptons (e^+, $2e^-$). This potential will be estimated in Section 2.

In Section 3, we will discuss the formation of the molecular complex and investigate its evolution and stability after switching on the new BO potential, using a classical trajectory approach for the nuclei. The stable channels yield a new $[\alpha, \bar{p}, e^+, 2e^-]_{n',l'}$ atomcule, as will be discussed in Section 4. The dissociative channels leading to antihydrogen synthesis will be considered in Section 5.

2 The Born-Oppenheimer He-$\bar{\text{H}}$ potential at the Hartree-Fock level

The BO potential of the He-$\bar{\text{H}}$ complex was obtained by computing the total energy of the three leptons ($e^-e^+e^-$) at a given (fixed) α-$\bar{\text{p}}$ separation and adding the α–$\bar{\text{p}}$ electrostatic attraction. The wave function and the energy of the lepton subsystem were calculated in the framework of the self-consistent field (SCF) Hartree-Fock approximation [9]. The latter can be introduced in a standard manner, by treating separately the two electrons and the positron. Care should be taken because of the unusual signs of the electrostatic interactions in the system. One gets a set of coupled equations for the wave functions of the electrons and of the positron, which should be solved iteratively. For the closed-shell singlet state of the two electrons one has

$$\left[-\tfrac{1}{2}\Delta - \frac{2}{r_\alpha} + \frac{1}{r_{\bar{p}}} + \hat{J}(\varphi) - \hat{J}(\chi)\right]\varphi \equiv \left[\hat{h}_e + \hat{J}(\varphi) - \hat{J}(\chi)\right]\varphi = \varepsilon_e\varphi, \quad (2)$$

$$\left[-\tfrac{1}{2}\Delta + \frac{2}{r_\alpha} - \frac{1}{r_{\bar{p}}} \quad - 2\hat{J}(\varphi) \quad\right]\chi \equiv \left[\hat{h}_p \quad - 2\hat{J}(\varphi) \quad\right]\chi = \varepsilon_p\chi, \quad (3)$$

and

$$E^S_{lcpt.} = 2 < \varphi|\hat{h}_e|\varphi > + < \varphi\varphi|\varphi\varphi > + < \chi|\hat{h}_p|\chi > -2 < \varphi\chi|\varphi\chi > . \quad (4)$$

r_α and $r_{\bar{p}}$ represent the distance from the respective heavy particles, $\varphi = \varphi(\vec{r}_e)$ is the doubly filled spatial orbital of the electrons, $\chi = \chi(\vec{r}_p)$ is the spatial orbital of the positron, $\hat{J}$ is the usual Coulomb operator and $< \varphi\psi|\mu\nu >$ is a short-hand for the integral $< \varphi(1)\psi(2)|\frac{1}{r_{12}}|\mu(1)\nu(2) >$.

In the case of the triplet electronic subsystem, there are two singly occupied electronic orbitals φ_1 and φ_2; as the two electrons have the same spin, they exhibit exchange interaction as well. The respective equations are:

$$\left[\hat{h}_e + \sum_{j=1}^{2}\left(\hat{J}(\varphi_j) - \hat{K}(\varphi_j)\right) - \hat{J}(\chi)\right]\varphi_i = \varepsilon^i_e\varphi_i, \quad (5)$$

$$\left[\hat{h}_p \quad - \hat{J}(\varphi_1) - \hat{J}(\varphi_2) \quad\right]\chi = \varepsilon_p\chi, \quad (6)$$

and

$$E^T_{lept.} = < \varphi_1|\hat{h}_e|\varphi_1 > + < \varphi_2|\hat{h}_e|\varphi_2 > + < \varphi_1\varphi_2|\varphi_1\varphi_2 > - < \varphi_1\varphi_2|\varphi_2\varphi_1 > + < \chi|\hat{h}_p|\chi > - < \varphi_1\chi|\varphi_1\chi > - < \varphi_2\chi|\varphi_2\chi > . \quad (7)$$

In (5), $\hat{K}(\varphi_j)$ is the usual exchange operator (note that $[\hat{J}(\varphi_i) - \hat{K}(\varphi_i)]\varphi_i \equiv 0$).

The equations were solved in the standard algebraic approximation used in quantum chemistry: each function φ, χ was expanded as a linear combination of a set of pre-selected basis functions, permitting to replace the integro-differential Hartree-Fock equations of the form $\hat{F}\psi = \varepsilon\psi$ by a generalized matrix pseudo-eigenvalue equation of type $\mathbf{Fc} = \varepsilon\mathbf{Sc}$, $\mathbf{S}$ being the overlap (metric) matrix of the basis and $\mathbf{c}$ the vector of expansion coefficients of ψ.

Standard He and H basis orbitals are adequate for the description of the (He + $\bar{\text{H}}$) output channel. In the ($[\bar{\text{p}}\text{He}^+]_{nl}$) input channel, the $\bar{\text{p}}$ strongly perturbs the electronic cloud around the α, and thus specific polarization orbitals are needed on both nuclei to model the "anti-bounding". Exponents ξ for such polarization orbitals were experimented in order to approach the SCF limit for representative α–$\bar{\text{p}}$ separations of the molecular complex. For the $\bar{\text{p}}$, we complemented the hydrogen's 311G basis set [10] with a set of 4 shared exponents sp orbitals (ξ= 1, 3, 10, 30) and 1 cartesian d function (ξ= 0.6). For the α, we expanded the helium's 311++G basis set [10] into an uncontracted set of 3 s (ξ= 98.1243, 14.7689, 0.086), 3 sp (ξ= 3.31883, 0.874047, 0.244564) and 1 cartesian d (ξ= 1) functions. This resulted in a total of 46 basis functions.

We estimated the importance of correlation effects to be about 0.04 au, using 4^{th} order perturbation theory for the comparable 3-lepton He-H system. Thus, correlation effects amount to a few percents of representative interaction energies and Hartree Fock calculations should provide a good estimation. Total Born-Oppenheimer energies $\epsilon^{S,T}(R)$ were obtained by adding the α-$\bar{\text{p}}$ electrostatic attraction to the corresponding leptonic energies $E_{lept}^{S,T}$. Total Born-Oppenheimer energies for input/output channels are presented in Fig. 1. The statistical weight ratio between the e^- spin singlet state (light grey) and the e^- spin triplet state (dark grey) is 1 : 3, respectively, assuming that no selection effects take place during the formation of the molecular complex.

3 Formation and dynamical evolution of the molecular complex

3.1 Formation

Prior to the possible formation of a molecular complex, the associative reaction of atomcules with light positronium cannot be treated within the Born-Oppenheimer (BO) framework. However, propensity rules can be guessed from the constraints imposed by (a) the conservation of total angular momentum and energy and (b) the probability of Auger emission for the electrons or collisional deexcitation.

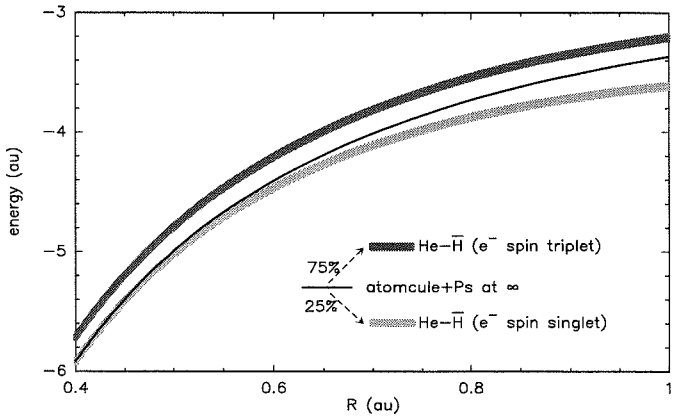

Fig. 1. Total Born-Oppenheimer energies for input/output channels. Solid line: input channel ($\bar{p}He^+$, Ps at infinity); light gray line: total BO energy for the output channel (He-$\bar{H}$) in the e^- spin singlet state; dark grey line: same for the e^- spin triplet state. The thickness of the last two curves indicates the expected magnitude of electronic correlation effects (see text).

(a) Since the Ps carries little impulse and kinetic energy[1], the *total* angular momentum and energy of the (α, $\bar{p}$, e^+, $2e^-$) molecular complex should be conserved. Considering Fig. 1, the formation of the e^- triplet spin state is strongly endothermic with a 0.25 au energy gap, which corresponds to a transition with $\Delta n \sim -4$ ($\Delta l = 0$) for the original atomcule [3]. On the other hand, the formation of the e^- singlet spin state is slightly exothermic in the range 0.4-0.7 au, especially if e^- correlation is taken into account. Therefore, it is expected to be more likely, as only a $\Delta n \sim +1$ transition ($\Delta l = 0$) is required to conserve the total energy.

(b) For the original $[\bar{p}He^+]_{nl}$ atomcule, the metastability domain is a narrow domain of circular or quasi-circular states with $(n, l \sim n-1)$ [1]. Elliptic states with $l \lesssim 35$ and inner circular states with $n \lesssim 33$ are destroyed by Auger emission of the remaining electron [8], while outer states with $n > 40$ are quenched by collisions during the thermalisation stage [13]. For the 3-lepton molecular complex, we expect the corresponding domain to be narrower, due to additional Auger decay channels. Nevertheless, assuming the same boundaries of metastability, the only state supporting a $\Delta n \sim -4$ transition is the level with $(n, l) = (40, 35)$, which would thus lead to an e^- spin triplet state with $(n, l) = (36, 35)$. Alternatively, all states adjacent to an Auger-dominated

[1] Thermalized Ps have kinetic energy $E_T \sim 10^{-3}$ au at 300 K, much smaller than the spacing of the atomcule energy levels, about 10^{-1} au. The maximum angular momentum brought in by the Ps is approximately given by $\Delta l_{max} \sim a\sqrt{2m_{Ps}E_T}$, a being the maximum impact parameter. Since the bound $\bar{p}$ is formed most likely at a radius which overlaps the wave function of the displaced electron [1], a is close to the Bohr radius of the electron in He. Thus, we estimate $\Delta l_{max} \sim 4\,10^{-2} \ll 1$.

short-lived level would be destroyed during the $\Delta n \sim 1$ transition required for the formation of a singlet spin state. These qualitative arguments should be kept in mind for refining the upper-bounded $\bar{H}$ formation probability to be derived hereafter. Besides, the reverse process consisting in the dissociation of the molecular complex to Ps and $\bar{p}He^+$ may also limit the reaction rates.

3.2 Dynamical evolution

Once the complex has formed, the BO framework becomes usable for studying the dynamical evolution of the (α, $\bar{p}$, e^+, $2e^-$) molecular complex, which we studied in a classical trajectory approach for the α-$\bar{p}$ nuclei. However our investigation of the collision in two independent steps (formation *and* evolution) raises the question of (a) the time scale and nature of the branching of the new BO potential and (b) the classical initial conditions for the new dynamical orbits.

(a) The time scale of an atomcule-Ps collision with thermal kinetic energy E_T is approximately given by $t \sim r/\sqrt{2E_T/m_{Ps}}$, where r denotes the reactive range of the $\bar{p}He^+$–Ps interaction, and m_{Ps} the reduced mass of Ps relative to the $\bar{p}He^+$ atom. Assuming an interaction range of a few au, t is about 10^{-15} s and is comparable to the classical orbiting time of the $\bar{p}$. Moreover, the attractive long range interaction is likely to accelerate the complex formation in the exoenergetic e^- singlet channel. Accordingly, the branching of the new potential is expected to occur during a single $\bar{p}$ revolution or less. Could the branching of the new BO potential drive the dissociation of the atomcule and lead to $\bar{H}$ formation?

(b) The initial antiprotonic Rydberg states were described by enforcing a semi-classical quantization of the orbits in the effective $[\bar{p}He^+]_{n,l=J}$ potential, which is the sum of the ground state BO electronic potential $\epsilon(r)$ and of the centrifugal potential [2]. Reproducing theoretical energies [3] of given n states constrains the classical orbit of the circular state and semi-major axis of the elliptic ones, as illustrated in Fig. 2. Alternatively, we predict the energies of the circular states with a relative accuracy of a few 10^{-3} [13], by using a Bohr quantization.

Starting from such initial orbits, the dynamical stability of the molecular complex was studied by smoothly branching the new $[\bar{p}e^+e^-e^-\alpha]_{n,l}$ BO potential and by integrating the classical equations of motion for the $\bar{p}$ and α nuclei. For elliptic states, several random initial conditions representative of all possible $\bar{p}$ phases were considered. The results were insensitive to the time scale of

[2] We computed the BO electronic potential $\epsilon(r)$ [13] at the Hartree-Fock limit, which is exact for this one electron system.

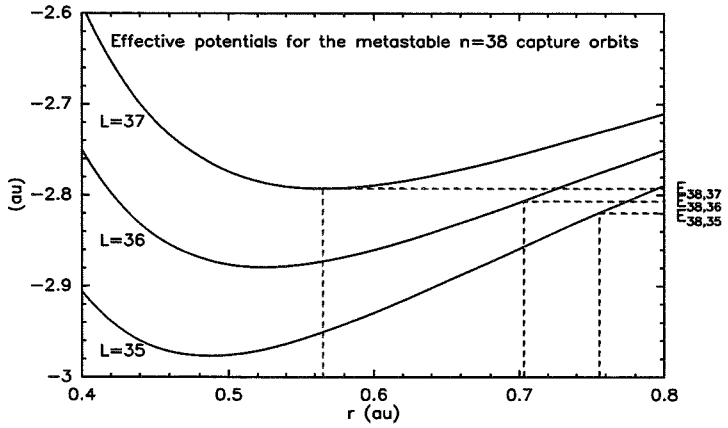

Fig. 2. Semi-classical quantization of the effective $[\bar{p}He^+]_{n,l=J}$ potential [13] (solid lines). Reproducing theoretical energies [3] of given (n, l) states constrains the classical orbit of the circular state $(n, n-1)$ and semi-major axis of the elliptic ones (dashed lines). The semi-minor axis is constrained analogously.

the branching. In all simulations, $n \geq 38$ e^- singlet spin states were found to dissociate to $\bar{H}$, whereas $n < 38$ e^- singlet spin states (and all n e^- triplets) remained bound, for all l values corresponding to observed metastable atomcules [11]. Two typical simulations are shown in Fig. 3.

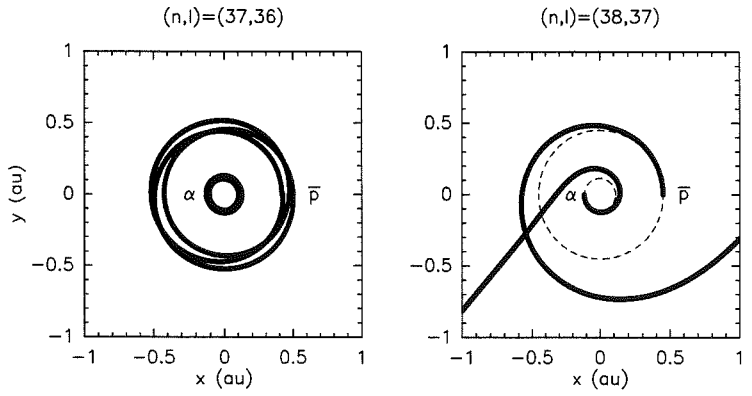

Fig. 3. Classical trajectory simulations for the α-$\bar{p}$ particles moving in the BO potential of the He-$\bar{H}$ system (e^- spin singlet), starting from a circular state (n= 37 or 38). $n \geq 38$ e^- singlet spin states dissociate to $\bar{H}$, whereas $n < 38$ e^- singlet states remain bound (solid fat lines represent α and $\bar{p}$ trajectories in the new BO potential, whereas dashed lines show the initial circular orbits).

4 Bound states

For orbits which remain bound classically, the $\bar{p}He^+$-Ps reaction may yield a new class of atomcules, involving both leptons and anti-leptons. These new atomcules are expected to present a mean lifetime comparable to the positronium's (a few 100 ns), assuming the e^+e^- annihilation is the main destructive channel.

Energies of the circular bound states were obtained by a Bohr quantization in the new [α, $\bar{p}$, e^+, $2e^-$] BO potential. Electronic spin singlets up to the $n = 37$ circular state (as well as all triplets) are predicted to be bound, in agreement with the dynamical approach of Sec. 3. Energy levels of the circular bound states are featured in Table 1 and 2 for the e^- spin singlet and triplet, respectively. For the e^- singlet spin states, transition wavelengths are strongly red-shifted with respect to those of the $\bar{p}He^+$ atomcule, whereas the orbit radii are larger. For the triplet spin states however, the red-shift is much smaller and the orbit radii are similar. Elliptic states could be easily derived analytically [12] by fitting a Morse potential to the effective potential.

n	R_n (au)	E_n (au)	$\Delta\lambda^n_{n-1}$ (nm)
37	0.578 (0.524)	-3.111 (-2.879)	544.1 (467.6)
36	0.517 (0.487)	-3.195 (-2.977)	458.6 (415.7)
35	0.472 (0.453)	-3.294 (-3.086)	396.7 (370.6)
34	0.435 (0.422)	-3.409 (-3.209)	346.9 (330.9)
33	0.401 (0.393)	-3.540 (-3.347)	305.8 (295.8)

Table 1
Classical radius, energy levels and transition wavelengths for the $[\alpha\bar{p}e^+2e^-]_{n,l=n-1}$ circular bound states (e^- spin singlet), compared to those obtained for the $[\alpha\bar{p}e^-]_{n,l=n-1}$ circular ones (values in parenthesis).

$\bar{p}He^+$ atomcules can be observed because the repulsive exchange interaction dramatically reduces the quenching cross sections with surrounding He atoms [13]. We expect the new atomcule to be more stable with respect to collisions, since the exchange will now involve two electrons instead of one. On the other hand, Auger transition rates should be greater also, thus reducing the lifetime of these states. Laser spectroscopy measurements are eagerly anticipated to confirm the existence of this composite [α, $\bar{p}$, e^+, $2e^-$] metastable atomcule.

n	R_n (au)	E_n (au)	$\Delta\lambda^n_{n-1}$ (nm)
40	0.670	-2.642	696.0
39	0.615	-2.707	604.8
38	0.567	-2.783	531.1
37	0.526	-2.868	469.3
36	0.488	-2.965	416.8
35	0.454	-3.075	371.8
34	0.422	-3.197	331.1
33	0.393	-3.335	295.8

Table 2
Classical radius, energy levels and transition wavelengths for the $[\alpha\bar{p}e^+2e^-]_{n,l=n-1}$ circular bound states (e^- spin triplet).

5 $\bar{H}$ formation and conclusions

We investigated the evolution and stability of the intermediate complex (α, $\bar{p}$, e^+, $2e^-$) resulting from the reactive association of antiprotonic atomcules with positroniums. When the two electrons of the molecular complex form a singlet state, we predict two possible channels: inner $\bar{p}$ orbits with $n < 38$ remain bound classically, whereas $n \geq 38$ dissociate to $\bar{H}$. Alternatively, assuming that the e^- triplet spin state can be formed, we predict that all orbits remain bound, and thus no $\bar{H}$ formation should occur in this case.

In order to derive an effective formation cross section for $\bar{H}$ from the atomcule-Ps reaction, the individual populations $P(n \geq 38, l)$ of the $\bar{p}He^+$ metastable states would be required. According to our estimations [13], the states with $n \geq 38$ would constitute about 40% of the total delayed fraction. Inasmuch as e^- singlet spin states are formed in a 1 : 3 ratio, one would expect that about 10% of the thermalized Ps which encounter $\bar{p}He^+$ in high pressure He gas will lead to $\bar{H}$. This estimation provides an upper bound as it does not take into account competing processes, such as Auger decay of the molecular complex, or reverse dissociation. Therefore, we predict that $\bar{H}$ formation cross sections [6] has been overestimated by one order of magnitude at least.

Alternatively, a new class of metastable atomcules (α, $\bar{p}$, e^+, $2e^-$) is expected to be formed with a similar branching ratio and could provide an original benchmark for correlation in composite lepton-antilepton systems, as all theoretical predictions could be tested by high-resolution laser-spectroscopy.

We emphasize that chemical physics might open the way to a better understanding of exotic processes involving antiprotonic atomcules. Alternatively,

the study of such exotic systems and of their quenching by molecular contaminants [14] might provide a new insight into the physico-chemistry of cold terrestrial and interstellar radicals.

References

[1] T. Yamazaki, E. Widmann, R.S. Hayano, M. Iwasaki, S.N. Nakamura, K. Shigaki, F.J. Hartmann, H. Daniel, T.v. Egidy, P. Hofmann, Y.-S. Kim, J. Eades, Nature 361 (1993) 238.

[2] N. Morita, T. Yamazaki, F.J. Hartmann, D. Horváth J. Eades et al., Phys. Rev. Lett. 72 (1994) 1180.

[3] V.I. Korobov, Hyp. Int. 101/102 (1996), 479.

[4] S. N. Nakamura, R.S. Hayano, M. Iwasaki, K. Shigaki, E. Widmann, T. Yamazaki, H. Daniel, T.v. Egidy, F.J. Hartmann, P. Hofmann, Y.-S. Kim, J. Eades, Phys. Rev. A 49 (1994) 4457.

[5] E. Widmann, I. Sugai, T. Yamazaki, R.S. Hayano, M. Iwasaki, S.N. Nakamura, H. Tamura, T.M. Ito, A. Kawachi, N. Nishida, W. Higemoto, Y. Ito, N. Morita, F.J. Hartmann, H. Daniel, T.v. Egidy, W. Schmid, J. Hoffmann, J. Eades, Phys. Rev. A53 (1996) 3129.

[6] Y. Ito, E. Widmann, T. Yamazaki, Hyp. Int. 76 (1993) 163.

[7] R. Ahlrichs, O. Dumbrajs, H. Pilkuhn, H.G. Schlaile, Z. Phys. A306 (1982) 297.

[8] I. Shimamura, Phys. Rev. A46 (1992) 3776.

[9] W.J. Hehre, L. Radom, P.v.R. Schleyer, J.A. Pople, Ab Initio Molecular Orbital Theory, Ed. Wiley & Sons, United States, 1986.

[10] R. Krishnan, J.S. Binkley, R. Seeger, J.A. Pople, J. Chem. Phys. 72 (1980) 650.

[11] T. Yamazaki, E. Widmann, J. Eades, M. Kumakura, N. Morita, H.A. Torii, M. Hori, T. Ishikawa, F.E. Maas, H. Tamura, R.S. Hayano, I. Sugai, Y. Fujita, B. Ketzer, H. Daniel, F.J. Hartmann, M. Hasinoff, R. Pohl, R. Schmidt, T.v. Egidy, D. Horváth, Phys. Rev. A 55 (1997) R3295.

[12] L. Landau, E. Lifchitz, Quantum Mechanics, Mir Pub., Moscow, 1980, p 91.

[13] S. Sauge, P. Valiron, accepted in Chemical Physics.

[14] B. Ketzer, F.J. Hartmann, T.v. Egidy, C. Maierl, R. Pohl, J. Eades, E. Widmann, T. Yamazaki, M. Kumakura, N. Morita, R.S. Hayano, M. Hori, T. Ishikawa, H.A. Torii, I. Sugai, D. Horváth, J. Chem. Phys., 109 (1998) 424.

Chapter 6

Other possible metastable systems

6.1 Antiproton helium polarization states

Antiproton helium polarization states have been proposed by Carbonell *et al.* (1995): these are systems in which the antiproton would be trapped in the tail of the long range attractive polarization potential. However, we may expect these states to be unstable by collisions, owing to the absence of shielding of the $\bar{p}$ by the electronic cloud.

6.2 Other antiprotonic atomcules

We may also consider other antiprotonic atomcules. Again, such systems will probably be unstable, either by collisions or by Auger emission of the valence electron, inducing Stark annihilation (see Fig. 6.1).

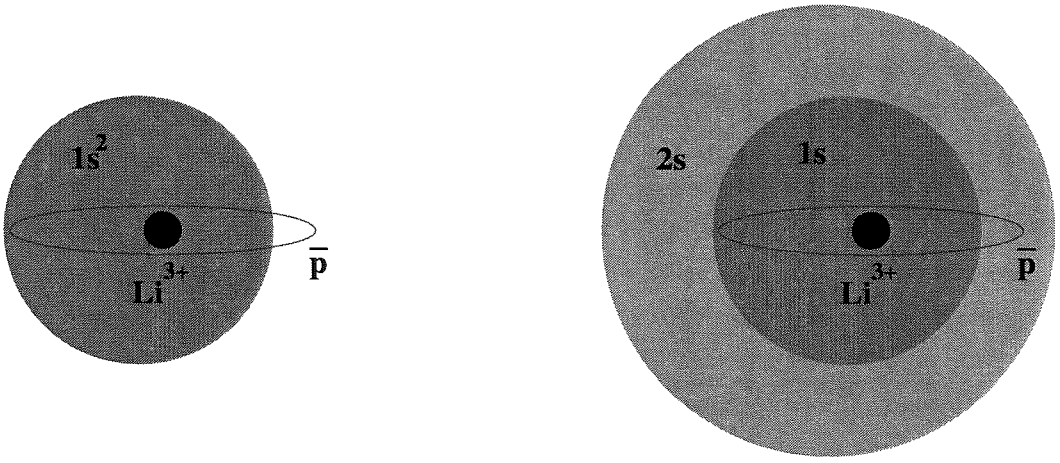

Figure 6.1: Antiprotonic Lithium atomcules. On the left plot, Pauli shielding of the $\bar{p}$ is too weak to prevent collisional quenching. On the right plot, the antiproton is screened, but fast Auger emission is more likely.

6.3 Molecular Rydbergs

The metastability of molecular Rydbergs might be investigated as well (Fig. 6.2). The antiproton would be closer to nuclei than for polarization states, and could therefore be shielded by the surrounding electronic cloud. On the other hand, other processes might compete for quenching these states, such as Auger expulsion of the outer valence electron, or radiative transitions induced by ro-vibronic excitation of the cluster:

$$[He_2^+, \vec{p}]_{nl} \rightarrow [He_2^{+\star}, \vec{p}]_{n'l'} \tag{6.1}$$

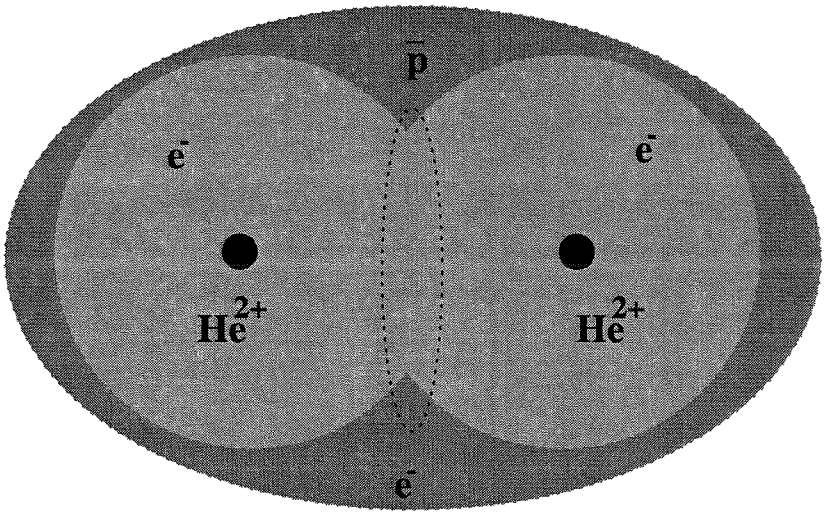

Figure 6.2: Molecular Rydberg $[He_2^+,\bar{p}]_{nl}$. It may describe an intermediary state in the $\bar{p}He^+$-He collision, just before annihilation.

6.4 Towards ground-state antiproton trapping?

As an alternative for non-metastable antiprotonic trapping schemes, we may consider the insertion of $\bar{p}$ within nanometric cages, hoping to provide ground-state antiproton trapping. We cannot expect any electrostatic confinement, since electrostatic forces vanish inside closed cages, according to the Gauss theorem. Similarly, polarization terms are always attractive towards the atomic cage, and thus also dispersive. However, for highly conjugated systems such as fullerenes, we might consider phenomenons of cage retroaction: the distorsion of the electronic cloud by the $\bar{p}$ might induce a *chemical* repulsive force, which might confine the $\bar{p}$ if it happens to be stronger than the dispersive electrostatic and polarization forces. Preliminary calculations for C60 have shown no confinement effects so far.

Conclusion

L'étude des atomes d'helium antiprotonique $\bar{p}He^+$ a évolué au cours des années, passant du statut de "curiosité exotique" à celui d'un vaste champ d'investigation rendu accessible grâce à une spectroscopie haute précision. Les nouvelles méthodes spectroscopiques développées au CERN ont fourni la preuve expérimentale indubitable de l'existence d'atomcules métastables formés par capture d'antiprotons dans l'helium sur des orbites de Rydberg de grand moment angulaire $l \sim 40$. Avec l'amélioration conjointe des prédictions théoriques et des techniques expérimentales, ce système à trois corps original (α $\bar{p}$ e^-) a atteint un niveau de précision tel que la prise en compte des corrections de l'électrodynamique quantique est devenue nécessaire pour rendre compte des énergies de transition mesurées au niveau de sa structure hyperfine. Si cette évolution devait se poursuivre, l'atomcule $\bar{p}He^+$ pourrait bien surpasser l'atome d'helium en tant que système à trois corps dont la structure est prédite théoriquement et vérifiée expérimentalement avec une précision jamais atteinte. En devenant par ailleurs le premier système de laboratoire pour l'électrodynamique quantique de l'antiproton, l'atomcule trouve un rôle complémentaire à celui de l'atome d'anti-hydrogène, tout en restant plus facile à synthétiser.

En dehors des études structurales de l'atomcule, les aspects de leur interaction avec d'autres atomes, molécules ou systèmes exotiques constitue un vaste champ d'investigation pour la physique des collisions et la physico-chimie moléculaire, balisé par une spectroscopie qui permet d'étudier l'interaction des états individuels avec leur environnement. Mon travail de thèse s'est inscrit dans cette dynamique. L'intérêt premier de ces recherches a été de confirmer que les concepts usuels de physique moléculaire sont effectivement transposables - voire indispensables - à l'étude de ces processus exotiques. Dans ce cadre, nos travaux ont permis de rendre compte de la grande diversité de comportements collisionnels observés ou présumés:

- la stabilité collisionnelle des atomcules dans l'helium pur est attribuée à l'existence d'une barrière d'activation élevée: le nuage électronique protège l'antiproton des collisions mais cet écrantage devient insuffisant pour les états externes ($n \geq 42$) qui sont détruits. Par ailleurs la thermalisation des atomcules formés avec une énergie cinétique supérieure à la hauteur des barrières détruit toutes les populations métastables de façon significative (50 % au moins), portant la fraction estimée des états de capture de 20 à 3 %.

- le fort "quenching" collisionnel par H_2 à basse température ($\sim$ 30 K) est sous-tendu par l'existence de très faibles barrières d'activation ($\sim$ 100 μH) qui rendent compte qualitativement des sections efficaces de destruction géométriques mesurées expérimentalement. A cet égard, nous soulignons l'impossibilité de faire des prédictions quantitatives sans une détermination très précise de l'interaction moléculaire, impliquant le recours à des techniques de chimie quantique *ab initio*. En dehors du cadre de ces expériences, l'étude de ces systèmes éclaire également la physico-chimie des radicaux terrestres et interstellaires froids. En montrant que l'extension spatiale des fonctions d'onde vibrationelles de molécules légères comme H_2 ne peut être ignorée pour des calculs très précis du potentiel d'interaction, nous anticipons que la réactivité chimique complexe de NH_3 ou H_2O pourrait être mieux comprise à la lumière de cet effet négligé en général.

- Une autre voie de synthèse de l'antihydrogène, par réaction d'atomcules antiprotoniques $\bar{p}He^+$ avec du positronium e^+e^-, est confirmée avec un rapport de branchement de 10 %. Par ailleurs, nous prédisons la formation d'une nouvelle classe d'atomcules exotiques métastables (α, $\bar{p}$, e^+, $2e^-$). Si la spectroscopie venait confirmer son existence, le nouvel atomcule pourrait constituer le premier test de référence pour le traitement de la corrélation dans des molécules composées de leptons et d'antileptons. On peut espérer que d'autres systèmes exotiques métastables verront bientôt le jour dans l'imagination des chercheurs ou les murs des laboratoires capables de produire des faisceaux d'antiprotons de basse énergie.

L'expérience LEAR s'est arrêtée en novembre 1996 pour laisser la place au montage du projet ASACUSA (Atomic Spectroscopy And Collisions Using Slow Antiprotons). Ce projet a pour objet d'étudier les états antiprotoniques liés et les états du continuum. En fonction du point de vue, de telles études constitueront un test des théories "few-body" ou des théorèmes d'invariance CPT (Charge-Parité-Temps). Si on suppose l'invariance des propriétés du proton et de l'antiproton par symétrie CPT, l'accord entre théorie et expérience constitue une validation des calculs QED pour les systèmes à trois corps en interaction coulombienne. En revanche, si on admet l'exactitude de ces calculs, il en résulte des contraintes sévères sur les constantes fondamentales de l'antiproton, ce qui constitue un test du théorème CPT.

Le projet ASACUSA qui achève sa phase de mise en route, devrait permettre le stockage prolongé d'antiprotons de très basse énergie (jusqu'à quelques eV), ouvrant ainsi de nouveaux champs d'investigation:

- Spectroscopie haute résolution des atomes d'helium antiprotonique: structure hyperfine, populations initiales et durée de vie des états individuels en fonction des conditions physico-chimiques (pression, température, densité de contaminants).

- Formation de clusters antiprotoniques dans des gaz très dilués voire in vacuo (i.e. en une seule collision) et étude spectroscopique des mécanismes de capture, par mesure de la population primordiale des états formés. Spectroscopie $p\bar{p}$ (hydrogène antiprotonique).

Ces expériences ouvrent la voie à une physico-chimie de l'antimatière, dont l'assise théorique pourrait être testée en complétant l'interprétation des mesures fournies par LEAR tout en suggérant de nouvelles expériences pour le projet ASACUSA. Ce ne sont pas les clés de la Cité qui aiguisent ici des désirs de conquête, mais celles de l'Antimonde.

Appendix

Chapter 7

Introduction to ab initio quantum chemistry

Contents

7.1 Introduction

The key to theoretical chemistry is molecular quantum mechanics. This is the science relating molecular properties to the motion and interactions of electrons and nuclei. Soon after its formulation in 1925, it became clear that solution of the Schrödinger equation could, in principle, lead to direct quantitative prediction of most, if not all, chemical phenomena using only the values of a small number of physical constants (Planck's constant, the velocity of light and the masses and charges of electrons and nuclei). Such a procedure constitutes an *ab initio* approach to chemistry, independent of any experiment other than the determination of these constants. It was also early recognized that solution of the Schrödinger equation was a formidable if not completly impossible mathematical problem for any but the very simplest of systems. In practice, the Schrödinger equation has to be replaced by approximate mathematical models for which the possibility of solution exists.

The theoretical models discussed in this chapter are all based on *molecular orbital (MO) theory*. This approximate treatment of electron distribution and motion assigns electrons to

one-electron functions termed *spin orbitals*. These comprise a product of spatial functions, termed *molecular orbitals*, $\psi_1(x,y,z)$, $\psi_2(x,y,z)$, $\psi_3(x,y,z)$, ..., and either α or β *spin components*. The spin orbitals are allowed complete freedom to spread throughout the molecule, their exact form being determined variationally to minimize the total energy. In the simplest version of the theory, a single assignment of electrons to orbitals (sometimes called an *electron configuration*) is made. These orbitals are then brought together to form a suitable *many-electron wave function* Ψ which is the simplest MO approximation to the solution of the Schrödinger equation.

In practical calculations, the molecular orbitals ψ_1, ψ_2, ..., are further restricted to be linear combinations of a set of N known one-electron functions $\phi_1(x,y,z)$, $\phi_2(x,y,z)$, ..., $\phi_N(x,y,z)$:

$$\psi_i = \sum_{\mu=1}^{N} c_{\mu i}\phi_\mu. \tag{7.1}$$

The functions $\phi_1(x,y,z)$, $\phi_2(x,y,z)$, ..., $\phi_N(x,y,z)$ are known as *one-electron basis functions*, or simply as *basis functions*. They constitute a *basis set*. If the basis functions are the *atomic orbitals* for the atoms making up the molecule, Eq. (7.1) is often described as the *linear combination of atomic orbitals (LCAO) approximation*, and is frequently used.

Given the basis set, the unknown coefficients $c_{\mu i}$ are determined so that the total electronic energy calculated from the many-electron wave function is minimized and, according to the *variational theorem*, is as close as possible to the energy corresponding to the exact solution of the Schrödinger equation. This energy and the corresponding wave function represent the best that can be obtained within the *Hartree-Fock approximation*, that is, the best given the constrained imposed by: (a) the use of a limited basis set in the orbital expansion, and (b) the use of a single assignment of electrons to orbitals.

Hartree-Fock models are the simplest to use for chemical applications and have been employed in many of the studies carried out to date. To specify the model in full, it is only necessary to define a unique basis set ϕ_1, ϕ_2, ..., ϕ_N for any nuclear configuration. This is conveniently done by having a standard set of basis functions for each nucleus, centered at the nuclear position, which depend only upon the corresponding atomic number. Thus, there would be a set of functions for each hydrogen atom and other sets for each carbon and so forth. In the simplest Hartree-Fock models, the number of basis functions on each atom will be as small as possible, that is only large enough to accomodate all the electrons and maintain spherical symmetry. As a consequence, the molecular orbitals (7.1) will have only limited flexibility. If larger basis sets are used, the number of adjustable coefficients in the variational procedure increases, and an improved description of the molecular orbitals are obtained. Very large basis sets will result in nearly complete flexibility. The limit of such an approach, termed the *Hartree-Fock limit*, represents the best that can be done with a single electron configuration.

The main deficiency of Hartree-Fock theory is its incomplete description of the *correlation* between motions of the electrons. Even with a large and completely flexible basis set, the full solution of the Schrödinger equation cannot be expressed in terms of a *single electron configuration*, that is, a unique assignment of electrons to orbitals. To correct for such a deficiency, it is necessary to use wave functions that go beyond the Hartree-Fock level, that is, that represent more than a single electron configuration. If Ψ_0 is the full Hartree-Fock many-electron wave function, the extended approximate form for the more accurate wave function is

$$\Psi = a_0\Psi_0 + a_1\Psi_1 + a_2\Psi_2 + \ldots \tag{7.2}$$

Here Ψ_1, Ψ_2, ... are wave functions for other configurations, and the linear coefficients a_0, a_1, ... are to be determined. Inclusion of wave functions for all possible alternative electron configurations (within the framework of a given basis set) is termed *full configuration interaction*. It represents the best that can be done using that basis set. Practical methods, which may be sequenced in order of increasing sophistication and accuracy, seek either to limit the number of configurations or to approximate the effect which their inclusion has on the total wave function.

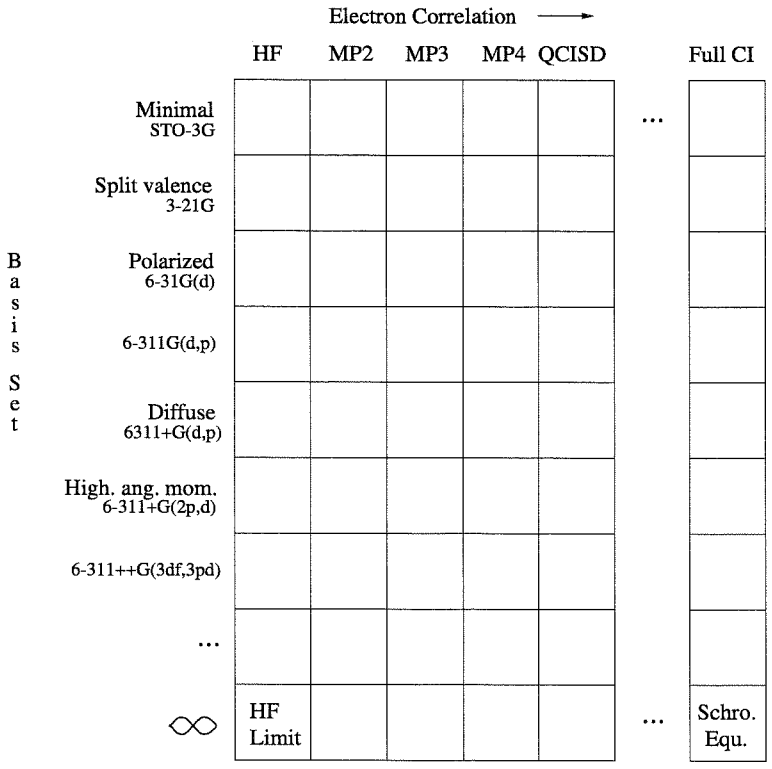

Figure 7.1: Schematic representation of theoretical models showing basis set improvement vertically and correlation improvement horizontally (Foresman & Frisch, 1993).

The two directions in which theoretical models may be improved can be shown with a two-dimensional chart as in Fig. 7.1. The simplest type of model is a Hartree-Fock treatment using a small basis set. This would be placed at the top left of the diagram. As more sophisticated models are applied, an investigation may move downwards (improvement of the basis set) or from left to right (improvement of correlation technique). The bottom row, which may be not realizable in practice, represents various methods using a completely flexible basis. The right-hand column, which may also be impractical, represents full configuration interaction with a given basis. The bottom righ-hand corner corresponds to full configuration interaction with a completely flexible basis set, i.e. the exact solution of the nonrelativistic Schrödinger equation. The following sections describe more explicitely the approximation techniques used by these various methods.

7.2 The Schrödinger equation

According to quantum mechanics, the energy and many properties of a stationary state of a molecule can be obtained by solution of the Schrödinger partial differential equation

$$\hat{H}\Psi = E\Psi, \tag{7.3}$$

where H is the *Hamiltonian*, a differential operator representing the total energy. E is the value of the energy of the state, that is, the energy relative to a state in which the constituent particles (nuclei and electrons) are infinitely separated and at rest. Ψ is the *wave function.* It depends on the cartesian coordinates of all particles (which may take any value from $-\infty$ to $+\infty$) and also on the spin coordinate (which may take only a finite number of values corresponding to spin angular momentum components in a particular direction). The square of the wave function, $|\Psi^2|$, is interpreted as a measure of the probability distribution of the particles within the molecule. The Hamiltonian $\hat{H}$, like the energy in classical mechanics is the sum of kinetic and potential parts

$$\hat{H} = \hat{T} + \hat{V}\,. \tag{7.4}$$

The kinetic energy operator $\hat{T}$ is a sum of differential operators,

$$\hat{T} = -\frac{h^2}{8\pi^2}\sum_i \frac{1}{m_i}\left(\frac{\partial^2}{\partial x_i^2} + \frac{\partial^2}{\partial x_i^2} + \frac{\partial^2}{\partial z_i^2}\right)\,. \tag{7.5}$$

The sum is over all particles i (nuclei + electrons) and m_i is the mass of particle i. h is *Planck's constant.* The potential energy operator is the coulomb interaction

$$\hat{V} = \sum_{i<j}\left(\frac{e_i e_j}{r_{ij}}\right)\,. \tag{7.6}$$

where the sum is over distinct pairs of particles (i, j) with electric charges e_i, e_j separated by a distance r_{ij}. For electrons, $e_i = -e$, while for a nucleus with atomic number Z_i, $e_i = Ze$.

The Hamiltonian described above is *nonrelativistic.* It ceases to be appropriate as the velocities of the particles, particularly electrons, approach the velocity of light. This effect becomes significant for the inner-shell electrons of heavy atoms. Certain small magnetic effects, such as spin orbit coupling or spin-spin interactions are also omitted in this Hamiltonian; these are usually of minor significance in discussions of chemical energies.

One other restriction has to be imposed on the wave functions. The only solutions of (7.3) that are physically acceptable are those with appropriate symmetry under interchange of identical particles. For *boson* particles, the wave function is unchanged, that is, *symmetric*, under such interchange. For *fermion* particles, the wave function must be multiplied by -1, that is, *antisymmetric.* Electrons are fermions, so that Ψ must be antisymmetric with respect to interchange of the coordinates of any pair of electrons. This is termed the *antisymmetry principle.* The Schrödinger equation for any molecule will have many solutions, corresponding to different *stationary states.* The state with lowest energy is the *ground state.* Most of the techniques and applications described hereafter are concerned with the ground states of molecules.

7.3 The Born-Oppenheimer approximation

The first major step in simplifying the general molecular problem in quantum mechanics is the separation of the nuclear and electronic motions. This is possible because the nuclear masses are much greater than those of the electrons, and, therefore, nuclei move much more slowly. As a consequence, the electrons in a molecule adjust their distribution to changing nuclear positions rapidly. This makes it a reasonable approximation to suppose that the electron distribution depends only on the instantaneous positions of the nuclei and not on their velocities. In other words, the quantum-mechanical problem of electron motion in the field of *fixed* nuclei may first be solved, leading to an *effective* electronic energy $E_{\text{eff}}(\mathbf{R})$ which depends on the relative nuclear coordinates denoted by $\mathbf{R}$. This effective energy is then used as a potential energy for a subsequent study of the nuclear motion. This separation of the general problem into two parts is frequently called the *adiabatic* or *Born-Oppenheimer approximation.* Quantitatively, the Born-Oppenheimer approximation may be formulated by writing down the Schrödinger equation for electrons in the field of fixed nuclei,

$$\hat{H}^{\text{elec}}\Psi^{\text{elec}}(\mathbf{r},\mathbf{R}) = E_{\text{eff}}(\mathbf{R})\Psi^{\text{elec}}(\mathbf{r},\mathbf{R})\,. \tag{7.7}$$

Here, Ψ^{elec} is the electronic wave function which depends on the electronic coordinates, $\mathbf{r}$, as well as on the nuclear coordinates, $\mathbf{R}$. The electronic Hamiltonian, $\hat{H}^{\text{elec}}$, corresponds to the motion of electrons only in the field of fixed nuclei and is

$$\hat{H}^{\text{elec}} = \hat{T}^{\text{elec}} + \hat{V}, \tag{7.8}$$

where $\hat{T}^{\text{elec}}$ is the electronic kinetic energy,

$$\hat{T}^{\text{elec}} = -\left(\frac{h^2}{8\pi^2 m_e}\right) \sum_{i}^{\text{electrons}} \frac{1}{m_i}\left(\frac{\partial^2}{\partial x_i^2} + \frac{\partial^2}{\partial x_i^2} + \frac{\partial^2}{\partial z_i^2}\right), \tag{7.9}$$

and $\hat{V}$ is the coulomb potential energy,

$$\hat{V} = -\sum_{i}^{\text{electrons}} \sum_{l}^{\text{nuclei}} \frac{Z_k e^2}{r_{ik}} + \sum_{i<j}^{\text{electrons}} \frac{e^2}{r_{ij}} + \sum_{k<l}^{\text{nuclei}} \frac{Z_k Z_l e^2}{R_{kl}}. \tag{7.10}$$

The first part of (7.10) corresponds to the electron-nuclear attraction, the second to the electron-electron repulsion, and the third to nuclear-nuclear repulsion. The last is independent of the electronic coordinates and is a constant contribution to the energy for any particular nuclear configuration. The main task of theoretical studies of electronic structure is to solve, by using the best possible approximation, the electronic Schrödinger equation (7.7).

The potential surface, $E^{\text{eff}}(\mathbf{R})$, is fundamental to the quantitative description of chemical structures and reaction processes. If we deal with the lowest energy solution of the electronic Schrödinger equation, $E^{\text{eff}}(\mathbf{R})$ is the ground-state potential energy surface. This surface will generally have a number of local minima. These are *equilibrium structures.* The geometry corresponding to a minimum of E(R) would be the geometry a molecule would have if the nuclei were in fact stationary. In practice , finite nuclear motions occurs because of *zero-point vibration*, even at low temperatures. Nevertheless, the potential minimum is usually a good approximation to the averaged structure.

7.4 Atomic units

Before discussing approximate electronic wave functions, it is useful to adopt new units which eliminate the fundamental physical constants from the electronic Schrödinger equation (7.3). This involves introduction of the *Bohr radius*, a_0, defined by

$$a_0 = \frac{\hbar^2}{4\pi^2 m e^2}. \tag{7.11}$$

This is the atomic unit of length (the *bohr*). New coordinates (x',y',z') may now be introduced:

$$x' = \frac{x}{a_0}. \tag{7.12}$$

In a similar way, we can introduce a new atomic unit of energy, E_H, which is the coulomb repulsion between two electrons separated by 1 bohr:

$$E_H = \frac{e^2}{a_0}. \tag{7.13}$$

This unit is termed the *hartree*. New energies (E') are given by

$$E' = \frac{E}{E_H}. \tag{7.14}$$

If (7.12) and (7.14) are substituted into the Schrödinger equation (7.3), we have

$$\hat{H}'\,\Psi' = E'\,\Psi', \tag{7.15}$$

where the hamiltonian, $\hat{H}'$, in atomic units, is

$$\hat{H}' = -\frac{1}{2}\sum_{i}^{electrons}\left(\frac{\partial^2}{\partial x_i'^2}+\frac{\partial^2}{\partial y_i'^2}+\frac{\partial^2}{\partial z_i'^2}\right) - \sum_{i}^{electrons}\sum_{s}^{nuclei}\left(\frac{Z_s}{r'_{is}}\right) + \sum_{i<j}^{electrons}\left(\frac{1}{r'_{ij}}\right) + \sum_{s<t}^{nuclei}\left(\frac{Z_s Z_t}{R'_{st}}\right). \tag{7.16}$$

Throughout the rest of this part, we assume atomic units.

7.5 Molecular orbital theory

Molecular orbital theory is an approach to molecular quantum mechanics which uses one-electron functions or *orbitals* to approximate the full wave function. A molecular orbital, $\psi(x,y,z)$, is a function of the cartesian coordinates x, y, z of a single electron. Its square modulus, $|\psi|^2$, is interpreted as the probability distribution of the electron in space. To describe the distribution of an electron completly, the dependance on the spin coordinates, ξ, also has to be included. This coordinate takes on one of two possible values($\pm\frac{1}{2}$),and measures the spin angular momentum component along the z axis in units of $h/2\pi$. For spin aligned along the positive z axis, the spin wave function is written $\alpha(\xi)$. Thus,

$$\alpha(+\frac{1}{2}) = 1, \qquad \alpha(-\frac{1}{2}) = 0\,. \tag{7.17}$$

Similarly, for spin along the negative z axis, the spin wave function is $\beta(\xi)$, so that

$$\beta(+\frac{1}{2}) = 0, \qquad \beta(-\frac{1}{2}) = 1\,. \tag{7.18}$$

The complete wave function for a single electron is the product of a molecular orbital and a spin function, $\psi(x,y,z)\alpha(\xi)$ or $\psi(x,y,z)\beta(\xi)$. It is termed a *spin orbital*, $\chi(x,y,z,\xi)$. It might appear that the simplest type of wave function appropriate for the description of an n-electron system would be in the form of a product of spin orbitals,

$$\Psi = \chi_1(1)\chi_2(2)...\chi_n(n) \tag{7.19}$$

where $\chi_i(i)$ is written for $\chi_i(x_i,y_i,z_i,\xi_i)$, the spin orbital of electron i. However, such a wave function is not acceptable, as it does not have the property of antisymmetry. If the coordinates of electrons i and j are interchanged in this wave function, the product $...\chi_i(i)...\chi_j(j)...$ becomes $...\chi_i(j)...\chi_j(i)...$ which is not equivalent to multiplication by -1. To ensure antisymmetry, the spin orbitals may be arranged in a *determinantal wave function*

$$\Psi = \frac{1}{\sqrt{n!}}\begin{vmatrix} \chi_1(1) & \chi_2(1) & ... & \chi_n(1) \\ \chi_1(2) & \chi_2(2) & ... & \chi_n(2) \\ ... & ... & ... & ... \\ \chi_1(n) & \chi_2(n) & ... & \chi_n(n) \end{vmatrix} \tag{7.20}$$

Here the elements of the first row of the determinant contain assignations of electron 1 to all the spin orbitals $\chi_1\chi_2...\chi_n$, the second row all possible assignations of electron 2, and so forth. Interchange of two electrons interchanges two rows in the Slater determinant, which multiplies the wave function by -1, ensuring antisymmetry. In such a wave function, no two electrons can be assigned to the same spin-orbital; this is the Pauli exclusion principle and is a consequence of the Pauli-principle antisymmetry requirement.

In building up a determinantal wave function, the usual practice choice is to choose a set of molecular orbitals $\psi_1, \psi_2, \psi_3, ..., \psi_n$, and then to assign electrons of α or β spin to these orbitals, as shown on Fig. 7.2. The electrons are represented by arrows ($\uparrow$ for α, $\downarrow$ for β), orbitals of lowest energy being at the bottom of the diagram.

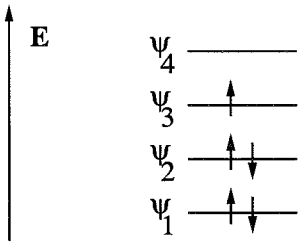

Figure 7.2: Electron configuration diagram for $(\psi_1\alpha)(\psi_1\beta)(\psi_2\alpha)(\psi_2\beta)(\psi_3\alpha)$. Electrons are denoted by arrows.

It is not possible for a molecular orbital to be occupied by two electrons of the same spin. This is the *Pauli exclusion principle*, which follows because the determinantal wave function (7.20) vanishes if two columns are identical. Hence orbitals may be classified as doubly occupied (ψ_1, ψ_2), singly occupied (ψ_3) or empty (ψ_4). Most molecules have an even number of electrons in their ground (lowest-energy) states and may be represented by *closed-shell wave functions* with orbitals either doubly occupied or empty.

7.6 Basis set

7.6.1 Basis set expansions

In practice, the individual molecular orbitals are expressed as linear combinations of a finite set of N prescribed one-electrons functions known as *basis functions*. If the basis functions are $\phi_1, \phi_2, ..., \phi_n$, then an individual orbital ψ_i can be written

$$\psi_i = \sum_{\mu=1}^{N} c_{\mu i}\phi_\mu, \tag{7.21}$$

where $c_{\mu i}$ are the *molecular orbital expansion coefficients*. These coefficients provide the orbital description with some flexibility, but clearly do not allow for complete freedom unless the ϕ_μ define a complete set. However, the problem of finding the orbitals is reduced from

finding complete descriptions of the three-dimensional function ψ_i to finding only a finite set of linear coefficients for each orbital.

In simple qualitative versions of molecular orbital theory, atomic orbitals of constituent atoms are used as basis functions. Such treatments are often described as *linear combination of atomic orbital (LCAO)* theories. Thus, a set of basis functions is associated with each nucleus, depending only on the charge of that nucleus. Such functions may have the symmetry properties of atomic orbitals, and may be classified as *s, p, d, f...* according to their angular properties. Two types of atomic basis functions have received widespread use. *Slater-type atomic orbitals* (STOs) have exponential radial parts. They are labeled like hydrogen atomic orbitals, $1s, 2s, 2p_x, ...$ and have the normalized form

$$\psi_{n,l,m}(r_a, \theta_a, \phi_a) = N r_a^{n-1} \exp(-\zeta r_a) Y_l^m(\theta_a, \phi_a) \,. \tag{7.22}$$

To simplify molecular integral evaluation, Boys proposed the use of *Gaussian-type functions* (GTFs) instead of STOs. A cartesian gaussian centered on atom a is defined as

$$g_{ijk} = N x_a^i y_a^j z_a^k \, e^{(-\alpha r_a^2)}, \tag{7.23}$$

where N is the normalization constant, i, j and k are nonnegative integers, and α is a positive orbital exponent. When $i+j+k = 0$, the GTF has an s type; when $i+j+k = 1$, we have a p-type Gaussian, which contains the factor x_a, y_a or z_a. When $i+j+k = 2$, we have a d-type Gaussian. There are six d-type Gaussians, with the factors $x_a^2, y_a^2, z_a^2, x_a y_a, x_a z_a$ et $y_a z_a$. If desired, five linear combinations (having the factors $x_a y_a, x_a z_a, y_a z_a, x_a^2 - y_a^2$ and $3z_a^2 - r_a^2$) can be formed to have the same angular behavior as the five real $3d$ AOs. Gaussian-type functions are less satisfactory than STOs as representations of atomic orbitals, particularly because they do not have a *cusp* at the origin [1]. Nevertheless, they have the important advantage that all integrals in the computations can be evaluated explicitly without recourse to numerical integration. In order to describe more precisely the electron-nucleus cusp region, it is common to use linear combinations of gaussian functions as basis functions. For example, an s-type basis function ϕ_μ may be expanded in terms of s-type gaussians,

$$\phi_\mu = \sum_s d_{\mu s} \, g_s \,. \tag{7.24}$$

Here the coefficients $d_{\mu s}$ are fixed. Basis functions of this type are called *contracted gaussians*, the individual g_s being termed *primitive gaussians*. By using contracted gaussians instead of primitive gaussians as the basis set, the number of variational coefficients to be determined is reduced, which gives large savings in computational time with little loss in accuracy if the contraction coefficients $d_{\mu s}$ are well chosen.

[1] The cusp or discontinuity in the first derivative of the electronic wave function arises because the electron-nucleus or electron-electron potential energy becomes infinite where two particles meet. The cusp conditions a proper wave function has to satisfy will be investigated in further details in Sec. 8.2.6.

7.6.2 Minimal basis sets

Minimal basis sets contain the minimum number of basis functions needed for each atom, as in the examples:

H 1s

C 1s, 2s, $2p_x$, $2p_y$, $2p_z$

Minimal basis sets use fixed-size atomic-type orbitals. For example, the STO-3G basis set uses three gaussian primitives per basis function, which accounts for the "3G" in its name. The STO-3G basis set approximates Slater orbitals with gaussian functions.

7.6.3 Split valence basis sets

The first way a basis set can be made larger is to increase the number of basis functions per atom. *Split valence basis sets*, such as 3-21G and 6-31G have two (or more) sizes of basis function for each valence orbital. For example, hydrogen and carbon are represented as

H 1s,1s'

C 1s, 1s', 2s, 2s', $2p_x$, $2p'_x$, $2p_y$, $2p'_y$, $2p_z$ $2p'_z$

where the primed and unprimed orbitals differ in size. The *double zeta* basis sets form all molecular orbitals from linear combinations of two sizes of functions for each atomic orbital. Similarly, *triple zeta* basis sets, like 6-311G, use three sizes of contracted functions for each orbital-type.

7.6.4 Polarized basis sets

Split valence basis sets allow orbitals to change size, but not to change shape. Besides, atomic orbitals are distorded (or polarized) upon molecule formation. To allow for this polarization, one must introduce basis-functions STOs with angular momentum beyond what is required for the ground state to the description of each free atom. For example, polarized basis sets add d functions to carbon atoms and f functions to transition metals, and some of them add p functions to hydrogen atoms.

7.6.5 Diffuse functions

Basis sets with diffuse functions are important for systems where electrons are relatively far from the nucleus: molecules with lone pairs, anions and other systems with significant negative charges, systems in their excited states, systems with low ionization potentials. Diffuse functions are large-size versions of s- and p-type functions (as opposed to the normal, contracted functions). They allow orbitals to occupy a larger region of space.

7.7 Hartree-Fock theory

Up to this point, we have described how a determinantal wave function may be constructed from molecular orbitals, and how the orbitals may, in turn, be expanded in terms of a set of

basis functions. It remains to specify a method for fixing the expansion coefficients. This is the realm of *Hartree-Fock theory.*

Hartree-Fock theory is based on the *variational method* in quantum mechanics. If Φ is *any* antisymmetric normalized function of the electronic coordinates, then an expectation value of the energy corresponding to this function can be obtained from the integral

$$E' = \int \Phi^* \hat{H} \Phi d\tau \,. \tag{7.25}$$

If Φ happens to be the exact wave function, Ψ, for the electronic ground state, it will satisfy the Schrödinger equation (7.3). Since Ψ is normalized, E' will therefore be the exact energy E,

$$E' = E \int \Psi^* \Psi d\tau = E \,. \tag{7.26}$$

However, if Φ is *any other* normalized antisymmetric function, it can be shown that E' is greater than E,

$$E' = \int \Phi^* \hat{H} \Phi d\tau > E \,. \tag{7.27}$$

Thus, the variational method may be applied to determine optimum orbitals in single-determinant wave functions (7.20). In practice, we select a bais set for orbital expansion, and the coefficients $c_{\mu i}$ (as in Eq. 7.21) may then be adjusted to minimize the expectation value of the energy E'. The resulting value of E' will then be as close to the exact energy E as is possible within the limitations imposed by: (a) the single-determinant wave function, and (b) the particular basis set employed. Hence the *best* single-determinant wave function, in an energy sense, is found by minimizing E' with respect to the coefficients $c_{\mu i}$. This implies the variational equations

$$\frac{\partial E'}{\partial c_{\mu i}} = 0 \,. \tag{7.28}$$

We first deal with these equations for closed-shell systems.

7.7.1 Closed-Shell Systems

The variational condition (7.28) leads to a set of algebraic equations for $c_{\mu i}$. They were derived independently for the closed-shell wave function by Roothaan et Hall. The *Roothaan-Hall equations* are

$$\sum_{\nu=1}^{N} (F_{\mu\nu} - \epsilon_i S_{\mu\nu}) c_{\nu i} = 0 \qquad \mu = 1, 2, ..., N \,. \tag{7.29}$$

with the normalization conditions

$$\sum_{\mu=1}^{N} \sum_{\nu=1}^{N} c^{\star}_{\mu\nu} S_{\mu\nu} c_{\nu} = 1 \,. \tag{7.30}$$

Here, ϵ_i is the *one-electron energy* of molecular orbital Ψ_i, $S_{\mu\nu}$ are the elements of an $N \times N$ matrix termed the *overlap matrix*,

$$S_{\mu\nu} = \int \phi_\mu^*(1)\phi_\nu(1)dx_1dy_1dz_1, \tag{7.31}$$

and $F_{\mu\nu}$ are the elements of another $N \times N$ matrix, the *Fock matrix*

$$F_{\mu\nu} = H_{\mu\nu}^{\text{core}} + \sum_{\lambda=1}^{N}\sum_{\sigma=1}^{N} P_{\lambda\sigma}[(\mu\nu|\lambda\sigma) - \frac{1}{2}(\mu\lambda|\nu\sigma)]\,. \tag{7.32}$$

In this expression, $H_{\mu\nu}^{\text{core}}$ is a matrix representing the energy of a single electron in a field of "bare" nuclei. Its elements are

$$\hat{H}^{\text{core}}(1) = -\frac{1}{2}\left(\frac{\partial^2}{\partial x_1^2} + \frac{\partial^2}{\partial y_1^2} + \frac{\partial^2}{\partial z_1^2}\right) - \sum_{\text{A}=1}^{M}\frac{Z_\text{A}}{r_{1\text{A}}}\,. \tag{7.33}$$

Here Z_A is the atomic number of atom A, and summation is carried out over all atoms. The quantities $(\mu\nu|\lambda\sigma)$ are *two-electron repulsion integrals*:

$$(\mu\nu|\lambda\sigma) = \int\int \phi_\mu^*(1)\phi_\nu(1)\left(\frac{1}{r_{12}}\right)\phi_\lambda^*(2)\phi_\sigma(2)dx_1dy_1dz_1dx_2dy_2dz_2\,. \tag{7.34}$$

They are multiplied by the elements of the one-electron *density matrix*, $P_{\lambda\sigma}$:

$$P_{\lambda\sigma} = 2\sum_{i=1}^{\text{occ}} c_{\lambda i}^* c_{\sigma i}\,. \tag{7.35}$$

The summation is over *occupied* molecular orbitals only. The factor of two indicates that *two electrons* occupy each molecular orbital. The electronic energy, E^{ee}, is now given by (7.36)

$$E^{\text{ee}} = \frac{1}{2}\sum_{\mu=1}^{N}\sum_{\nu=1}^{N} P_{\mu\nu}(F_{\mu\nu} + H_{\mu\nu}^{\text{core}}) \tag{7.36}$$

which, when added to (7.37), accouting for the internuclear repulsion,

$$E^{nr} = \sum_{\text{A<B}}^{M}\frac{Z_\text{A}Z_\text{B}}{R_{\text{AB}}} \tag{7.37}$$

(where Z_A and Z_B are the atomic numbers of atoms A and B, and R_{AB} is their separation) yields an expression for the total energy.

The Roothaan-Hall equations (7.29) are not linear since the Fock matrix $F_{\mu\nu}$ itself depends on the molecular orbital coefficients, $c_{\mu i}$, through the density matrix expression (7.35). Solution necessarily involves an iterative process. Since the resulting molecular orbitals are derived from their own effective potential, the technique is frequently call *self-consistent-field (SCF) theory.*

7.7.2 Open-Shell systems

For open-shell systems, in which electrons are not completly assigned to orbitals in pairs, the Roothaan-Hall equations need modification. This applies, for example, to doublet free radicals or triplet states, for which one component will have an excess of α electrons. For doublets, there will be one extra α electron, for triplets, two extra α electrons, and so forth.

Simple molecular orbital theory can be extended to open-shell systems in two possible ways. The first is described as *spin-restricted Hartree-Fock (RHF) theory.* In this approach, a single set of molecular orbitals is used, some being doubly occupied and some being singly occupied with an electron of α spin. This is the case illustrated for a five-electron doublet state in Fig. 7.2. The spin orbitals used in the single determinant are then $(\psi_1\alpha)(\psi_1\beta)(\psi_2\alpha)(\psi_2\beta)(\psi_3\alpha)$. The coefficients $c_{\mu i}$ are still defined by the expansion (7.21) and their optimum values are still obtained from the variational conditions (7.28). However, details are more complicated since different conditions apply to singly- and doubly-occupied orbitals.

The second type of molecular orbital theory in common use for open-shell systems is *spin-unrestricted Hartree-Fock (UHF) theory.* In this approach, different spatial orbitals are assigned to α and β electrons. Thus, there are two distinct sets of molecular orbitals $\psi_i^\alpha = \sum_{\mu=1}^{N} c_{\mu i}^\alpha \phi_\mu$ and $\psi_i^\beta \sum_{\mu=1}^{N} c_{\mu i}^\beta \phi_\mu$ $(i = 1, ..., N)$. The electron configuration for a five-electron doublet may be written as $(\psi_1^\alpha\alpha)(\psi_1^\beta\beta)(\psi_2^\alpha\alpha)(\psi_2^\beta\beta)(\psi_3^\alpha\alpha)$ and is illustrated in Fig. 7.3.

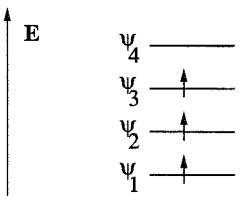

Figure 7.3: Electron configuration diagram for $(\psi_1^\alpha\alpha)(\psi_1^\beta\beta)(\psi_2^\alpha\alpha)(\psi_2^\beta\beta)(\psi_3^\alpha\alpha)$.

It is important to note that the previously doubly-occupied orbital ψ_1 is now replaced by two distinct orbitals, ψ_1^α and ψ_1^β. Since the RHF function is a special case of the UHF function, it follows from the variational principle that the optimized UHF energy must be below the optimized RHF value. On the other hand, UHF functions have the disadvantage that they are not true eigenfunctions of the total spin operator, unlike exact wave functions. Thus, the UHF wave functions which are designed for doublet states (as in the example shown in Fig. 7.2) are contaminated by functions corresponding to states of higher spin multiplicity, such as quartets.

In UHF theory, the two sets of molecular orbitals are defined by two sets of coefficients,

$$\psi_i{}^\alpha = \sum_{\mu=1}^{N} c_{\mu i}^\alpha \phi_\mu, \qquad \psi_i{}^\beta = \sum_{\mu=1}^{N} c_{\mu i}^\beta \phi_\mu \,. \tag{7.38}$$

These coefficients are varied independently, leading to the UHF generalizations of the Roothaan-Hall equations. These are

$$\sum_{\nu=1}^{N}(F_{\mu\nu}^{\alpha} - \epsilon_i^{\alpha} S_{\mu\nu})c_{\nu i}^{\alpha} = 0,$$

$$\sum_{\nu=1}^{N}(F_{\mu\nu}^{\beta} - \epsilon_i^{\beta} S_{\mu\nu})c_{\nu i}^{\beta} = 0, \qquad \mu = 1, 2, ..., N. \tag{7.39}$$

Here, the two Fock matrices are defined by

$$F_{\mu\nu}^{\alpha} = H_{\mu\nu}^{\text{core}} + \sum_{\lambda=1}^{N}\sum_{\sigma=1}^{N}[(P_{\lambda\sigma}^{\alpha} + P_{\lambda\sigma}^{\beta}(\mu\nu|\lambda\sigma) - P_{\lambda\sigma}^{\alpha}(\mu\lambda|\nu\sigma)],$$

$$F_{\mu\nu}^{\beta} = H_{\mu\nu}^{\text{core}} + \sum_{\lambda=1}^{N}\sum_{\sigma=1}^{N}[(P_{\lambda\sigma}^{\alpha} + P_{\lambda\sigma}^{\beta}(\mu\nu|\lambda\sigma) - P_{\lambda\sigma}^{\beta}(\mu\lambda|\nu\sigma)]. \tag{7.40}$$

The density matrix is also separated into two parts,

$$P_{\mu\nu}^{\alpha} = \sum_{i=1}^{\alpha\text{occ}} c_{\mu i}^{\alpha *} c_{\nu i}^{\alpha}, \qquad P_{\mu\nu}^{\beta} = \sum_{i=1}^{\beta\text{occ}} c_{\mu i}^{\beta *} c_{\nu i}^{\beta}. \tag{7.41}$$

The integrals $S_{\mu\nu}$, $H_{\mu\nu}^{core}$, and $(\mu\nu|\lambda\sigma)$ appearing in the UHF equations are the same as those already defined in the Roothaan-Hall procedure for closed-shell calculations.

7.8 The electronic correlation

The primary deficiency of Hartree-Fock theory is the inadequate treatment of the *correlation between motions of electrons.* In particular, single-determinant wave functions take no account of correlation between electrons with opposite spin. Correlation of the motions of electrons with the same spin is partially, but not completly, accounted for by virtue of the determinantal wave function. These limitations lead to calculated (Hartree-Fock) energies that are above the exact values. By convention, the difference between the Hartree-Fock and exact (nonrelativistic) energies is the *correlation energy*

$$E(\text{exact}) = E(\text{Hartree} - \text{Fock}) + E(\text{correlation}) \tag{7.42}$$

The neglect of correlation between electrons of opposite spin leads to a number of qualitative deficiencies in the description of electronic structure. One very important consequence is that the closed-shell Hartree-Fock function often does not dissociate correctly when nuclei are moved to infinite separation. For example, Hartree-Fock theory assigns both electrons in

the hydrogen molecule to a symmetric σ_g-type bonding orbital. The molecular orbital wave function corresponding to this electron configuration is given by

$$2^{-1/2}\sigma_g(1)\sigma_g(2)[\alpha(1)\beta(2) - \beta(1)\alpha(2)]\,. \tag{7.43}$$

As the two hydrogen nuclei are moved appart, this description continues to treat the motion of the electrons in the σ_g molecular orbital as uncorrelated. Within a minimal basis set framework, the form of this orbital at large separations is

$$\sigma_g = 2^{-1/2}[1s_A + 1s_B], \tag{7.44}$$

where $1s_A$ and $1s_B$ are the atomic $1s$ atomic orbitals for the constituent hydrogen atoms. Consequently, the cartesian part of the wave function is

$$\sigma_g(1)\sigma_g(2) = \frac{1}{2}[1s_A(1)1s_A(2) + 1s_A(1)1s_B(2) + 1s_B(1)1s_A(2) + 1s_B(1)1s_B(2)]\,. \tag{7.45}$$

According to this wave function, the two electrons spend half of the time on the same atom (both on A and both on B) and half of the time on different atoms (one and A and one on B), even when the centers are infinitely separated. This is clearly incorrect, since the molecule should dissociate into two neutral hydrogen atoms. In fact, the correct wave function for the singlet state of hydrogen at large separation,

$$\frac{1}{2}[1s_A(1)1s_B(2) + 1s_B(1)1s_A(2)][\alpha(1)\beta(2) - \beta(1)\alpha(2)], \tag{7.46}$$

cannot be expressed in terms of a single determinant.

7.8.1 Full Configuration Interaction

Consider a system comprising n electrons described by a basis set of N functions, ϕ_μ. There will then be $2N$ spin orbital basis functions of the type $\phi_\mu\alpha$ and $\phi_\mu\beta$, which in turn may be linearly combined into $2N$ spin orbitals χ_i. Suppose that we have already solved the Hartree-Fock problem using these basis functions and have obtained the single-determinant wave function ψ_0,

$$\Psi_0 = (n!)^{-1/2}|\chi_1\chi_2\cdots\chi_n|\,. \tag{7.47}$$

Note that the spin orbitals utilized in this determinant, $\chi_1\chi_2\cdots\chi_n$, are a subset of the total set which have been determined in the variational procedure. The unused spin orbitals correspond to unoccupied or *virtual* spin orbitals χ_a $(a = n+1, n+2, \ldots, 2N)$. We shall find it useful to denote occupied spin orbitals by subscripts $i, j, k, \ldots$ and virtual ones by $a, b, c, \ldots$.

Determinantal wave functions, other than the Hartree-Fock function Ψ_0, may now be constructed by replacing one or more of the occupied spin orbitals $\chi_i, \chi_j, \ldots$ in (7.47) by virtual spin orbitals $\chi_a, \chi_b, \ldots$. We shall denote these determinants as Ψ_s with $s > 0$. They

may be further classified into single-substitution functions, Ψ_i^a in which χ_i is replaced by χ_a, double substitution functions, Ψ_{ij}^{ab}, in which χ_i is replaced by χ_a and χ_j by χ_b, triple-substitution functions, and so forth. This series of substituted determinants goes all the way to n-substituted terms in which all occupied spin orbitals are replaced by virtual spin orbitals.

In the full configuration interaction method, a trial wave function

$$\Psi = a_0\Psi_0 + \sum_{s>0} a_s\Psi_s, \tag{7.48}$$

is used, where the summation $\sum_{s>0}$ is over all substituted determinants. The unknown coefficients, a_s, are then determined by the linear variational method, leading to (7.49)

$$\sum_s (H_{st} - E_i\delta_{st})a_{si} = 0, \qquad t = 0, 1, 2, ... \tag{7.49}$$

Here, H_{st} is a configurational matrix element,

$$H_{st} = \int \Psi_s H \Psi_t d\tau_1 d\tau_2 ... d\tau\,. \tag{7.50}$$

and E is an energy. The lowest root E of (7.49) leads to the energy of the electronic ground state. Note the similarity of (7.49) to the Roothan-Hall equations 7.29. The full configuration interaction method represents the most complete treatment possible within the limitations imposed by the basis-set. As the basis set becomes more complete, that is, as $N \to \infty$, the result of a full configuration interaction treatment will approach the exact solution of the nonrelativistic Schrödinger equation. The full CI method is well-defined, size-consistent, and variational. It is not practical except for very small systems, however, because of the vey large number of substituted determinants, the total number of which in (7.48) is (2N!)/[n!(2N-n)!].

7.8.2 Limited Configuration Interaction

The most straightforward way of limiting the length of the CI expansion is to truncate the series (7.48) at a given level of substitution. In practice, the simplest procedure to have any effect on the calculated energy is limited to simple and double substitutions only, and is termed *Configuration Interaction, Singles and Doubles* or CISD,

$$\Psi_{\mathrm{CISD}} = a_0\Psi_0 + \sum_{i}^{\mathrm{occ}}\sum_{a}^{\mathrm{virt}} a_i^a\Psi_i^a + \sum_{i<j}^{\mathrm{occ}}\sum_{a<b}^{\mathrm{virt}} a_{ij}^{ab}\Psi_{ij}^{ab}\,. \tag{7.51}$$

Here, all coefficients are varied to minimize the expectation value of the energy. As a matter of fact, the energy lowering due to inclusion of single substitutions is considerably less than that due to doubles. As a further simplification, the *frozen-core* approximation is often used. In this method, all virtual spin orbitals are included in the CI expansion, but those occupied spin orbitals which correspond principally to inner-shell electrons are omitted. The contributions to the total correlation energy due to inner-shell electrons are not particularly small, but appear to be relatively constant from one molecular environment to another. As a result, the shapes of potential surfaces are little affected by omission of these contributions.

7.8.3 Møller-Plesset Perturbation Theory

The perturbation theory of *Møller* and *Plesset*, closely related to *many-body perturbation theory*, is an alternative approach to the correlation problem. The approach is not to truncate the matrix as in limited CI but rather to treat it as the sum of two parts, the second being a parturbation of the first. Møller-Plesset models are formulated by first introducing a generalized electronic Hamiltonian, $\hat{H}_\lambda$, according to

$$\hat{H}_\lambda = \hat{H}_0 + \lambda\hat{V}, \tag{7.52}$$

where $\hat{H}_0$ is taken to be the sum of the one-electron Fock operators. The perturbation, $\lambda\hat{V}$, is defined by

$$\lambda\hat{V} = \lambda(\hat{H} - \hat{H}_0)\,. \tag{7.53}$$

The eigenvalue, E_s, corresponding to a particular determinant, Ψ_s, is the sum of the one-electron energies, ϵ_i, for the spin orbitals which are occupied in Ψ_s. Ψ_λ and E_λ, the exact or full CI (within a given basis set) ground-state wave function and energy for a system described by the Hamiltonian $\hat{H}_\lambda$, may now be expanded in powers of λ according to Rayleigh-Schrödinger perturbation theory

$$\Psi_\lambda = \Psi^{(0)} + \lambda\Psi^{(1)} + \lambda^2\Psi^{(2)} + ... \tag{7.54}$$

$$E_\lambda = E_0 + \lambda E_1 + \lambda^2 E_2 + ... \tag{7.55}$$

Practical correlation methods may now be formulated by setting the parameter $\lambda = 1$, and by truncation of the series in (7.54-7.55) to various orders. One refers to the methods by the highest-order energy term allowed, that is, truncation after second-order as MP2, after third-order as MP3 and so forth. The leading terms in expansions (7.54-7.55) are

$$\Psi^{(0)} = \Psi_0, \tag{7.56}$$

$$E_0 = \sum_i^{\text{occ}} \epsilon_i, \tag{7.57}$$

$$E_0 + E_1 = \int \Psi_0 H \Psi_0 d\tau_1 d\tau_2 ... d\tau_n = E_{\text{Hartree-Fock}}, \tag{7.58}$$

where Ψ_0 is the Hartree-Fock wave function and ϵ_i are the one-electron energies defined by (7.29). The MP energy to first order is thus the Hartree-Fock energy. Higher terms in the expansion involve other matrix elements of the operator $\hat{V}$. The first-order contribution to the wave function is

$$\Psi^{(1)} = \sum_{S>0} \frac{V_{S0}\Psi_S}{(E_0 - E_S)}, \tag{7.59}$$

where V_{S0} are matrix elements involving the perturbation operator, $\hat{V}$,

$$V_{S0} = \int \Psi_S \hat{V} \Psi_0 \, d\tau_1 \, d\tau_2 \ldots d\tau_n \tag{7.60}$$

One can demonstrate that V_{S0} vanishes unless S corresponds to a double substitution, so that only such substitutions contribute to the first order wave function. The second-order contribution to the MP energy is

$$E_2 = -\sum_S^D \frac{|V_{S0}|^2}{(E_0 - E_s)}, \tag{7.61}$$

where $\sum_S^D$ indicates that summation is to be carried out over all double substitutions. This probably represents the simplest approximate expression for the correlation energy. If Ψ_s is the double-substitution $ij \rightarrow ab$, the explicit expression for V_{S0} is

$$V_{S0} = (ij||ab), \tag{7.62}$$

where $(ij||ab)$ is a two-electron integral over spin orbitals, defined by

$$(ij||ab) = \int\int \chi_i^*(1)\chi_j^*(2) \left(\frac{1}{r_{12}}\right) [\chi_a(1)\chi_b(2) - \chi_b(1)\chi_a(1)] d\tau_1 d\tau_2 \, . \tag{7.63}$$

Here integrationis over all coordinates (cartesian and spin) for both electrons. The final formula for the second-order contribution to the energy then becomes

$$E_2 = -\sum_{i<j}^{occ} \sum_{a<b}^{virt} (\epsilon_a + \epsilon_b - \epsilon_i - \epsilon_j)^{-1} |(ij||ab)|^2 \, . \tag{7.64}$$

An important point to note is that, unlike the simple CID and CISD configuration interaction schemes, MP2 requires only a partial transformation of the two-electron integrals of (7.34) into a spin orbital basis. MP calculations are well defined and can be applied quite widely. Moreover, they do satisfy the size-consistency requirement. On the other hand, perturbation theory results, terminated at any order, are no longer variational, since they are not derived as expectation values of the Hamiltonian.

7.8.4 The Coupled-Cluster Method

The *coupled-cluster (CC) method* was introduced around 1958 by Coester and Kümmel in the context of studying the atomic nucleus. CC methods for molecular electronic calculations were developed by Pople and Bartlett. The fundamental equation in CC theory is

$$\Psi = e^{\hat{T}} \Psi_0, \tag{7.65}$$

where Ψ is the exact nonrelativistic ground-state molecular electronic wave function. Ψ_0 is the normalized ground-state Hartree-Fock wave function, the operator $e^{\hat{T}}$ is defined by the Taylor-series expansion

$$e^{\hat{T}} \equiv 1 + \hat{T} + \frac{\hat{T}^2}{2!} + \frac{\hat{T}^3}{3!} + \ldots = \sum_{k=0}^{\infty} \frac{\hat{T}^k}{k!}, \tag{7.66}$$

and the *cluster operator* $\hat{T}$ is

$$\hat{T} \equiv \hat{T}_1 + \hat{T}_2 + ... + \hat{T}_n, \tag{7.67}$$

where n is the number of electrons in the molecule and the operators $\hat{T}_1, \hat{T}_2, ...$ are defined below. The *one-particle excitation operator* $\hat{T}_1$ and the *two-particle excitation operator* $\hat{T}_2$ are defined by

$$\hat{T}_1\Psi_0 \equiv \sum_{b=n+1}^{\infty}\sum_{i=1}^{n} t_i^a \Psi_i^a, \qquad \hat{T}_2\Psi_0 \equiv \sum_{b=a+1}^{\infty}\sum_{a=n+1}^{\infty}\sum_{j=i+1}^{n}\sum_{i=1}^{n-1} t_{ij}^{ab}\Psi_{ij}^{ab}, \tag{7.68}$$

where Ψ_i^a is a singly excited Slater determinant with the occupied spin-orbital u_i replaced by the virtual spin-orbital u_a, and t_i^a is a numerical coefficient whose value depends on i and a and will be determined by requiring that Eq. (7.65) be satisfied. The operator $\hat{T}_1$ converts the Slater determinant Ψ_0 into a linear combination of all possible singly excited Slater determinants. Ψ_{ij}^{ab} is a Slater determinant with the occupied spin-orbitals u_i and u_j replaced by the virtual spin-orbitals u_a and u_b, respectively. The effect of the $e^{\hat{T}}$ operator is to express Ψ as a linear combination of Slater determinants that include Ψ_0 and all possible excitations of electrons from occupied to virtual spin-orbitals. A full CI calculation also expresses Ψ as a linear combination involving all possible excitations, and we know that a full CI calculation with a complete basis set gives the exact Ψ; hence, it is plausible that Eq. (7.65) is valid. The mixing into the wave function of Slater determinants with electrons excited from occupied to virtual spin-orbitals allows electrons to keep away from one another and thereby provides for electron correlation.

The aim of a CC calculation is to find the coefficients $t_i^a, t_{ij}^{ab}, ...$ To apply the CC method, two applications are made. First, instead of using a complete, and hence infinite, set of basis functions, one uses a finite basis set to express the spin-orbitals in the SCF wave function; one thus use only a finite number of virtual orbitals when forming excited determinants. As usual, we have a basis-set truncation error. Second, instead of including all the operators $\hat{T}_1, \hat{T}_2, \ldots, \hat{T}_N$, one approximates the operator $\hat{T}$ by including only some of these operators. Theory shows that the most important contribution to $\hat{T}$ is made by $\hat{T}_2$. The approximation $\hat{T} \approx \hat{T}_2$, gives

$$\Psi_{CCD} = e^{\hat{T}_2}\Phi_0\,. \tag{7.69}$$

Inclusion of only $\hat{T}_2$ gives an approximate CC approach called the *coupled-cluster doubles (CCD) method.* Since $e^{\hat{T}_2} = 1 + \hat{T}_2 + \frac{\hat{T}_2^2}{2!} + ...$, the wave function Ψ_{CCD} contains determinants with double substitutions, quadruple substitutions, hextuples, and so on. The next step in improving the CCD method is to include the operator $\hat{T}_1$ and take $\hat{T} = \hat{T}_1 + \hat{T}_2$ in $e^{\hat{T}}$. This gives the *CC singles and doubles (CCSD) method.* With $\hat{T} = \hat{T}_1 + \hat{T}_2 + \hat{T}_3$, one obtains the *CC singles, doubles and triples (CCSDT) method.* The exact basis-set correlation energy is obtained by full CI, by CC calculations with $\hat{T}$ not truncated, and by MP perturbation theory carried to infinite order. Various calculations on small molecules showed that the best results were obtained with the CCSDT model.

Chapter 8

Variational Monte Carlo determination of the $\bar{H}$-He potential

Contents

8.1 Introduction

Possible formation of antihydrogen via collision of metastable antiprotonic helium atomcules with positronium has been proposed lately by Ito & Yamazaki (1993)

$$[\bar{p}He^+]_{nl} + Ps \rightarrow \bar{H} + He + 6.8\ eV\,. \tag{8.1}$$

The determination of the Born-Oppenheimer $\bar{H}$-He potential is a first step, if one wants to investigate the output channels of the atomcule-Ps reaction. Energy calculations of mixed electron-positron systems requires a consistent treatment of interleptonic correlation, since cusps at electron-positron coalescence occur where the wave function is large. Hence CI methods as well as many-body perturbation theory are not the more appropriate in this case. Monte Carlo methods however fullfill the integrability requirement raised by arbitrary forms of Ψ, notably forms with explicit dependance to interleptonic coordinates.

8.2 Variational Monte Carlo (VMC) method

8.2.1 The variational method

We are here concerned with solving the non-relativistic, time-independant electronic Schrödinger equation

$$\mathcal{H}\Psi = E\Psi, \tag{8.2}$$

where $\mathcal{H}$ is the molecular hamiltonian operator. The expectation value of the energy of a trial wave function Ψ is given by

$$E[\Psi] = \frac{\int \Psi^* \mathcal{H} \Psi d\mathbf{R}}{\int \Psi^* \Psi d\mathbf{R}}. \tag{8.3}$$

According to the variational principle, $E[\Psi]$ will be a minimum for the exact ground state wave function. $E[\Psi]$ therefore provides an upper bound to the exact ground state energy; the best choice of Ψ may be obtained by minimizing $E[\Psi]$ with respect to the variation of its parameters $\{\alpha\}$.

8.2.2 Monte Carlo evaluation of $E[\Psi]$

Use of elaborate forms for Ψ imply numerical integration. On the other hand, uniform sampling to integrate $E[\Psi]$ is inefficient. An efficient method has to generate points based on the integrand. This can be done if one re-writes (8.3) as

$$E[\Psi] = \frac{\int \Psi^2 E_L(\mathbf{R})}{\int \Psi^2 d\mathbf{R}} \equiv \langle E_L \rangle_{\Psi^2}, \tag{8.4}$$

where E_L is the "local energy" defined as $E_L = \mathcal{H}\Psi(\mathbf{R})/\Psi(\mathbf{R})$. This rewriting allows now to interpret $E[\Psi]$ as an average of $E_L(\mathbf{R})$ sampled from the probability density $P_L(\mathbf{R}) = \Psi^2 / \int \Psi^2 d\mathbf{R}$ rather than an operator expectation value. Moreover, E_L is rigorously equal to eigenstate E_k, providing Ψ is – ideally – eigenfunction Φ_k, which means that E_k may be obtained with zero variance. If electronic configurations $\mathbf{R}$ are sampled from $P_L(\mathbf{R})$, then the Monte Carlo estimate of the energy is

$$E[\Psi] = \langle E_L \rangle_{\Psi^2} = \lim_{n\to\infty} \frac{1}{N} \sum_{i=1}^{N} E_L(\mathbf{R_i}). \tag{8.5}$$

Assuming uncorrelated sampling, the variance of the mean value is given by

$$\sigma^2(E[\Psi]) = \frac{\langle E_L^2 \rangle_{\Psi^2} - \langle E_L \rangle_{\Psi^2}^2}{N-1}. \tag{8.6}$$

In general, Ψ^2 is not of a form for which the distribution can be sampled directly. Metropolis algorithm provides a powerful method to sample electronic configuration space from Ψ^2.

8.2.3 Random walks, Markov chain and Metropolis sampling

A stationary distribution Ψ^2 can arise from a Markov chain of random moves (over electronic configuration space) governed by a transition probability $P(\mathbf{R_{old}} \rightarrow \mathbf{R_{new}})$ (Hammond *et al.*, 1994). Metropolis method (Metropolis *et al.*, 1953) gives the appropriate step P to drive the "walkers" towards the desired equilibrium distribution. Simple Metropolis algorithm is an acceptance/rejection game of chance with acceptance probabilities

$$P(\mathbf{R_{old}} \rightarrow \mathbf{R_{new}}) = \min(\frac{\Psi^2(\mathbf{R_{new}})}{\Psi^2(\mathbf{R_{old}})}, 1), \tag{8.7}$$

to account for both cases in which the ratio of the Ψ^2 are > 1 and < 1 [1]. Starting from a given configuration the next one is constructed as follows. First, a new configuration is proposed by moving successively each electron from a random vector sampled uniformly from a cube with linear dimension d_0 chosen to give an acceptance ratio of about 0.5. The proposed configuration is accepted as the next configuration with probability P, otherwise the old configuration is kept as the next one. Initially, one must wait for equilibrium (i.e. convergence to Ψ^2, within statistical fluctuations) before computing any expectation values. As can be noted, one main advantage of the Metropolis algorithm is that it only requires evaluating Ψ for the proposed move, the unknown normalisation $\int \Psi d\mathbf{R}$ is not required.

8.2.4 Generating independant configurations

Monte Carlo theorems relative to estimation of statistical errors are concerned with *independant* configurations. Estimation of correlation length τ i.e. the number of moves required to produce independant configurations has been investigated by Jacucci and Rahman (Jacucci & Rahman, 1984). The usual procedure to get a numerical estimate of $E[\Psi]$ is by taking the mean $\overline{E_L}$. $\sigma^2(\overline{E_L})$ is then obtained by using estimate of τ and $\sigma^2 = \frac{1}{N}\sum_{i=1}^{N}(E_L(\mathbf{R_i}) - \overline{E_L})^2$ according to

$$\sigma^2(\overline{E_L}) \simeq \tau\frac{\sigma^2}{N}, \tag{8.9}$$

[1] Let $\Phi^2(\mathbf{R_{old}})$ and $\Phi^2(\mathbf{R_{new}})$ be the current contribution of electronic configurations to probability density with $\Phi^2(\mathbf{R_{new}}) < \Phi^2(\mathbf{R_{old}})$. Then walkers at $\mathbf{R_{new}}$ will move to $\mathbf{R_{old}}$ since $P = 1$. On the other hand, walkers at $\mathbf{R_{old}}$ will move to $\mathbf{R_{new}}$ with probability $\frac{\Psi^2(\mathbf{R_{new}})}{\Psi^2(\mathbf{R_{old}})}$. Therefore, the net balance between contributions $\mathbf{R_{old}}$ and $\mathbf{R_{new}}$ will be

$$\delta\Phi = 1 \times \Phi^2(\mathbf{R_{new}}) - \frac{\Psi^2(\mathbf{R_{new}})}{\Psi^2(\mathbf{R_{old}})} \times \Phi^2(\mathbf{R_{old}}) \tag{8.8}$$

If $\frac{\Phi^2(\mathbf{R_{new}})}{\Phi^2(\mathbf{R_{old}})} = \frac{\Psi^2(\mathbf{R_{new}})}{\Psi^2(\mathbf{R_{old}})}$, then $\delta\Phi = 0$ and we are at equilibrium. If $\frac{\Phi^2(\mathbf{R_{new}})}{\Phi^2(\mathbf{R_{old}})} > \frac{\Psi^2(\mathbf{R_{new}})}{\Psi^2(\mathbf{R_{old}})}$ then $\delta\Phi > 0$ and the contribution of electronic configuration $\mathbf{R_{new}}$ to Ψ^2 will decreases, driving this inequality toward equality and equilibrium. Likewise, if $\frac{\Phi^2(\mathbf{R_{new}})}{\Phi^2(\mathbf{R_{old}})} < \frac{\Psi^2(\mathbf{R_{new}})}{\Psi^2(\mathbf{R_{old}})}$ then $\delta\Phi < 0$ and the contribution of $\mathbf{R_{new}}$ to Ψ^2 will increases until equilibrium has been reached.

where $\tau = 1$ for independant configurations. In order to estimate τ, the statistical inefficiency s is defined as

$$s = \lim_{N_b \to \infty} \frac{N_b \sigma^2(\overline{E_b})}{\sigma^2}, \tag{8.10}$$

where the N sequential configurations have been divided into b blocks of N_b configurations for which average energy $\overline{E_b}$ and variance of the block average $\sigma^2(\overline{E_b})$ are respectively

$$\overline{E_b} = \frac{1}{N_b} \sum_{i=1}^{N_b} E_L(\mathbf{R_i}), \tag{8.11}$$

$$\sigma^2(\overline{E_b}) = \frac{1}{b} \sum_{1}^{b} (\overline{E_b} - \overline{E_L})^2 . \tag{8.12}$$

One efficient procedure to determine τ is to plot s as a function of $\frac{1}{N_b}$ and extrapolate to get $\tau = s(0)$. In order to generate N independant configurations, it is therefore necessary to retrieve one every τ moves for a total number of $N\tau$ moves.

8.2.5 Monte Carlo optimization

The most commonly used technique is attributable to Umrigar *et al.* (1988). For the optimization of the trial wave function, he proposed to minimize the variance [2] of a fixed set of N electronic configurations $\mathbf{R_i}$ sampled from $|\Psi(\mathbf{R}, \alpha_0)|^2$ where α_0 is an initial estimate of variational parameters. The variance is given by (Mushinski & Nightingale, 1994)[3]

$$\sigma^2(\alpha) = \frac{\sum_{i=1}^{N} [E_L(\alpha, \mathbf{R_i}) - \overline{E(\alpha)}]^2 W_i}{\sum_{i=1}^{N} W_i}, \tag{8.15}$$

where

$$W_i = \frac{|\Psi(\alpha, \mathbf{R_i})|^2}{|\Psi(\alpha_0, \mathbf{R_i})|^2}, \tag{8.16}$$

[2] the idea of using variance of the energy as a measure of the quality of a variational trial wave function is reviewed by Goedecker & Maschke (1991).

[3]

$$\sigma(\alpha)^2 = \frac{\int \Psi^*(\alpha) (\mathcal{H} - \overline{E(\alpha)})^2 \Psi(\alpha) \, d\mathbf{R}}{\int \Psi^2(\alpha) \, d\mathbf{R}} = \frac{\int |\Psi(\alpha_0)|^2 (\mathcal{H} - \overline{E(\alpha)})^2 W_i \, d\mathbf{R}}{\int |\Psi(\alpha_0)|^2 W_i \, d\mathbf{R}}, \tag{8.13}$$

where

$$\overline{E(\alpha)} = \frac{\int \Psi^*(\alpha) \mathcal{H} \Psi(\alpha) \, d\mathbf{R}}{\int \Psi^2(\alpha) \, d\mathbf{R}} = \frac{\int |\Psi(\alpha_0)|^2 (\frac{\mathcal{H}\Psi_\alpha}{\Psi_\alpha} W_i) \, d\mathbf{R}}{\int |\Psi(\alpha_0)|^2 W_i \, d\mathbf{R}} = \frac{\sum_{i=1}^{N} E_L(\alpha, \mathbf{R_i}) W_i}{\sum_{i=1}^{N} W_i}. \tag{8.14}$$

Since $\mathcal{H}$ and $\overline{E(\alpha)}$ commut, expanding $(\mathcal{H} - \overline{E(\alpha)})^2$ operator and expressing all integrals as a Monte Carlo average lead effectively to (8.15).

and

$$\overline{E(\alpha)} = \frac{\sum_{i=1}^{N} E_L(\alpha, \mathbf{R_i}) W_i}{\sum_{i=1}^{N} W_i}. \tag{8.17}$$

The chief advantage of this procedure is that only a small number of configurations are required to perform the optimization. There are two reasons for this. First, the optimization technique incorporates correlated sampling i.e. the same set of configurations is used to evaluate σ^2 for each set of variational parameters during the whole optimization procedure, providing re-weighting factors W_i to convert the distributions from $|\Psi(\alpha_0)|^2$ to $|\Psi(\alpha)|^2$. Hence the difference in the σ's for two sets of variational parameters will be much more accurately determined than the values of the σ's themselves. Second, (8.15) is in the form of a least square fit. So if the true wave function were representable by an n-parameter trial wave function, then only n configurations would be necessary to determine the n parameters exactly. Another advantage is that the quantity being minimized has a known lower bound (namely zero), whereas the minimum of the energy is not known. There is a last argument in favour of variance minimisation: if one optimises the energy directly, the wave function obtained has an associated energy which is not very smooth, instead it contains small regions of space where the energy is much lower than average. This does indeed lower the overall energy in the optimization procedure but it does not produce a wave function which is closer to the true ground state wave function. Hence, VMC calculation using the optimized variational parameters will give a final value of the energy considerably higher than the final value obtained from the optimization scheme. This is in direct contrast to the results obtained from a variance optimization scheme, where the energy does not rise significantly.

8.2.6 Variational trial wave function

Most variational methods rely on a double basis-set expansion in 1-electron primitive functions and in N-electron Slater determinants. A unique characteristic of Monte Carlo methods is their ability to use arbitrary wave function forms – including ones with explicit interleptonic distance dependancies – enabling treatments beyond forms constructed solely with one-electron functions. Given this flexibility, it is important to recall properties a trial function ideally should possess. In particular, we focus on electron correlation, and the capability of various variational forms of many-electron wave functions to describe it.

Cusp conditions

An important corollary of the Schrödinger eigenvalue equation is that the local energy is constant everywhere in space for an eigenstate Φ_k. In particular, the singularity of the Coulomb potential must be cancelled by a corresponding term in the local kinetic energy. This condition results in a *cusp*, i.e., a discontinuity in the first derivative of Φ_k where two charged particles meet. With a sufficiently flexible trial function, one can include appropriate degrees of freedom which are then determined by the *cusp condition*. To examine the cusp

condition, let us take the simplest case: the electron-nucleus cusp of a hydrogenic atom. This is shown in Fig. 8.1.

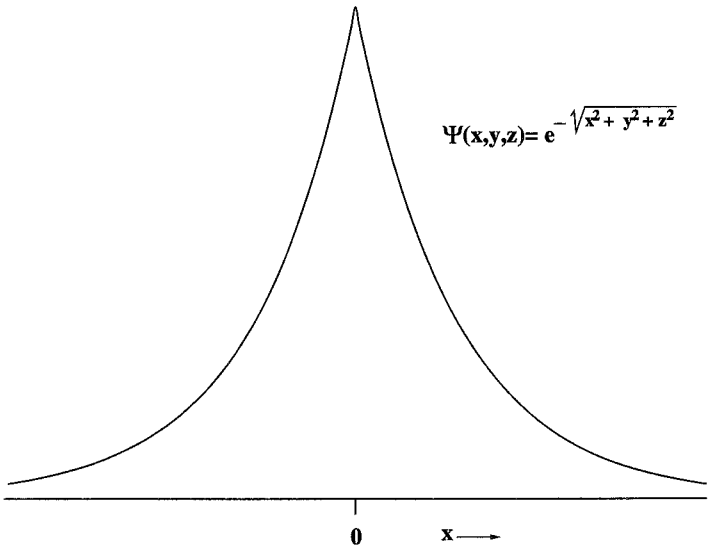

Figure 8.1: The electron-nucleus cusp in a hydrogenic atom

For hydrogenic atoms one can write the exact wavefunction in spherical polar coordinates, (r, θ, ϕ), as the product of a radial function, $R(r)$, and an angular function, $\Omega(\theta, \phi)$ (which is related to the spherical harmonics), i.e.,

$$\Phi_k(r, \theta, \phi) = R_k(r)\, \Omega_k(\theta, \phi)\,. \tag{8.18}$$

In focusing on the electron-nucleus cusp, we are only interested in the behavior of Φ as $r \to 0$. So let us examine the radial function, which is the solution of the radial Schrödinger equation,

$$\left(\frac{d^2}{dr^2} + \frac{2}{r}\frac{d}{dr} + \frac{2Z}{r} - \frac{l(l+1)}{r^2} + 2E\right) R(r) = 0, \tag{8.19}$$

where Z is the atomic charge. For $l = 0$ (i.e., S states), we see that the two r^{-1} terms must cancel, which leads to the cusp condition

$$\left(\frac{1}{R(r)}\frac{dR(r)}{dr}\right)\Big|_{r=0} = -Z\,. \tag{8.20}$$

If we solve (8.20) for R, we find that R must be an exponential in r. What of the $l \neq 0$ case, and what happens to (8.20) if $R(0) = 0$? Let us treat the latter issue and show that it adresses the former. To treat the case of $R \to 0$ at the origin, we can explicitly factor out the leading r dependance, i.e.,

$$R(r) = r^m \rho(r), \tag{8.21}$$

so that $\rho(r)$ is a function that does not go to zero at the origin. Substituting into (8.19), we find that the r^{-2} terms cancel if $m = l$, yelding the following equation for ρ:

$$\left(\frac{2\,(l+1)}{r}\frac{\rho'}{\rho} + \frac{2\,Z}{r} + \frac{\rho''}{\rho} + 2E\right) r^l \rho = 0\,. \tag{8.22}$$

The choice of $m = l$ should not be too surprising, for it corresponds to the known behavior of the eigenfunctions of the hydrogenic atoms with respect to angular momentum. Now, by equating the r^{-1} terms in (8.22), one gets the general electron-nucleus cusp condition,

$$\left.\frac{\rho'}{\rho}\right|_{r=0} = -\frac{Z}{l+1} \tag{8.23}$$

For hydrogenic systems, thsi cusp condition uniquely determines the overall exponential behavior of the wave function for each value of l, i.e., $R(l=0) \propto e^{-Zr}$, $R(l=1) \propto e^{-Zr/2}$, $R(l=2) \propto e^{-Zr/3}$, etc.

The extension to the many-electron case is straightforward. As any single electron approaches the nucleus (with all other fixed), the exact wave function behaves asymptotically as in the one-electron case, and (8.23) holds for each electron individually. In the same way, an extension of this argument to the electron-electron cusp is possible. In this case, as electron i approaches electron j one has essentially a two-body problem similar to the hydrogenic atom. However, now both electrons give kinetic energy contributions. Expanding the wave function in spherical polar coordinates centered on electron i, leads to the "radial" equation

$$\left(2\frac{d^2}{dr_{ij}} + \frac{4}{r_{ij}}\frac{d}{dr_{ij}} + \frac{2}{r_{ij}} - \frac{l(l+1)}{r_{ij}^2} + 2E\right) R_{ij}(r_{ij}) = 0\,. \tag{8.24}$$

Therefore, following the discussion for the hydrogenic systems, we obtain the cusp condition to be

$$\left.\frac{\rho'_{ij}}{\rho_{ij}}\right|_{r_{ij}=0} = \frac{1}{2(l+1)} \tag{8.25}$$

With a flexible form of the wave function, we can satisfy both (8.23) and (8.25).

General trial function forms

The exact wave function can be approximated in a number of ways through series expansions in the electronic coordinates. Hylleraas (1929) had great success for He with trial functions of the form

$$\Psi_{Hylleraas} = \left(\sum_{k=1}^{N} d_k r^{a_k} s^{b_k} t^{e_k}\right) e^{-\frac{1}{2}s}, \tag{8.26}$$

where r is the electron-electron separation (which was previously designated as r_{ij}), $s = r_1 + r_2$, and $t = r_1 - r_2$. Here r_1 and r_2 are the distances from electrons to nucleus. The electron-nucleus cusp condition is satisfied by the exponential term, and the electron-electron

cusp is satisfied by choosing the proper values for the coefficients. Because all the interparticle distances are represented, very accurate descriptions of the He wave function may be obtained with relatively few terms. Although (8.26) is written explicitely for two electrons, it is easily generalized to larger systems.

Helium has long served as a testing ground for atomic trial functions because of its simplicity. For example, a nine-term Hylleraas function yields an energy of -2.9035 hartrees, while a 1078 term function yields -2.90372375 hartrees. Clearly, convergence is not fast. On the other hand, by adding terms with powers of $\ln s$ and negative powers of s, we can obtain -2.903724377033 hartrees with only 246 terms. It was argued that comparable accuracy in a CI calculation would require 10^5 one-electron basis functions and approximately 10^{12} configurations. Thus, the functional form is very important. However, even with Monte Carlo integration, the task of determining hundreds or thousands of parameters remain an obstacle.

Molecular orbital theory

Unlike the forms just discussed, the most widely used methods in *ab initio* electronic structure theory are based on molecular orbital (MO) expansions and the Hartree-Fock approximation. As a first approximation, the N-electron wave function Ψ_D is represented by a Slater determinant of spin-orbitals. Each spin orbital, $\widetilde{\phi}_i$ consists of a spatial function, ϕ_i, multiplied by an electron spin function (α or β). The orbital approach is motivated by a simple generalization of the one-electron description of the H atom, building in the antisymmetry required by the Pauli principle. The determinantal part of the probability distribution, Ψ_D^2, depends on the product $\phi_1^2\phi_2^2...\phi_n^2$ of one-electrons probabilities. Since no terms involve conditional probabilities of two or more electrons, each particle acts independently of the others. This independant-particle approximation differs fundamentally from Hylleraas-type functions which include r_{ij} terms explicitly. Hence a single determinant wave function alone does not satisfy the electron-electron cusp condition. In contrast, Ψ_D can be made to satisfy the electron-nucleus cusp condition because the atomic orbitals explicitly depend upon electron-nucleus distance r_{iA}. Consider the most common case, where Ψ_D does not go to zero at $r_{iA} \to 0$. Then,

$$\left.\frac{1}{\Psi_D}\frac{\partial \Psi_D}{\partial r_{iA}}\right|_{r_{iA}=0} = -Z_A\,. \tag{8.27}$$

One can show than (8.27) can be enforced if for each MO (i.e., for each k) one requires

$$\left.\frac{1}{\phi_k}\frac{\partial \phi_k}{\partial r_{iA}}\right|_{r_{iA}=0} = -Z_A\,. \tag{8.28}$$

Therefore, for Ψ_D to satisfy (8.27), each orbital must individually satisfy (8.28).

Correlated molecular orbital functions

In the above discussion, the importance of r_{ij} terms was underlined. On the other hand Hartree-Fock and post Hartree-Fock wave functions, which do not explicitly contain these terms, lead to molecular integrals that are substancially more convenient for integration. Correlated molecular orbital (CMO) methods incorporate the best of both. Typically, CMO functions are constructed as a determinant of orbitals where each orbital is multiplied by a function of the interleptonic coordinates $f(r_{ij}) \equiv f_{ij}$. Explicitly,

$$\Psi_{CMO} = \mathcal{A}\phi_1(x_1)\phi_2(x_2)...\phi_n(x_n)f_{12}f_{13}f_{23}...f_{n-1,n}, \tag{8.29}$$

where $\mathcal{A}$ is the antisymmetrizer operator. Most often the form of f_{ij} is independant of the orbitals, making Ψ_{CMO} a simple product function

$$\Psi_{CMO} = \Psi_D\Psi_C, \tag{8.30}$$

where Ψ_D is the determinantal part and Ψ_C is a product of correlation functions. One advantage of this form is that we can now satisfy the electron-electron cusp condition, because f_{ij} depends explicitly on r_{ij}. Using the results of Sec 8.2.6 describing the r_{ij} dependance of Ψ_D, we obtain the cusp of Ψ_{CMO} by constraining Ψ_C so that for like-spin electrons,

$$\left.\frac{1}{\Psi_C}\frac{\partial\Psi_C}{\partial r_{ij}}\right|_{r_{ij}=0} = \frac{1}{4}, \tag{8.31}$$

while for opposite spin electrons,

$$\left.\frac{1}{\Psi_C}\frac{\partial\Psi_C}{\partial r_{ij}}\right|_{r_{ij}=0} = \frac{1}{2}. \tag{8.32}$$

We can distinguish between two classes of functions Ψ_C. In the first class, Ψ_C contains polynomials in r_{ij}, similar to the Hylleraas functions. The second class is an exponential or Jastrow form

$$\Psi_C = e^U, \tag{8.33}$$

where U contains all the r_{ij} dependence. One of the most commonly form used in Monte Carlo calculations is the Padé-Jastrow function

$$U = \sum_{i=1}^{N}\sum_{j,i}^{N}\frac{a_1 r_{ij} + a_2 r_{ij}^2 + ...}{1 + b_1 r_{ij} + b_2 r_{ij}^2 + ...}. \tag{8.34}$$

The general behavior of e^U is shown in Fig. 8.2, beginning at unity for $r_{ij} = 0$ and asymptotically approaching a constant value for large r_{ij}. In the simplest case, where only a_1 and b_1 are non-zero, this asymptotic value is e^{a_1/b_1}. One can verify that the electron-electron cusp condition requires a_1 to be $1/2$ for unlike spins and $1/4$ for like spins. The linear Padé-Jastrow form has only one free parameter, namely b_1, with which to optimize the wave function.

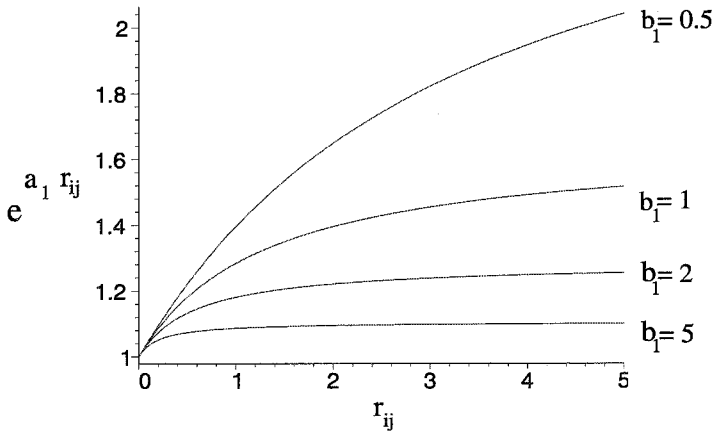

Figure 8.2: Dependence of the linear Pade-Jastrow function on r_{ij}. The coefficient a_1 is set to 0.5 to satisfy the electron-electron cusp condition.

For CMO wave functions one can optimize the Jastrow parameters, the molecular orbital coefficients, and the atomic orbital exponents. Clearly, practical limitations will be reached for very large systems, but such optimization has been done for several systems. Use of a three-parameter correlation function for Li_2 led to 55 % of the correlation energy. A 21 parameter function, that included all combinations of r_i, r_j, and r_{ij} to fourth order, including electron-electron-nucleus terms, obtained essentially all the correlation energy for two-electrons systems, 99 % of the correlation energy for Be, and 86 % of the correlation energy for Ne. These results are impressive, and show that VMC can be as attractive quantum chemistry technique in its own right. We are finishing the writing of a VMC production code. Validation tests are in progress at the present time.

8.3 Helium-antihydrogen interaction

8.3.1 Molecular hamiltonian

In the Born-Oppenheimer approximation, the spinless non-relativistic Hamiltonian (in atomic units) is

$$\mathcal{H}(1,2;3) = -\frac{1}{2}\triangle_1 - \frac{1}{2}\triangle_2 - \frac{1}{2}\triangle_3 + V, \tag{8.35}$$

where

$$V = -2(\frac{1}{r_{\alpha 1}} + \frac{1}{r_{\alpha 2}} - \frac{1}{r_{\alpha 3}}) + (\frac{1}{r_{\bar{p}1}} + \frac{1}{r_{\bar{p}2}} - \frac{1}{r_{\bar{p}3}}) + (\frac{1}{r_{12}} - \frac{1}{r_{13}} - \frac{1}{r_{23}}) - \frac{2}{r_{\alpha\bar{p}}}. \tag{8.36}$$

1 and 2 refer to electrons, 3 to positron.

8.3.2 Trial wavefunction

For the He-$\bar{H}$ system, we plan to use a first variational trial wave function adapted from those choosed by Kolos and Wolniewicz for their treatment of the H-$\bar{H}$ (Kolos *et al.*, 1975) and He-H^+ (Kolos & Wolniewicz, 1965) interactions. It is an expansion in elliptical coordinates which contains exponential factors and Pade-Jastrow functions, ensuring lepton-nucleus and lepton-lepton cusp condition, respectively. The necessary flexibility is secured by expressing the rest of the function as a power series in the 6 variables involving lepton-nucleus distances. Thus, the trial wave function is

$$\Psi = \sum_i c_i \Psi_i(1,2;3), \tag{8.37}$$

where

$$\begin{aligned}
\Psi_i(1,2;3) &= [\Phi_i(1,2) \pm \Phi_i(2,1)]\, \Phi_i(3) \\
\Phi_i(1,2) &= e^{(-\alpha_1\mu_1 - \alpha_2\mu_2 + \beta_1\nu_1 + \beta_2\nu_2)}\, e^{\frac{a_{12}r_{12}+c_{12}r_{12}^2}{1+b_{12}r_{12}+d_{12}r_{12}^2}}\, \mu_1^{s_{i1}}\, \nu_1^{t_{i1}}\, \mu_2^{s_{i2}}\, \nu_2^{t_{i2}} \\
\Phi_i(2,1) &= e^{(-\alpha_1\mu_2 - \alpha_2\mu_1 + \beta_1\nu_2 + \beta_2\nu_1)}\, e^{\frac{a_{12}r_{12}+c_{12}r_{12}^2}{1+b_{12}r_{12}+d_{12}r_{12}^2}}\, \mu_2^{s_{i1}}\, \nu_2^{t_{i1}}\, \mu_1^{s_{i2}}\, \nu_1^{t_{i2}} \\
\Phi_i(3) &= e^{(-\gamma_1\mu_3 + \gamma_2\nu_3)}\, e^{\frac{a_{13}r_{13}+c_{13}r_{13}^2}{1+b_{13}r_{13}+d_{13}r_{13}^2}}\, e^{\frac{a_{23}r_{23}+c_{23}r_{23}^2}{1+b_{23}r_{23}+d_{23}r_{23}^2}}\, \mu_3^{u_{i1}}\, \nu_3^{u_{i2}}\,.
\end{aligned}$$

The + or − sign in $\Psi_i(1,2;3)$ results in an eletronic spin singlet or triplet state, respectively. μ_i, ν_i denote elliptic coordinates [4]; and r_{ij} are interleptonic distances. The coefficients c_i and α_j, β_j, γ_j $(j = 1, 2)$, as well as b_{kl}, c_{kl}, d_{kl} $(0 < k < l \leq 3)$ are variational parameters. The electron-electron cusp condition requires $a_{12} = 1/2$ in the singlet case and $a_{12} = 1/4$ in the triplet case. For the electron-positron cusp, we have $a_{13} = a_{23} = 1/2$ (Schrader, 1970). s_{kl}, t_{kl}, u_{kl} are integers.

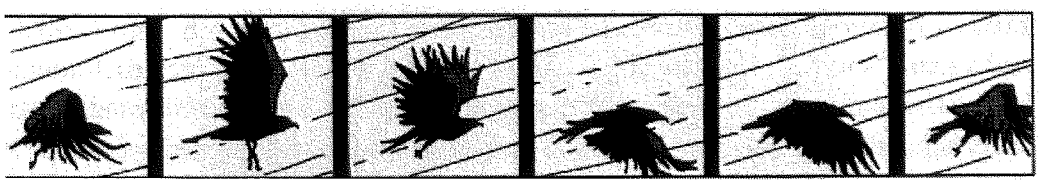

[4] Let the distances between α, $\bar{p}$ nuclei and i^{th} lepton carry the usual symbol $R_{\alpha\bar{p}}$, $r_{\alpha i}$, $r_{\bar{p}i}$. Then elliptic coordinates are

$$\mu_i = \frac{r_{\bar{p}i} + r_{\alpha i}}{R_{\alpha\bar{p}}} \text{ and } \nu_i = \frac{r_{\bar{p}i} - r_{\alpha i}}{R_{\alpha\bar{p}}} \tag{8.38}$$

Références Bibliographiques

Bakalov, D. et Korobov, V. I. 1998, Hyperfine strucutre of antiprotonic helium energy levels, *Physical Review A* **57**, 1662.

Beck, W. A., Wilets, L. et Alberg, M. A. 1993, Semiclassical description of antiproton capture on atomic helium, *Physical Review A* **48**, 2779.

Carbonell, J., Ciesielski, F. et Gignoux, C. 1995, Antiproton helium polarization states, dans *Few-body systems supplement*, vol. 8, pp. 428–432.

Condo, G. T. 1964, On the absorption of negative pions by liquid helium, *Physics Letters* **9**, 65.

Elander, N. et Yarevsky, E. 1997, Finite-element calculations of the antiprotonic helium atom including relativistic and QED corrections, *Physical Review A* **56**, 1865.

Fedotov, S. I., Kartavtsev, O. I. et Monakhov, D. E. 1996, Auger decay rates for $^{3,4}He^{+}\bar{p}$, *Physics of Atoms and Nuclei* **59**, 1717.

Foresman, J. B. et Frisch, A. 1993, *Exploring chemistry with electronic structure methods*, Gaussian Inc.

Gabrielse, G., Fei, X., Orozco, L. A., Tjoelker, R. L., Haas, J., Kalinowsky, H., Trainor, T. A. et Kells, W. 1990, Thousandfold improvement in the measured antiproton mass, *Physical Review Letters* **65**, 1317.

Goedecker, S. et Maschke, K. 1991, Comment on "criterion for a good variational wave function, *Physical Review B* **44**, 10365.

Hammond, B. L., A., L. W. et J., R. P. 1994, *Monte Carlo Methods in ab initio quantum chemistry*, World Scientific.

Hartmann, F. J., Ketzer, B., Maierl, C., Pohl, R., Von Egidy, T., Hayano, R. S., Hori, M., Ishikawa, T., Tamura, H., Torii, H. A., Kumakura, M., Morita, N., Sugai, I., Horváth, D. *et al.* 1998, Laser spectroscopy of metastable states in the $v = 2$ cascade of antiprotonic ^{3}He, *submitted in Physical Review A* .

Hori, M., Torii, H. A., Hayano, R. S., Ishikawa, T., Maas, F. E., Tamura, H., Ketzer, B., Hartmann, F. J., Pohl, R., Maierl, C., Hasinoff, M., Von Egidy, T., Kumakura, M., Morita, N. *et al.* 1998, Laser spectroscopic studies of state-dependent collisional quenching of the lifetimes of metastable antiprotonic helium atoms, *Physical Review A* **57**, 1698.

Hugues, R. J. et Deutch, B. I. 1992, Electric charge of positrons and antiprotons, *Physical Review Letters* **69**, 578.

Hylleraas, E. A. 1929, Neue Berechnung der Energie des Heliums in Grand-austande, sowie des tiefsten terms von ortho-Helium, *Zeitshrift für Physik* **54**, 374.

Ito, Y. Widmann, E. et Yamazaki, T. 1993, Possible formation of antihydrogen atoms from metastable antiprotonic helium atoms and positrons/positroniums, *Hyperfine Interactions* **76**, 163.

Iwasaki, M., Nakamura, S. N., Shigaki, K., Shimizu, Y., Tamura, H., Ishikawa, T. et Hayano, R. S. 1991, Discovery of antiproton trapping by long-lived metastable states in liquid helium, *Physical Review Letters* **67**, 1246.

Jacucci, G. et Rahman, A. 1984, Comparing the efficiency of Metropolis Monte Carlo and molecular-dynamics Methods for configuration space sampling, *Il Nuovo Cimento* **4**, 341.

Ketzer, B. 1999, Laserspektroskopie Von etastabilem antiprotonischen Helium unter dem Einfluβ Von Fremdgasbeimischungen, *pHD* .

Ketzer, B., Hartmann, F. J., Daniel, H., Von Egidy, T., Niestroj, A., Schmid, S., Schmid, W., Yamazaki, T., Sugai, I., Nakayoshi, K., Hayano, R. S., Maas, F. E., Torii, H. A., Ishikawa, T. *et al.* 1996, Isotope effects on delayed annihilation time spectra of antiprotonic helium atoms in low-temperature gas, *Physical Review A* **53**, 2108.

Ketzer, B., Hartmann, F. J., Von Egidy, T., Maierl, C., Pohl, R., Eades, J., Widmann, E., Yamazaki, T., Kumakura, M., Morita, N., Hayano, R. S., Hori, M., Ishikawa, T., Torii, H. A. *et al.* 1998, Quenching of metastable states of antiprotonic helium atoms by collisions with H_2 molecules, *Journal of Chemical Physics* **109**, 424.

Kino, Y., Kamimura, M. et Kudo, H. 1998, High-accuracy 3-body coupled-channel calculation of metastable states of antiprotonic helium atoms, *Nuclear Physics A* **631**, 649c.

Kolos, W., Morgan, D. L., Schrader, D. M. et Wolniewicz, L. 1975, Hydrogen-antihydrogen interactions, *Physical Review A* **11**, 1792.

Kolos, W. et Wolniewicz 1965, Potential-energy curves for the $\mathbf{X}\,^1\Sigma_g^+$, $\mathbf{b}\,^3\Sigma_u^+$, and $\mathbf{C}\,^1\Pi_u$ states of the hydrogen molecule, *Journal of Chemical Physics* **43**, 2429.

Korenman, G. Y. 1996, The dynamics of antiprotonic metastable states in helium, *Hyperfine Interactions* **103**, 341.

Korobov, V. I. 1996, Variational calculation of energy levels in $\bar{p}He^+$ molecular systems, *Physical Review A* **54**, 1749.

Korobov, V. I. 1998, Metastable states of antiprotonic helium atoms, dans *Proceedings of the Workshop on Frontier Tests of Quantum Electrodynamics and Physics of the Vacuum. Sandansky.*

Korobov, V. I. et Bakalov, D. D. 1997, Energies and relativistic corrections for the metastable states of antiprotonic helium atoms, *Physical Review Letters* **79**, 3379.

Korobov, V. I. et Shimamura, I. 1997, Auger transition rates for metastable states of antiprotonic helium $He^+\bar{p}$, *Physical Review A* **56**, 4587.

Maas, F. E., Hayano, S. T., Ishikawa, T., Tamura, H., Torii, H. A., Morita, N., Yamazaki, T., Sugai, I., Nakayoshi, K., Hartmann, F. J., Daniel, H., Von Egidy, T., Ketzer, B., Niestroj, A. *et al.* 1995, Laser-induced resonant transition at 470.724 nm in the $v = n - l - 1 = 2$ cascade of metastable antiprotonic helium atoms, *Physical Review A* **52**, 4266.

Metropolis, N., Rosenbluth, A. W., Rosenbluth, M. N., Teller, A. H. et Teller, E. 1953, Equation of state calculations by fast computing machines, *Journal of Chemical Physics* **21**, 1087.

Morita, N., Kumakura, M., Yamazaki, T., Widmann, E., Masuda, H., Sugai, I., Hayano, R. S., Maas, F. E., Torii, H. A., Hartmann, F. J., Daniel, H., Von Egidy, T., Ketzer, B., Müller, W. *et al.* 1994, First observation of laser-induced resonant annihilation in metastable antiprotonic helium atoms, *Physical Review Letters* **72**, 1180.

Morita, N., Ohtsuki, K. et Yamazaki, T. 1993, Laser spectroscopy of metastable antiprotonic helium atomcules, *Nuclear Instruments & Methods in Physics Research A.* **330**, 439.

Mushinski, A. et Nightingale, M. P. 1994, Many-body trial wave functions for atomic systems and ground states of small noble gas clusters, *Journal of Chemical Physics* **101**, 8831.

Pohl, R., Hori, M., Torii, H. A., Hayano, R. S., Ishikawa, T., Hartmann, F. J., Ketzer, B., Maierl, C., , Von Egidy, T., Eades, J., Widmann, E., Yamazaki, T., Kumakura, M. *et al.* 1998, Influence of oxygen admixtures on the lifetimes of metastable antiprotonic helium atoms, *Physical Review A* **58**, 4406.

Russell, J. E. 1969, Metastable states of $\alpha\pi^-e^-$, αK^-e^- and $\alpha\bar{p}e^-$ atoms, *Physical Review Letters* **23**, 63.

Russell, J. E. 1970, Distorsion of the elctron wave function in $\alpha\pi^-e^-$, αK^-e^- and $\alpha\bar{p}e^-$ atoms, *Physical Review A* **1**, 735.

Schrader, D. M. 1970, Self-consistent-field theory for one-positron many-electron systems, *Physical Review A* **1**, 1070.

Shimamura, I. 1992, Moleculelike metastable states of antiprotonic and mesic helium, *Physical Review A* **46**, 3776.

Torii, H. A., Hayano, R. S., Hori, M., Ishikawa, T., Morita, N., Kumakura, M., Sugai, I., Yamazaki, T., Ketzer, B., Hartmann, F. J., Von Egidy, T., Pohl, R., Maierl, C., Horváth, D. *et al.* 1999, Laser measurements of the density shifts of resonance lines in antiprotonic helium atoms and stringent constraint on the antiproton charge and mass, *Physical Review B* **404**.

Umrigar, C. J., Wilson, K. G. et Wilkins, J. W. 1988, Optimized trial wave functions for quantum Monte Carlo calculations, *Physical Review Letters* **60**, 1719.

Voronin, A. et Dalkarov, O. 1998, Collisional dynamics of metastable antiprotonic atoms in helium, *private communication* .

Widmann, E., Daniel, H., Eades, J., Von Egidy, T., Hartmann, F. J., Hayano, R. S., Higemoto, W., Hofmann, J., Ito, T. M., Ito, Y., Ishikawa, T., Kawachi, A., Nakamura, S. N., Nishida, N. *et al.* 1993, Antiproton trapping in various helium media: report of the HELIUMTRAP experiment at LEAR, *Nuclear Physics A* pp. 679c–688c.

Widmann, E., Eades, J., Yamazaki, T., Torii, H. A., Hayano, R. S., Hori, M., Ishikawa, T., Kumakura, M., Morita, N., Sugai, I., Hartmann, F. J., Von Egidy, T., Ketzer, B., Maierl, C. *et al.* 1997, Hyperfine structure of the metastable $\bar{p}He^+$ atomcule revealed by a laser-induced $(n,l) = (37,35) \rightarrow (38,34)$ transition, *Physics Letters B* **404**, 15.

Widmann, E., Sugai, I., Yamazaki, T., Hayano, R. S., Ishikawa, T., Nakamura, S. N., Tamura, H., Ito, T. M., Kawachi, A., Nishida, N., Higemoto, W., Ito, Y., Morita, N., Hartmann, F. J. *et al.* 1996, Effects of impurity atoms and molecules on the lifetime of antiprotonic helium atoms, *Physical Review A* **53**, 3129.

Widmann, E., Sugai, I., Yamazaki, T., Hayano, R. S., Ishikawa, T., Nakamura, S. N., Tamura, H., Ito, T. M., Kawachi, A., Nishida, N., Ito, Y., Morita, N., Hartmann, F. J., Daniel, H. *et al.* 1995, Phase and density dependence of the delayed annihilation of metastable antiprotonic helium atoms in gas, liquid, and solid helium, *Physical Review A* **51**, 2870.

Wind, H. 1965, *Journal of Chemical Physics* **42**, 2371.

Yamazaki, T. 1992, A possible way to promote antihydrogen formation via metastable antiprotonic helium atoms, *Zeitschrift für Physik A - Hadrons and nuclei* **341**, 223.

Yamazaki, T. 1994, Prospects of spectroscopy with antiprotonic exotic atoms, dans *Invited talk at the International Conference on Low-Energy Antiproton Physics LEAP94*.

Yamazaki, T. 1998, An exotic three-body System - Antiprotonic helium atomcules, dans *Few-body systems supplement 10: Few-body problems in physics'98*, pp. 151–159, Springer-Verlag/Wien.

Yamazaki, T., Ketzer, B., Widmann, E., Eades, J., Daniel, H., Hartmann, F. J., Hasinoff, M., Pohl, R., Schmidt, R., Von Egidy, T., Horváth, D., Kumakura, M., Morita, N., Sugai, I. *et al.* 1997a, Laser resonance studies of the interactions of metastable antiprotonic helium atomcules $\bar{p}^4He^+$ with surrounding H_2 molecules, *Chem. Physics Letters* **265**, 137.

Yamazaki, T. et Ohtsuki, K. 1992, Atomic core-polarization effects in metastable hadronic helium atoms, *Physical Review A* **45**, 7782.

Yamazaki, T., Widmann, E., Eades, J., Kumakura, M., Morita, N., Torii, H. A., Hori, M., Ishikawa, T., Maas, F. E., Tamura, H., Hayano, R. S., Sugai, I., Fujita, Y., Ketzer, B. *et al.* 1997b, High-precision structural studies of the antiprotonic helium atom $\bar{p}^4He^+$ by observing laser resonances with $\Delta v = \Delta(n-l-1) = 2$, *Physical Review A* **55**, 3295.

Yamazaki, T., Widmann, E., Hayano, R. S., Iwasaki, M., Nakamura, S. N., Shigaki, K., Hartmann, F. J., Daniel, H., Von Egidy, T., Hofmann, P., Kim, Y. S. et Eades, J. 1993, Formation of long-lived gas phase antiprotonic helium atoms and quenching by H_2, *Nature* **361**, 238.

Résumé

Environ 3% des antiprotons ($\bar{p}$) stoppés dans l'helium survivent plusieurs microsecondes, contre quelques picosecondes dans tout autre matériau. Cette métastabilité inhabituelle résulte d'une capture sur des états liés de l'atome exotique $\bar{p}He^+$, dénommé atomcule car il s'apparente à la fois à un atome de Rydberg quasi-circulaire quasi-classique de grand moment angulaire $l \sim n - 1 \sim 37$ et à une molécule diatomique composée d'un noyau chargé négativement et caractérisée par une forte excitation rotationnelle $J = l$. En dehors de cette structure duale originale accessible par spectroscopie laser, la physico-chimie de leur interaction avec d'autres atomes ou molécules a fait l'objet de mesures résolues en état. Alors que les atomcules résistent à des millions de collisions dans l'helium pur, des contaminants moléculaires comme H_2 les détruisent immédiatement, même à basse température.

Dans le cadre Born-Oppenheimer, nous interprétons l'interaction moléculaire, calculée par des techniques de chimie quantique *ab initio*, en termes de chemins réactifs classiques, qui présentent des barrières d'activation compatibles avec celles mesurées pour He et H_2. Nous montrons par une approche Monte Carlo de trajectoires classiques que la thermalisation détruit fortement les populations initiales, portant la fraction estimée des états de capture à 3 %. Nous étudions aussi la recombinaison dissociative $\bar{p}He^+ + e^+e^-$ dans une approche de trajectoires classiques pour les noyaux: nous prédisons la synthèse d'antihydrogène avec un rapport de branchement de 10 %, ainsi qu'une nouvelle classe d'atomcules métastables (α, $\bar{p}$, e^+, $2e^-$), qui pourrait être confirmée par spectroscopie. Ce travail illustre la transférabilité des concepts de chimie physique à l'étude de processus exotiques en présence d'antimatière, et apporte un éclairage nouveau sur la physico-chimie des radicaux interstellaires froids.

Mots-clés: physico-chimie exotique en présence d'antimatière, atomcules antiprotoniques métastables, collisions moléculaires, chemins réactifs classiques, barrières d'activation, chimie quantique *ab initio*.

Summary

About 3% of antiprotons ($\bar{p}$) stopped in helium are long-lived with microsecond lifetimes, against picoseconds in all other materials. This unusual longevity has been ascribed to the trapping of $\bar{p}$ on metastable bound states in $\bar{p}He^+$ helium atom-molecules thus named atomcules. Apart from their unique dual structure investigated by laser spectroscopy - a near-circular quasi-classical Rydberg atom with $l \sim n - 1 \sim 37$ or a special diatomic molecule with a negatively charged $\bar{p}$ nucleus in high rotational state with $J = l$ - the chemical physics aspects of their interaction with other atoms or molecules constitute an interesting topic for molecular physics. While atomcules may resist to million collisions in helium, molecular contaminants such as H_2 are likely to destroy them in a single one, down to very low temperatures.

In the Born-Oppenheimer framework, we interpret the molecular interaction obtained by *ab initio* quantum chemical calculations in terms of classical reactive channels, with activation barriers accounting for the experiments carried out in He and H_2. From classical trajectory Monte Carlo simulations, we show that the thermalization stage strongly quenches initial populations, thus reduced to a recovered 3 % trapping fraction. Alternatively, we investigate the reactive association of $\bar{p}He^+$ with e^+e^- in a classical trajectory approach for nuclei: we predict antihydrogen synthesis with 10 % branching ratio and a new class of metastable atomcules (α, $\bar{p}$, e^+, $2e^-$), which could be confirmed by spectroscopy. This work illustrates the pertinence of chemical physics concepts to the study of exotic processes involving antimatter. New insights into the physico-chemistry of cold interstellar radicals are anticipated.

Keywords: exotic physico-chemistry in the presence of antimatter, metastable antiprotonic atomcules, molecular collisions, classical reactive channels, activation barriers, *ab initio* quantum chemistry.